

2010

Highly efficient selection, enumeration, enrichment, and molecular profiling of low-abundance biological cells

Udara R. Dharmasiri Rasika Dharmasiri

Louisiana State University and Agricultural and Mechanical College, udaraud1@gmail.com

Follow this and additional works at: https://digitalcommons.lsu.edu/gradschool_dissertations



Part of the [Chemistry Commons](#)

Recommended Citation

Dharmasiri, Udara R. Dharmasiri Rasika, "Highly efficient selection, enumeration, enrichment, and molecular profiling of low-abundance biological cells" (2010). *LSU Doctoral Dissertations*. 3081.

https://digitalcommons.lsu.edu/gradschool_dissertations/3081

This Dissertation is brought to you for free and open access by the Graduate School at LSU Digital Commons. It has been accepted for inclusion in LSU Doctoral Dissertations by an authorized graduate school editor of LSU Digital Commons. For more information, please contact gradetd@lsu.edu.

HIGHLY EFFICIENT SELECTION, ENUMERATION, ENRICHMENT, AND MOLECULAR PROFILING OF LOW-ABUNDANT BIOLOGICAL CELLS

A Dissertation

Submitted to the Graduate Faculty of the
Louisiana State University and
Agricultural and Mechanical College
in partial fulfillment of the
requirements for the degree of
Doctor of Philosophy

in

The Department of Chemistry

by

Udara R. Dharmasiri

B.S. University of Peradeniya, 2004

M.S., Post-Graduate Institute of Science,
University of Peradeniya, Sri Lanka, 2006

December, 2010

DEDICATION

This dissertation is dedicated to my loving parents, Sarath Chandralatha Kaldera and A.W. Dharmasiri. I am grateful for their sacrifices that have made this education possible. To my grandparents, brother and sisters of my mother and father, tremendous sacrifices have been made by all in my attempt to make a difference in the world of education.

ACKNOWLEDGEMENTS

I would like to thank first and foremost my advisor, Prof. Steven A. Soper, for his encouragement and unwavering support throughout my thesis research. His infectious enthusiasm, constructive criticism and unlimited zeal for excellence made this work fantastic. Dr. Soper, your quest for knowledge and the wisdom you provided will serve me for a lifetime. Of course, I thank my dissertation committee members; Prof. Jayne Garno, Prof. Joseph Francis, Prof. David Spivak, Prof. Evgueni Nesterov, Prof. Donghui Zhang, who taught, inspired and encouraged me.

I wish also to thank Andre A. Adams and Dr. Subramaniam Balamurugan (Bala) for their much appreciated comments and support in my early cell analysis and aptamer work. Also, a very heartfelt thanks to Dr. Witek and Dr. Hupert, who offered much needed support, friendship, interest and fun that helped me get through the day-to-day research and graduate school.

I have been privileged to work with talented Soper research group members. I thank them all, past members including Jason, John, Paul, Annie, Catherine and Johnhoon as well as current members including Dr. Hong, Dr. Chantiwas, Dr. Nesterova, Jerry, Edith, Mike, Joyce, Swathi, Katrina, Brandon, Brandy, Franklin, Kumuditha, Nyote, and Sudha. Special thanks to Samuel for many enlightening discussions and friendship throughout my career in LSU. I am grateful to Wonbae for helping me with computer issues. Frankly, Soper research group provided me an excellent work environment for the past four years.

Finally, I would like to thank LSU and the United States of America for affording me every opportunity to achieve.

TABLE OF CONTENTS

DEDICATION	ii
ACKNOWLEDGMENTS	iii
LIST OF TABLES	viii
LIST OF FIGURES	ix
LIST OF SCHEMES	xvi
ABBREVIATIONS AND ACRONYMS	xvii
ABSTRACT	xx
CHAPTER 1. MICROSYSTEMS FOR CAPTURE OF LOW-ABUNDANT CELLS	1
1.1 Low-Abundant Cells.....	1
1.2 Methods for Low-Abundant-Cell Selection	3
1.2.1 Macroscale Techniques for Selecting Low-Abundant Cells.....	5
1.2.1.1 Immunomagnetic-Assisted Cell Sorting	5
1.2.1.2 Size-Based Selection	7
1.2.1.3 Fluorescence-Activated Cell Sorting	8
1.2.1.4 Molecular Methods.....	9
1.2.2 Challenges Associated with Macroscale Methods for Low-Abundant-Cell Selection	10
1.3 Microsystems for Low-Abundant-Cell Selection.....	11
1.3.1 Low-Abundant-Cell Selection via Immunoaffinity Interactions.....	12
1.3.2 Low-Abundant-Cell Selection via Physical Criteria.....	21
1.3.3 Low-Abundant-Cell Selection via Dielectrophoresis.....	23
1.3.4 Low-Abundant-Cell Selection via Magnetic Interactions	27
1.3.5 Microfluidic Fluorescence-Activated Cell Sorting	29
1.4 Conclusions	30
1.5 References	32
CHAPTER 2. CIRCULATING TUMOR CELLS: A LITERATURE REVIEW	38
2.1 Introduction.....	38
2.2 Anatomy of Tumor Metastasis	38
2.3 Morphology of CTCs	42
2.4 Biomarkers Found in CTC Membranes.....	45
2.5 Abundance of CTCs in Cancer Patients.....	46
2.6 Clinical Significant of CTCs.....	47
2.7 Statistical Considerations for CTC Analysis	49
2.8 Conclusions	51
2.9 References.....	52

CHAPTER 3. HIGHLY EFFICIENT CAPTURE AND ENUMERATION OF LOW-ABUNDANT PROSTATE CANCER CELLS USING PROSTATE-SPECIFIC MEMBRANE ANTIGEN APTAMERS IMMOBILIZED TO A POLYMERIC MICROFLUIDIC DEVICE..... 55

3.1 Introduction..... 55

3.2 Materials and Methods..... 60

3.2.1 Buffers and Reagents..... 60

3.2.2 Cell Suspensions 61

3.2.3 HTMSU with Integrated Conductivity Sensor Fabrication..... 61

3.2.4 Antibody Immobilization to the HTMSU 63

3.2.5 Aptamer Immobilization onto PMMA Films and the HTMSU Device 63

3.2.6 Determination of Aptamer Surface Density on UV-Modified PMMA 65

3.2.7 LNCaP Cell Capture Using the HTMSU..... 66

3.2.8 LNCaP Cell Release from the HTMSU 66

3.2.9 Conductivity Enumeration of Released Cells..... 67

3.3 Results and Discussion 67

3.3.1 LNCaP Cell Selectivity and Specificity Using Aptamer Recognition 67

3.3.2 Cell Translational Velocity Optimization 70

3.3.3 Selection of Other CTC-Types Using the HTMSU with Immobilized PSMA
Aptamers 74

3.3.4 Cell Detachment from the Capture Surfaces..... 74

3.3.5 Conductivity Enumeration of the CTCs 76

3.4 Conclusions 79

3.5 References 80

CHAPTER 4. ENRICHMENT AND DETECTION OF ESCHERICHIA COLI O157:H7 FROM WATER SAMPLES USING AN ANTIBODY MODIFIED MICROFLUIDIC CHIP..... 84

4.1 Introduction..... 84

4.2 Materials and Methods..... 86

4.2.1 Reagents and Buffers 86

4.2.2 Microfluidic Chip Fabrication and Assembly..... 87

4.2.3 Antibody Immobilization 89

4.2.4 Fluorescence Microscopy 90

4.2.5 Flow Dynamics..... 91

4.2.6 Water Sample Collection..... 91

4.2.7 Water Sample Filtration..... 92

4.2.8 *E. coli* Detection via Culturing 93

4.2.9 Polymerase Chain Reaction (PCR) and Real-Time qPCR..... 93

4.2.10 Slab Gel Electrophoresis..... 94

4.3 Results and Discussion..... 95

4.3.1 Low-Abundant *E. coli* O157:H7 Cell Processing 95

4.3.2 Water Sample Filtration..... 97

4.3.3 *E. coli* Flow Dynamics in Microfluidic Channels 98

4.3.4 Nonspecific Cell Selection..... 100

4.3.5 *E. coli* O157:H7 Cell Release from the Channel Surface 101

4.3.6 Cell Recovery..... 101

4.3.7 Cell Enumeration in Water Samples	105
4.3.8 Cellstripper™ Effects on Real-Time Quantitative PCR (RT qPCR).....	108
4.4 Conclusions	109
4.5 References.....	110
CHAPTER 5.HIGH-THROUGHPUT SELECTION,ENUMERATION, ELECTROKINETIC MANIPULATION, AND MOLECULAR PROFILING OF LOW-ABUNDANT CIRCULATING TUMOR CELLS USING A MICROFLUIDIC SYSTEM	113
5.1 Introduction	113
5.2 Materials and Methods.....	120
5.2.1 Reagents and Cells.....	120
5.2.2 Cell Culturing	121
5.2.3 Microscopy	121
5.2.4 Fabrication of HTMSU.....	122
5.2.5 Antibody Immobilization to the HTMSU.....	124
5.2.6 SW620 Cell Capture/Release and Enumeration Using the HTMSU	124
5.2.7 Electrokinetic Cell Manipulation	125
5.2.8 Measurement of the Electroosmotic Flow (EOF)	126
5.2.9 DNA Extraction from SW620 Cells.....	126
5.2.10 PCRs, LDRs, Gel Electrophoresis and Capillary Electrophoresis	127
5.3 Results and Discussion.....	128
5.3.1 SW620 Cell Selection.....	130
5.3.2 Cell Detachment from the Capture Surface	132
5.3.3 Conductivity Enumeration of the CTCs	132
5.3.4 Electrokinetic Enrichment of SW620 Cells	135
5.3.5 PCR and LDR Mutation Profiling.....	141
5.4 Conclusions	145
5.5 References.....	146
CHAPTER 6. FUTURE WORK: HIGHLY EFFICIENT SEPARATION OF PURE HEMATOPOIETIC STEM CELLS FROM WHOLE BLOOD	151
6.1 Introduction	151
6.2 Materials and Methods.....	154
6.2.1 Cell Suspensions	154
6.2.2 Cell-SELEX Library and Primers	154
6.2.3 Cell-SELEX Procedures for Generation of Panel of Aptamers for HSCs	155
6.2.4 ultra-High-Throughput Microsampling Unit (uHTMSU) Fabrication	156
6.2.5 Aptamer Immobilization.....	156
6.2.6 HSCs Selection Using the uHTMSU	156
6.2.7 HSCs Release from the uHTMSU.....	157
6.3 Expected Results and Significance.....	157
6.4 Dissertation Summary.....	158
6.5 Immediate Projections.....	160
6.6 References.....	161

APPENDIX : PERMISSIONS	158
VITA	181

LIST OF TABLES

Table 1.1 Low-abundant cell types (<1000 targets mL ⁻¹) and methods for their selection	2
Table 2.1 Summary of CTC counts in 7.5 mL of blood from patients with various types of carcinomas	46

LIST OF FIGURES

- Figure 1.1** Sample-processing time as a function of the fluidic conduit cross-sectional area at three different linear velocities: 1, 10, and 100 mm s⁻¹ 4
- Figure 1.2 (A-C)** Schematic of the immunomagnetic-assisted cell-sorting process. Blue and tan circles represent normal and circulating tumor cells, respectively. **(D)** Schematic of a fluorescence-activated cell-sorting instrument. 6
- Figure 1.3** Isolation of circulating tumor cells (CTCs) from whole blood, performed with a microfluidic device (CTC chip) fabricated in silicon via reactive ion etching. **(A)** The workstation setup for CTC isolation from whole blood. **(B)** The CTC chip with microposts etched into the silicon. **(C)** Micrograph of whole blood flowing through the CTC chip. **(D)** An image of a captured NCI-H1650 lung cancer cell spiked into blood (pseudo-colored red). The inset shows a high-magnification view of the captured cell. **(E)** CTC recovery as a function of flow rate. **(F)** Regression analysis of capture efficiency for various target-cell concentrations in whole-blood samples versus lysed-blood samples. **(G-N)** High-magnification images of captured CTCs and hematologic cells stained with 4',6-diamidino-2-phenylindole (DAPI), cytokeratin, and CD45. Merged images identify CTCs in panels **G, I, K** and **M** and hematologic cells in panels **H, J, L**, and **N**. 16
- Figure 1.4** Schematic of a microchip-based high-throughput microsampling unit (HTMSU) fabricated in poly(methylmethacrylate) via microreplication for selection of circulating tumor cells (CTCs). **(A)** An AutoCAD[®] diagram of the sinusoidally shaped capture channels with bright-field optical micrographs showing **(B)** the integrated conductivity sensor consisting of cylindrical Pt electrodes with a 75 μm diameter and a 50 μm gap; **(C)** the single port exit, where the HTMSU's width tapers from 100 μm to 50 μm and the depth tapers from 150 μm to 80 μm over a 2.5 mm region that ends 2.5 mm from the Pt electrodes; **(D)** the sinusoidal cell-capture channels (5x magnification); **(E)** three-dimensional projection of the topology of the HTMSU obtained at 2.5 μm resolution via noncontact optical profilometry (arrows, Pt electrode conduits); and **(F)** the capture efficiency of CTCs in spiked whole-blood samples as a function of the cells' translational velocity. The microchannels were 35 μm wide (red down triangles, sinusoid; purple circles, straight) and 50 μm wide (blue up triangles)..... 18
- Figure 1.5 (A)** Chemical steps for the immobilization of aptamers to the surfaces of a poly(methylmethacrylate) (PMMA)-based high-throughput microsampling unit (HTMSU) used for the positive selection of LNCaP cells. **(B)** Conductometric responses generated for 1.0 mL of whole blood seeded with 20±1 LNCaP cells (red) and 0 LNCaP cells (blue), at a linear flow velocity of 2.5 mm s⁻¹, processed with an HTMSU. The arrows designate peaks that were identified as LNCaP cells on the basis of a signal-to-noise threshold of 3. 20

Figure 1.6 Dielectrophoretic separation of MDA231 human metastatic breast cancer cells from diluted peripheral blood. **(A)** Initial separation of cells in the chamber inlet well after the electrical sweep signal was applied. **(B)** Blood cells focused into bands that flowed between the electrode tips, leaving the cancer cells behind. **(C)** Cancer cells that remained on the electrode tips after the blood cells were swept downstream through the dielectrophoresis column. **(D)** Close to the chamber outlet well, where only blood cells in focused bands were moving. 25

Figure 1.7 **(A)** Schematic of an integrated reverse-transcription polymerase chain reaction (RT-PCR) chip with a cell-selection unit for the magnetic capture of target cells. A microtemperature module, a bead-collection module, and a microfluidic control module are integrated into the chip. **(B)** A mixture of dengue virus (10^2 PFU) and enterovirus 71 (10^2 PFU) was incubated with antidengue antibody (lanes 1 and 2) or antienterovirus 71 antibody-conjugated magnetic beads (lanes 3 and 4); RT-PCR was then performed with dengue group-specific primers (lanes 1 and 3) or enterovirus 71-specific primers (lanes 2 and 4). The lanes marked with the letter L represent signals generated from DNA size markers. Results on the left and right are from a benchtop instrument and the integrated chip, respectively. 28

Figure 2.1 The metastatic cascade. Tumor cells are released from the primary tumor mass, and thus become circulating tumor cells (CTCs). The CTCs in the blood are subjected to the shear forces generated by the flow of blood, immune response attack and anoikis. CTCs that do survive can reach a target organ and attach to the endothelial cell lining within the capillary bed of the target site. After invading the endothelium, a secondary tumor mass can develop. Reprinted with permission.⁸ 40

Figure 2.2 Example of CTC types identified from the patient with breast cancer. **(A)** Wright-Giemsa-stained CTCs (100x oil). **(B)** Same cells as **(A)** showing initial fluorescent image of corresponding CTCs stained with anti-CK-Alexa Fluor 488 (green) and DAPI (4',6-diamidino-2-phenylindole) (blue) (image taken at 20 and enlarged for comparison purposes). **(C)** Example of probable CTC undergoing final stages of apoptosis, with no detectable nucleus. These events are not counted as CTCs in our patient statistics. Reprinted with permission.²⁵ 44

Figure 2.3 Kaplan-Meier estimates of probabilities of progression-free survival and overall survival in patients with metastatic breast cancer for those with <5 CTCs per 7.5 mL of whole blood and those in the group with >5 CTCs in 7.5 mL of whole blood at the first follow-up visit after initiation of a newline of therapy. All patients in the trial ($n=177$) are included in these Figures. **(A)** progression-free survival from baseline. **(B)** overall survival from baseline. Reprinted with permission.³⁵ 50

Figure 3.1 **(A)** Diagram of the HTMSU made via micro-replication into PMMA from a metal mold master. The capture bed consisted of curvilinear channels that

were 30 μm wide and 150 μm deep (51 channels). **(B)** Process operation of the HTMSU used for the positive selection of LNCaP cells. Also shown is the chemistry used for the immobilization of the cell selection elements, aptamers, to the PMMA surface. The first step involved the UV-irradiation (15 mW cm^{-2}) of PMMA and in this case, the irradiation was carried out on just the capture bed so that positive cell selection occurred only in this region. 64

Figure 3.2 (A) Brightfield (left) and fluorescence (right) images for the positive selection of LNCaP cells infused into the HTMSU at a constant volumetric flow rate. The cells were suspended in a PBS buffer ($\sim 1000 \text{ cells mL}^{-1}$) and following infusion of the cell suspension, the device was washed with PBS buffer prior to imaging. In all cases, the entire capture bed was imaged by scanning the microscope stage. The cells were stained with the fluorescein membrane probe prior to introduction into the HTMSU to allow fluorescence visualization. **(B)** Comparison of LNCaP cell capture efficiencies using anti-PSMA aptamers or anti-EpCAM antibodies cell recognition elements. In both cases, the HTMSU capture bed was modified with UV light to create the functional scaffold for covalent attachment of the antibody or 50-labeled aptamer. The graph shows the cell capture efficiency versus cells' translational velocity. Red squares and blue circles represent the capture efficiencies for anti-PSMA aptamers and anti-EpCAM antibodies, respectively. In these experiments, ~ 1000 LNCaP cells were seeded into a PBS buffer ($\text{pH}=7.4$) with the number of captured cells determined via brightfield microscopy and subsequently verified using fluorescence microscopy. 68

Figure 3.3 Brightfield and fluorescence micrographs showing anti-PSMA aptamer captured LNCaP cells in a PMMA microchannel. **(A)** Brightfield micrographs taken at 40x magnification and **(B)** the corresponding fluorescence micrographs verifying the captured cell is the fluorescently labeled LNCaP cell. The inset shown in panel **(B)** is a fluorescent-stained LNCaP cell in a PMMA microchannel that was not decorated with anti-PSMA aptamers indicating the spherical shape of these cells..... 73

Figure 3.4 (A) Time-lapse micrographs showing trypsin enzyme mediated release of a captured LNCaP cell upon application of 0.25% w/w trypsin in PBS buffer ($\text{pH}=7.4$). **(a)** At $t=0$ or prior to exposure of the captured cells to the trypsin releasing buffer. **(b)** At $t=2.0\text{min}$, disruption of the binding complex is evident. **(c)** At $t=6.5\text{min}$, the cell appears to be released from the capture surface. **(d)** At $t=7.5\text{min}$, the cell was completely released from the surface and swept away from the capture surface to the detection region by the hydrodynamic flow. **(B)** Plot of cell release efficiency versus time. In each experiment the number of cell releasing events, >25 , in three curvilinear channel were counted. The error bars represents the standard deviation of the results obtained for three replicate experiments. 75

Figure 3.5 (A) Conductometric responses generated for 1.0 mL of whole blood seeded with 20 ± 1 LNCaP cells (black) or 0 LNCaP cells (red) at a linear flow velocity of 2.5 mm s^{-1} processed using the HTMSU. The captured LNCaP cells were

released from the capture surface using the release buffer comprised of 0.25% w/w trypsin and transported through the conductivity sensor at a volumetric flow rate of 0.05 mL min⁻¹. The arrows designate peaks that were identified as LNCaP cells based on a signal-to-noise threshold of 3. The crossed arrows represent non-LNCaP cell events. The insets shown in the figure represent a magnified view of sections of the data stream. The blue line represents the threshold level, which represents 3x the average background level, which was used to differentiate “true” events from noise. The data presented here was smoothed by the Savitsky-Golay method (25 point smoothing function). Also shown in this plot is a sample of whole blood containing no LNCaP cell that was processed with the HTMSU device (red line). **(B)** Calibration plot ($m=0.990$, $r^2=0.99997$) for the number of LNCaP cells seeded (10–250 cells mL⁻¹) into 1.0 mL of whole blood versus the number of conductivity responses using the Pt-conductivity sensor. 77

Figure 4.1 **(A)** A picture of the PMMA fluidic system for the positive selection of rare *E. coli* cells containing 8 different devices with each device comprised of 16 selection channels. **(B)** Schematic of the entire cell selection chip and **(C)** an expanded view of an individual cell selection device. Each device contained 9.5 mm long 16 curvilinear channels that were 15 μm in width and 80 μm in depth with a radius of curvature of 120 μm with respect to the channel center. **(D-E)** SEM of the brass molding tool. 89

Figure 4.2 **A** and **C** are pictures of 0.1 μm PCTE membranes after filtration and washing, respectively, while **B** and **D** correspond to 40x microscope images of the same membranes after filtration and washing, respectively. The insert in **B** shows a micrograph of the membrane before filtration. The sample processed here was that taken from Lake Granbury in Texas. 97

Figure 4.3 Histograms of the radial position of bacterial cells in an unmodified sinusoidally-shaped microchannel at linear velocities of **(A)** 1, **(B)** 5, **(C)** 40, and **(D)** 100 mm s⁻¹. The dashed lines designate the channel walls. The cells were imaged using fluorescence microscopy with the cells stained using PKH67. The coordinate system adopted used 0 as the channel centroid, (-) values refer to locations with respect to the outer edge of the channel and (+) values represent radial positions in the direction of the inner edge of the channel. 99

Figure 4.4 Fluorescence images of a microchannel with **(A)** *E. coli* O157:H7 cells and **(B)** *E. coli* K12 cells captured on an antibody modified PMMA surface. The dashed lines designate the edges of the channel. 100

Figure 4.5 Time-lapse micrographs showing Cellstripper™ and hydrodynamic shear-mediated release of a captured fluorescently-labeled *E. coli* O157:H7 cell (circled in red) from the capture surface. **(A)** A brightfield image prior to exposure of the captured cell to the stripping solution. **(B)** A fluorescence image of the same spot at $t=0.1$ min following incubation with the Cellstripper™ solution. **(C)** A bright field image at $t=3.4$ min after introduction

of the Cellstripper™ solution was infused into the channel and disruption of the binding complex was evident by the bacterial cell being released from the surface. **(D)** A fluorescence image at $t=3.5$ min following introduction of the stripping solution – the cell appears to be released from the capture surface. The stripping solution was hydrodynamically pumped through the fluidic chip at a linear velocity of 25 mm s^{-1} 102

Figure 4.6 Real-time PCR amplification plots for the *slt1* gene using RT qPCR with a master mix containing different concentrations of Cellstripper™ in standard samples (indicated with arrows in the figure). The protocol involved a three-step cycle: (1) 10 min at $95 \text{ }^\circ\text{C}$, 46 cycles; (2) 30 s at $95 \text{ }^\circ\text{C}$, 60 s at $58 \text{ }^\circ\text{C}$; and (3) 60 s at $72 \text{ }^\circ\text{C}$. The PCR products were observed in real-time using a SYBR Green dye..... 103

Figure 4.7 (A) Capture efficiency data of *E. coli* O157:H7 as a function of the cells' translational velocity using the microfluidic chip shown in Figure 4.1. The number of captured cells was determined via real-time qPCR. **(B)** Cell capture efficiency as a function of the channel width using a translational velocity of 5 mm s^{-1} . Channels used contained a variable width (10, 20, and $30 \text{ }\mu\text{m}$) but the same depth ($30 \text{ }\mu\text{m}$) and length (3 cm). **(C)** Standard curves for the real-time, qPCR analysis of *E. coli* O157:H7 using *slt1* (filled squares) and *uidA* (filled circles) genes. C_t values of known samples were plotted against the corresponding cfu of the bacteria. The linear regression analysis for *slt1*: $y = -3.456\log(x) + 37.12$ ($r^2 = 0.997$) and *uidA*: $y = -3.373\log(x) + 40.99$ ($r^2 = 0.996$). **(D)** A fluorescence agarose gel image of the 252 bp and 348 bp PCR products for *uidA* and *slt1* genes, respectively. The amplicons were generated with 10×10^3 cfu/reaction of the *E. coli* O157:H7 serotype..... 104

Figure 4.8 (A) Amplification plots for the *slt1* gene using real-time qPCR for serial dilutions of *E. coli* O157:H7 ($6 - 60 \times 10^3$ cfu/reaction). **(B)** Dissociation curves for amplicons obtain in **(A)**. The PCR protocol used involved a three-step procedure: (1) 10 min at $95 \text{ }^\circ\text{C}$; 46 cycles consisting of (2) 30 s at $95 \text{ }^\circ\text{C}$, 60 s at $58 \text{ }^\circ\text{C}$, 60 s at $72 \text{ }^\circ\text{C}$; and (3) 81 cycles of ramping the temperature between 55 and $95 \text{ }^\circ\text{C}$ ($0.2 \text{ }^\circ\text{C s}^{-1}$)..... 107

Figure 4.9 *E. coli* colonies formed on the modified mTEC agar surface. The *E. coli* colonies are represented as dark spots. **(A)** Baton Rouge Lake water, filtered volumes: **a** – 100 mL sample, **b** – 25 mL, **c** – 10 mL, **d** – 5 mL, **e** – 0.1 mL, **f** – blank. The membrane filter in sample (a) was used to calculate the number of colonies of *E. coli* per 100 mL of water. The *E. coli* concentration was calculated as $(\# \text{ colonies/volume processed}) \times 100$. **(B)** A waste water sample processed using the mTEC agar surface; volumes processed: **a** – 1 mL; **b** – 0.1 mL; **c** – 0 mL (blank). The membrane filter in sample b has the acceptable number of colonies to calculate the number of *E. coli* per 100 mL of waste water..... 108

Figure 5.1 Diagrams of the microfluidic system made via micro-replication into PMMA from a metal mold master. **(A)** Cell selection HTMSU. The capture bed

consisted of curvilinear 51 channels that were 30 μm wide and 150 μm deep. (Electro-manipulation unit consists of 80 μm wide, 100 μm deep and 5 cm long linear channels. The solution flow H arriving from HTMSU is divided at the T junction into a major flow (H_{eb}) and a minor flow (H_{ec}). Conductometrically enumerated SW620 cells were introduced to system at 'a' entrance port. The 'a' entrance port connects with b-c channel at the T intersection. 'b' exit is the sample waste reservoir and c exit is cell reservoir. Both 'b' and 'c' reservoirs host Pt external electrodes; cathode and anode embedded in sample reservoir, 'b' and waste reservoir, 'c', respectively. **(B)** Brightfield (left) and fluorescence (right) micrographs (43x) for the positive selection of SW620 cells infused into the HTMSU at a constant linear velocity flow of 2 mm s^{-1} . The cells were suspended in a whole blood (100 cells mL^{-1}) and following infusion of the cell suspension, the device was washed with PBS buffer prior to imaging. In all cases, the entire capture bed was imaged by scanning the microscope stage. The cells were stained with the fluorescein membrane probe prior to introduction into the HTMSU to allow visualization. **(C)** The selected SW620 cells enriched in the sample reservoir at the end of c channel. Positive Pt electrode is also in the Figure. Total volume of the reservoir is 2 μL 131

Figure 5.2 (A) Conductometric responses generated for 1.0 mL of whole blood seeded with 10 SW620 cells **(a)**, 0 SW620 cells (ash) **(b)** and 32 HT29 **(c)** at a linear flow velocity of 2.0 mm s^{-1} processed using the HTMSU. The captured SW620 cells were released from the capture surface using the release Tris-Glycine buffer comprised of 0.25% w/v trypsin and transported through the conductivity sensor at a volumetric flow rate of 1 $\mu\text{L min}^{-1}$. Peaks were identified as SW620/HT29 cells based on a signal-to-noise threshold of 3. The insets shown in the figure represent a magnified view of sections of the data stream. The data presented here was smoothed by the Savitsky-Golay method (25 point smoothing function). The conductometrically enumerated cell samples were subjected to PCR followed LDR analysis. Two μL of amplicons from PCR were used for analyzing point mutation in the K-ras gene. The LDR products were analyzed using capillary electrophoresis. The capillary electrophoresis responses for the sample after processing blood with no SW620 **(B)**, Sample after processing blood with 50 HT29 cells **(C)** and sample after processing blood with 10 SW620 cells **(D)**. Peak 'a' represents the primer and peak 'b' is the LDR product for SW620..... 133

Figure 5.3 Micrographs (43x) showing SW620 cell manipulation in the electro-manipulation unit. The SW620 cells resident in Tris-Glycine buffer were introduced from inlet of channel 'a'. **A, B, C** The cells are travelling at 1 $\mu\text{L min}^{-1}$ flow rate. The hydrodynamic flow direction is given in white arrow. The majority (90%) of the cells are travelling from a-b, which has less pressure drop (0.7 psi at 1 $\mu\text{L min}^{-1}$) compared to the pressure drop of a-c (7 psi at 1 $\mu\text{L min}^{-1}$). **D, E, F** The SW620 cells movement in the presence of electric field strength of 100 V cm^{-1} . The electrophoretic movement direction of cells is given in red arrow. 137

Figure 5.4 Agarose gel electrophoresis of the PCR products. PCR was set for 32 cycles, with initial denaturation of 2 min and final extension of 7 min. Each cycle consisted of: 94 °C (30 s), 60 °C (30 s), 72 °C (40 s). Gel stained with ethidium bromide were run at 4.8 V cm⁻¹. **(A)** Gel electropherogram for PCR performed on standard SW620 samples **(a)** no gDNA template, Negative control; **(b)** DNA from 10 SW620 cells; **(c)** DNA from 20 SW620 cells; **(d)** DNA from 50 SW620 cells; **(e)** DNA from 100 SW620 cells; **(f)** DNA from 500 SW620 cells; **(g)** DNA from 1,000 SW620 cells; **(h)** DNA from 5,000 SW620 cells; **(i)** gDNA template from SW620, Positive control; Lanes a-i contains 3 µL of DNA amplicons. **(B)** Gel Electropherogram for PCR performed on SW620 cells obtained from HTMSU selection followed by electrokinetic enrichment **(a)** gDNA template from SW620, Positive control; **(b)** PCR product from 10 SW620 cells selected from whole blood using HTMSU **(c)** PCR product from whole blood with no SW620 cells **(d)** no gDNA template, negative control. Lanes a-d contains 3 µL of DNA amplicons. 142

Figure 5.5 The LDR mixtures with a discriminating and common primers for *K-ras* c12.2V, could selectively detect this mutation. Two µL of amplicons from PCR with SW620 (mutant) and HT29 were used for analyzing point mutation in the *K-ras* gene. LDR was set for 20 cycles. Initial denaturation 95 °C for 2 min. Each cycle consisted of: 95 °C (30s), 65 °C (2 min), and 4 °C as final hold. LDR was performed at capillary temperature of 60°C, denaturation temperature of 90 °C (3 min), Injection at 2.0 kV (30 s) and separation at 6.0 kV (20 min). Peak a represent the primer and peak b represents the LDR product. Capillary electrophoresis products for **A)** 0 **B)** 10 **C)** 20 **D)** 50 **E)** 100 **F)** 500 and **G)** 5000 cells of SW620. The insets in A and B show the magnified scaled plot of products. **H)** LDR product for 50 cells of HT29. 144

LIST OF SCHEMES

Scheme 4.1 Overview for the Processing Strategy Adopted for Analysis of Extremely Low Abundant <i>E. coli</i> O157:H7 and Other Serotypes Using Positive Selection and Enrichment via a Microfluidic Chip with Subsequent Quantification through Real-Time qPCR.....	96
Scheme 5.1 Overview for the cell selection, enumeration, electrokinetic enrichment and molecular profiling strategy adopted for analysis of extremely low-abundant SW620 cells resident in patients' blood.....	129

ABBREVIATIONS AND ACRONYMS

CTC	-	circulating tumor cells
μ FACS	-	microfabricated fluorescence activated cell sorter
ELISA	-	enzyme-linked immunosorbent assay
BT-20	-	breast cancer cell line
MDA-435	-	breast cancer cell line
MDA231	-	breast cancer cell line
MCF-7	-	breast cancer cell line
CD	-	cluster of differentiation
CD34+	-	hematopoietic stem cells
CD45-	-	leukocyte-specific antibody
cfu	-	colony forming units
CV	-	coefficient of variance
DAPI	-	4',6-diamidino-2-phenylindole
K_o	-	encounter rate
P	-	probability
Δ	-	dimensionless Damköhler number
k_{in}	-	intrinsic antigen-antibody reaction rate
a	-	encounter radius
Λ	-	dimensionless encounter time
U	-	cell-translational velocity
D	-	cell diffusion coefficient
F_A	-	adhesion force
F_S	-	shear force
f_c	-	bond strength between a single antigen-antibody complex
C_s	-	contact area of the cell
r_p	-	cell radius
h and h'	-	cell-separation distances from the surface upon binding
NCI-H1650	-	lung cancer cell line
EDC	-	1-ethyl,-3-(3-dimethylaminopropyl)carbodiimide
NHS	-	N-hydroxysuccinimide
fNRBC	-	fetal nucleated red blood cell
ϵ_M	-	permittivity of the suspending medium
ERMS	-	electric field strength
FDEP	-	dielectrophoresis force
ϵ_C^*	-	complex permittivities of the cell
ϵ_M^*	-	complex permittivities of the medium
DEP	-	dielectrophoresis
DEP/G-FFF	-	dielectrophoretic /gravitational field-flow fractionation
DEP-FFF	-	dielectrophoretic field-flow fractionation
DNA	-	deoxyribonucleic acid
DRIE	-	deep reactive ion etching
EID	-	effective infective dose
EpCAM	-	epithelial cell adhesion molecules
FACS	-	fluorescence-activated cell sorting
FITC	-	fluorescein isothiocyanate
HIV	-	human immunodeficiency virus

HTMSU	-	high-throughput microsampling unit
IMAC	-	Immunomagnetic Affinity Capture
LNCaP	-	prostate cancer cell lines
LOD	-	limit of detection
mAb	-	monoclonal antibodies
MACS	-	magnetic-activated cell sorting
mRNA	-	messenger ribonucleic acid
NG2+	-	putative progenitor cell line
pAb	-	polyclonal antibodies
PBMC	-	peripheral blood mononucleated cells
PDMS	-	patterned poly-(dimethylsiloxane)
PMMA	-	poly(methylmethacrylate)
PSMA	-	prostate-specific membrane antigen
Pt	-	Platinum
RT-PCR	-	reverse transcription polymerase chain reaction
SELEX	-	systematic evolution of ligands by exponential enrichment
TCID ₅₀	-	50% tissue culture infectious dose
UV	-	ultra violet
WBC	-	white blood cell
BM	-	basement membrane
ECM	-	extracellular matrix
VEGF	-	endothelial growth factor
FGF	-	fibroblast growth factor
STC	-	solid tumor cells
N/C	-	nuclear/cytoplasmic ratio
CK	-	cytokeratins
EGFR	-	epidermal growth factor receptor
EMT	-	epithelial-to-mesenchymal transition
PC3	-	bone metastasis prostate cancer cells
LNCaP	-	lymph node metastasis prostate cancer cells
22Rv1	-	prostate cancer cell line localized to prostate
A	-	Adenine
C	-	Cytosine
G	-	Guanine
T	-	Thymine
MES-2-(4-morpholino)	-	ethane sulfonic acid
PSMA _M	-	mannose-rich PSMA
PSMA _C	-	glycosylated form of PSMA
EPA	-	environmental protection agency
PCTE	-	polycarbonate track etched membranes
HPMM	-	high precision micromilling
R _e	-	Reynolds number
U	-	velocity
mTEC	-	membrane-Thermotolerant E. coli agar
FP	-	forward primer
RP	-	reverse primer
SEM	-	scanning electron microscopy

dRn	-	reference dye normalized fluorescence
LDR	-	ligase detection reaction
CRC	-	colorectal cancer
FOBT	-	fecal occult blood test
FDA	-	food and drug administration
gDNA	-	genomic deoxyribonucleic acid
CE	-	capillary electrophoresis
PKH67	-	fluorescein derivative
SW620	-	colon cancer cells
K_D	-	dissociation constant
H	-	total flow
ΔP	-	pressure drop
EOF	-	Electroosmotic flow
z	-	zeta Potential
Q	-	net negative surface charge
ρ	-	charge density
U_h	-	hydrodynamic flow velocity
U_{EOF}	-	velocity due to electroosmosis flow
FITC	-	fluorescence isothiocyanate
HSCs	-	hematopoietic stem cells
CD34, CD59, CD38, SCA-1 and Thy1	-	membrane biomarkers
ssDNA	-	single stranded deoxyribonucleic acid
uHTMSU	-	ultra high-throughput microsampling unit

ABSTRACT

Prostate tumor cells over-express a prostate-specific membrane antigen (PSMA) that can be used as a marker to select these cells from highly heterogeneous clinical samples, even when found in low abundance. In this study, anti-PSMA aptamers were immobilized onto the surface of a capture bed poised within a PMMA, microchip, which was fabricated into a high-throughput micro-sampling unit (HTMSU) used for the selective isolation of rare circulating prostate tumor cells resident in a peripheral blood matrix. The HTMSU capture bed consisted of 51 ultra-high-aspect ratio parallel curvilinear channels with a width similar to the prostate cancer cell dimensions. Using a linear velocity (2.5 mm s^{-1}) for optimal cell capture in the aptamer tethered HTMSU, a recovery of 90% of LNCaP cells (prostate cancer cell line; used as a model in this example) was found. Due to the low abundance of these cells, the input volume required was 1 mL and this could be processed in 29 min using an optimized linear flow rate of 2.5 mm s^{-1} . Captured cells were subsequently released intact from the affinity surface using 0.25% w/v trypsin followed by counting individual cells using a contact conductivity sensor integrated into the HTMSU that provided high detection and sampling efficiency (100%) and did not require staining of the cells for enumeration.

Next, an alternative fluidic device was designed and fabricated to select *E. coli* O157:H7 cells from water samples using antibody-based positive selection followed by the accurate identification and quantification via RT qPCR. The assay offers the ability to evaluate recreational water quality without the need for bacterial cell culturing. Due to the smaller size of these cells (1-2 μm) compared to CTCs (20 μm), fluidic transport properties of *E. coli* cells were characterized and found to depend less on centrifugal forces to increase the encounter rate of the cells with the surface-immobilized antibodies used for their selection compared to the larger CTCs. Through fundamental studies to optimize the transport rate, *E. coli* cells could be recovered at 72%, with the RT qPCR assay limit-of-detection equal to ~ 6 cells. The enrichment procedure provided many advantages compared to existing EPA methods for *E. coli* analysis; (i) recognizes O157 antigens from intact and virulent cells and in stressed and non-culturable cells, which also can produce Shiga-like toxins; (ii) cells enriched on-chip were free from potential interferences that may hamper the nucleic acid-based measurements; and (iii) preconcentrate cells by nearly 10^5 from samples that are 100 mL in total volume.

Finally, I report on a microfluidic technique for selective isolation, enumeration, and electrokinetic enrichment of low-abundance (~ 10 cells mL^{-1}) circulating tumor cells (CTCs) directly from whole blood. Enriched CTCs can then be genetically profiled for marker mutations which can provide important clinical information. In here I integrated high-throughput CTC selection ability of HTMSU with electrokinetic enrichment step for pre-concentration of selected CTCs for molecular profiling of rare genetic mutation in genomic DNA. SW620 cells (colorectal cancer cell line) over-express the integral membrane protein EpCAM, and as such could be immuno-specifically selected using the HTMSU activated with the EpCAM antibodies. Selected CTCs were then enzymatically released intact from the antibody capture surface and hydrodynamically transported through a pair of Pt electrodes for conductivity-based enumeration without a need for fluorescent labeling. Following enumeration, CTCs were hydrodynamically transported at a flow rate of $1 \mu\text{L min}^{-1}$ to an on-chip electro-manipulation unit. At an electric field strength of 100 V cm^{-1} , the negatively charged CTCs migrated against both the EOF and hydrodynamic flow and were enriched in the anodic receiving reservoir to a final volume of $2 \mu\text{L}$. The collected CTCs could then be genetically profiled to search for point mutations using a PCR/LDR/capillary electrophoresis assay.

CHAPTER 1 MICROSYSTEMS FOR CAPTURE OF LOW-ABUNDANT CELLS*

1.1 Low-Abundant Cells

What distinguishes a low-abundance cell from one that is not, and what applications require the ability to analyze low-abundance cells? On the basis of the data presented in Table 1.1, we consider any sample containing less than 1,000 target cells mL⁻¹ to contain low-abundance cells. Typical examples of low-abundance cells are circulating tumor cells (CTCs), circulating fetal cells, and stem cells. The abundance of these cells, as well as others, is highly variable and depends upon factors such as the age of the sample, the stage of the disease, and the cellularity, which is defined as the state of a tissue or cell with regard to the degree, quality, or condition of cells present.¹ However, environmental samples containing biopathogens are categorized on the basis of the effective infectious dose level that can lead to the outbreak of disease (Table 1.1).

The ability to select and enumerate low-abundance cells and their subsequent analyses have many important applications (Table 1.1), such as cancer research,² forensic science, homeland security, space exploration, environmental analysis,³ isolation and characterization of intact fetal cells in maternal blood for noninvasive prenatal diagnosis,⁴ use of stem cells for cell-based therapies,⁵ detection of CTCs in blood for differential diagnosis and prognosis,⁶⁻¹¹ and detection of T lymphocytes for determining the progression rate of human immunodeficiency virus infections^{12,13} or autoimmune disease.¹⁴ Another fast-growing area requiring low-abundance cell analysis is the isolation and detection of pathogens and protozoan parasites such as *Escherichia coli* O157:H7, swine influenza virus, and *Cryptosporidium* in various food and water

* Reproduced with permission from *Annual Reviews of Analytical Chemistry*

Table 1.1 Low-abundance cell types (<1000 targets mL⁻¹) and methods for their selection

	Rare cell type	Resident material	Cell abundance (cells mL ⁻¹)	Isolation method	Ref.
CTC	Lung, Breast, Prostate, Pancreatic, Colon, Cervical, Bladder	Peripheral, Cord blood, Bone marrow, Lymph Fluid, Thymus, Urine	<0.7	MACS, FACS, Immunoaffinity columns	(6,9, 42, 18)
Fetal	Trophoblasts, Lymphocytes, Nucleated Erythrocytes	Maternal and cord blood	1-15	MACS, FACS, Charge flow separation, Density gradient centrifugation (DGC)	(83)
Stem	Multipotent Stem Cells	Peripheral, Cord blood, Bone marrow	400	MACS, FACS, Immunoaffinity columns, DGS	(19-22)
Somatic	Sperm	Vaginal swab	380	Differential extraction, FACS	(84)
Infected	HIV infected T cells <i>S. spp</i> infected lymphocytes	Peripheral blood Lymph	300	MACS, FACS, Immunoaffinity columns, ELISA	(23, 24) (88)
Bacterial	<i>E. hirae</i> , <i>E. gallinarum</i> <i>E. casseliflavus</i> , <i>S. pneumoniae</i> <i>E. coli</i> O157:H7*, <i>V. Cholerae</i> *	Waste, River, Drinking Waters	0.01-1	Bacteria Culture, ELISA, PCR/RT-PCR	(94, 25) (26)
Viruses	<i>Adenoviruses</i> * <i>Enteroviruses</i> * <i>Hepatitis A and E</i> *	Waste, River, Drinking Waters	0.01-1	Viral cultures, Immunoaffinity column, RT-PCR, ELISA	(26)
	Dengue	Peripheral Blood	1000		(25)
	Swine flu Bovine Diarrhea	Lymph	610 10		(64)
Protozoa /Helminthes	<i>C. parvum</i> <i>C. cayetanensis</i> , <i>E.histolytica</i> , <i>N. fowleri</i> <i>D. medinensis</i> , <i>S. spp.</i>	Waste, River, Drinking Waters	0.01-1	Fluorescence antibody, Filtration, PCR/RT-PCR, ELISA	(26)

samples.^{15–17}

The challenge in any analytical strategy for low-abundance cells begins with the selection of the target cells from a heterogeneous population in which the target is a minority. For example, in the case of CTCs, in 1 mL of whole blood there are more than 10^9 red blood cells (RBCs) and typically one to five CTCs, requiring an enrichment factor less than 10^9 . For the isolation of low-abundance cells, four important metrics must be considered: (a) throughput, the number of cell-identification or -sorting steps per unit time; (b) recovery, an indicator of the fraction of target cells collected from the input sample; (c) purity, which depends on the number of so-called interfering cells excluded from the final analysis; and (d) viability, that is, whether the isolated cells retain their biological function after the selection process.^{27,28} Additionally, highly efficient quantification of the number of enriched low-abundance cells must be provided in most cases.²⁹

1.2 Methods for Low-Abundant-Cell Selection

Two basic formats can be used for selecting low-abundance cells from mixed populations: macro and microscale formats. Macroscale formats provide high throughput for selecting low-abundance cells due to their ability to process large input volumes quickly, whereas microscale formats typically lack that ability (see Figure 1.1).³⁰ High-throughput processing is required due to the necessity for sampling large input volumes to generate a high statistical confidence for successfully securing the target cells from the processed sample. Throughput is directly proportional to (a) the cross-sectional area of the conduit through which the sample is delivered and (b) the rate of sample delivery. The input sample volume required for the assay is determined

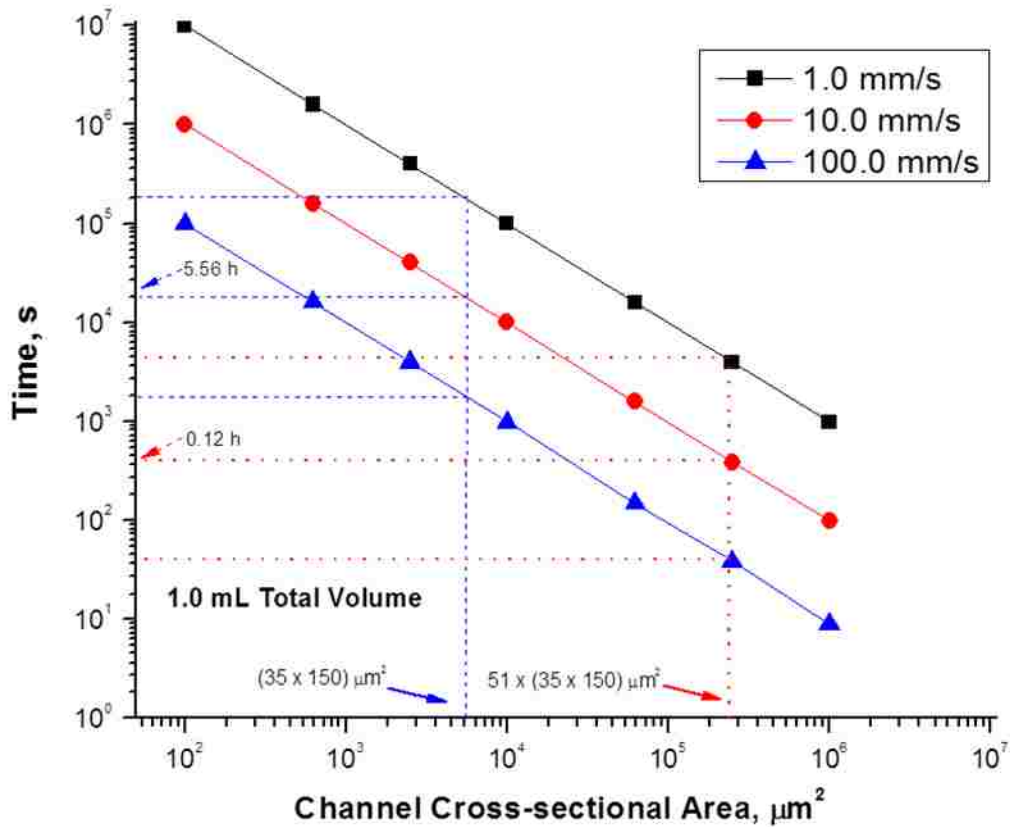


Figure 1.1 Sample-processing time as a function of the fluidic conduit cross-sectional area at three different linear velocities: 1, 10, and 100 mm s⁻¹.

by the frequency of rare cell appearance. For example, at 5 cells mL⁻¹, a sampling volume of 1 μL would produce a probability of only 0.5% of finding the target cells in that volume. Because low-abundance cells appear at frequencies less than 1,000 cells mL⁻¹, high-volume sampling (≥1 mL) is required to increase the probability of isolating these rare events. If cross-sectional dimensions of 35 μm×35 μm were employed for a fluidic conduit to exhaustively search for rare cells, and if the transport rate through the conduit were 10 mm s⁻¹ with a required input volume of 1.0 mL, the sampling time would be approximately 278 h. For a single rectangular conduit with dimensions of 150 μm×35 μm under conditions similar to those given above, the sampling time would be reduced to ~5.6 h. If the 150 μm×35 μm conduits were highly parallelized through the incorporation of 51 conduits, the processing time would drop to 0.12 h (Figure 1.1).

1.2.1 Macroscale Techniques for Selecting Low-Abundant Cells

Commonly used macroscale formats for enriching low-abundance cells include (a) magnetic capture that employs micrometer-sized ferromagnetic beads coated with molecular recognition elements, typically referred to as immunomagnetic-assisted cell sorting (IMACS);³⁵⁻³⁷ (b) size-based separations that use nuclear-tracked membranes;^{38,39} (c) fluorescence-activated cell sorting (FACS);^{40,41} and (d) reverse-transcription polymerase chain reaction (RT-PCR) of messenger RNAs (mRNAs), which are used as surrogates for cell identification.⁴² In the following sections, we briefly discuss these macroscale processing techniques.

1.2.1.1 Immunomagnetic-Assisted Cell Sorting

CellSearch® procedure and OncoQuick® system are two commercially available immunomagnetic isolation kits for selecting CTCs from peripheral blood samples.⁴³ Both kits employed anti-epithelial cell adhesion molecules (EpCAM) antibodies for selecting the cancer cells. Both procedures employed density gradient centrifugation followed by a series of washes in order to remove the red blood cell (RBC) fraction from the whole blood sample prior to magnetic isolation of the low abundance cells. Centrifugation of the RBC depleted sample is next performed at 800xg for 10 min to remove the blood plasma. The resulting cellular pellets are resuspended in 10 mL of buffer, and incubated with carboxylate-functionalized ferromagnetic particles that are coated with anti-EpCAM. Immunomagnetically-labeled cells are concentrated using an external magnetic field (see Figure 1.2). Following magnetic isolation, the processed sample is incubated with leukocyte specific anti-cytokeratin antibodies labeled with Alexa Fluor 555, nuclear specific 4',6-diamidino-2-phenylindole (DAPI), and a CTC specific anti-EpCAM antibody conjugated to a fluorescein derivative. Under these conditions, white blood cells and tumor cells harbor blue

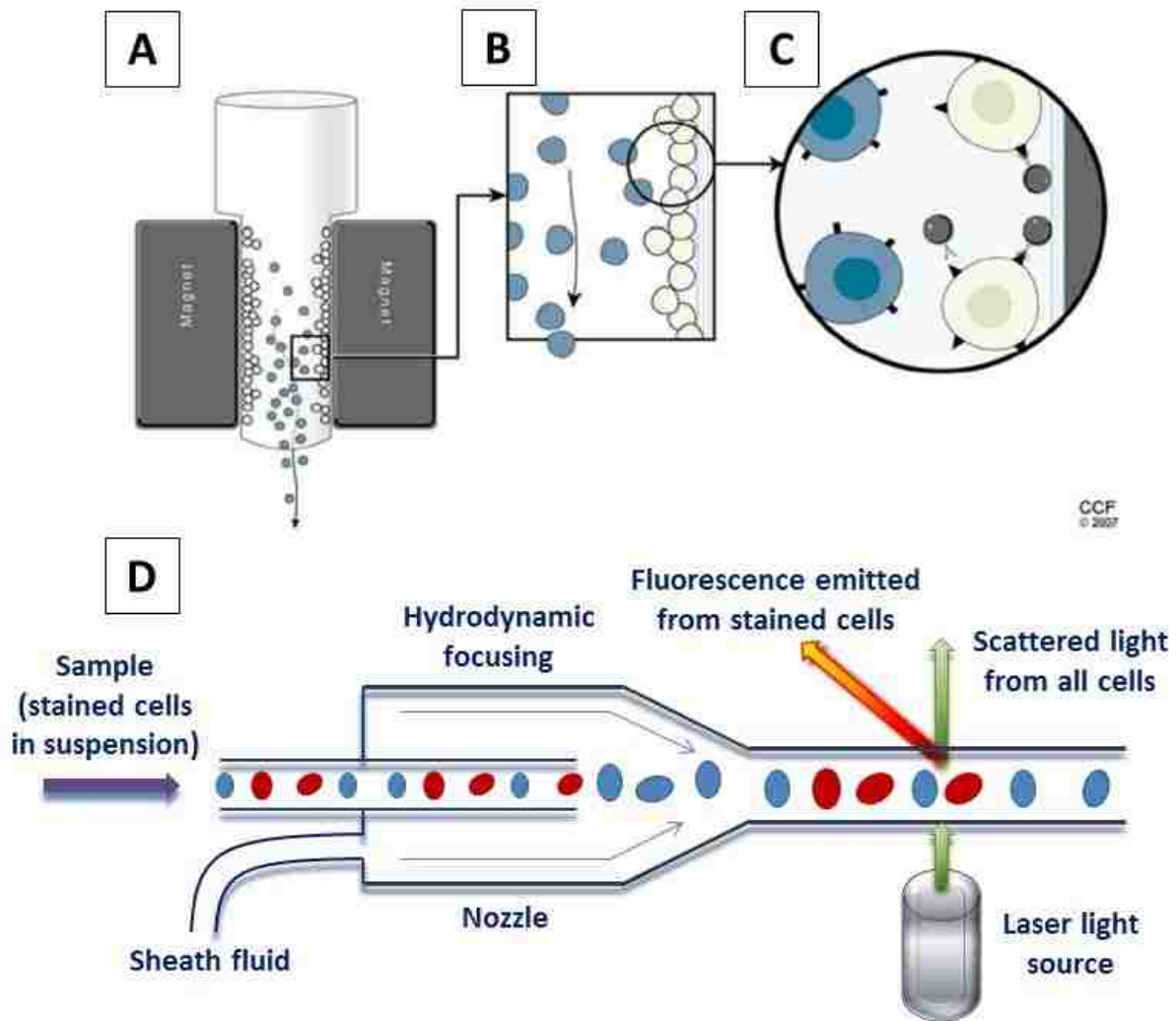


Figure 1.2 (A-C) Schematic of the immunomagnetic-assisted cell-sorting process. Blue and tan circles represent normal and circulating tumor cells, respectively. **(D)** Schematic of a fluorescence-activated cell-sorting instrument.

fluorescing nuclei; however, the fluorescent signatures of the FITC derivative selectively placed a green “halo effect” about the blue nuclei of the CTCs. The orange fluorescent halo from the Alexa Fluor 555 about the nuclei of the leukocytes is used for exclusion. The CTC recovery rates data is significantly better using the CellSearch system (60% recovery) compared to the OncoQuick system (26% recovery). In addition, the CellSearch system requires a smaller input volume compared to the OncoQuick system. The non-metastatic samples with both kits show the detection of at least one CTC in the blood of healthy

individuals in 12% of these samples analyzed. For the confirmed metastatic cancer cases, CellSearch is capable of producing positive responses in 54% of these samples resulting in a relatively high rate of false negatives.⁴³ The OncoQuick system demonstrated poorer detection accuracy as only 23% of the samples are reported positive for metastatic disease. In 5 of the 6 varieties of cancer studied, CellSearch is twice as effective as OncoQuick at detecting metastatic disease and CellSearch is also found to be more sensitive in common positive tests often identifying more CTCs within similar amounts of peripheral blood.

1.2.1.2 Size-Based Selection

Tracked polycarbonate membranes with varying pore sizes (8–14 μm) are employed to filter large (9.0–18 mL) blood samples spiked with known quantities of CTCs.³⁶ Prior to filtration using the membrane, the samples are diluted at a 1:1 (v/v) ratio of spiked blood:PBS containing an anticoagulant EDTA. Simple gravimetric filtration through these polycarbonate membranes is sufficient to reduce the erythrocyte content by $>10^5$ cells mL^{-1} . After the initial filtration using the polycarbonate filter, the isolated cells are washed and incubated for 1 h with anti-pan-cytokeratin directed against cytokeratin 5, 6, 8, 17 and 19)-FITC. After a wash to remove the unbound anti-cytokeratin antibodies, nuclei-specific propidium iodide is added, and an additional incubation of 30 min performed. The cells retained by the polycarbonate membrane are analyzed using a combination of laser scanning cytometry (LSC) and microscopy. After analysis, all the cytokeratin positive cells are relocated and examined “by eye” to exclude any false- positive events. Only positive cells with the appropriate nuclear:cytoplasmic ratio are counted as positive events.

False positives are evident in the case of MCF-7 cells, and the authors attributed this to the presence of adhesion molecules on the cells’ periphery. The most prominent

reduction in leukocyte frequency is demonstrated for 9 mL blood samples that originally contained 5×10^7 leukocytes, which is reduced to 7,000 leukocytes after the filtration step. These membranes are demonstrated to isolate nearly 85–100% of the CTCs, but significant numbers of white blood cells are also retained due to their similar size with respect to the CTCs complicating the enumeration process. Also, the process requires pre or post treatment of retained cells with a variety of fluorescent stains before the LSC could be utilized.

Microarrays are also used in the isolation of target cells. Various “cluster of differentiation” (CD) antigens are affinity-captured onto the arrays containing immobilized antibodies.⁴⁰ The arrays contain several surface-immobilized antibodies directed toward target antigenic species, which are used to spatially isolate cells. These methods are limited by slow mass transport but are promising for multiplexed analyses; the array elements are not individually addressable making collecting isolated cells from a multiplexed analysis difficult due to the single chamber of the arrays. Most often in order to isolate a particular phenotype, subsequent processing is required. Belov et al. presented an array technique based on cluster of differentiation in leukemia.⁴⁰ The CD antigens can be used to phenotype leukocytes based on characteristic abnormal patterns of antigen expression. Microarray technology is also used to screen HIV positive blood against normal as well as blood from those undergoing therapy and those deemed long term non-progressors.⁴¹

1.2.1.3 Fluorescence-Activated Cell Sorting

FACS can be used to select low-abundance cells from mixed populations by monitoring the presence of antigenic species indigenous only to the target cells (see <http://www.abcam.com/technical>). FACS samples individual cells in a high-throughput

fashion ($\sim 50,000$ cells s^{-1}) by monitoring the fluorescence signature elicited by each cell type (Figure 1.2D). For example, FACS has been used to detect and enumerate an immortalized breast cancer cell line (BT-20 cells) that was seeded into peripheral blood mononucleated cells (PBMCs) at frequencies of 10^{-5} , 10^{-6} , and 10^{-7} .³⁷ The flow cytometer employed three excitation wavelengths, 325, 488, and 633 nm, allowing for discrimination between the PBMCs and the BT-20 cells. A panel of fluorescently labeled antibodies allowed the BT-20 cells to produce distinct colors for their identification from the PBMCs. BT-20 cells were also characterized by a cocktail containing three anti-cytokeratin antibodies, each tagged with a different-colored dye. Through the use of a color-discrimination algorithm, BT-20 cells were detected with a 20% recovery for frequencies at 10^{-5} and 10^{-6} . The challenges associated with this assay format were the extensive amount of time required for the immunofluorescent staining (~ 20 h), the need to remove the RBCs from the blood sample prior to processing, and the extensive equipment required for the measurements. The recovery was low due to the loss of target cells during removal of the RBC fraction and the extensive staining and processing steps required. For this approach to reliably assess rare CTCs at frequencies of 10^{-7} in the presence of PBMCs, ~ 200 mL of blood would be needed.

1.2.1.4 Molecular Methods

Another approach employed for the analysis of low-abundance cells in clinical or environmental samples is RT-PCR, in which mRNAs are used as markers to report on the presence of specific low-abundance cells. For example, reports have documented RT-PCR's ability to detect low-abundance cells in 10^6 PBMCs via an appropriate marker panel.³⁸ Gene expression-based assays have high sensitivity but can generate poor selectivity, which can lead to false-positive results. Also, as with many low-abundance cell-

based assays for whole blood, the RBC fraction must be removed with, for example, Ficoll-Hypaque density-gradient centrifugation (DGC), which can reduce cell recovery. Notably, these assays are prone to high interlaboratory variability.³⁹

1.2.2 Challenges Associated with Macroscale Methods for Low-Abundant-Cell Selection

Enrichment of target cells via macroscale systems typically employs either positive selection (for example, IMACS or FACS) or negative selection. Negative selection gives low purity (0.01%–0.1%) due to insufficient removal of interfering cells.⁴² When the sample matrix is whole blood, negative selection performed on the basis of size is often marred by interferences resulting from leukocytes, due to the similarity in size between these cells and the CTCs, for example.^{45,46} Attempts to further preconcentrate targets and remove WBCs introduce a significant risk of target loss. For example, monocytes were found to interfere with the selection of comparably sized stem cells.⁴⁷

The challenges associated with positive selection using IMACS or FACS assays are the extensive amount of time required for the immunofluorescent staining (~20 h) and, in many cases, the need to remove the RBCs from a blood sample prior to processing. Furthermore, semi-automated processes requiring operator intervention and the variability in reagent and laboratory protocols lead to poor interlaboratory standardization and data collection, assessment, and management.⁴⁸ Additionally, downstream processing of the collected rare cells requires samples with high purity that are in a viable form (i.e., following cell culturing). For example, the magnetic field used for IMACS may produce perturbations on stem cell differentiation.⁴⁹ Finally, in the case of positive selection, the recovery can depend upon the expression level of the antigenic membrane protein used for their selection.⁹

Many macroscale techniques also rely on DGC preselection. Differences in density between cell types can be small, and individual cell types can be heterogeneous in size and density.⁵⁰ Consequently, particular cell types can distribute throughout a density-gradient medium, rather than precisely segregate at a discrete area; this results in reduced recovery of the desired cells and/or contamination with undesired cell types.⁴⁵ Procedures such as DGC that enrich for low-abundance blood cell types, such as hematopoietic progenitor cells, can lead to significant loss or reduced yields due to poor segregation with potential interfering cells. For example, conventional density-gradient methods to isolate progenitor cells (e.g., CD34+ hematopoietic stem cells) from umbilical cord blood results in significant loss of the desired stem cells.⁴⁶

1.3 Microsystems for Low-Abundant-Cell Selection

Microsystem technologies allow the dissemination of new sample-processing capabilities to a broader user community due to their potentially smaller footprint, lower power consumption, reduced reagent requirements, and process automation, as compared with their benchtop counterparts. Additionally, improved performance is fundamental to high-sensitivity cellular analysis technologies.^{53,54} In particular, microsystem platforms enable one to handle small numbers of cells without loss. Such a task is difficult to achieve with instruments such as conventional flow cytometers, which typically require a starting population of more than 100,000 cells.⁵⁵ Furthermore, low-abundance cell-selection mechanisms such as affinity, physical characteristics, dielectrophoresis (DEP), and magnetic interactions can be integrated into a microsystem, along with downstream molecular processing of the intracellular contents of the selected cells, to provide important clinical or environmental information. The challenge for imposing low-abundance cell-selection assays to microsystems is sampling; to generate a high statistical probability of

selecting the low-abundance cells, large input volumes (>1 mL) must be processed, and most microsystems cannot handle large-volume inputs in reasonable times (i.e., they have poor throughput; see Figure 1.1). Therefore, novel design approaches must be implemented to accommodate the necessary sampling volume. In the following sections, we review microfluidic-based systems for selecting low-abundance cells.

1.3.1 Low-Abundant-Cell Selection via Immunoaffinity Interactions

Affinity-based selection of low-abundance cells is often employed in microsystems. This approach exploits the specific but noncovalent interactions between a ligand, such as an antibody, aptamer, or peptide, and a target-specific receptor, such as a membrane protein.⁵⁶ Affinity-based cell selection via microsystems can be carried out by either positive or negative selection. Negative selection requires the complete removal of the nontarget cells with minimal target-cell capture and is an attractive approach when the specific markers for target cells are not fully known. In contrast, positive selection involves directly capturing the target cell through the use of a membrane protein(s) unique to that cell type.⁹

In most cases, cell selection involves a solid phase in which (a) the recognition element(s) is covalently tethered to the surface of a fluidic conduit and (b) the sample containing the low-abundance cells is moved through this conduit to invoke the selection process. The operational criteria mentioned in Section 1 are important to this phase, as are (a) nonspecific interactions, (b) target cell–recognition element adhesion strength, (c) conduit architecture, (d) recognition element immobilization chemistry, and (e) ligand surface density.

As noted in Section 1, throughput—namely, the number of cell-identification or -sorting steps per unit time—is a critical metric to optimize. One can improve throughput

by increasing the transport rate of sample through the selection conduit. However, cell recovery can degrade at certain transport rates, indicating that there is an optimal flow rate at which the system can be operated. The analytical model used to explain this observation is based on cell adhesion between a surface-tethered antibody and a moving antigen.⁵⁷ This model describes a two-state process. The first state accounts for transport of the solution-cell antigen to the surface-bound antibody, which describes the encounter rate (k_o). The second state gives the probability (P) that an association event will occur during the time the antigen is in close proximity to the tethered antibody. The encounter rate, k_o , increases linearly with flow velocity, whereas P decreases. These states can be used to calculate the rate of capture per antigen-antibody pair (k_f , s^{-1}) via the following equation:⁵⁷

$$k_f = k_o P \quad (1)$$

P can be estimated from Equation 2,

$$P = \lambda \delta / (1 + \lambda \delta) \quad (2)$$

where δ is the dimensionless Damköhler number (calculated from $a^2 k_{in} / D$; k_{in} is the intrinsic antigen-antibody reaction rate; a is the encounter radius) and λ is the dimensionless encounter time [calculated from $\tau / (a^2 / D)$; $\tau = 8a / (3U\pi)$; U is the cell-translational velocity; D is the cell diffusion coefficient].^{33,57} Equation 1 indicates that the recovery increases with translational velocity due to increases in k_o but that, beyond an optimal velocity, the recovery degrades due to insufficient reaction time (i.e., lower P).

Critical to affinity-based cell selection that uses surface-immobilized recognition elements and flow processing is the adhesion force (F_A) between the cell and the antibody-decorated surface, which must be greater than the shear force (F_S) generated by the solution flow to prevent target cell loss. F_A can be determined from the bond

strength between a single antigen-antibody complex (f_c), the cell-contact area with the recognition surface (A_c), and the number of receptors poised on the surface within the contact area of the cell (C_s). F_A is calculated from³³

$$F_A = f_c \times A_c \times C_s \quad (3)$$

If the cell is assumed to be a nondeformable object once it adheres to the capture surface, the contact area can be calculated from Equation 4,⁵⁸

$$A_c = \pi \{ r_p \sin[\cos^{-1}(r_p - h' + h)/r_p] \}^2 \quad (4)$$

where r_p is the cell radius and h and h' represent the characteristic cell-separation distances from the surface upon binding. When the F_S generated by the flow is equal to or greater than F_A , the cell can be removed from the surface. The velocity-dependent F_S can be determined from Stoke's law,⁵⁹

$$F_S = 6\pi\eta r_p v_c, \quad (5)$$

where r_p is the cell radius, η is the solution viscosity, and v_c is the critical linear velocity that can induce cell detachment.

The application of mAB based microsystem for CTCs selection kept pace with their increasing availability. Monoclonal antibody-poised microsystem was designed by Du et al. to recognize and select cervical cancer cells (HCCC) in a mixed cell population.⁶⁰ The channel dimensions of microsystem were rather large, 500 $\mu\text{m} \times 500 \mu\text{m}$, and 2.0 cm long. The anti- $\alpha 6$ -integrin antibody was immobilized on the surface against overexpressed $\alpha 6$ -integrin antigen on cervical cancer cell membrane. The capture efficiency of 30% was obtained at average velocity of 1.3 mm s^{-1} and surface antibody concentration of 1:50, while normal cell capture efficiency was less than 5% reported indicating insufficient separation efficiency with low purity to track rare cell events. It is found that separation purity and cancer cell capture efficiency were altered

by the specificity of the antibody, flow rate and surface immobilized antibody concentration. Increasing the flow rate caused both increased dissociation of antigen and decreased antigen–antibody interaction time. The high non-specific binding of normal cells at low flow rates were observed and it was likely a result of the high surface to volume ratio of the microchannel.

Nagrath et al.⁹ developed a microsystem for selecting CTCs directly from peripheral blood. The CTCs originated from solid lung, colorectal, breast, prostate, brain, and neck tumors and were selected through use of anti-EpCAM monoclonal antibodies tethered to the walls of a microfluidic channel and posts. The device contained 78,000 microposts that were 100 μm tall and 100 μm wide with a total surface area of 970 mm^2 (Figure 1.3). Anti-EpCAM monoclonal antibodies provided the specificity for CTC recovery from unfractionated blood because EpCAM is specifically overexpressed by adenocarcinomas.^{9,33} The essential parameters that determined recovery by the CTC chip were flow velocity, shear force, and cellular EpCAM expression level, as noted in Equations 1–5. At a flow rate of 1 mL h^{-1} , 65% of the CTCs were recovered, and 98% of the cells remained viable. As the processing flow rate was increased to 3 mL h^{-1} , the recovery was reduced to 25%, as shown in Figure 1.3E. Enrichments from whole blood provided ~50% purity, and as a result the CTCs had to be differentiated from the major impurity, leukocytes, through use of fluorescently labeled cytokeratin and CD45 antibodies (Figure 1.3G-N). The same CTC chip was also used to select low-abundance lung cancer cells from whole blood.⁵⁹ Extensive clinical studies have been successfully completed with the use of this CTC chip. For example, with this chip CTCs were isolated in 100% of patients with early-stage prostate cancer. Furthermore, the potential utility of this CTC chip in monitoring response to anticancer therapy was also

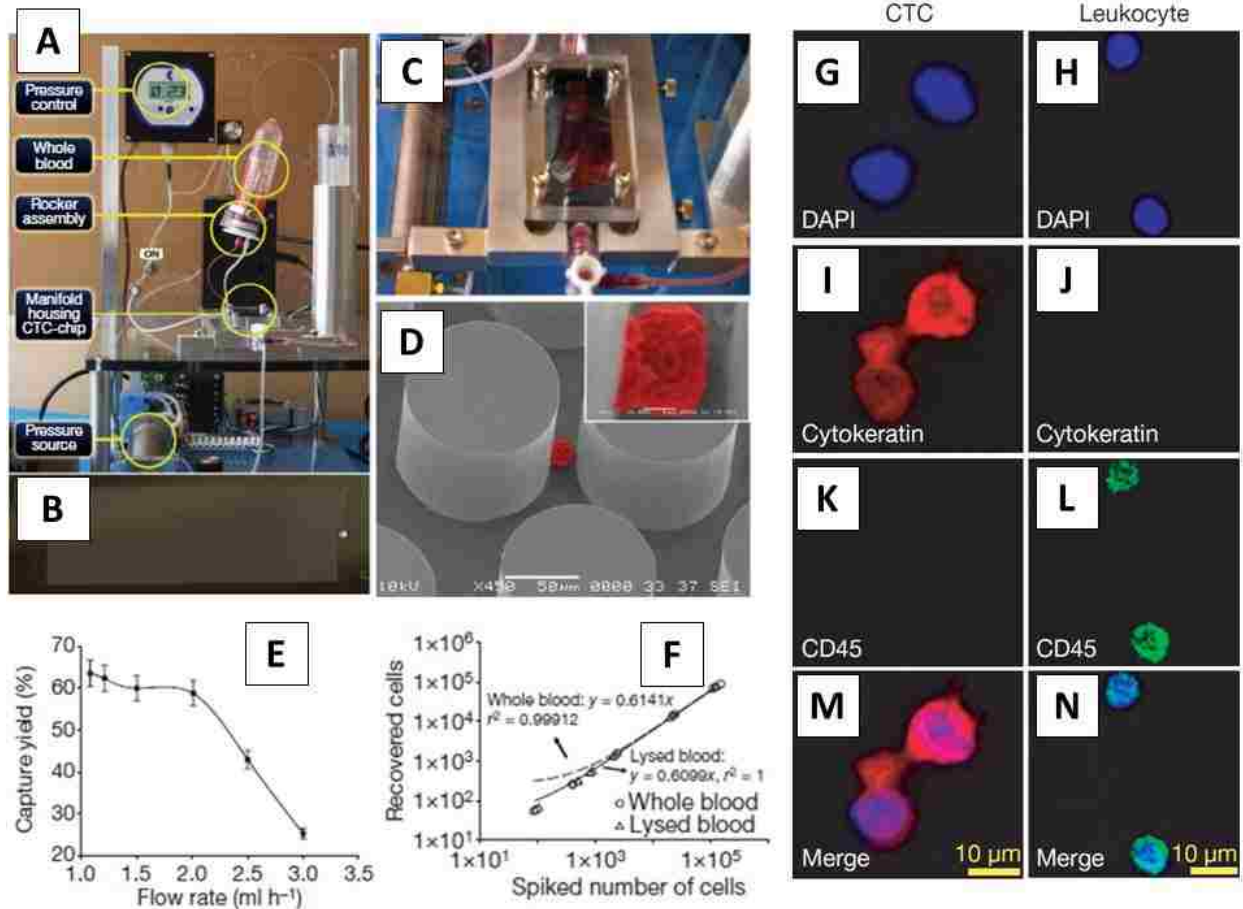


Figure 1.3 Isolation of circulating tumor cells (CTCs) from whole blood, performed with a microfluidic device (CTC chip) fabricated in silicon via reactive ion etching. **(A)** The workstation setup for CTC isolation from whole blood. **(B)** The CTC chip with microposts etched into the silicon. **(C)** Micrograph of whole blood flowing through the CTC chip. **(D)** An image of a captured NCI-H1650 lung cancer cell spiked into blood (pseudo-colored red). The inset shows a high-magnification view of the captured cell. **(E)** CTC recovery as a function of flow rate. **(F)** Regression analysis of capture efficiency for various target-cell concentrations in whole-blood samples versus lysed-blood samples. **(G-N)** High-magnification images of captured CTCs and hematologic cells stained with 4',6-diamidino-2-phenylindole (DAPI), cytokeratin, and CD45. Merged images identify CTCs in panels **G**, **I**, **K** and **M** and hematologic cells in panels **H**, **J**, **L**, and **N**.

investigated. In a small cohort of patients with metastatic cancer who were undergoing systemic treatment, temporal changes in CTC numbers correlated well with the clinical course of the disease.^{9,59}

Adams et al.³³ introduced a microchip-based high-throughput microsampling unit (HTMSU) capable of selecting very low abundance CTCs from whole blood in a single

step. The HTMSU was fabricated from poly(methylmethacrylate) (PMMA) via microreplication and consisted of 51 ultrahigh-aspect ratio, parallel, curvilinear channels and a Pt-conductivity sensor to allow for cell enumeration (Figure 1.4). The capture channels were functionalized, via a carboxylate scaffold, with anti-EpCAM monoclonal antibodies. The authors found that the CTC-capture efficiency varied with channel width; the highest recovery (97%) was obtained for channels that had similar widths (35 μm) to the CTC dimensions (15–30 μm) (Figure 1.4F). The device was capable of high-throughput operation at an optimal linear fluid velocity of 2 mm s^{-1} in each channel (51 parallel channels), allowing 1 mL samples to be exhaustively interrogated in ~ 37 min. The captured CTCs were subsequently removed from the capture surface via trypsin and were quantitatively counted one at a time via conductivity detection.

Microsystems have also been applied to immunoassay-based recognition for pathogen detection. Static forward light scattering was investigated for the analysis of bovine viral diarrhoea virus in a complex matrix mimicking a body fluid.⁶¹ The assay was based on the use of microparticles coated with antibodies directed against bovine viral diarrhoea virus, and the reaction was monitored in a Y-shaped poly(dimethylsiloxane) (PDMS) fluidic device with optical fibers oriented at a 45° angle to measure light scatter from single virus cells. Bovine viral diarrhoea virus concentrations of 10 $\text{TCID}_{50} \text{ mL}^{-1}$ (where TCID_{50} stands for 50% tissue-culture infectious dose) were detected with this microfluidic chip. Application of antigen/antibody-recognition strategies for low-abundance-cell selection is, in some cases, limited by the availability of antibodies directed against membrane proteins uniquely found on the target rare cells.⁶² Additionally, most positive selection tools require surface immobilization of the antibody, which can result in reduced recovery or adhesion strength between the cell

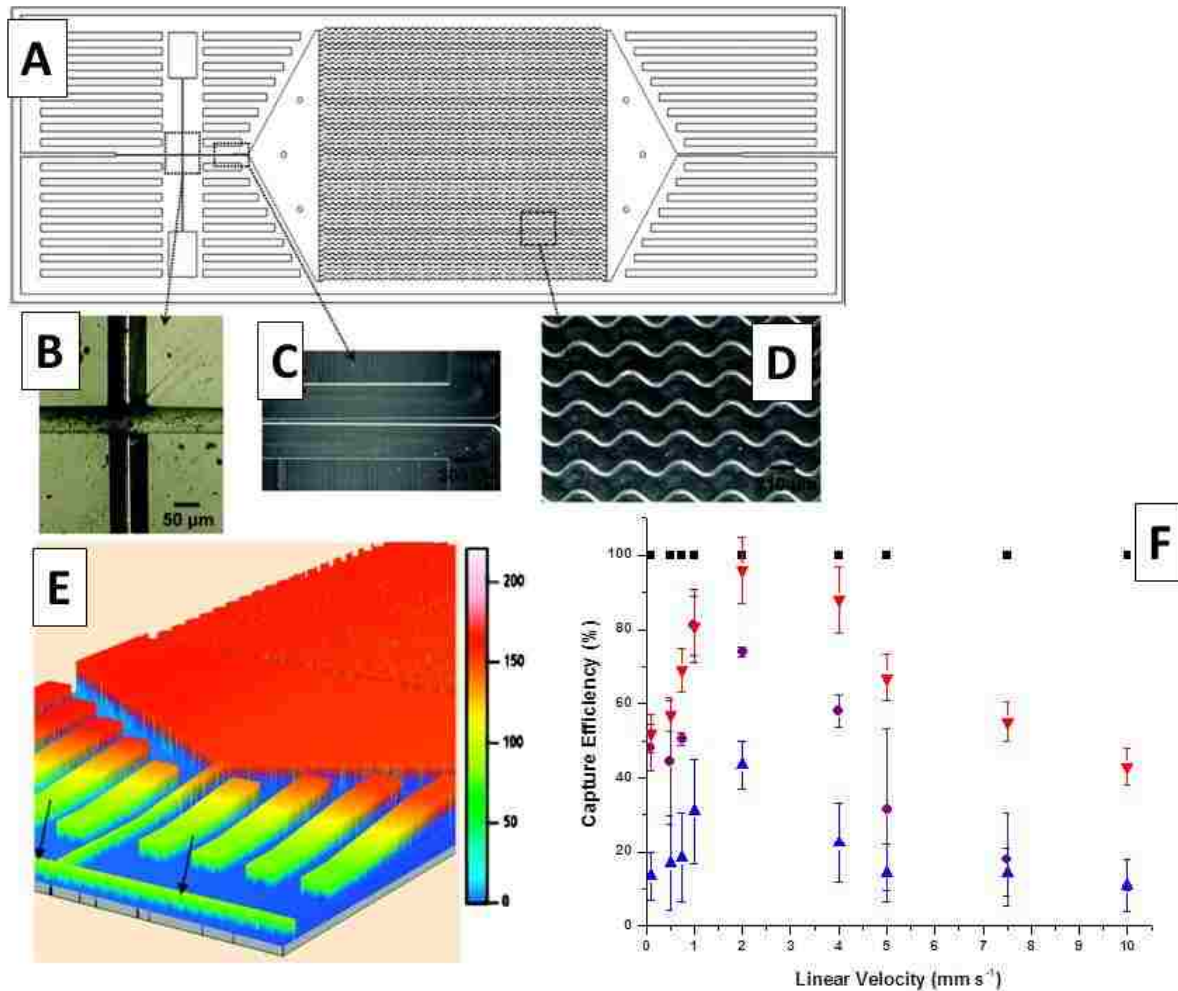


Figure 1.4 Schematic of a microchip-based high-throughput microsampling unit (HTMSU) fabricated in poly(methylmethacrylate) via microreplication for selection of circulating tumor cells (CTCs). (A) An AutoCAD[®] diagram of the sinusoidally shaped capture channels with bright-field optical micrographs showing (B) the integrated conductivity sensor consisting of cylindrical Pt electrodes with a 75 μm diameter and a 50 μm gap; (C) the single port exit, where the HTMSU's width tapers from 100 μm to 50 μm and the depth tapers from 150 μm to 80 μm over a 2.5 mm region that ends 2.5 mm from the Pt electrodes; (D) the sinusoidal cell-capture channels (5x magnification); (E) three-dimensional projection of the topology of the HTMSU obtained at 2.5 μm resolution via noncontact optical profilometry (arrows, Pt electrode conduits); and (F) the capture efficiency of CTCs in spiked whole-blood samples as a function of the cells' translational velocity. The microchannels were 35 μm wide (red down triangles, sinusoid; purple circles, straight) and 50 μm wide (blue up triangles).

and the surface-tethered antibody due to the stochastic nature of the immobilization chemistry. Antibodies may also show variation in antigen binding, exhibit instability when bound to solid surfaces, and have limited binding sites.⁶³ Finally, environmental

factors may affect antibody-antigen interactions.^{64,65} Therefore, alternatives to antibodies for low-abundance cell selection have been investigated.

Aptamers, single-stranded nucleic acid oligomers, possess highly specific recognition affinities to molecular targets through interactions other than classical Watson-Crick base pairing.⁶⁶ Compared with antibodies, aptamers have lower molecular weights, remain stable during long term storage, sustain reversible denaturation, have low toxicity, and can be produced against targets via highly automated technologies [e.g., SELEX (systematic evolution of ligands by exponential enrichment)].⁶⁷ Additionally, their immobilization chemistry is highly oriented: End-point attachment occurs exclusively through the 5' or 3' end of the aptamer, which bears a functional group. These advantages make aptamers highly desirable as potential molecular recognition elements for low-abundance-cell selection.⁶⁸

Aptamers have been employed in a microsystem for the capture of prostate cancer cells that used a LNCaP cell line as a model. This cell line overexpresses a prostate-specific membrane antigen (PSMA) that was used as a marker for the selection of these cells.⁶⁹ Nuclease-stabilized and in vitro-generated PSMA aptamers were immobilized onto ultraviolet-modified PMMA capture channels (Figure 1.4A-D). The authors used carbodiimide-coupling chemistry and the appropriate linker structure to enhance the accessibility of the surface-bound aptamer to the solution borne cells (Figure 1.5A). Following selection and isolation, the captured cells were released from the capture surface via enzymatic digestion of the extracellular domain of PSMA for subsequent conductivity enumeration. CTCs possess unique electrical properties that arise from their characteristic chemical composition (compared with those of erythrocytes).

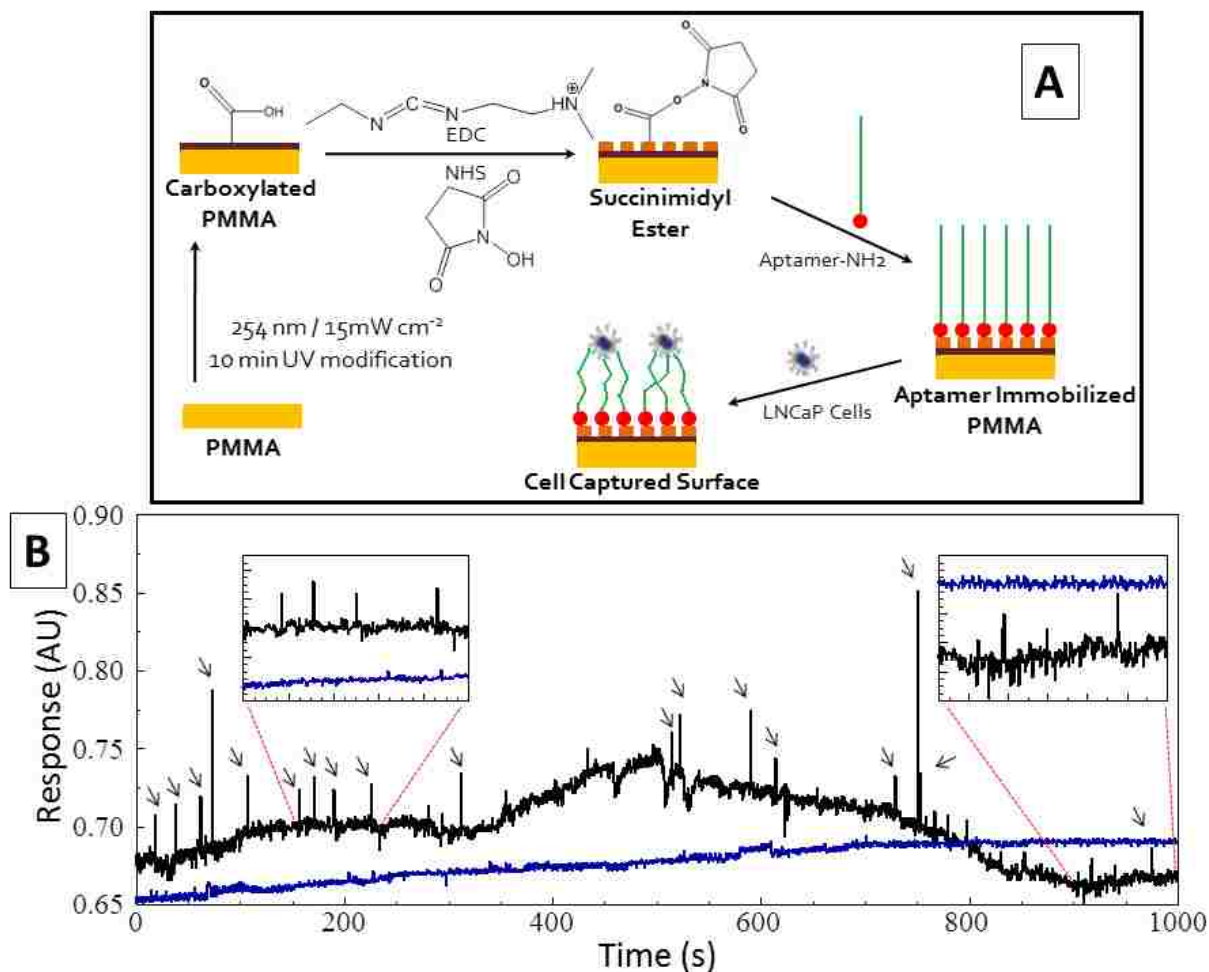


Figure 1.5 (A) Chemical steps for the immobilization of aptamers to the surfaces of a poly(methylmethacrylate) (PMMA)-based high-throughput microsampling unit (HTMSU) used for the positive selection of LNCaP cells. (B) Conductometric responses generated for 1.0 mL of whole blood seeded with 20 ± 1 LNCaP cells (red) and 0 LNCaP cells (blue), at a linear flow velocity of 2.5 mm s^{-1} , processed with an HTMSU. The arrows designate peaks that were identified as LNCaP cells on the basis of a signal-to-noise threshold of 3.

For example, the overexpression of membrane glycoproteins—such as PSMA and EpCAM, which are associated with many tumor or cancer cells—results in an increase in the number of negatively charged sialic acid molecules that cap the extracellular domains of these integral membrane proteins.⁵⁸ As shown in Figure 1.5B, only positive signals were designated as LNCaP cells due to their electrical properties. The system required no sample pretreatment and provided high throughput (processing time for 1 mL was 29 min), a recovery of 90%, and a purity of 100%.

1.3.2 Low-Abundant-Cell Selection via Physical Criteria

Differences in cell size, density, shape and deformability can be exploited in microsystems to select low-abundance cells on the basis of mechanical restriction.^{71,72} Such microsystems are relatively easy to build with common microfabrication technologies.¹⁹

Forensic DNA analysis of sexual assault evidence requires separation of DNA from epithelial (victim) and sperm (perpetrator) cells collected on vaginal swabs. Because the cells in sexual assault evidence are rarely viable, biological adhesion is less likely, but adsorption to the glass is possible and could be used to selectively isolate the epithelial cells from solution using microsystem, either alone or in conjunction with the sedimentation rate differences.¹⁹ Specific gravity differences are small but perceptible, with sperm cell density on the order of 1.12 g mL^{-1} ⁷³ and epithelial cell densities in the range of $1.04\text{-}1.08 \text{ g mL}^{-1}$.⁷⁴ These values characterize differences in the rate at which cells would settle to the bottom of the inlet reservoir. The microsystem prepared by Horsman et al. contained a straight channel with the dimensions of 2.5 cm long, 50 μm deep and 90 μm wide at half-height. The larger surface area of the epithelial cells and their high concentration of cell surface binding proteins, which are capable of specific interaction with surfaces, present the possibility for binding to glass substrates. Because, the method does not use mobilization of the epithelial cells, clogging of the microchannel by epithelial cells, was not encountered here. Separation speed and throughput was low, because the flow rates achievable using gravity forces were slow, not easily controlled. It was demonstrated that increasing the flow rate to achieve a faster separation can dislodging the epithelial cells from the reservoir. A 20 min separation (~380 sperm cells) provided sufficient material for DNA extraction and

PCR amplification of a 380-bp fragment of β -globin, which is a representative human gene. Though the system generated 100% theoretical purity, the real life forensic samples are contaminated with bacteria and purity of separation can be deteriorated and bacteria can interfere with effective counting of sperm cells using optical means.

The size and deformation characteristics of fetal nucleated red blood cells (fNRBCs) were used to isolate them from maternal blood.¹⁹ fNRBCs range between 9 and 12 μm in size and were demonstrated to deform and pass through fluidic obstacles fabricated in PDMS that were as small as 2.5 $\mu\text{m}\times 5 \mu\text{m}$. WBCs ranging in diameter between 10 and 20 μm could not deform and thus were retained by the fluidic channels of similar dimensions. The authors¹⁹ isolated low-abundance fNRBCs from umbilical blood that was preconcentrated using DGC. Unfortunately, the low processing rate of $<0.35 \text{ mL h}^{-1}$ posed a major challenge to this system, given that $\sim 10 \text{ mL}$ of blood had to be processed to accommodate sampling these low-abundance cells.

A series of massively parallel microfabricated sieving structures were used to separate neuroblastoma (NB) tumor cells from blood constituents on the basis of size characteristics.⁷² The reported devices consisted of four successively narrowing regions of channels. The size-based selection of tumor cells was carried out through the use of diluted blood (1:10) (v/v) containing the NB cells. As the NB cells traversed the device, they were retained in the 10 $\mu\text{m}\times 20 \mu\text{m}$ channels, but other blood cells migrated to the output. It was observed that in shallow channels NB cells tended to adhere to the walls upstream of where freely moving cells were retarded. A shorter (3.5 cm) device with deeper (20 μm) channels reduced the device flow resistance and adhesion problems. Experiments that used undiluted whole blood (2 mL) took approximately 3 h to analyze.

The authors⁷² noted that the enriched cells obtained from the device had low purity and that the interfering cells were composed of residual erythrocytes and leukocytes.

1.3.3 Low-Abundant-Cell Selection via Dielectrophoresis

DEP uses the electrical polarization of cells in nonuniform fields to induce translational motion and/or reorientation of the cells.⁷⁵ The induced polarization depends on multiple factors related to the cells' condition, such as bilipid membrane characteristics, internal structure, and size of the nucleus.⁷⁶ DEP has been used to study the physiology of bacterial,⁷⁷ yeast,⁷⁸ plant,⁷⁹ and mammalian cells⁸⁰ and to investigate cellular alterations accompanying physiological changes, such as mitotic stimulation and induced differentiation. The variability in particular cells' response to electric fields can be used not only to differentiate cell types but also to distinguish the activation states of similar cells.⁸¹ DEP devices can differentiate among cell types by changing the field frequency or amplitude.⁸²⁻⁸⁴

The DEP force (F_{DEP}) acting on a cell can be calculated via⁸⁵

$$F_{DEP} = 2\pi\epsilon_M r_p^3 R_e[f_{CM}(\omega)] \nabla E_{RMS}^2, \quad (6)$$

where ϵ_M is the permittivity of the suspending medium, r_p is the cell radius, E_{RMS} is the electric field strength, and $R_e[f_{CM}(\omega)]$ is the real part of the dipolar Clausius-Mossotti factor. This factor is the relative polarization of the cell versus that of the surrounding medium and is given by⁸⁵

$$f_{CM}(\omega) = [\epsilon_C^*(\omega) - \epsilon_M^*(\omega)] / [\epsilon_C^* + 2\epsilon_M^*(\omega)] \quad (7)$$

where ϵ_C^* and ϵ_M^* are the complex permittivities of the cell and medium, respectively. The DEP forces can be either negative, $R_e[f_{CM}(\omega)] < 0$ (i.e., the cell is repelled by a region of higher electric field), or positive, $R_e[f_{CM}(\omega)] > 0$ (i.e., the cell is attracted to a region of higher electric field). As shown by Equations 6 and 7, the polarizability of the

cell is frequency dependent; thus, changing ω can result in the selection of certain cell types.

A dielectric affinity column was used to select tumor cells (MDA231) from diluted blood,⁸⁶ from which the cells were captured by balancing gravity, DEP, fluid drag, and hydrodynamic lift effects (Figure 1.6) and released by reducing the frequency of the applied electric field. Efficient selection was obtained when (a) the product of the cell radii and dielectric polarizability was sufficiently different and (b) the ratio of fluid velocity to the square of the applied voltage was within the specified range, determined by the type of cell. The column sorted cells at a rate of $\sim 10^3 \text{ s}^{-1}$; larger devices increased this rate by two orders of magnitude. The viability of the excluded cells was 98%, indicating that the cell-membrane barrier function was maintained. The total number of cells analyzed with this device in a single run was 1.2×10^6 , and the ratio of tumor cells to normal hematopoietic cells was 1:3.

The electrical conductivity of RBC membranes increases sharply when they become infected with malarial parasites such as *Plasmodium falciparum*. When challenged by a suspension in a low-conductivity medium, infected cells lose internal ions, whereas uninfected cells retain them.²⁴ The resulting dielectric differences between infected and noninfected cells were exploited in order to sort these cells via DEP.²⁴ Parasitized cells were isolated by steric dielectric field–flow fractionation (DEP-FFF) and were focused at the center of a spiral electrode array, identified, and counted. The spiral microelectrode array had a 2 mm^2 surface area and was composed of five complete turns of four parallel spiral elements. On the spiral array, cells were distinguished through differences in their DEP properties. More than 99.5% of the

normal erythrocytes were trapped, and 90% of the parasitized cells were preconcentrated 50- to 200-fold.

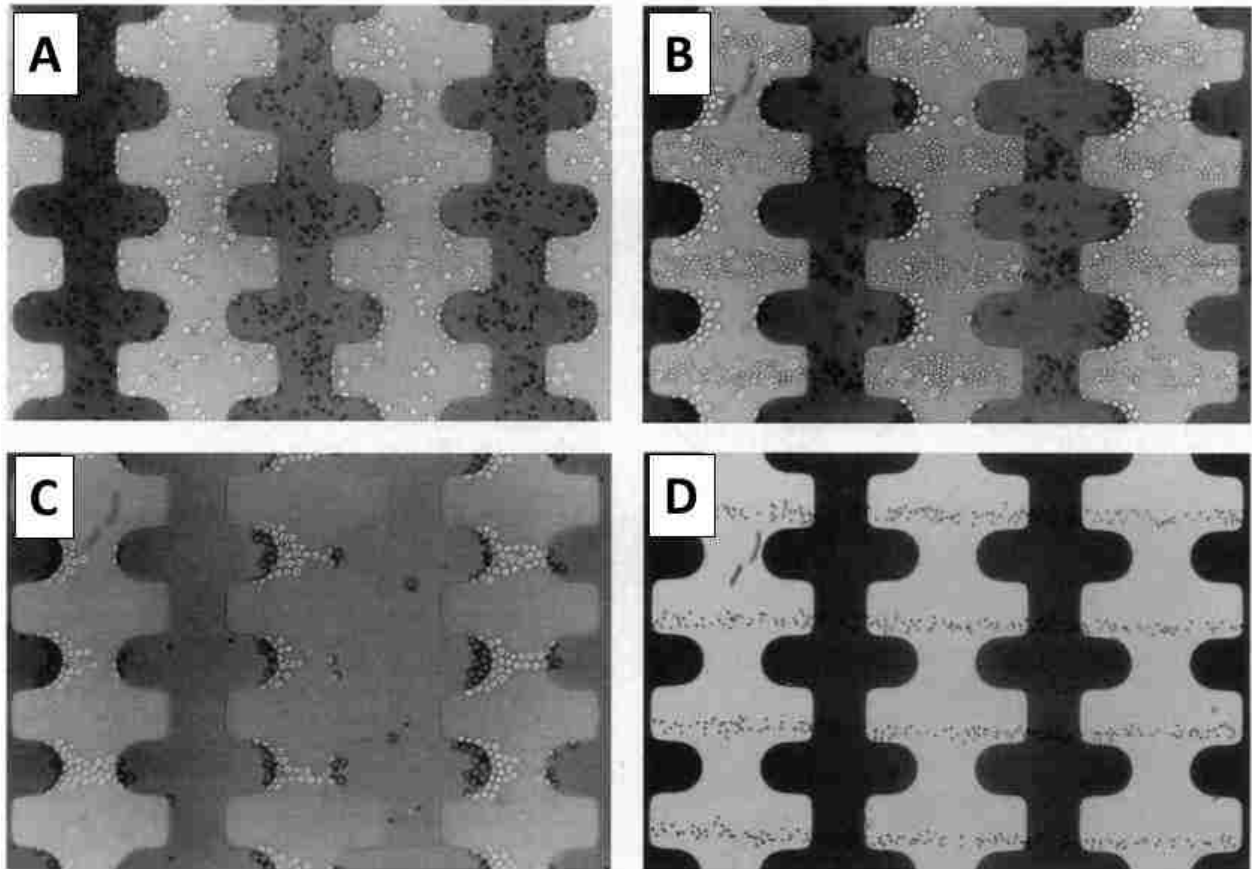


Figure 1.6 Dielectrophoretic separation of MDA231 human metastatic breast cancer cells from diluted peripheral blood. (A) Initial separation of cells in the chamber inlet well after the electrical sweep signal was applied. (B) Blood cells focused into bands that flowed between the electrode tips, leaving the cancer cells behind. (C) Cancer cells that remained on the electrode tips after the blood cells were swept downstream through the dielectrophoresis column. (D) Close to the chamber outlet well, where only blood cells in focused bands were moving.

Using a similar approach, Reichmuth et al. developed a microfluidic chip with an integrated membrane for simultaneous concentration and detection of swine influenza virus with necessary sensitivity for diagnosis.⁸⁷ The membrane was created in a small section (100 μm wide \times 25 μm deep \times 150 μm long) of the microchannel. The immunoassays recognized the membrane viral proteins using antibodies. Open channel electrophoresis was used to detect by observing formation of an antibody–antigen (virus

particle) complex. The size-exclusion properties of the *in situ* polymerized polyacrylamide membrane were exploited to simultaneously concentrate viral particles and separate the virus/fluorescent antibody complex from the unbound antibody. The filtration step eliminated the need for washing, commonly required with surface-based immunoassays and increased the speed of the assay. With integrated preconcentration, a LOD of 610 TCID₅₀ mL⁻¹ could be obtained for <50 µL sample in less than 6 min. The most common failure mode of the chip was accumulation of dust or other particulates at the membrane element. Therefore, sample prepreparation is required to remove large particles (> micrometer-size).

Differences in cell-dielectric properties were exploited to separate and identify cells without extensive cell manipulation.⁸⁸ For applications such as stem cell research, it is highly preferable that the isolated cells be unlabeled and minimally manipulated to preserve their integrity. Vykoukal and coworkers⁸⁹ applied DEP-FFF for the rapid, label-free enrichment of progenitor cells from a stromal vascular fraction. Different cell types were driven to different flow lamina in a DEP-FFF separator on the basis of the aggregate effect of their density and specific dielectric properties. Low-abundance putative progenitor cells, NG2 cells (<2% in the starting mixture), were enriched up to 14-fold, yielding 28% NG2⁺ cells in the most enriched fraction. This device is therefore ideally suited for batch-mode isolation and recovery of moderate quantities of cells (<10⁶ cells per run).

Although these approaches are applicable to many cell-processing problems, they demand that the dielectric properties of the target cells be significantly different from those of the interfering cells. For this reason, DEP/gravitational field-flow fractionation (DEP/GFFF), which has a potentially higher discriminatory ability, has been

developed.^{90,91} GFFF is a process by which particles are allowed to settle while under the influence of an axial flow.⁹² In DEP/GFFF, the balance of DEP and gravitational forces controls cell position in the gravitational flow profile.⁹¹ This technique was applied to the separation of a breast cancer cell line (MDA435) from RBCs.⁹² Results suggested that the MDA435 cells could be separated from erythrocytes in a 10 μL sample containing a total of $\sim 50,000$ cells. The enriched fractions of the MDA435 cells and erythrocytes were reported to be $>98\%$ and $>99\%$, respectively.

1.3.4 Low-Abundant-Cell Selection via Magnetic Interactions

Target cells can be specifically labeled with antibody-conjugated magnetic beads, and the selection and enrichment of the low-abundance cells can be achieved through the use of a magnetic field. Using this principle, Lee and coworkers²⁷ developed an integrated system capable of selecting RNA viruses, such as dengue virus and enterovirus, through use of antibody-conjugated magnetic beads and one-step RT-PCR in an integrated microfluidic system. The target virus in the sample was captured with modified magnetic beads and manipulated via microelectromagnets (Figure 1.7A). The integrated microfluidic system performed the entire process automatically with a rotary micropump and microvalves for fluid control. Following isolation, the viruses selected were subjected to thermolysis, RNA extraction, and RT-PCR on a single chip. The authors' results were similar to those obtained with benchtop instruments (Figure 1.7B).

Furdui and Harrison adopted this technique in order to enrich Jurkat cells (T cell leukemia) from blood.⁹³ The model samples contained Jurkat cells to erythrocyte cells ratios of 1:10,000 with a total of $1-2 \times 10^{10}$ RBCs mL^{-1} with a Jurkat cell frequency of 1×10^6 mL^{-1} . The magnetic beads were initially functionalized with protein A prior to incubating with

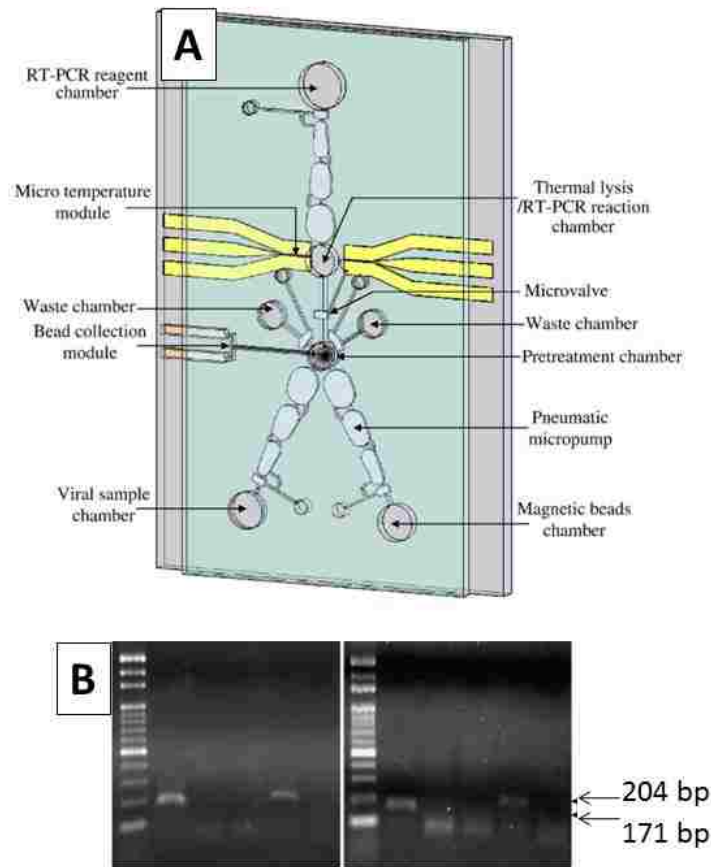


Figure 1.7 (A) Schematic of an integrated reverse-transcription polymerase chain reaction (RT-PCR) chip with a cell-selection unit for the magnetic capture of target cells. A microtemperature module, a bead-collection module, and a microfluidic control module are integrated into the chip. **(B)** A mixture of dengue virus (10^2 PFU) and enterovirus 71 (10^2 PFU) was incubated with antidengue antibody (lanes 1 and 2) or antienterovirus 71 antibody-conjugated magnetic beads (lanes 3 and 4); RT-PCR was then performed with dengue group-specific primers (lanes 1 and 3) or enterovirus 71-specific primers (lanes 2 and 4). The lanes marked with the letter L represent signals generated from DNA size markers. Results on the left and right are from a benchtop instrument and the integrated chip, respectively.

anti-human CD43. The results of the incubation yielded antibody-functionalized beads, where the antibodies were bound to protein A via their F_c domain. A magnetic zone was used to selectively isolate the magnetic particles bound to the target cells in the microfluidic device. Subsequent to a rinsing step, the captured cells were eluted after removal of the magnetic field and initiation of hydrodynamic pumping. Following optimization, the authors were able to isolate 37% of the spiked T-cells with a throughput that corresponded to $3 \mu\text{L min}^{-1}$ from a $2 \mu\text{L}$ sample that consisted of 1,070 Jurkat cells.

Beyor and coworkers⁹⁴ presented an *E. coli* O157:H7-detection microsystem with integrated cell capture, sample preparation, and PCR with capillary electrophoresis analysis. Immunomagnetic beads were coupled to polyclonal antibodies specific to the *E. coli* phenotype of interest. Sample volumes ranging from 10 to 100 μL were introduced and driven through immunomagnetic bead beds to capture the target cells. A detection limit of 0.2 colony-forming units μL^{-1} was achieved for an input volume of 50 μL .

1.3.5 Microfluidic Fluorescence-Activated Cell Sorting

Replacing the conventional flow chamber in FACS with microfabricated devices could allow more sensitive optical detection, easier mechanical setup, and more innovative sorting schemes. Another advantage is that multiple cell sorters can be fabricated in parallel on a single chip, allowing increased throughput or successive enrichment steps.

Fu et al.⁹⁵ demonstrated a complete microfabricated fluorescence-activated cell sorting (μFACS) device for *E. coli* HB101 cells. The chip was mounted on an inverted optical microscope, and fluorescence readout with a photomultiplier tube was accomplished at a T-shaped fluidic junction on the chip, with the cells manipulated electrokinetically. An advantage of the μFACS system is the small detection volume, typically 250 fL, which greatly reduces background fluorescence from the cell suspension and chamber material. Low-abundance cells are sorted by implementing a specific sorting algorithm. When a cell of interest is detected, the flow is stopped and the cell of interest is recovered by running the flow backward at a slow speed until the cell is moved into a collection channel. At that point, the cell is collected, and the device is once again run at a high speed in the forward direction. This reversible sorting method cannot be performed with standard FACS machines. The μFACS system offers several advantages over traditional FACS: (a) Because the channels are made with micrometer-size dimensions, the volume of the

interaction region can be precisely controlled, eliminating the need for hydrodynamic focusing; (b) the planar geometry of the device allows for the use of high-numerical aperture optics, increasing the limit of detection of the optical system; and (c) the disposability of the sorting device obviates the need for cleaning and sterilizing the instrument and prevents cross contamination between samples. However, the throughput obtained with this μ FACS is 20 cells s^{-1} , considerably lower than that of conventional FACS.

Another example of low-abundance-cell sorting via μ FACS was presented by Simonnet & Groisman,⁹⁴ who attempted to port conventional high-throughput, high-resolution cell sorting using flow cytometry to a PDMS microsystem. The integrated cell sorter was incorporated with various components, including peristaltic pumps, dampers, and input and output wells, to perform cell sorting in a coordinated and automated fashion. DEP and pressure switching were used to create a valveless device for the separation of cells within microchannels. The standard forward and reverse sorting algorithms were implemented. Conventional FACS uses flow rates of $\sim 10 \text{ m s}^{-1}$, corresponding to sampling rates of $1,000\text{--}50,000 \text{ cells s}^{-1}$. Using this platform, the authors processed up to $17,000 \text{ cells s}^{-1}$. An 83-fold enrichment was achieved in a single pass, yielding 40% recovery. As with the macroscale version of FACS, sorting and enumerating low-abundance cells require specific staining protocols as well as sample-preprocessing steps.

1.4 Conclusions

IMACS, FACS, and size-based selection techniques of low-abundance cells can be transitioned to microscale systems, and they can produce results that are similar if not superior to their macroscale counterparts. The high automation potential of microfluidic

systems and their ability to process samples in closed architectures provide a venue in which to analyze mass-limited samples, such as low-abundance cells, which is free from contamination.

However, Microsystems for rare cell selection need to be designed to sample larger input volumes in reasonable times (i.e., higher throughput) to accommodate extremely low abundance cells. In this dissertation, I investigate the use of surface modification, rare cell enumeration and electro-manipulation techniques in polymer-based microfluidic devices as a means of separation, enumeration and enrichment low-abundance cells in complex matrices such as whole blood and environmental water samples. The selection and enumeration of low-abundance cells are often not the terminal steps in the processing pipeline of these cells. For example, CTCs selected via immunoaffinity, with EpCAM as the molecular target, can originate from a variety of different cancers, such as colorectal, prostate, bladder, lung, or breast. To determine the specific type of cancer, it is necessary to molecularly profile the selected cells. A major challenge concerns the mass-limited samples encountered when analyzing low-abundance cells. For example, in a single eukaryotic cell two copies of the genome and approximately 300 copies of each different mRNA molecule are present, requiring highly sensitive genotyping techniques to characterize these molecular entities.

Therefore, I also investigate to optimize genotyping techniques such as RT-qPCR and PCR/LDR/CE for quantitation and molecular profiling of low-abundance genetic molecular entities. Overall, highly integrated low-abundance cell-based microfluidic devices that can molecularly profile such cells will find applications in medicine at the point of care; national security and counterterrorism; police, paramedics,

and fire departments; veterinary medicine; and environmental and food safety monitoring.

1.5 References

1. Berger MJ, Adams SD, Tigges BM, Sprague SL, Wang XJ, et al. **2006**. *Cytotherapy* 8:480–87.
2. Mostert B, Sleijfer S, Foekens JA, Gratama JW. **2009**. *Cancer Treat. Rev.* 35:463–74.
3. Utikal J, Polo JM, Stadtfeld M, Maherali N, Kulalert W, et al. **2009**. *Nature* 460:1145–48.
4. Elisavet K, Aggelki K, Nikolas P, Aris A. **2009**. *Chromosome Res.* 17(Suppl. 1):230–31.
5. de Wynter E, Ploemacher RE. **2001**. *J. Biol.Regul. Homeost. Agents* 15:23–27.
6. Allard WJ, Matera J, Miller MC, Repollet M, Connelly MC, et al. **2004**. *Clin. Cancer Res.* 10:6897–904.
7. Bertazza L, Mocellin S, Nitti D. **2008**. *Curr. Oncol. Rep.* 10:137–46.
8. Mocellin S, Hoon D, Ambrosi A, Nitti D, Rossi CR. **2006**. *Clin. Cancer Res.* 12:4605–13.
9. Nagrath S, Sequist LV, Maheswaran S, Bell DW, Irimia D, et al. **2007**. *Nature* 450:1235–39.
10. Siewert C, Herber M, Hunzelmann N, Fodstad O, Miltenyi S, et al. **2001**. *Recent Results Cancer Res.* 158:51–60.
11. Wuelfing P, Borchard J, Buerger H, Heidl S, Zaenker KS, et al. **2006**. *Clin. Cancer Res.* 12:1715–20.
12. Jansen CA, De CIM, Hooibrink B, Van DBAK, van Baarle D, Miedema F. **2006**. *Blood* 107:1427–33.
13. Ramirez de Arellano E, Martin C, Soriano V, Alcamí J, Holguin A. **2007**. *Virus Genes* 34:111–16.
14. Collins DP, Luebering BJ, Shaut DM. **1998**. *Cytometry* 33:249–55.
15. Deng MQ, Cliver DO, Mariam TW. **1997**. *Appl. Environ. Microbiol.* 63:3134–38.
16. Islam D, Lindberg AA. **1992**. *J. Clin. Microbiol.* 30:2801–6.

17. Seesod N, Nopparat P, Hedrum A, Holder A, Thaithong S, et al. **1997**. *Am. J. Trop. Med. Hyg.* 56:322–28.
18. Sumi S, Arai K, Kitahara S, Yoshida KI. **2000**. *Clin. Chim. Acta* 296:111–20.
19. Mohamed H, Turner JN, Caggana M. **2007**. *J. Chromatogr. A* 1162:187–92.
20. Liang X, Xu K, Xu J, Chen W, Shen H, Liu J. **2009**. *J. Magn. Magn. Mater.* 321:1885–88.
21. Gangopadhyay NN, Shen H, Landreneau R, Luketich JD, Schuchert MJ. **2004**. *J. Immunol. Methods* 292:73–81.
22. Muscari C, Gamberini C, Carboni M, Basile I, Farruggia G, et al. **2007**. *J. Cell. Biochem.* 102:992–1001.
23. Horsman KM, Barker SLR, Ferrance JP, Forrest KA, Koen KA, Landers JP. **2005**. *Anal. Chem.* 77:742–49.
24. Gascoyne P, Mahidol C, Ruchirawat M, Satayavivad J, Watcharasit P, Becker FF. **2002**. *Lab Chip* 2:70–75.
25. Terry VH, Johnston ICD, Spina CA. **2009**. *Virology* 388:294–304.
26. Wagner C, Kotsougiani D, Pioch M, Prior B, Wentzensen A, Haensch GM. **2008**. *Immunology* 125:503–09.
27. Lee W-C, Lien K-Y, Lee G-B, Lei H-Y. **2008**. *Diagn. Microbiol. Infect. Dis.* 60:51–58.
28. Yang S-Y, Lien K-Y, Huang K-J, Lei H-Y, Lee G-B. **2008**. *Biosens. Bioelectron.* 24:855–62.
29. WHO. http://www.who.int/water_sanitation_health/gdwqrevision/watpathogens.pdf.
30. Kubota-Koketsu R, Mizuta H, Oshita M, Ideno S, Yunoki M, et al. **2009**. *Biochem. Biophys. Res. Commun.* 387:180–86.
31. El-Ali J, Sorger PK, Jensen KF. **2006**. *Nature* 442:403–11.
32. Kodituwakku AP, Jessup C, Zola H, Robertson DM. **2003**. *Immunol. Cell Biol.* 81:163–70.
33. Adams AA, Okagbare PI, Feng J, Hupert ML, Patterson D, et al. **2008**. *J. Am. Chem. Soc.* 130:8633–41.

34. Adams AA. 2008. Novel Devices and Protocols Enabling Isolation and Enumeration of Low Abundant Biological Cells from Complex Matrices. Baton Rouge: La. State Univ. 190 pp.
35. Said TM, Agarwal A, Zborowski M, Grunewald S, Glander H-J, Paasch U. **2008**. *J. Androl.* 29:134–42.
36. Zabaglo L, Ormerod MG, Dowsett M. **2000**. *Cytometry* 41:166–71.
37. Gross HJ, Verwer B, Houck D, Hoffman RA, Recktenwald D. **1995**. *Proc. Natl. Acad. Sci. USA* 92:537–41.
38. Bosma AJ, Weigelt B, Lambrechts AC, Verhagen OJHM, Pruntel R, et al. **2002**. *Clin. Cancer Res.* 8:1871–77.
39. Helo P, Cronin AM, Danila DC, Wenske S, Gonzalez-Espinoza R, et al. **2009**. *Clin. Chem.* 55:765–73.
40. Belov L, Huang P, Chrisp JS, Mulligan SP, Christopherson RI. **2005**. *J. Immunol. Methods* 305:10– 19.
41. Pappas D, Wang K. **2007**. *Anal. Chim. Acta* 601:26–35.
42. Sitar G, Brambati B, Baldi M, Montanari L, Vincitorio M, et al. **2004**. *Exp. Cell Res.* 302:153–61.
43. Balic M, Dandachi N, Hofmann G, Samonigg H, Loibner H, et al. **2005**. *Cytom. B Clin. Cytom.* 68:25–30.
44. Russell TR, McGann P, Music M, Ciocci M. **2004**. *US Patent Appl.* No. 2002–208939 2004023222.
45. Chen Z, Zhang S, Tang Z, Xiao P, Guo X, Lu Z. **2006**. *Surf. Interface Anal.* 38:996–1003.
46. Lord BI. **1997**. *WO Patent Appl.* No. 96–GB2006 9706817.
47. Hamada S, Hara K, Hamada T, Yasuda H, Moriyama H, et al. **2009**. *Diabetes* 58:1321–32.
48. Graham HA, Gorman JG, Rowell JP. **2007**. *US Patent Appl.* No. 2007–715411 2007172899.
49. Pan WJ, Haut PR, Olszewski M, Kletzel M. **1999**. *J. Hematother. Stem Cell Res.* 8:561– 64.

50. Iacone A, Quaglietta AM, D'Antonio D, Accorsi P, Dragani A, et al. **1991**. *Haematologica* 76(Suppl. 1):18–21.
51. Wagner JE Jr. **1993**. *J. Hematother.* 2:225–28.
52. Beebe DJ, Moore JS, Yu Q, Liu RH, Kraft ML, et al. **2000**. *Proc. Natl. Acad. Sci. USA* 97:13488–93.
53. Lagally ET, Simpson PC, Mathies RA. **2000**. *Sens. Actuators B* 63:138–46.
54. Mairhofer J, Roppert K, Ertl P. **2009**. *Sensors* 9:4804–23.
55. Koo OK, Liu YS, Shuaib S, Bhattacharya S, Ladisch MR, et al. **2009**. *Anal. Chem.* 81:3094–101.
56. Chang KC, Hammer DA. **1999**. *Biophys. J.* 76:1280–92.
57. Katkov II, Mazur P. **1999**. *Cell Biochem. Biophys.* 31:231–45.
58. Maheswaran S, Sequist LV, Nagrath S, Ulkus L, Brannigan B, et al. **2008**. *N. Engl. J. Med.* 359:366–77.
59. Du Z, Colls N, Cheng KH, Vaughn MW, Gollahon L. **2006**. *Biosensors & Bioelectronics* 21: 1991.
60. Heinze BC, Song J-Y, Lee C-H, Najam A, Yoon J-Y. **2009**. *Sens. Actuators B* 138:491–96.
61. Lin P, Ghetti A, Shi W, Tang M, Harvie GI, et al. **2008**. *US Patent Appl.* No. 2007–777962 2008057505.
62. Hayes DF, Smerage J. **2008**. *Clin. Cancer Res.* 14:3646–50.
63. Sardana G, Jung K, Stephan C, Diamandis EP. **2008**. *J. Proteome Res.* 7:3329–38.
64. Steeg PS. **2006**. *Nature* 12:895–904.
65. Diener JL, Hatala P, Killough JR, Wagner-Whyte J, Wilson C, Zhu S. **2006**. *WO Patent Appl.* No. 2006–US8193 2006096754.
66. Tombelli S, Minunni M, Mascini M. **2007**. *Biomol. Eng.* 24:191–200.
67. Shangguan D, Tang Z, Mallikaratchy P, Xiao Z, Tan W. **2007**. *ChemBioChem* 8:603–6.
68. Hakomori S. **1990**. *J. Biol. Chem.* 265:18713–16.

69. Harrison DJ, Manz A, Fan Z, Luedi H, Widmer HM. **1992**. *Anal. Chem.* 64:1926–32.
70. Mohamed H, McCurdy LD, Szarowski DH, Duva S, Turner JN, Caggana M. **2004**. *IEEE Trans. Nanobiosci.* 3:251–56.
71. Curry MR, Millar JD, Tamuli SM, Watson PF. **1996**. *Biol.f Reprod.* 55: 1325.
72. Matter ML, Laurie GW. **1994**. *J. Cell Biol.* 124: 1083.
73. Baek SH, Chang W-J, Baek J-Y, Yoon DS, Bashir R, Lee SW. **2009**. *Anal. Chem.* 81:7737–42.
74. Hakota M, Hibino H, Fukuda H, Shiba Y. **2009**. *Jpn. Patent Appl.* No. 2007–247809 2009077638.
75. Yoo J, Cha M, Lee J. **2008**. *Proc. NSTI Nanotechnol. Conf. Trade Show* 2:611–14.
76. Huang J-T, Wang G-C, Tseng K-M, Fang S-B. **2008**. *J. Ind. Microbiol. Biotechnol.* 35:1551–57.
77. Saito M, Horikiri S, Matsuoka H. **2003**. *Electrochemistry* 71:446–48.
78. Gascoyne PRC, Noshari J, Anderson TJ, Becker FF. **2009**. *Electrophoresis* 30:1388–98.
79. An J, Lee J, Lee SH, Park J, Kim B. **2009**. *Anal. Bioanal. Chem.* 394:801–9.
80. Hu Q, Joshi RP, Beskok A. **2009**. *J. Appl. Phys.* 106:024701.
81. Jang L-S, Huang P-H, Lan K-C. **2009**. *Biosens. Bioelectron.* 24:3637–44.
82. Wang M-W. **2009**. *J. Electrochem. Soc.* 156:G97–102.
83. Gascoyne PRC, Vykoukal J. **2002**. *Electrophoresis* 23:1973–83.
84. Becker FF, Wang X-B, Huang Y, Pethig R, Vykoukal J, Gascoyne PRC. **1995**. *Proc. Natl. Acad. Sci. USA* 92:860–64.
85. Reichmuth DS, Wang SK, Barrett LM, Throckmorton DJ, Einfeld W, Singh AK. **2008**. *Lab on a Chip* 8: 1319.
86. Labeed FH, Coley HM, Hughes MP. **2006**. *Biochim. Biophys. Acta Gen. Subj.* 1760:922–29.
87. Vykoukal J, Vykoukal DM, Freyberg S, Alt EU, Gascoyne PRC. **2008**. *Lab Chip* 8:1386–93.

88. Huang Y, Wang X-B, Becker FF, Gascoyne PRC. **1996**. *Biochim. Biophys. Acta Biomembr.* 1282:76–84.
89. Markx GH, Rousselet J, Pethig R. **1997**. *J. Liq. Chromatogr. Relat. Technol.* 20:2857–72.
90. Yang J, Huang Y, Wang X-B, Becker FF, Gascoyne PRC. **1999**. *Anal. Chem.* 71:911–18.
91. Furdui VI, Harrison DJ. **2001**. *Proc. Micro Total Anal. Syst. Symp., 5th, Monterey*, pp. 289–90. Enschede, Neth.: Kluwer Acad.
92. Beyor N, Seo TS, Liu P, Mathies RA. **2008**. *Biomed. Microdevices* 10:909–17.
93. Fu AY, Chou H-P, Spence C, Arnold FH, Quake SR. **2002**. *Anal. Chem.* 74:2451–57.
94. Simonnet C, Groisman A. **2006**. *Anal. Chem.* 78:5653–63

CHAPTER 2 CIRCULATING TUMOR CELLS: A LITERATURE REVIEW

2.1 Introduction

The first observation of blood-borne cells shed from a solid tumor was reported in the 19th century from an Australian physician named Thomas Ashworth from a patient who died of metastatic cancer.¹ Originally these cells were referred to as 'carcinocythemia,' but now they have been named circulating tumor cells (CTCs).² A fraction of these CTCs originate from the primary tumor and consequently, are one of the initial steps in the process of metastasis, whereas a majority of these CTCs are derived from metastatic lesions. Because the ultimate fate of cancer patients is largely determined by metastases and the number of CTCs is likely to reflect the aggressiveness of a tumor, CTC detection, characterization and enumeration have been considered to have great potential in the therapeutic management of cancer-related diseases.³

2.2 Anatomy of Tumor Metastasis

Metastasis is the process by which cancer cells leave the primary tumor site, disseminate and form secondary tumors at anatomically remote sites.⁴ Understanding the metastatic process is indeed a critical process in cancer fatalities; 90% of cancer patients do not die from their primary tumor, but from metastatic disease.⁵ In 1889, Paget proposed the 'seed and soil hypothesis' for understanding the process of metastasis. He proposed that metastatic spread was a consequence of particular tumor cells ('seeds') finding a suitable environment ('soil') in which to develop and grow.⁴ An alternative hypothesis, that of mechanical entrapment, was proposed by Ewing in 1928;

he suggested that CTCs accumulate through entrapment in the first vascular bed they encounter.⁴

As such, metastasis is often delineated as a 'cascade' of events (Figure 2.1), because there are a series of steps that are involved:^{4,6-8}

- (1) The development of a new blood supply to the proliferating tumor (angiogenesis).
- (2) The elude of tumor cells from the primary tumor mass.
- (3) Incursion of, and migration through, the basement membrane (BM) and extracellular matrix (ECM) surrounding the tumor epithelium and subsequent invasion of the BM supporting the endothelium of local blood vessels (or lymphatics).
- (4) Intravacation of the tumor cells into the blood vessel (or lymphatic), prior to hematogeneous (lymphagenous) dissemination to distant anatomical sites.
- (5) Adhesion of the CTCs to the endothelial cell lining at the capillary bed of the target organ site.
- (6) Incursion of the tumor cells through the endothelial cell layer and surrounding BM (extravasation) and target organ tissue.
- (7) The growth of secondary tumor foci at the target organ site.

Angiogenesis is the formation of new blood vessels from pre-existing vasculature. Without the formation of an intra-tumor blood supply, tumors would be unable to obtain the oxygen and nutrients necessary to flourish.⁷ Angiogenesis is stimulated by the release of growth factors, such as vascular endothelial growth factor (VEGF) and fibroblast growth factor (FGF).⁹ As a result of angiogenesis, tumors gain access to a blood supply in conjunction with co-option of existing blood vessels and also vasculogenicmimicry, where the tumor cells themselves carve blood vessel-like conduits.¹⁰

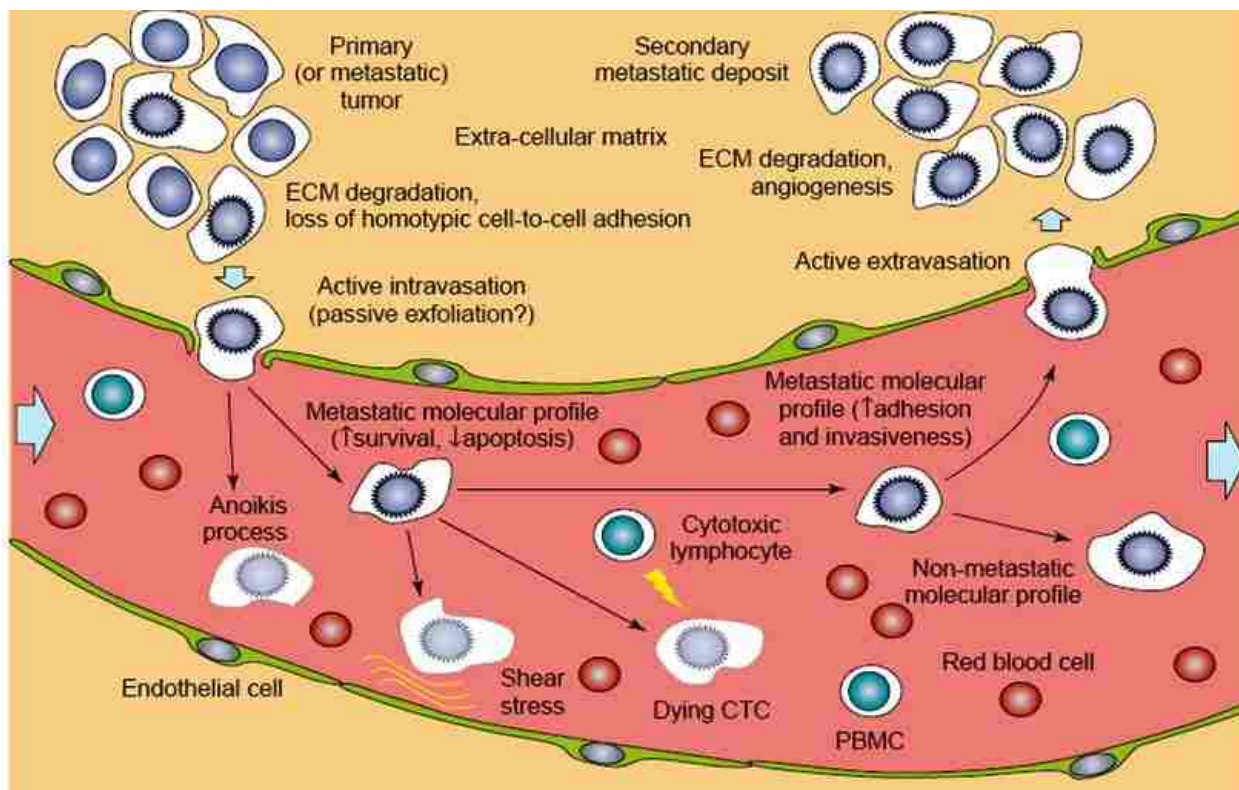


Figure 2.1 The metastatic cascade. Tumor cells are released from the primary tumor mass, and thus become circulating tumor cells (CTCs). The CTCs in the blood are subjected to the shear forces generated by the flow of blood, immune response attack and anoikis. CTCs that do survive can reach a target organ and attach to the endothelial cell lining within the capillary bed of the target site. After invading the endothelium, a secondary tumor mass can develop. Reprinted with permission.⁸

Loss of cell–cell adhesion within the primary tumor mass permits disaggregation of tumor cells and hence, aids in the initial phases of dissemination.¹¹ Cadherin/catenin expression in the primary tumor is also altered resulting in the loss of cell–cell adhesion. It has been reported that abrogation of E-cadherin is associated with the metastatic phenotype.¹² During metastasis, the dissolution of the ECM is achieved through the action of several hydrolytic enzymes, released either by the tumor cells themselves or by cells surrounding the tumor.¹³ From model systems, it has been estimated that $\sim 1 \times 10^6$ CTCs per gram of solid tumor tissue can be introduced daily into the bloodstream.⁸

Once released from the primary tumor site, many cancer cells possess the ability to migrate and do so in several different ways: (1) Moving collectively as groups or as single cells; (2) adopting an elongated mesenchymal morphology; or (3) crawling in an amoeboid manner.⁹ Tumor cells initially attach to the BM and ECM via interactions with the integrin family of adhesion receptors and subsequently traverse these structures as proteolytic enzymes help their invasion and ultimately allow the tumor cells access to the vasculature. Tumor cells also move through collagenous matrices by physically deforming their shapes.¹⁴

The endothelial cells can retract, thus allowing the detached tumor cells to pass into systemic circulation. Once tumor cells are in the blood stream, they are subject to events which can threaten their survival including the shear forces generated by the flow of blood and an immune response attack.¹⁵ Upon being shed, the CTCs are fragile and lack interactions with blood borne fibrin and platelets and as a result, the membrane can be easily destroyed by shear stress imparted by blood flow.¹⁶ In addition, natural killer cells, Pit cells and Kupffer cells, attack the neoplastic cells immediately upon release.^{17,18} It has been reported that the presence of CTCs in the peripheral blood triggers as much as an 80% increase in the number of natural killer cells present within peripheral blood in a matter of minutes. As such, the vast majority of carcinoma cells are killed within a few hours of dissemination through the natural defense system.¹⁹ Also, most tumor cells are either mechanically destroyed from the shear stress of blood flow rupturing the cells' membrane or the CTC undergoes a process called anoikis, a special form of cell death resulting from an adhesion deficiency.²⁰ Single tumor cells are more likely to be destroyed compared to cells travelling in clumps because the cells at the center of the complex are physically shielded.²¹

Most often, tumors develop in organs proximal to capillary beds owing in part to metastatic CTCs surviving the natural protections provided by the circulatory system. Survival is further supported by the CTCs developing a protective barrier consisting of fibrin and platelets sufficient to prevent lysis from blood flow related shear by providing a stabilizing reinforcement and barrier-like protective coating from natural killer cells.

Surviving CTCs can eventually reach the capillary bed of a target organ, where they can adhere to the micro-vessel endothelium, which stimulates endothelial cell retraction. The CTCs pass through the BM via the action of proteases and thus, establishing a secondary tumor at a new site. Once tumor cells reach the secondary site, they may be destroyed – most undergo apoptosis within 24 h, may lie dormant, or they may proliferate to form secondary tumors. It has been recently revealed that CTCs can reach the peripheral blood from tumor deposits every few hours and can remain there for as long as 22 years.⁸ Recent evidence suggests that tumor cell dormancy may account for the observation that some tumors – for example, melanoma and breast cancer – may present metastases many years after eradication of the primary tumor.⁷

It has been suggested that distant sites may be pre-conditioned to become fertile ground for the establishment of metastases; the ‘metastatic niche’. Hematopoietic stem cells migrate to tissues causing remodeling of the ECM and growth factor milieu, such that a microenvironment is formed that both attracts tumor cells and supports their proliferation.²²

2.3 Morphology of CTCs

Both solid tumor cells (STCs) and cultured CTCs have been found to have irregular nuclei. Many CTCs exhibit conspicuous intracellular compartments containing numerous small vesicles and large amounts of amorphous material. They are also

surrounded by a ribosome decorated membrane. These inclusions may have a size equal to or exceeding that of the nucleus and are not seen in STCs. CTCs have a significantly larger mean cell diameter (CTC-15 μm) and cell volume (CTC-1730 μm^3) compared to STCs (STC-11 μm , STC-735 μm^3 , respectively). In contrast, STCs have a larger nuclear/cytoplasmic (N/C) ratio (CTCs-27.1%, STCs-28.9%) and 'excess' membrane (CTCs-46.8%, STC-60.9%).²³

The deformability of STCs and CTCs differ significantly as well. Small deformations are rapid and of similar magnitudes for both cell types, but large deformations are considerably slower in the case of CTCs. Microscopic observations indicate that CTCs' large nucleus resists deformation. In addition, it has been speculated that the large, multi-vesicular intracellular accumulations of CTCs contribute to their low cytoplasmic deformability.²⁴

Marrinucci et al. investigated the morphology of CTCs using metastatic breast cancer cells. They observed different subcategories of CTCs within the same patient's blood sample. It was discovered that 22.9% of CTCs had a higher N/C ratio than the surrounding white blood cells (WBCs) (Figure 2.2). They also exhibited a scant rim of amphophilic to eosinophilic cytoplasm with round to oval to occasionally lobated nuclei without sharp irregularities. The chromatin was vesicular with prominent, generally eosinophilic nucleoli. This category of CTCs was termed well-differentiated adenocarcinoma cells.²⁵ In addition, their eccentrically located nuclei were slightly smaller than neighboring WBC nuclei. The chromatin was often coarse and hyperchromatic in these CTCs with a moderate rim of dense appearing orangeophilic

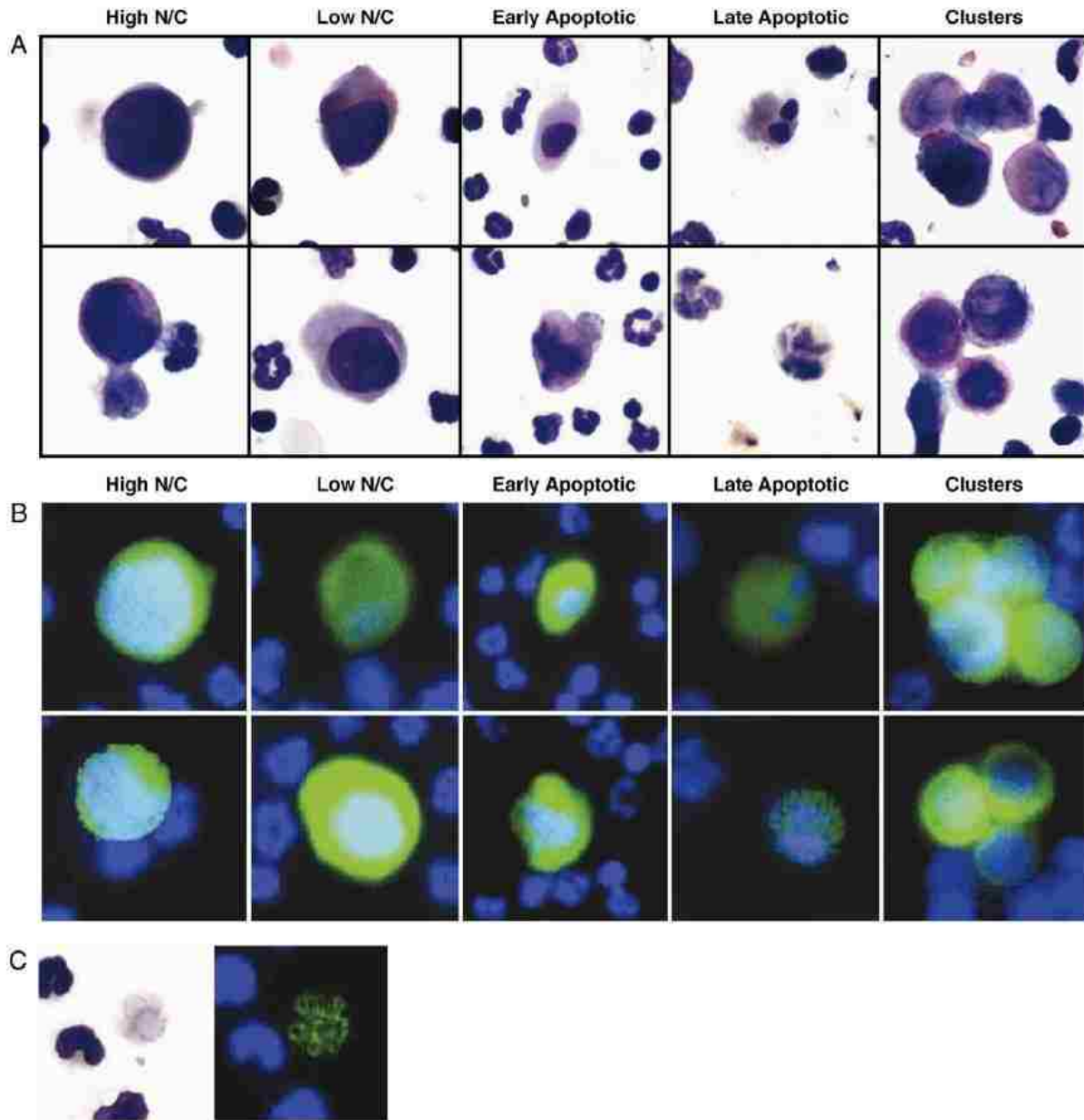


Figure 2.2 Example of CTC types identified from the patient with breast cancer. **(A)** Wright-Giemsa–stained CTCs (100x oil). **(B)** Same cells as **(A)** showing initial fluorescent image of corresponding CTCs stained with anti-CK-Alexa Fluor 488 (green) and DAPI (4',6-diamidino-2-phenylindole) (blue) (image taken at 20 and enlarged for comparison purposes). **(C)** Example of probable CTC undergoing final stages of apoptosis, with no detectable nucleus. These events are not counted as CTCs in our patient statistics. Reprinted with permission.²⁵

cytoplasm. This category of cells meets the cytological criteria for moderately to well-differentiated adenocarcinoma cells.²⁶ 31.9% and 34.7% of the total CTC population exhibited morphologic evidence of both early- and late-stage apoptosis (Figure 2.2),

respectively. Early apoptotic changes included condensation and shrinkage of nuclear material yielding hyperchromatic glassy-appearing nuclei with loss of nuclear detail on Wright-Giemsa staining.^{26,27} Also, clusters of CTCs were noted with a 4% frequency. Ten doublets, one triplet, and one quartet were observed by Marrinucci et al. The composition within clusters was a heterogeneous mixture of cell types.²⁵

2.4 Biomarkers Found in CTC Membranes

CTCs express two distinct marker types on their membrane, which are tumor type-specific and epithelial-specific markers. Tumor type-specific markers are expressed exclusively on tumor cells that have disseminated from a particular tumor.²⁸ Markers of this type include mammoglobin, HER2-neu, mucin 1 (breast cancer), prostate specific antigen (prostate cancer), and carcinoembryonic antigen (colorectal and gastric cancers).^{3,29} Although these types of markers may offer the potential advantages of specifically identifying a particular organ tumor cell rather than just epithelial cells, they also provide some insight into their molecular characteristics.

Epithelial-specific markers are expressed by all tumor cells of epithelial origin as well as by normal epithelial cells, although they are unlikely to be present in the peripheral blood stream. The most commonly used markers in this category include the epithelial cell adhesion molecule (EpCAM, also known as ESA, CD326, HEA125, TROP II, or TACSTD1) and cytokeratins (CK) 7, 8, 18, 19, and/or 20.³⁰ The majority of leukocytes do not express epithelial markers, however, they occasionally have been observed to become positive for such antigens when in an activated state.^{3,31}

2.5 Abundance of CTCs in Cancer Patients

Allard et al. evaluated the abundance of CTCs in the blood of healthy subjects and patients with a variety of malignant diseases (Table 2.1).³² The number of CTCs in metastatic cancer patients ranged from 0 to 23,618 in 7.5 mL of patient's blood. The

Table 2.1 Summary of CTC counts in 7.5 mL of blood from patients with various types of carcinomas

	No. of patients	No. of specimens	Mean \pm SD	Median with ≥ 2	No. (%) ≥ 2	No. (%) ≥ 5	No. (%) ≥ 10	No. (%) ≥ 50
Subject								
Healthy	145	145	0.1 \pm 0.2	N/A	0(0)	0(0)	0(0)	0(0)
Nonmalignant	199	199	0.1 \pm 0.3	3	1(1)	0(0)	0(0)	0(0)
Metastatic cancer type								
Prostate cancer	123	188	75 \pm 333	13	107(57)	77(41)	61(32)	27(14)
Unknown cancer	11	27	16 \pm 35	13	14(52)	13(48)	8(30)	2(7)
Ovarian cancer	29	53	6 \pm 16	9	20(38)	12(23)	1(23)	9(17)
Breast cancer	422	1316	84 \pm 885	10	489(37)	340(26)	256(19)	129(10)
Gastric cancer	9	13	24 \pm 83	3	4(31)	1(8)	1(8)	1(8)
Colorectal cancer	196	333	4 \pm 11	5	99(30)	56(17)	30(9)	5(2)
Bladder cancer	7	7	42 \pm 107	146	2(29)	2(29)	1(14)	1(14)
Renal cancer	11	12	1 \pm 1	2	3(25)	0(0)	0(0)	0(0)
;Lung cancer	99	168	30 \pm 178	9	34(20)	24(14)	16(10)	10(6)
Pancreatic cancer	16	21	2 \pm 6	3.5	4(19)	1(5)	1(5)	0(0)
Assorted other cancer	41	45	1 \pm 4	11	5(11)	4(9)	3(7)	0(0)
Combined cancers	964	2183	61 \pm 696	9	781(36)	530 (24)	386 (18)	176(8)

NOTE. The group labeled unknown are patients with metastatic disease with unknown primary tumor; the assorted others are carcinomas with <5 specimens.

Abbreviation: N/A, not applicable. Reprinted with permission.³²

highest proportion of positive specimens was seen in patients with metastatic prostate cancer, followed by patients with metastatic cancer of unknown origin, ovarian cancer, and breast cancer.³³ The presence of CTCs and the mean number of CTCs varied widely in samples. Differences in carcinomas, vascularization of the tumors, sites of metastasis, and aggressiveness of the tumor were factors that contribute to these differences.³⁴

It has also been found that the CTC frequency varies highly depending on the form of therapeutic treatment. Studies carried out on pancreatic and colorectal cancer patients indicated that decreases in CTC numbers were seen immediately after surgery.³⁵ By contrast, radiofrequency ablation of liver secondaries led to an immediate increase in CTC number and there was speculation that coagulative necrosis caused by the energy waves might induce cancer cell seeding.³⁶

Correlation between CTC number and the response of the primary tumor to chemotherapy was not observed, which is unusual given the fact that CTCs levels are normally correlated to treatment response.³⁷ This observation was explained by the discovery that CTCs can be different from the primary tumor in terms of their genome and protein expression patterns, such as p53 mutations and expression of Bcl-2, heat shock proteins, topo-isomerase II-a, ER/PR, and HER2.³⁸ For example, a subset of patients with HER2-negative primary tumors developed HER2-positive CTCs during disease progression and this change might have consequences as to the response of the tumor cells to therapy.³⁰

2.6 Clinical Significant of CTCs

Elucidating the presence and number of CTCs in peripheral blood is emerging as an effective tool for differential diagnosis and prognosis, risk determination, disease recurrence, screening, and prediction of specific benefits from particular therapies for the management of cancer-related diseases.²⁰ Moreover, the growing ability to detect and analyze CTCs could galvanize the development of drugs designed to block metastasis. Compared to waiting for secondary tumors to appear, monitoring CTC numbers may provide a simple way to determine whether an anti-metastasis drug works for a particular patient.³⁰

The initial primary tumor specimen may not always be representative of metastatic deposits. A primary example is prostate cancer, which often presents itself with multifocal localized disease and may recur many years later with bony lesions that are not readily biopsied.³⁹ CTCs can reflect the molecular changes in a person's cancer that would point toward particular and effective treatments (*i.e.*, personalized medicine). For example, only women with breast cancer whose tumor cells express the receptor HER2 respond to the drug Herceptin. It has been found that some women whose primary tumors were HER2-negative later had CTCs that were positive for HER2, suggesting their cancer had mutated.⁴⁰ Monitoring CTCs might therefore identify women who were initially ineligible for Herceptin but who would later qualify for the drug. These important observations support the argument that the detection of CTCs and determination of their gene amplification, mutation or expression can be used for better tailoring therapies.

Researchers have also begun to analyze CTCs for certain gene variants or proteins that indicate a patient's tumor is susceptible to a particular drug.⁴¹ This kind of "liquid biopsy," will allow physicians to follow cancer changes over time and tailor the treatments. Also driving the interest in CTCs has been the recent development of molecularly targeted cancer therapies that work best on patients whose tumors have a particular mutation.⁴²

Receptor profiles of tumors change over time; it was noted that epidermal growth factor receptor (EGFR) is consistently expressed in CTCs for patients with metastatic breast cancer.⁴³ In patients with non-small cell lung cancer, EGFR-activating mutations have been detected in CTCs as well, including the T790M mutation that confers drug resistance. The ability to stain CTCs directly for a variety of markers and potentially

analyze the mutations within them could enable therapeutic trials to be designed with CTC-based endpoints.³⁹

It was recently reported that highly tumorigenic cells possessing properties consistent with those of stem cells can be isolated from human cancers. These cancer stem cells may be detectable in the peripheral blood and bone marrow of patients.⁴⁴ The identification of these CTC subpopulations is likely to further the discovery of tumor stem-cell biomarkers and help resolve the issue of what exactly a cancer stem cell is. Hence, the development of therapies specifically targeting cancer stem cells will have great benefit for patients.

2.7 Statistical Considerations for CTC Analysis

The success of rare CTC detection is affected by many parameters, including quality of the starting sample, frequency of the events of interest, sample preparation, specificity and expression level of the chosen markers, robustness of the assay, and objective and reproducible readouts.²⁹ All of these factors contribute to the statistical probability of accurately detecting and quantifying CTCs and therefore, are important to consider when designing and interpreting CTC assays for clinical use.

The CellSearch™ system employs the Kaplan-Meier statistic for the interpretation of CTC counts at baseline and follow-up blood collections of the patient (Figure 2.3). The survival curves are compared using log-rank testing and cox proportional hazards regression to determine univariate and multivariate hazard ratios for overall survival.^{45,46} For example, a threshold of 5 CTC/7.5 mL was used to stratify patients with metastatic breast cancer into those with favorable outcomes (CTC <3 or <5) and those with unfavorable outcomes (CTC ≥3 or ≥5). These statistical outcomes on CTC levels were used to predict survival, therapeutic benefits and stratify patients into

low-risk, moderate-risk, and high-risk groups (Figure 2.3).³⁵ It was found that both univariate and multivariate analysis of CTC levels were significantly correlated with overall survival.^{47,48}

In most cases, Poisson statistics apply when accounting for randomly distributed CTCs due to limitations with the volume of blood that can be sampled. Another important consideration is whether the blood sample volume is large enough to detect

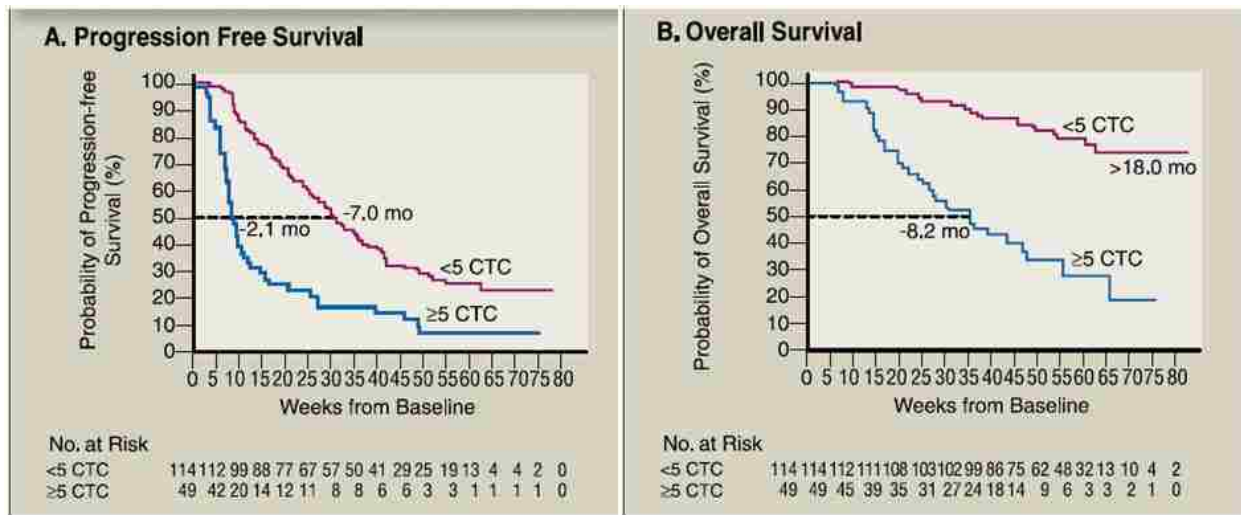


Figure 2.3 Kaplan-Meier estimates of probabilities of progression-free survival and overall survival in patients with metastatic breast cancer for those with <5 CTCs per 7.5 mL of whole blood and those in the group with >5 CTCs in 7.5 mL of whole blood at the first follow-up visit after initiation of a newline of therapy. All patients in the trial ($n=177$) are included in these Figures. **(A)** progression-free survival from baseline. **(B)** overall survival from baseline. Reprinted with permission.³⁵

and enumerate a very small number of CTCs.²⁹ For cell-based assays, the size of sample (n) that will provide a given precision is given by;²⁸

$$n = \frac{(100)^2}{CV} (1)$$

where CV is the coefficient of variation of a known positive control. From the perspective of CTCs, to reduce the CV to $\sim 10\%$ (and hence improve the accuracy), many events would need to be assessed. Therefore, analysis of multiple blood samples

from the same patient at the same time significantly improves the probability of accurately detecting rare CTCs.

These statistical factors also suggest that some caution should be employed when using a threshold number (i.e., ≥ 5 CTC versus < 5 CTCs) to stratify cancer patients into poor prognosis versus good prognosis groups for the purposes of clinical decision making. From a statistical point of view, there is a higher probability of correctly identifying CTCs when > 5 are detected, and/or there is a greater probability of incorrect identification when 1–4 CTCs are detected.⁴⁸

2.8 Conclusions

CTC presence is one of several crucial steps in the metastatic process of solid malignancies. CTCs are detected in peripheral-blood samples, which are easy to obtain (with minimal discomfort for patients) compared with other sites, such as bone marrow and lymph nodes, where minimal residual disease might be present. Therefore, the detection of CTCs is emerging as an attractive strategy for tailoring cancer treatment on a single-patient basis. Because metastatic cells can have a very different molecular profile from the solid tumor of origin, sensitivity to conventional chemotherapeutic drugs and molecularly targeted anticancer agents might be better tested in CTCs than in the primary tumor. Accordingly, any advance in the knowledge of CTC biology might lead to significant progress in both anticancer drug development and better definition of patient diagnosis and prognosis.

However, many investigators have reported a positive correlation between detection of CTCs and patient diagnosis and prognosis, but the number of clinical trials enrolled in each case is low (50-1,000 patients). Therefore, implementation of CTC detection in biological studies of large-scale clinical trials must prove the prognostic

power of CTC detection. In addition, CTCs are low-abundance cells scattered among millions of peripheral-blood mononucleated cells. The application of novel technologies, such as high-throughput technologies, single-cell genomics and proteomics must fulfill the promise of comprehensively describing the molecular signature of CTCs of solid malignancies. Dissection of CTC biology should define the molecular profile of those CTCs that can metastasize. These insights should enable investigators to identify an ideal marker (or set of markers) to detect only prognostically informative CTCs and/or to design more effective anticancer drugs.

2.9 References

1. Ashworth, T. *Aust. Med. J.* **1869**, 14, 146.
2. Carey RW, TP., Bennett, JM. *Am. J. Med.* **1976**, 60, 273.
3. Sleijfer, S.; Gratama, J-W.; Sieuwerts, AM.; Kraan, J.; Martens, JWM.; Foekens, JA. *Euro. J. Cancer* **2007**, 43, 2645.
4. Brooks, SA.; Lomax-Browne, HJ.; Carter, TM.; Kinch, CE.; Hall, DMS. *Acta Histochem.* **2010**, 112, 3.
5. Klaus, P., Catherine A-P. *Cell* **2010**, In press.
6. Fidler, IJ. *J. Natl. Cancer Inst.* **1970**, 45, 773.
7. Chambers, AF.; Groom, AC.; MacDonald, IC. *Nature Rev. Cancer* **2002**, 2, 563.
8. Mocellin, S.; Keilholz, U.; Rossi, CR.; Nitti, D. *Tren. Mole. Med.* **2006**, 12, 130.
9. Blood, CH.; Zetter, BR. *Biochim. Biophys. Acta, Rev. Cancer* **1990**, 1032, 89.
10. Hendrix, MJC.; Seftor, EA.; Kirschmann, DA.; Quaranta, V.; Seftor, REB. *Annal. NY Acad. Sciences* **2003**, 995, 151.
11. Cavallaro, U.; Christofori, G. *Nature Rev. Cancer* **2004**, 4, 118.
12. Perl, A-K.; Wilgenbus, P.; Dahl, U.; Semb, H.; Christofori, G. *Nature* **1998**, 392, 190.
13. Price, JT.; Bonovich, MT.; Kohn, EC. *Crit. Rev. Biochem. Mole. Biol.* **1997**, 32, 175.

14. Friedl, P.; Wolf, K. *Cancer Res.* **2008**, 68, 7247.
15. Dietmaier, W.; Hartmann, A.; Wallinger, S.; Heinmoller, E.; Kerner, T.; Endl, E.; Jauch, K-W.; Hofstadter, F.; Ruschoff, F. *Cancer* **1999**, 154, 83.
16. Gassmann, P.; Haier, J. *Clin. Exp. Metastasis* 2008, 25, 171.
17. Wisse, E.; van't Noordende, JM.; van der Meulen, J.; Daems, WT. *Cell Tissue Res.* **1976**, 173, 423.
18. Wiltrout, RH. *Immunol. Rev.* **2000**, 174, 63.
19. Timmers, M.; Vekemans, K.; Vermijlen, D.; Asosingh, K.; Kuppen, P.; Bouwens, L.; Wisse, E.; Braet, F. *Int. J. Cancer* **2004**, 112, 793.
20. Logothetis, CJ.; Navone, NM.; Lin, S-H. *Clin. Cancer Res.* **2008**, 14, 1599.
21. Nash, GF.; Turner, LF.; Scully, MF.; Kakkar, AK. *Lancet Oncol.* **2002**, 3, 425.
22. Kaplan, RN.; Riba, RD.; Zacharoulis, S.; Bramley, AH.; Vincent, L.; et al. *Nature* **2005**, 438, 820.
23. Nannmark, U.; Johansson, BR.; Bagge, U. *Clin. Exp. Metastasis* **1991**, 9, 119.
24. Neri, A.; Nicolson, GL. *Int. J. Cancer* **1981**, 28, 731.
25. Marrinucci, D.; Bethel, K.; Bruce Richard, H.; Curry Douglas, N.; Hsieh, B.; et al. **2007** Case study of the morphologic variation of circulating tumor cells.
26. Mehes, G.; Ambros, P. F.; Gadner, H. *Haematologia* 2001, 31, 97.
27. Schmidt, H.; De Angelis, G.; Bettendorf, O.; Eltze, E.; Semjonow, A.; et al. *Int. J. Biol. Markers* **2004**, 19, 93.
28. Allan Alison, L.; Keeney, M. *J. Oncol.* **2010**, 2010, 426218.
29. Tibbe Arjan, GJ.; Miller, MC.; Terstappen Leon, WMM. *Cytometry. Part A: J. Int. Soc. Anal. Cytol.* **2007**, 71, 154.
30. Pantel, K.; Brakenhoff, RH.; Brandt, B. *Nature Rev. Cancer* **2008**, 8, 329.
31. Jung, R.; Kruger, W.; Hosch, S.; Holweg, M.; Kroger, N.; Gutensohn, K.; Wagener, C.; Neumaier, M.; Zander, AR. *Br. J. Cancer* **1998**, 78, 1194.
32. Allard, WJ.; Matera, J.; Miller, MC.; Repollet, M.; Connelly Mark, C.; et al. *Clin. Cancer Res.* **2004**, 10, 6897.

33. Meng, S.; Tripathy, D.; Shete, S.; Ashfaq, R.; Saboorian, H.; et al. *J. Proc. Natl. Acad. Sciences USA* **2006**, 103, 17361.
34. Cristofanilli, M.; Hayes DF.; Budd, GT.; Ellis MJ.; Stopeck, A.; et al. *J. Clin. Oncol.* **2005**, 23, 1420.
35. Cristofanilli, M.; Budd, GT.; Ellis, MJ.; Stopeck, A.; Matera, J.; et al. *New Eng. J. Med.* **2004**, 351, 781.
36. Jiao Long, R.; Apostolopoulos, C.; Jacob, J.; Szydlo, R.; Johnson, N.; et al. *J. Clin. Oncol.* **2009**, 27, 6160.
37. Xenidis, N.; Ignatiadis, M.; Apostolaki, S.; Perraki, M.; Kalbakis, K.; et al. *J. Clin. Oncol.* **2009**, 27, 2177.
38. Hayes, D. F.; Cristofanilli, M.; Budd, GT.; Ellis, M J.; Stopeck, A.; et al. *Clin. Cancer Res.* **2006**, 12, 4218.
39. Maheswaran, S.; Haber, DA. *Curr. Opin. Gen. Dev.* **2010**, 20, 96.
40. Shin SJ.; Hyjek, E.; Early, E.; Knowles DM. *Intl. J. Surg. Pathol.* **2006**, 14, 279.
41. Xi, L.; Nicastrì, DG.; El-Hefnawy, T.; Hughes, SJ.; Luketich, JD.; Godfrey, TE. *Clin.Chem.* **2007**, 53, 1206.
42. Yang, J.; Mani, SA.; Weinberg, RA. *Cancer Res.* **2006**, 66, 4549.
43. Payne, RE.; Yague, E.; Slade, MJ.; Apostolopoulos, C.; Jiao, LR.; et al. *Pharmacogenomics* **2009**, 10, 51.
44. Al-Hajj, M.; Wicha, MS.; Benito-Hernandez, A.; Morrison, SJ.; Clarke, MF. *Proc. Natl. Acad. Sciences USA* **2003**, 100, 6890.
45. Miller, MC.; Doyle Gerald, V.; Terstappen LWMM. *J. Oncol.* **2010**, 2010, 617421.
46. Hayes, DF.; Smerage, J. *Clin.Cancer Res.* **2008**, 14, 3646.
47. Cohen SJ.; Punt CJA.; Iannotti, N.; Saidman BH.; Sabbath KD.; et al. *J. Clin. Oncol.* **2008**, 26, 3213.
48. de Bono, JS.; Scher, HI.; Montgomery, RB.; Parker, C.; Miller, MC.; et al. *Clin. Cancer Res.* **2009**, 15, 1506.

CHAPTER 3 HIGHLY EFFICIENT CAPTURE AND ENUMERATION OF LOW-ABUNDANT PROSTATE CANCER CELLS USING PROSTATE-SPECIFIC MEMBRANE ANTIGEN APTAMERS IMMOBILIZED TO A POLYMERIC MICROFLUIDIC DEVICE*

3.1 Introduction

Prostate cancer is the most common non-cutaneous malignancy, accounting for 9% of all male cancer-related deaths in the US; there is a 1 in 6 probability of men in the US developing prostate cancer.^{1,2} In 2007, ~220,000 new cases of prostate cancer were recorded and 27,050 prostate cancer related deaths occurred in the US alone.³ For more than a decade, determinations of prostate-specific antigen (PSA) levels in human serum followed by digital rectal examination have been the predominate diagnostic methods for prostate cancer screening.⁴ Men with an abnormal digital rectal examination, as evidenced by the existence of polyps, or elevated PSA levels are typically referred for biopsy to assess the presence of prostate cancer. The five-region prostate biopsy technique is typically utilized in conjunction with a sextant biopsy.⁵ Using these rather invasive diagnostic strategies, up to 30% of prostate cancers are still undiagnosed.⁶ Unfortunately, certain medications (e.g. Finasteride), ejaculation, and prostate manipulation (e.g. catheterization, prostate massage) can alter PSA levels and as such, the determination of PSA levels in clinical settings remains controversial.⁴

Mortalities associated with malignant tumors are primarily due to metastasis, which results from the invasion of tissues and organs distant from the primary tumor.⁷ The early detection of metastasis is a critical factor for determining the probability of survival for many cancers.⁸ At present, reports have noted that circulating tumor cells (CTCs) can be present in peripheral blood for many adenocarcinomas prior to detection

* Reproduced with permission from *Electrophoresis*

of the primary tumor via conventional screening modalities.⁹ Therefore, elucidating the presence and number of CTCs in peripheral blood is emerging as an effective tool for risk determination, screening, differential diagnosis and prognosis, disease recurrence, and prediction of specific benefits from particular therapies for the management of cancer-related diseases.¹⁰

CTCs are an extremely rare component within human blood ($\sim 10^1$ cells mL^{-1} of whole blood) with the majority cellular components being erythrocytes ($\sim 10^9$ cells mL^{-1} of whole blood) and leukocytes ($\sim 10^6$ cells mL^{-1} of whole blood).¹¹ To discriminate CTCs from these highly abundant species, morphological or chemical differences between the target CTCs and normal hematopoietic components have been exploited,¹² but typically provide low recovery and/or purity.

Disseminated prostate tumor cells can infiltrate the bone marrow, peripheral blood, lymph nodes, stomach, or the penis and the question becomes; can these disseminated tumor cells be used as a clinical marker for prostate cancer staging? Certain cell lines derived from prostate cancers can be used as model systems for the design and evaluation of new assays directed toward prostate cancer using for example CTCs as the diagnostic marker. These cell lines are categorized as to their final metastatic destination, such as bone metastasis – PC3, lymph node metastasis – LNCaP, and those localized to prostate – 22Rv1.¹³ Lymph node based metastasis occur in the very early stages of prostate cancer where high cure rates abound, whereas bone metastasis typically occur in the advanced stages of this disease and is accompanied by significantly reduced quality of life.¹⁴ It has been hypothesized that tumor cells released from a primary tumor site into peripheral blood can be correlated with patient survival or other indicators, such as the presence of regional lymph node metastases.

But the use of CTCs as a diagnostic marker is unclear due to the lack of efficient tools for their isolation and enumeration.¹⁵ Therefore, the development of highly efficient CTC isolation and detection systems to search peripheral blood for LNCaP type cells can potentially generate an effective diagnostic/prognostic tool for prostate cancer.

LNCaP-like cells typically possess a high-expression level of the integral membrane protein, prostate-specific membrane antigen (PSMA). PSMA is a homodimeric type II transmembrane glycoprotein consisting of 750 amino acids having a molecular weight of 100 kDa,¹⁶ making PSMA an excellent candidate for tracking LNCaP-type cells to diagnose prostate cancer or to monitor its progression and/or therapeutic response to treatment.^{17–19}

Due to the low abundance nature of CTCs in peripheral blood with respect to erythrocytes and leukocytes, the efficiency of CTC isolation is basically characterized by throughput, recovery and purity.²⁰ Until now, different techniques, such as flow assisted cell sorting and immunomagnetic selection have been employed for the isolation of rare cells from complex clinical samples and are typically fraught with the limitation of choosing between high purity with poor recovery or high recovery with low purity.^{21,22}

While microfluidic systems are emerging as effective tools for biomedical research and diagnostics having such advantages as low reagent consumption, short analysis times and process integration,²² they are fraught with some limitations, for example the inability to exhaustively sample large input volumes required to search for extremely rare events, such as CTCs in peripheral blood. Two recent examples have appeared in which rare cellular events were accumulated from clinical samples using a microfluidic platform. Nagrath et al. described an immunoaffinity approach in which anti-epithelial cell adhesion molecules (EpCAM) antibodies were affixed to micropillars

poised within a microfluidic chip capable of extracting CTCs from peripheral whole blood samples with ~50% purity.¹¹ A polymer-based high-throughput microfluidic system was described by Adams et al. in which EpCAM-specific monoclonal antibodies were tethered to parallelized-high-aspect ratio microchannels, which were employed to isolate breast cancer cells (MCF-7) from whole blood demonstrating a recovery of 97% and nearly 100% purity.²⁰ A compelling attribute of this microfluidic device was its ability to specifically enumerate the CTCs on-chip using an integrated conductivity sensor, which demonstrated a single-cell detection efficiency of 100% without requiring cell labeling.²⁰

Though various techniques have been applied to isolate and characterize CTCs, many of them share a similar principle, they use antibody-based selection with integral membrane protein antigens. Application of this molecular recognition strategy for CTC detection is limited by the availability and specificity of antibodies directed against the necessary biomarkers, such as membrane proteins found on different tumor cells.⁹ In addition, most of these cell selection tools require surface immobilization of an antibody, which can result in reduced cell recoveries or adhesion strength between the cell and the surface-tethered antibody due to the stochastic nature of the immobilization chemistry.

Aptamers, single-stranded nucleic acid oligomers, possess highly specific recognition affinities to molecular targets through interactions other than classical Watson-Crick base pairing.²³ Compared with antibodies, aptamers have lower molecular weights, demonstrate faster tissue penetration, remain stable during long-term storage, sustain reversible denaturation, low toxicity, and can be produced against targets, such as membrane proteins, using highly automated technologies (i.e.

SELEX).²⁴ In addition, a wealth of literature exists on the immobilization of aptamer recognition elements to solid supports, such as glass,²⁵ polymers,²⁶ and gold.²⁶ Additionally, the immobilization chemistry is highly oriented with end-point attachment occurring exclusively through the 5'- or 3'-end of the aptamer, which bears a functional group, such as a primary amine. These advantages make aptamers highly desirable as potential molecular probes for diagnostics.²⁷

Many aptamers have been developed to target the extracellular domains of integral membrane proteins that are over-expressed on cancer cells.²⁸ Lupold et al. first reported RNA aptamers directed against the tumor-associated PSMA membrane antigen and the first application of RNA aptamers that targeted LNCaP cells via the PSMA biomarker. The affinity of this aptamer for PSMA was quantified and suggested that the aptamer identified a unique extra-cellular domain of PSMA.²⁹

Herein, we report on the use of PSMA-specific aptamers tethered to a high-throughput micro-sampling unit (HTMSU) with an integrated conductivity sensor employed for the highly efficient isolation and enumeration of rare circulating prostate tumor cells (LNCaP used as a model in these studies) from whole blood without the need for preprocessing of the blood prior to introduction into the microfluidic device nor staining of the CTCs for enumeration. Nuclease stabilized and in vitro generated RNA aptamers were immobilized onto ultraviolet (UV)-modified curvilinear capture channels comprising the capture bed contained within the microfluidic device using carbodiimide coupling chemistry and the appropriate linker structure to enhance the accessibility of the surface-bound aptamer to the solution-borne cells.³⁰ The linear velocity of sample introduction into the device was optimized in order to achieve high-CTC recovery from blood. After selection and isolation, the captured cells could be released from the

capture surface via enzymatic digestion of the extra-cellular domain of PSMA using trypsin for subsequent conductivity enumeration.²⁰ Recently, Phillips et al. has reported on the use of aptamers decorating PDMS microchannel walls for the selection of T-cell acute lymphocytic leukemia cells seeded in an aqueous buffer that was also loaded with a noncancerous cell line.³¹ Unfortunately, this work did not use whole blood as the input sample, which contains extremely high levels of interfering cells and the cell concentration was much higher ($\sim 1 \times 10^6$ cells mL^{-1}) than typically encountered for CTCs found in clinical samples (~ 10 cells mL^{-1}). The results reported here used whole blood as the input with CTC concentrations as small as 10 cells mL^{-1} .

3.2 Materials and Methods

3.2.1 Buffers and Reagents

PMMA was used as the HTMSU substrate and cover plate (0.5 mm thickness) and were purchased from Good Fellow (Berwyn, PA). Platinum wires for the conductivity sensor were purchased from Alfa Aesar (Boston, MA). Polyimidecoated fused silica capillaries were purchased from Polymicro Technologies (Phoenix, AZ). Chemicals used for the PMMA surface cleaning and modification included reagent grade isopropyl alcohol, 1-ethyl-3-[3-dimethylaminopropyl] carbodimide hydrochloride (EDC), N-hydroxysuccinimide (NHS), fetal bovine serum and 2-(4-morpholino)-ethane sulfonic acid (MES) and these were purchased from Sigma-Aldrich (St. Louis, MO). The nuclease-resistant RNA aptamer, $(\text{NH}_2-(\text{CH}_2)_6-(\text{OCH}_2\text{CH}_2)_6-(\text{ACCAAGACCUGACUUCUAACUAAGUCUACGUUCC})$, was obtained from Eurogentec (San Diego, CA). Random sequence oligonucleotides were obtained from Integrated DNA Technologies (Coralville, IA). Monoclonal anti-EpCAM antibody was obtained from R & D Systems (Minneapolis, MN). The LNCaP (prostate cancer cell line), MCF-7 (breast cancer cell line), growth media, HEPES buffer, PBS and

trypsin were all purchased from American Type Culture Collection (Manassas, VA). Citrated rabbit blood was purchased from Colorado Serum Company (Denver, CO). Tris-glycine buffer was obtained from Bio-Rad Laboratories (Hercules, CA). All solutions were prepared in nuclease-free water, purchased from Invitrogen (Carlsbad, CA). Nuclease-free microfuge tubes were purchased from Ambion (Foster City, CA) and were used for preparation and storage of all samples and reagents. A fluorescein derivative, PKH67, which contained a lipophilic membrane linker for cell staining, was purchased from Sigma-Aldrich.

3.2.2 Cell Suspensions

LNCaP and MCF-7 cells were cultured to 80% confluence in Dulbecco's Modified Eagle's Medium supplemented with high glucose containing 1.5 g L^{-1} sodium bicarbonate (NaHCO_3), 15 mM HEPES buffer, and 10% fetal bovine serum. A 0.25% trypsin solution was prepared in 150 mM PBS and used to harvest the LNCaP and MCF-7 cells from the culturing plate.

LNCaP and MCF-7 cells were stained with PKH67 for microscopic visualization experiments using fluorescence. A modified protocol for cell staining was implemented whereby the dye concentration was increased twofold resulting in more evenly distributed fluorescent labels over the cell's periphery. Cell counts for seeding experiments into whole blood were determined by counting three aliquots of cells in succession using a hemacytometer. The cell count accuracy was $\pm 10\%$.

3.2.3 HTMSU with Integrated Conductivity Sensor Fabrication

A detailed description of the HTMSU fabrication has been given by Adams et al. with a schematic of the device shown in Fig. 3.1A.²⁰ Briefly, the HTMSU was hot embossed into PMMA substrates via micro-replication from a metal mold master. The

HTMSU consisted of a series of 51 high-aspect ratio curvilinear channels that in concert formed the cell capture bed. Each channel was 150 μm (depth) \times 30 μm (width) and shared common inlet/outlet ports. Curvilinear shaped capture channels were used to improve the cell capture efficiency. The cell-free marginal zone apparent in straight channels was not observed in curvilinear channels and the cell radial distribution was unaffected by changes in cell translational velocity. Cells migrate to the outside of the curved channels due to centrifugal forces acting on the cells and the cross-stream velocity component due to the reversal of the direction of curvature.²⁰ The result is an increase in the aptamer/antigen encounter rate as the cells moved through the capture beds at the relatively high-linear velocities used here. The channel width of the cell capture bed (30 μm) was comparable with the average target cell diameter, which was used to increase the probability of cell–aptamer interactions with the solution-borne target cells. The large channel depth (150 μm) was selected to reduce the pressure drop in high-volume flow rates and also, to increase sample processing throughput.

Appropriately cleaned PMMA HTMSUs devices and cover plates were exposed through a mask to UV radiation resulting in the formation of carboxylate moieties only in the exposed areas of the PMMA. The exposed areas were restricted to only the cell capture bed region of the device.²⁰ UV irradiation was performed through an aluminum mask for 10 min at 15 mW cm^{-2} to facilitate the formation of the carboxylated scaffold. These parts were then aligned and clamped together between two borosilicate plates. The cover plate was thermally fusion bonded to the substrate by placing the clamped pieces inside a convective oven and heating to ~ 101 $^{\circ}\text{C}$, slightly above the glass transition temperature of the UV-modified material. The temperature was increased from 50 to 101 $^{\circ}\text{C}$ at a rate of 20 $^{\circ}\text{C min}^{-1}$ and held at 101 $^{\circ}\text{C}$ for 15 min. Polyimide-

coated fused silica capillaries were then inserted into the inlet port of the assembled HTMSU to provide the introduction of samples into the device using a programmable syringe pump (Harvard, Holliston, MA).

Pt electrodes ($d=76\ \mu\text{m}$) served as the contact conductivity sensor in the detection zone of the HTMSU and were placed into guide channels that were positioned orthogonal to the fluidic output channel following thermal assembly. Insertion of the electrodes was monitored using a microscope to carefully control the inter-electrode gap ($50\ \mu\text{m}$). The cell constant of the Pt conductivity sensor, K , was $\sim 0.01\ \mu\text{m}^{-1}$, which allowed for the specific detection of LNCaP cells based on their average size (diameter= $25\ \mu\text{m}$).

3.2.4 Antibody Immobilization to the HTMSU

Antibody immobilization was carried out in a two-step process. The UV-modified thermally assembled HTMSU device was loaded with a solution containing $4\ \text{mg mL}^{-1}$ EDC, $6\ \text{mg mL}^{-1}$ NHS in $150\ \text{mM MES}$ ($\text{pH}=6$) for 1 h at room temperature to obtain the succinimidyl ester intermediate. After this incubation, the EDC/NHS solution was removed by flushing nuclease-free water through the device. Then, an aliquot of $1.0\ \text{mg mL}^{-1}$ of the monoclonal anti-EpCAM antibody solution contained in $150\ \text{mM PBS}$ ($\text{pH}=7.4$) was introduced into the HTMSU and allowed to react for 4 h. The device was then rinsed with a solution of PBS ($\text{pH}=7.4$) to remove any non-specifically bound anti-EpCAM antibodies.

3.2.5 Aptamer Immobilization onto PMMA Films and the HTMSU Device

A schematic of the aptamer immobilization process is given in Fig. 3.1B. Aptamer immobilization to PMMA surfaces was carried out in a single step. Following PMMA

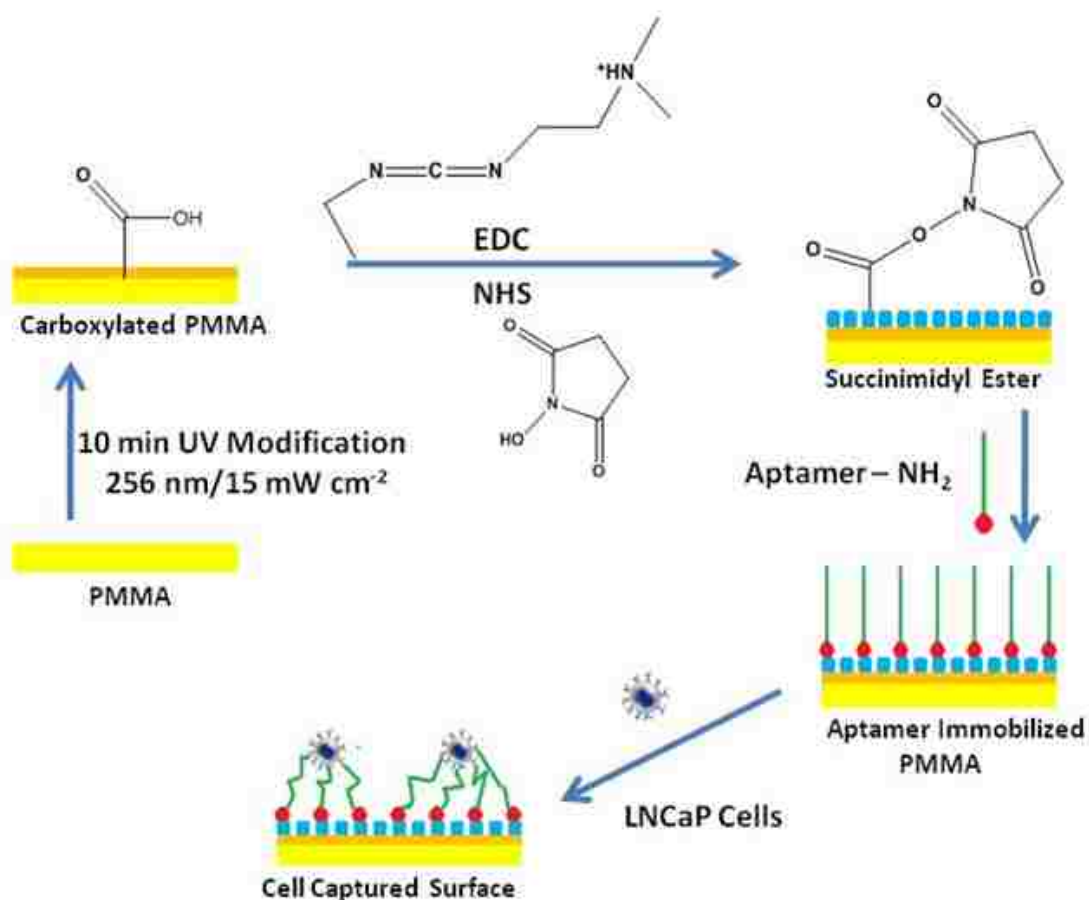
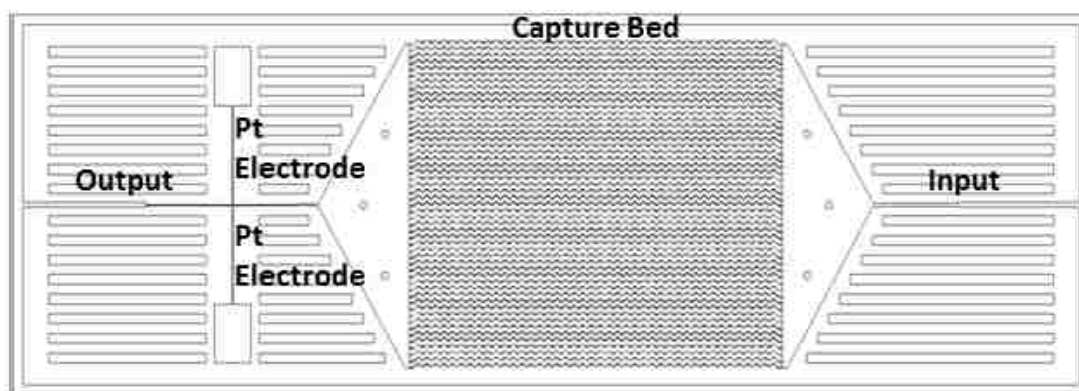


Figure 3.1 (A) Diagram of the HTMSU made via micro-replication into PMMA from a metal mold master. The capture bed consisted of curvilinear channels that were $30 \mu\text{m}$ wide and $150 \mu\text{m}$ deep (51 channels). (B) Process operation of the HTMSU used for the positive selection of LNCaP cells. Also shown is the chemistry used for the immobilization of the cell selection elements, aptamers, to the PMMA surface. The first step involved the UV-irradiation (15 mW cm^{-2}) of PMMA and in this case, the irradiation was carried out on just the capture bed so that positive cell selection occurred only in this region.

activation using UV light to generate the carboxylic acid functional scaffold, the activated PMMA surfaces were incubated with a solution containing 10 mM of an oligonucleotide with a random sequence or the PSMA aptamer, 4 mg mL⁻¹ EDC and 6 mg mL⁻¹ NHS in 150 mM MES (pH=6), and allowed to incubate for 3 h at room temperature. For PMMA films, the planar surface was immersed in the reaction solution. Following reaction, the PMMA surface was rinsed with a solution of PBS (pH=7.4) to remove any non-specifically bound constituents.

In the case of the HTMSUs, the assembled devices were loaded with a 10 mM anti-PSMA aptamer solution also containing 4 mg mL⁻¹ EDC and 6 mg mL⁻¹ NHS in 150 mM MES (pH=6). This solution was allowed to incubate in the device for 2 h at room temperature. The device was then rinsed with a solution of PBS (pH=7.4) at 20 mL min⁻¹ flow rate to remove any non-specifically bound constituents.

3.2.6 Determination of Aptamer Surface Density on UV-Modified PMMA

A clean SPR gold sensor surface was coated with 300 µL of a PMMA solution (1.0 mg of PMMA in 10 µL of CH₂Cl₂) in a custom built spin coater and spun at 1500 rpm for 1 min. The PMMA film was then subjected to UV light and aptamer immobilization was undertaken using identical conditions as those described in Section 2.5. The SPR response, which was measured using a BIACORE X SPR instrument (Piscataway, NJ), was recorded after each treatment using DI water as a buffer. The difference in SPR response before and after aptamer immobilization was determined and the SPR response unit was converted into molecules cm⁻² using the manufacturer's conversion factor of 10 response unit=1 ng cm⁻² and the molecular weight of the aptamer.³⁰

3.2.7 LNCaP Cell Capture Using the HTMSU

To connect the HTMSU to the pump, a luer lock syringe (Hamilton, Reno, NV) was placed on the pump equipped with a luer-to-capillary adapter (Inovaquartz, Phoenix, AZ). This was then attached to the capillary that was sealed to the input port of the HTMSU. A pre-capture rinse was performed with 0.2 mL of 150 mM PBS at 50 mm s^{-1} linear velocity to maintain isotonic conditions. Then, the appropriate volume of a cell suspension was introduced at the appropriate volumetric flow rate to produce the desired linear velocity in each microchannel comprising the capture bed. Next, a post-capture rinse was performed with 0.2 mL of 150 mM PBS at 50 mm s^{-1} to remove any non-specifically adsorbed cells.

In cases where the cells required optical visualization to assist in the operational optimization of the HTMSU, the PMMA devices were fixed onto a programmable motorized stage of an Axiovert 200M (Carl Zeiss, Thornwood, NY) microscope and video images were collected during each experiment at 30 frames per second using a monochrome CCD (JAI CV252, San Jose, CA). A Xe arc lamp was used to excite the fluorescent dyes incorporated into the cells' membrane.

3.2.8 LNCaP Cell Release from the HTMSU

Following a post cell capture rinse performed with 0.2 mL of 150 mM PBS, a trypsin solution consisting of 0.25% w/v trypsin in Tris-Glycine buffer (pH=7.4) was infused into the HTMSU. The captured cells could be observed (microscopically) until they were removed by the tryptic digestion and Stoke's force using both brightfield video measurements to evaluate release efficiency.

3.2.9 Conductivity Enumeration of Released Cells

The released cells from the capture surface were traversed at 1 mL min⁻¹ volume flow rate through a set of Pt electrodes. We used a specially designed circuit as described earlier²⁰ to measure the changes in solution conductivity due to single cells as a function of time to create the desired conductivity trace from which cell numbers were determined.

3.3 Results and Discussion

Although sophisticated imaging reagents and hardware have been developed for the diagnosis and prognosis of many cancer-related diseases, there are still significant advancements that need to be made that can provide earlier diagnosis and staging of cancers following surgical intervention or monitoring disease recurrence.¹⁵ In this work, we exploited the potential utility of CTCs as a diagnostic and prognostic marker for cancer using microfluidics for the high-efficiency recovery and subsequent enumeration of prostate tumor cells. The molecular recognition of these cells from clinical samples, such as blood, was enabled by the expression of PSMA into lymph node metastasized LNCaP cells. The selective isolation of these cells directly from whole blood was affected through the use of immobilized anti-PSMA aptamers decorating the walls of a capture bed poised within a HTMSU fabricated in a polymer, which could process large input volumes and search for extremely rare events. The HTMSU contained a conductivity sensor that was used to enumerate the isolated LNCaP cells following chemical release from the capture surface.

3.3.1 LNCaP Cell Selectivity and Specificity Using Aptamer Recognition

Specific selection of LNCaP cells was based on the recognition capabilities of anti-PSMA aptamers that were tethered to the HTMSU capture beds to select only cells

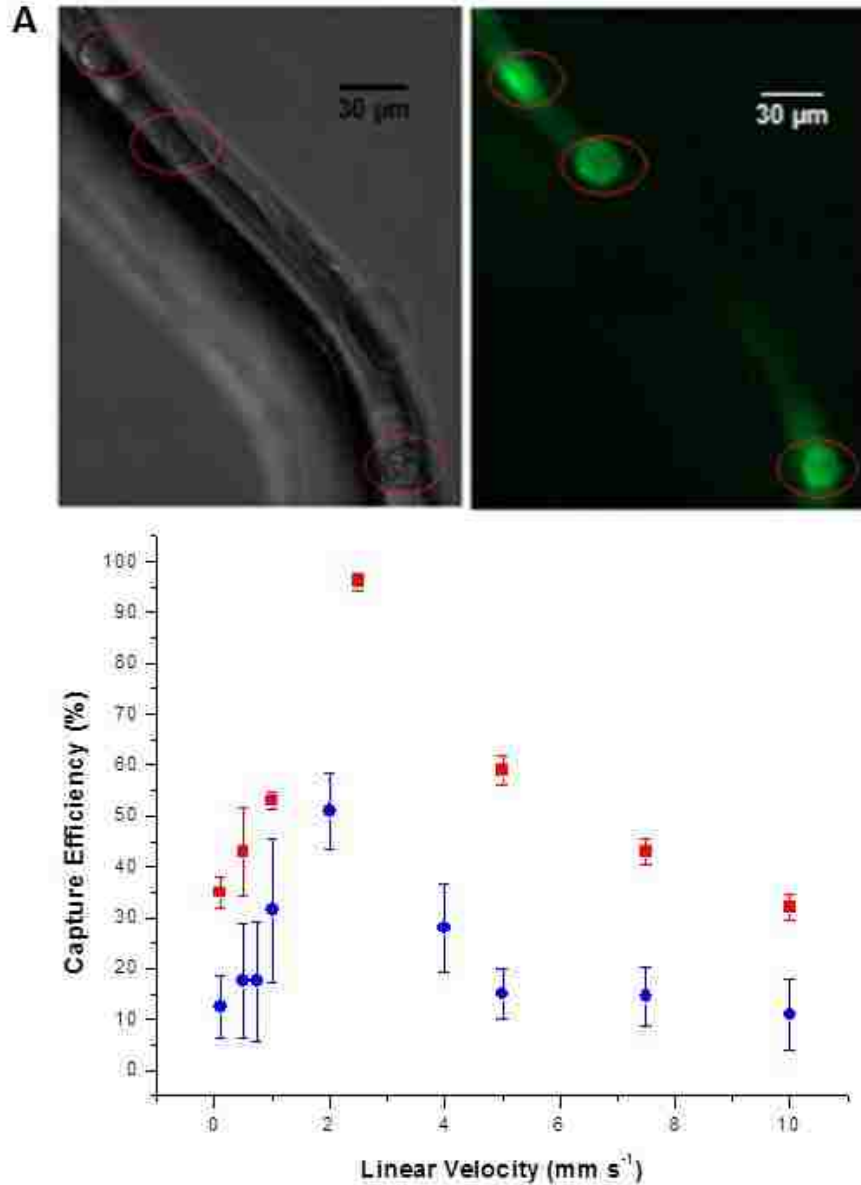


Figure 3.2 (A) Brightfield (left) and fluorescence (right) images for the positive selection of LNCaP cells infused into the HTMSU at a constant volumetric flow rate. The cells were suspended in a PBS buffer (~ 1000 cells mL^{-1}) and following infusion of the cell suspension, the device was washed with PBS buffer prior to imaging. In all cases, the entire capture bed was imaged by scanning the microscope stage. The cells were stained with the fluorescein membrane probe prior to introduction into the HTMSU to allow fluorescence visualization. (B) Comparison of LNCaP cell capture efficiencies using anti-PSMA aptamers or anti-EpCAM antibodies cell recognition elements. In both cases, the HTMSU capture bed was modified with UV light to create the functional scaffold for covalent attachment of the antibody or 50-labeled aptamer. The graph shows the cell capture efficiency versus cells' translational velocity. Red squares and blue circles represent the capture efficiencies for anti-PSMA aptamers and anti-EpCAM antibodies, respectively. In these experiments, ~ 1000 LNCaP cells were seeded into a PBS buffer (pH=7.4) with the number of captured cells determined via brightfield microscopy and subsequently verified using fluorescence microscopy.

that expressed PSMA even when these cells were of extremely low abundance. The specificity of the PSMA-mediated cell selection by aptamers was investigated by using different surface chemistries, pristine PMMA, UV-modified PMMA, and a capture bed surface decorated with random DNA sequences or PSMA-specific aptamers. These initial experiments used the HTMSU with the adhered cells determined via inspection with fluorescence and brightfield microscopy. In these experiments, the LNCaP cells were seeded into PBS buffer (pH=7.4) at ~ 1000 cells mL^{-1} and pumped through the HTMSU using a syringe pump (linear velocity= 2.5 mm s^{-1}). Because fluorescence microscopy was used for visualization, the cells were fluorescently stained using a fluorescein membrane probe. From these experiments, we noticed negligible amounts of cell adhesion of the LNCaP cells to the channel walls of pristine PMMA. UV irradiation of the polymer modifies the PMMA surface by introducing carboxylic acids and other carbonyl groups onto its surface, making this surface more hydrophilic compared with pristine PMMA.³² When the LNCaP cell suspension was pumped through this HTMSU device, no LNCaP cells were found to adhere to the UV-modified PMMA surface. Repeating this experiment using a UV-activated PMMA surface that was reacted with 50-amine containing DNA oligonucleotides possessing a random sequence, no LNCaP cells were detected in the capture bed following fluorescence and brightfield microscopic interrogation. These results suggested that the adhesion forces of the LNCaP cells to these surfaces were not strong enough to withstand the hydrodynamic shear produced by the laminar fluid flow. The random DNA sequences tethered to the PMMA surface did not possess recognition capabilities for the PSMA integral membrane protein. However, when PSMA-specific aptamers were tethered to

the capture bed walls, microscopic inspection of the capture beds clearly indicated the presence of captured LNCaP cells (see Fig. 3.2A).

3.3.2 Cell Translational Velocity Optimization

Because the capture aptamers are tethered to the channel walls, dynamic interactions between the cell membrane's receptors and the channel wall containing the recognition elements is important in determining the recovery of the rare cells. Chang's model³³ of cell adhesion in flowing systems has been applied in previous reports to describe the encounter rate between the solution-borne cells and the surface-tethered cell selection elements.²⁰ When the flow velocity is beyond an optimal value, a decrease in the interaction time between a particular cell's membrane antigen and the capture molecule available for binding is observed, thereby reducing the number of potential binding events. This model also predicts that too small of a velocity leads to a decrease in the encounter rate between the cell bound antigen and the immobilized recognition element. Therefore, an optimal linear velocity would be expected for each flowing system to guarantee the highest frequency of binding between capture molecules and antigen based on a balance between the interaction time and the encounter rate.³³ In addition, because the solution is driven hydrodynamically through the capture bed, shear force can cause release of the captured cells if the shear force is greater than the adhesion force, which in this case is determined by the PSMA/aptamer dissociation constant and the number of molecular association complexes between the surface and cell.²⁹

We therefore carried out experiments to determine the optimal linear velocity to provide the maximum recovery of rare tumor cells found in peripheral blood using aptamer recognition elements. The results of these investigations are presented in Fig.

3.2B. From these results, the maximum cell capture efficiency was found to occur at a translational velocity equal to 2.5 mm s^{-1} under the conditions employed in this study. LNCaP cell capture studies using an EpCAM antibody-tethered HTMSU followed the same capture efficiency trend for that observed for the anti-PSMA aptamer, indicating that the cell capture efficiency is governed by the same principal as that described by the Chang model and seen in our previous work for anti-EpCAM captured MCF-7 cells using this HTMSU.²⁰ However, the optimum linear cell translational velocity for maximum cell capture for the anti-EpCAM immobilized HTMSU was slightly lower (2.0 mm s^{-1}) than that observed for the anti-PSMA aptamer (2.5 mm s^{-1}) indicating that the reaction rate for the anti-EpCAM/EpCAM interaction is slightly less than that observed for the anti-PSMA aptamer/PSMA interaction. The molecular weight of EpCAM, 33 kDa,³⁴ is far less compared with 100 kDa for PSMA.¹⁶ The extra-cellular domain of EpCAM contains only 242 amino acid residues whereas PSMA contains 707 extra-cellular amino acid residues potentially giving extended accessibility of the extracellular domain of PSMA to its recognition element. However, the rate of association will depend also on the location of the recognition epitope as well as the conformational reorganization occurring during a binding event. These factors may provide a faster rate of reaction observed in the case of the anti-PSMA aptamer/PSMA complex. In addition, the expression level of PSMA (1×10^6 molecules cell⁻¹) is approximately twice the expression level of EpCAM within the LNCaP cell's membrane.³⁵⁻³⁷ This higher expression level and the bulky extra-cellular domain of PSMA may hinder accessibility of anti-EpCAM/EpCAM interactions due to molecular crowding effects. Moreover, the smaller molecular weight anti-PSMA aptamer, 10 kDa, is able to efficiently bind to the larger molecular weight PSMA due to its capability to quickly fold into

thermodynamically stable secondary and tertiary structures to form complexes through molecular forces that specify target interaction.³⁸

Another issue that must be addressed is the adhesion strength between the captured cell and its surface immobilized recognition element due to the fact that the shear force exerted by the solution can potentially dislodge the cell from the capture surface. This would occur if the adhesion strength (or force) was less than the shear force (F_S). The adhesion force (F_A) between the cell and the anti-PSMA aptamer decorated surface can be determined from the bond strength between a single antigen–aptamer complex (f_C), the cell contact area with the PMMA surface (A_C) and the number of receptors poised on the PMMA surface within the contact area of the cell (C_S) from:²⁰

$$F_A = f_C \times A_C \times C_S \quad (1)$$

If the cell is assumed to be a non-deformable object upon adhesion to the capture surface, the contact area can be calculated using,³⁹

$$A_C = \pi(r_p \sin(\cos^{-1}(r_p - h' + h)/r_p))^2 \quad (2)$$

where r_p is the cell radius and h and h' represent the characteristic cell separation distances from the surface upon binding. Using h and h' as 100 and 400 Å, respectively,⁴⁰ the calculated contact area was determined to be 1.88 μm^2 for the LNCaP cells ($r_p \approx 12.5 \mu\text{m}$). If the cell is assumed to flatten and elongate after contact, as observed experimentally (see Figs. 3.2 and 3.3), the resulting contact area A_C was calculated to be $\sim 380 \mu\text{m}^2$.⁴¹

The single PSMA-anti-PSMA aptamer adhesion force was estimated using the formalism by Bell,⁴² who developed the following expression for deriving the critical force required to break a single bond;

$$f_C = kT/r_o a_C \quad (3)$$

where k is Boltzman's constant, T is the absolute temperature, r_o is the separation distance between receptors at the minimum breaking force and $a_C=K_D C_S$ (K_D =PSMA-anti-PSMA aptamer equilibrium constant). Using a value of $K_D=4.76 \times 10^8 \text{ M}^{-1}$,²⁹ and $r_o=0.5 \text{ nm}$,³³ the value calculated for the adhesion force per association complex was

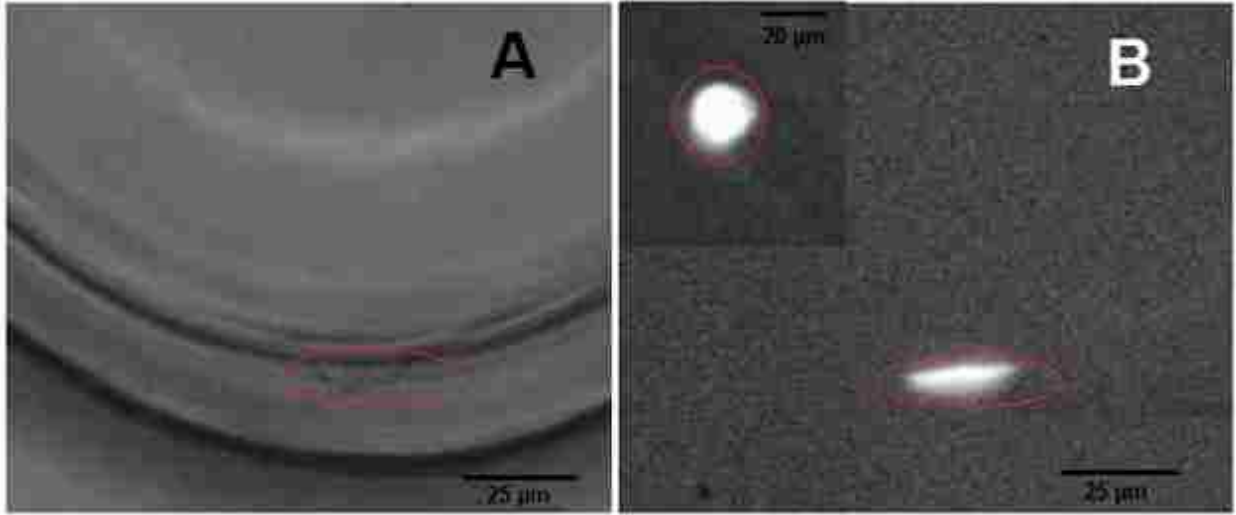


Figure 3.3 Brightfield and fluorescence micrographs showing anti-PSMA aptamer captured LNCaP cells in a PMMA microchannel. (A) Brightfield micrographs taken at 40x magnification and (B) the corresponding fluorescence micrographs verifying the captured cell is the fluorescently labeled LNCaP cell. The inset shown in panel (B) is a fluorescent-stained LNCaP cell in a PMMA microchannel that was not decorated with anti-PSMA aptamers indicating the spherical shape of these cells.

determined to be $4.55 \times 10^{-11} \text{ N}$. For the LNCaP cells shown in Fig. 3.3A, F_A was calculated to be $5.5 \times 10^{-5} \text{ N}$.⁴¹ F_S was determined from Stokes' law;⁴³

$$F_S = 6\pi\eta r_p v_C \quad (4)$$

where r_p is the cell radius ($\sim 12.5 \mu\text{m}$ for LNCaP cells),⁴⁴ η is the solution viscosity (4.8 C_p for whole blood with a hematocrit level of 0.4)⁴⁵ and v_C is the critical linear velocity that can induce cell detachment. Rearrangement of Eq.4 produced a value of $6.0 \times 10^3 \text{ cm s}^{-1}$ for v_C . This value is significantly greater than the linear velocities used in the present experiments for optimizing the capture efficiency. Several captured cells were

observed continuously during experiments in which linear velocities up to 10.0 cm s^{-1} were implemented and no cell damage or disruption of cell–wall adhesion was observed.

3.3.3 Selection of Other CTC-Types Using the HTMSU with Immobilized PSMA Aptamers

Non-specific adsorption or recognition of other CTC-types was also evaluated using a breast cancer cell line (MCF-7) as an example, which does not express PSMA, but does overexpress the EpCAM. The existence of PSMA genes in normal and non-prostate-specific tumor cells, such as the MCF-7 cell line, has been reported, however, protein assay results for the MCF-7 cell lines failed to detect the PSMA antigen.⁴⁶ Our results indicated that no MCF-7 cells were found in the PMMA capture beds when decorated with the anti-PSMA aptamers as deduced from microscopic interrogation of these beds using brightfield microscopy (data not shown). These cell capture experiments were carried out under dynamic laminar flow conditions in the HTMSU microfluidic channels using the optimized LNCaP linear velocity of 2.5 mm s^{-1} . Therefore, the presence of the hydrodynamic shear would most likely detach any non-specifically bound material due to weak adhesion forces exerted on these cells.

3.3.4 Cell Detachment from the Capture Surfaces

Releasing the cells intact from the capture bed was critical for the subsequent conductivity enumeration of the LNCaP CTCs. The mechanism we evaluated for cell release was the use of enzymatic digestion of the extra-cellular domain of the PSMA protein using trypsin to reduce the cell's adhesion strength to the aptamer surface. There are two main biosynthetic forms of PSMA within the LNCaP cell membrane, which are either mannose-rich PSMA (PSMA_M) or the glycosylated form of PSMA (PSMA_C). PSMA_M is completely sensitive to trypsin, whereas PSMA_C is trypsin resistant

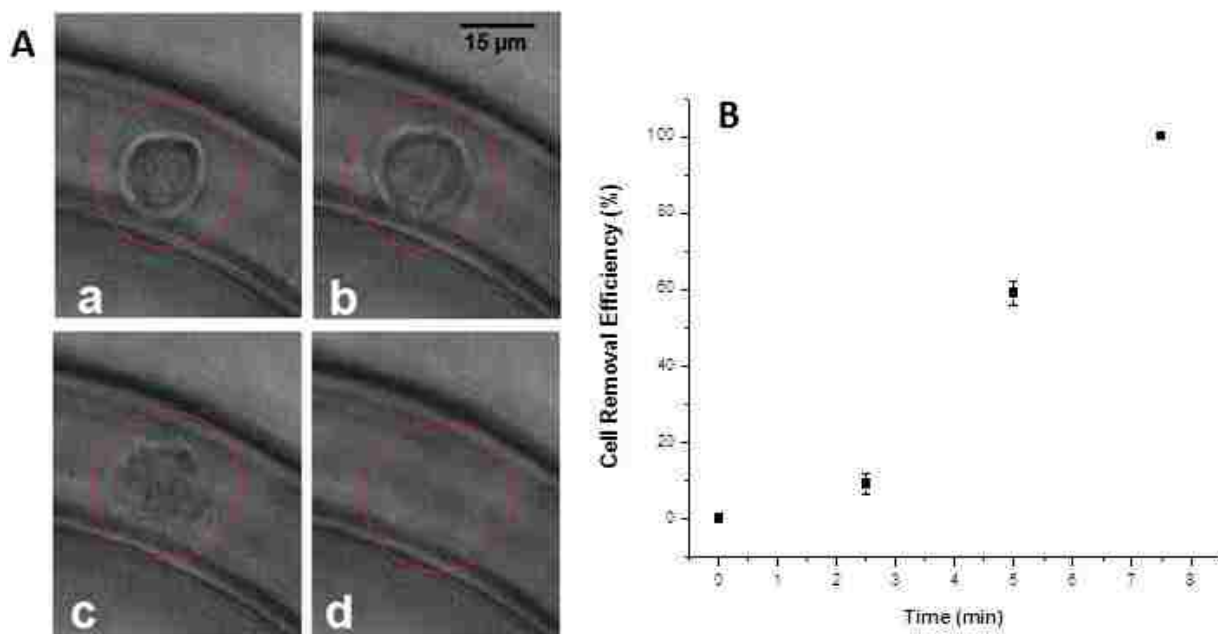


Figure 3.4 (A) Time-lapse micrographs showing trypsin enzyme mediated release of a captured LNCaP cell upon application of 0.25% w/w trypsin in PBS buffer (pH=7.4). (a) At $t=0$ or prior to exposure of the captured cells to the trypsin releasing buffer. (b) At $t=2.0$ min, disruption of the binding complex is evident. (c) At $t=6.5$ min, the cell appears to be released from the capture surface. (d) At $t=7.5$ min, the cell was completely released from the surface and swept away from the capture surface to the detection region by the hydrodynamic flow. **(B)** Plot of cell release efficiency versus time. In each experiment the number of cell releasing events, >25, in three curvilinear channel were counted. The error bars represents the standard deviation of the results obtained for three replicate experiments.

due to transport blockage at the Golgi complex associated with their secretory pathway.⁴⁷

Introduction of a trypsin solution into the capture bed to allow for tryptic digestion of PSMA to provide release of the captured LNCaP cells was found to effectively release these cells from the aptamer-decorated surface indicating the dominate component was PSMAM as the attachment partner between PSMA and the anti-PSMA aptamers. Figure 3.4A represents time-lapse micrographs of a captured cell that was processed using a trypsin digestion solution. Close investigation of the time-lapse micrographs indicated efficient release of the intact LNCaP cells from the capture

surface. The cell releasing efficiency increased with increasing incubation time according to Fig. 3.4B. Complete cell detachment (~100%) was achieved in less than 7 min of incubation time. We also note that brightfield inspection at the Pt electrode pair readout point of the device was performed of the released cells following trypsin processing and these inspections confirmed that the cells were intact at this point.

3.3.5 Conductivity Enumeration of the CTCs

The conductivity detector, which consists of a pair of Pt electrodes with a 50 μm spacing (cell constant= $0.01 \mu\text{m}^{-1}$), was fabricated specifically to transduce the larger CTCs compared with the smaller leukocytes and/or erythrocytes that may appear in the enumeration phases of the assay providing false positive signals due to the universal nature of the conductivity response. Also, the CTCs possess unique electrical properties due to their characteristic chemical composition compared with erythrocytes and leukocytes to provide efficient conductivity readout.⁴⁸ For example, the over-expression of membrane glycoproteins, such as PSMA, associated with many tumor or cancer cells result in an increase in the number of negatively charged sialic acid molecules that cap the extra-cellular domains of these integral membrane proteins.²⁰ This can produce a cell with a higher electrical conductivity compared with one that does not over-express these types of proteins.

One milliliter of whole blood was seeded with 20 ± 1 LNCaP cells and was processed using the HTMSU. The captured cells were subsequently released using the trypsin releasing buffer and enumerated with the conductivity transducer with a typical data stream shown in Fig. 3.5A. The conductivity transducer measured changes in the conductivity releasing buffer induced by the presence of single CTCs between the Pt electrode pair. Therefore, the responses generated in the data shown in Fig. 3.5A were

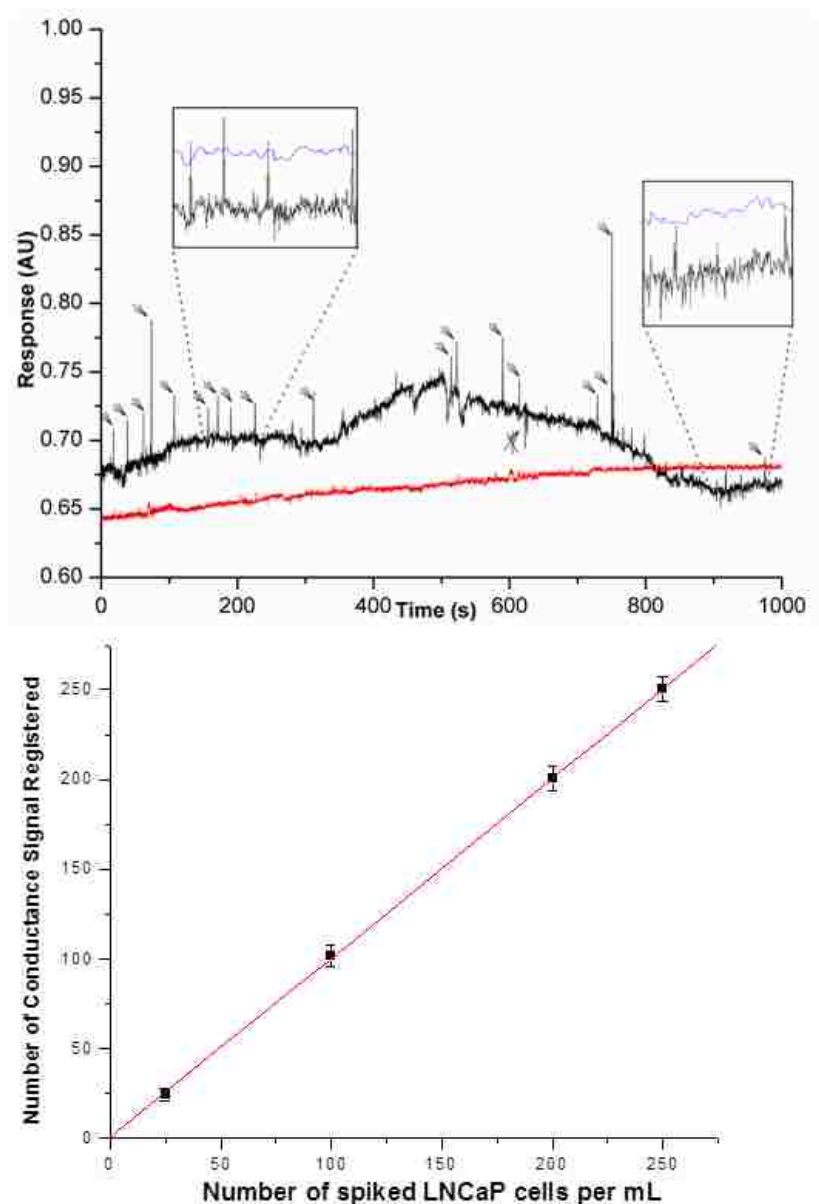


Figure 3.5 (A) Conductometric responses generated for 1.0 mL of whole blood seeded with 20 ± 1 LNCaP cells (black) or 0 LNCaP cells (red) at a linear flow velocity of 2.5 mm s^{-1} processed using the HTMSU. The captured LNCaP cells were released from the capture surface using the release buffer comprised of 0.25% w/w trypsin and transported through the conductivity sensor at a volumetric flow rate of 0.05 mL min^{-1} . The arrows designate peaks that were identified as LNCaP cells based on a signal-to-noise threshold of 3. The crossed arrows represent non-LNCaP cell events. The insets shown in the figure represent a magnified view of sections of the data stream. The blue line represents the threshold level, which represents 3x the average background level, which was used to differentiate “true” events from noise. The data presented here was smoothed by the Savitsky-Golay method (25 point smoothing function). Also shown in this plot is a sample of whole blood containing no LNCaP cell that was processed with the HTMSU device (red line). **(B)** Calibration plot ($m=0.990$, $r^2=0.99997$) for the number of LNCaP cells seeded ($10\text{--}250 \text{ cells mL}^{-1}$) into 1.0 mL of whole blood versus the number of conductivity responses using the Pt-conductivity sensor.

generated from single cells. Tris-Glycine buffer was selected as the major component in the release buffer due to its low conductance, hence, the sensitivity of the conductivity detection for single cells was enhanced and the resultant peaks should exhibit a positive response due to the higher conductance of the LNCaP cells with respect to the release buffer. There were 18 peaks in the conductance response given in Fig. 3.5A that could be assigned to single LNCaP cells based on a signal-to-noise threshold of 3 (99.7% confidence level) giving a recovery of ~90% (see insets to Fig. 3.5A showing the discrimination threshold used). As seen in Fig. 3.5A, only positive signals were designated as LNCaP cells and the negative spikes were assigned to particulates due to their lower conductance compared with the Tris-Glycine buffer. Variation of the peak response for each cell is most likely due to differences in the cells' morphology and chemical composition, which is determined by the state of mitosis of the cell.

One milliliter of a blank sample, which consisted of whole blood seeded with no LNCaPs cells, was analyzed by the HTMSU and enumeration via conductivity under the same conditions as described for the whole blood sample seeded with LNCaP cells and the resultant trace is shown in Fig. 3.5A. In this case, no single-cell spikes were seen in the data trace indicating that the signal spikes seen in the conductivity trace for the LNCaP seeded whole blood was indeed due to these tumor cells. Therefore, the purity of LNCaP cell selection was determined to be 100%.

The HTMSU with conductivity enumeration was further evaluated for the detection of various seed levels of LNCaP cells into whole blood to produce a calibration plot. A range of 10–250 LNCaP cells per mL of whole blood was evaluated. The best-fit linear function to the data plotted in Fig. 3.5B had a slope of 0.990 with an intercept near zero ($r^2=0.9997$). Interestingly, even at the lowest LNCaP cell load, the

data still fit along this linear function indicating that even at extremely low levels of LNCaP cells found in whole blood, we could still quantitatively analyze these cells using the HTMSU. We should note that for 1 mL of whole blood, $\sim 2.5 \times 10^9$ erythrocytes are present. Therefore, the enrichment factor for this assay can be calculated as 2.5×10^8 for the lowest LNCaP cell load investigated. At the 2.5 mm s^{-1} employed to provide maximum LNCaP recovery, the processing time for exhaustively processing 1 mL of blood would be ~ 29 min.

3.4 Conclusions

The HTMSU described in this manuscript utilized an aptamer-based positive selection approach for the isolation of prostate-specific CTCs (LNCaP) directly from whole blood with subsequent quantification of these rare cells using a non-labeling approach. The compelling advantage of this methodology is that no sample pre-treatment was necessary and the throughput (29 min processing time for 1 mL input), recovery (90%) and purity (100%) were extremely high, contrary to what is seen in other rare cell selection formats utilizing size or affinity capture. The ability to quantify the selected cells with near 100% detection efficiency using a conductivity readout format allows for the use of this simple system at the point-of-care for the management of cancer-related diseases from a simple blood test. In addition, molecular profiling of the selected CTCs could be used for determining therapeutic treatment regimens as well as identifying the organ of origin of the selected CTC from whole blood. Molecular profiling of rare CTCs in whole blood could not be done directly on the clinical sample due to the low copy number of the mutated DNA originating from the CTCs as well as potential interferences on downstream molecular processing by the highly abundant red and white blood cells found in whole blood. We are currently in the process of developing

sensitive genotyping assays that can be performed directly on the selected CTCs for providing this valuable clinical information.

Previously, it has been reported²⁰ a positive selection of MCF-7 breast cancer cells from peripheral blood using anti-EpCAM antibodies and this HTMSU. In this report, aptamers were used for the positive cell selection, in this case for selecting LNCaP cells from peripheral blood. The recovery, purity, and throughput were similar in both cases as well as the specificity for the target cells. The attractive features of aptamers compared with antibodies is the ordered nature of their attachment to the solid surface (50-end attachment) as opposed to a stochastic one associated with antibodies (primary amine groups on the antibody), the ability to carefully control the aptamer/surface distance to improve accessibility and the robust nature of the molecular recognition elements. For example, aptamers can be stored at room temperature without degrading their recognition performance, whereas antibodies must be stored in more controlled conditions to maintain their activity.

3.5 References

1. Serda, RE., Adolphi, NL., Bisoffi, M., Sillerud, LO., *Mol. Imaging* **2007**, 6, 277–288.
2. Martin-Orozco, RM., Almaraz-Pro, C., Rodriguez-Ubreva, FJ., Cortes, MA., Roperro, S., Colomer, R., Lopez-Ruiz, P., Colas, B., *Neoplasia* **2007**, 9, 614–624.
3. Moon, C., Park, JC., Chae, YK., Yun, JH., Kim, S., *Cancer Lett.* **2008**, 266, 116–134.
4. Loeb, S., Catalona, WJ., *Oncologist* **2008**, 13, 299–305.
5. Eskew, LA., Bare, RL., McCullough, DL., *J. Urology* **1997**, 157, 199–202
6. Rosser, CJ., Broberg, J., Case, D., Eskew, LA., McCullough, D., *Urology* **1999**, 54, 853–856.
7. Cristofanilli, M., Budd, GT., Ellis, MJ., Stopeck, A., Matera, J., *et al.*, *N. Engl. J. Med.* **2004**, 351, 781–791.

8. Feldstein, M., Zelen, M., *Breast cancer Res. Treat.* **1984**, 4, 3–10.
9. Lin, P., Ghetti, A., Shi, W., Tang, M., Harvie, Gl., Tao, H., *et al.*, Application: US, **2008**, pp 38pp, Cont -in-part of U S Ser No 497,919.
10. Logothetis, CJ., Navone, NM., Lin, SH., *Clin. Cancer Res.* **2008**, 14, 1599–1602.
11. Nagrath, S., Sequist, LV., Maheswaran, S., Bell, DW., Irimia, D., *et al.*, *Nature* **2007**, 450, 1235–1239.
12. Hayes, DF., Smerage, J., *Clin. Cancer Res.* **2008**, 14, 3646–3650.
13. Sardana, G., Jung, K., Stephan, C., Diamandis, EP., *J. Proteome Res.* **2008**, 7, 3329–3338.
- 14 Schuur, ER., Henderson, GIA., Kmetec, LA., Miller, JD., Lamparski, HG., Henderson, DR., *J. Bio. Chem.* **1996**, 271, 7043–7051.
15. Steeg, PS., *Nature Med.* **2006**, 12, 895–904.
- 16 Silver, DA., Pellicer, I., Fair, WR., Heston, WD., Cordon-Cardo, C., *Clin. Cancer Res.* **1997**, 3, 81–85.
17. Rosenthal, SA., Haseman, MK., Polascik, T., *J. Tech. Urology* **2001**, 7, 27–37.
18. Tasch, J., Gong, M., Sadelain, M., Heston, WDW., *Crit. Rev. Immunol.* **2001**, 21, 249–261.
19. Liu, T., Wu, LY., Kazak, M., Berkman, CE., *Prostate* **2008**, 68, 955–964.
20. Adams, AA., Okagbare, PI., Feng, J., Hupert, ML., Patterson, D., Gottert, J., McCarley, RL. *et al.*, *J. Am. Chem. Soc.* **2008**, 130, 8633–8641.
21. Dainiak, MB., Kumar, A., Galaev, IY., Mattiasson, B., *Adv. Biochem. Eng./Biotechnol.* **2007**, 106, 1–18.
22. Liu, Y-J., Guo, S-S., Zhang, Z-L., Huang, W-H., Baigl, D., Xie, M., Chen, Y., Pang, D.-W., *Electrophoresis* **2007**, 28, 4713–4722.
23. Diener, JL., Hatala, P., Killough, JR., Wagner-Whyte, J., Wilson, C., Zhu, S., (Archemix Corp., USA). Application: WO, **2006**, pp. 207
24. Tombelli, S., Minunni, M., Mascini, M., *Biomol. Eng.* **2007**, 24, 191–200.
25. Potyrailo, RA., Conrad, RC., Ellington, AD., Hieftje, GM., *Anal. Chem.* **1998**, 70, 3419–3425.

26. Balamurugan, S., Obubuafo, A., Soper, SA., Spivak, DA., *Anal. Bioanal. Chem.* **2008**, *390*, 1009–1021.
27. Shangguan, D., Tang, Z., Mallikaratchy, P., Xiao, Z., Tan, W., *Chembiochem* **2007**, *8*, 603–606.
28. Vorhies, JS., Nemunaitis, JJ., *Biologics* **2007**, *1*, 367–376.
29. Lupold, SE., Hicke, BJ., Lin, Y., Coffey, DS., *Cancer Res.* **2002**, *62*, 4029–4033.
30. Balamurugan, S., Obubuafo, A., Soper, SA., McCarley, RL., Spivak, DA., *Anal. Chem.* **2008**, *80*, 9630–9634.
31. Phillips, JA., Xu, Y., Xia, Z., Fan, ZH., Tan, W., *Anal. Chem.* **2009**, *81*, 1033–1039.
32. Witek, MA., Wei, S., Vaidya, B., Adams, AA., Zhu, L., et al., *Lab Chip* **2004**, *4*, 464–472.
33. Chang, KC., Hammer, DA., *Biophys. J.* **2000**, *79*, 1891–1902.
34. Chen, YH., Yu, T., Bai, Y., Zhao, N., *Cancer Lett.* **1999**, *144*, 101–105.
35. Heston, WD., *Urology* **1997**, *49*, 104–112.
36. Balzar, M., Winter, MJ., De Boer, CJ., Litvinov, SV., *J. Mol. Med.* **1999**, *77*, 699–712.
37. Schmittgen, TD., Teske, S., Vessella, RL., True, LD., Zakrajsek, BA., *Int. J. Cancer* **2003**, *107*, 323–329.
38. Jayasena, SD., *Clin. Chem.* **1999**, *45*, 1628–1650.
39. Cozens-Roberts, C., Quinn, JA., Lauffenburger, DA., *Biophys. J.* **1990**, *58*, 107–125.
40. Clausen, J., *Immunochemical techniques for the identification and estimation of macromolecules, In laboratory Techniques in Biochemistry and Molecular Biology*, **1981**: Vol. 1.
41. McCarley, RL., Vaidya, B., Wei, S., Smith, AF., Patel, AB., et al., *J. Am. Chem. Soc.* **2005**, *127*, 842–843. [42] Bell, G. I., *Science* 1978, *200*, 618–627.
43. Katkov, II., Mazur, P., *Cell Biochem. Biophys.* **1999**, *31*, 231–245.
44. Hong, S., Shamik, K., Enmon, RM., O'Connor, KC., *In vitro Cellul. Dev. Biol. Anim.* **2004**, *40*, 262–267.
45. Kameneva, MV., Watach, MJ., Borovetz, HS., *Clin. Hemorheol. Microcirc.* **1999**, *21*, 357–363.

46. Gala, JL., Heusterspreute, M., Loric, S., Hanon, F., Tombal, B., et al., *Clin. Chem.* **1998**, *44*, 472–481.
47. Castelletti, D., Alfalah, M., Heine, M., Hein, Z., Schmitte, R., et al., *Biochem. J.* **2008**, *409*, 149–157.
48. Hakomori, S., *Immun. Allergy Clin.* **1990**, *10*, 781–802.

CHAPTER 4 ENRICHMENT AND DETECTION OF ESCHERICHIA COLI O157:H7 FROM WATER SAMPLES USING AN ANTIBODY MODIFIED MICROFLUIDIC CHIP*

4.1 Introduction

Threats to human health from *Escherichia coli* contamination of aquatic environments are becoming highly prevalent. Several major waterborne outbreaks have been reported in aquatic systems ranging from freshwater to marine, where *E. coli* accumulates in the water column and sediments.^{1,2} To better understand *E. coli* ecology in aquatic environments, to provide monitoring over time scales appropriate for the study of *E. coli* outbreaks,³⁻⁵ and to protect human populations, monitoring techniques for *E. coli* are needed that have low detection thresholds even for extremely rare cells and rapid processing times.

The U.S. EPA allowable levels of *E. coli* are 0, 200, and 1000 cfu per 100 mL of drinking, swimming, and recreational (boating) waters, respectively, and the minimum infectious dose is very low, ~10 cells.⁶ To detect *E. coli* corresponding to doses this low, preenrichment of cells is required, especially in drinking and recreational waters, by processing large input volumes to accommodate the readout phases of the measurement assay. There are different technologies for isolating rare cells from heterogeneous samples to aid in their analysis such as fluorescence assisted cell sorting,⁷ flow-through filtrations,⁸ enzyme linked immunosorbent assays (ELISA),⁹ and immunomagnetic assisted cell sorting.¹⁰ These methods, however, rely on time-consuming culturing protocols.

The U.S. EPA has approved an *E. coli* detection test for the examination of drinking water, which is based on β -D glucuronidase, an enzyme associated with *E. coli*

* Reproduced with permission from *Analytical Chemistry*

colonies.¹¹ This method (EPA Method 1603) detects the presence of all coliforms but not specifically the *E. coli* O157:H7 strain due to a two-base frame shift insertion within its genome that yields an inactive *uidA* gene and lack of β -D glucuronidase production.¹² Detection of pathogenic *E. coli* O157:H7 is usually performed with EPA Method 9260F,¹³ which employs a series of incubations at low temperatures for extended periods of time (72 h).

The presence of naturally and anthropogenically derived dissolved substances in aquatic systems, such as humic materials and residual pharmaceuticals,¹⁴ along with other dominant native bacterial species, can act as interfering agents that may alter the accuracy of the aforementioned colorimetric tests. In addition, microbiological studies have indicated that stressed *E. coli* O157: H7 become nonculturable even though they may be viable and still capable of producing Shiga-like toxin.¹⁵ More recently, nucleic acid-based methods for pathogen detection, such as polymerase chain reaction (PCR), have been developed to target unique bacterial genes. PCR itself, although very sensitive, detects the presence of bacteria but does not allow isolation of rare bacterial cells, which is required to determine the etiological agent responsible for an outbreak.¹⁶

Recent work has shown that cells can be accumulated from biological samples using a microfluidic platform.¹⁷⁻¹⁹ These microfluidic devices utilized the surface of a microchannel or beads trapped within a microchannel for positive cell selection. Liu et al. generated a device for processing *E. coli* cells from input volumes of 1 mL with the cell limit-of-detection (LOD) of ~ 1 cfu μL^{-1} .²⁰ Beyor and co-workers reported a microfluidic system that could process ~ 50 μL of input and search for target cells, such as K-12 or O157:H7 *E. coli*.²¹ The LOD reported was 0.2 cfu μL^{-1} . With an *E. coli* O157:H7 concentration level of <200 cells per 100 mL, the probability of securing a target cell in

50 μ L would only be 0.01. Therefore, sampling statistics would require processing larger input volumes to provide higher confidence that a target could be processed.

We present a method for the isolation, identification, and quantification of *E. coli* O157:H7 cells from recreational waters. Once the cells were enriched, their quantification was accomplished using off-chip real-time quantitative PCR (qPCR). We used an engineered chip consisting of high-aspect ratio capture beds decorated with polyclonal antibodies (pAbs) specific for antigenic membrane proteins expressed in *E. coli* O157:H7. The method was further demonstrated to be capable of detecting *E. coli* O157:H7 cells in lake and wastewater samples. The benefits of this methodology include: (i) preselectivity, which is extremely important because the detection is often difficult due to the combination of the high number of nonpathogenic bacteria and the low number of pathogens of interest;¹⁶ (ii) the microfluidic chip provides a cell purification platform (cells are washed while attached to the surface) and prepares the selected cells for immediate qPCR analysis free from potential interfering agents; and (iii) rapid analysis as compared to conventional methods relying on culturing.

4.2 Materials and Methods

4.2.1 Reagents and Buffers

Heat-inactivated *E. coli* O157:H7 cells and goat polyclonal anti-*E. coli* O157 antibodies were purchased from K & P Laboratories Inc. (Gaithersburg, MD). Reagents used for the PMMA microfluidic chip surface cleaning and modification included reagent grade isopropyl alcohol, 1-ethyl-3-[3-dimethylaminopropyl] carbodiimide hydrochloride (EDC), N-hydroxysuccinimide (NHS), and 2-(4-morpholino)-ethane sulfonic acid (MES), which were purchased from Sigma-Aldrich (St. Louis, MO) and used as received. Phosphate buffered saline (PBS) was purchased from American Type Culture

Collection (Manassas, VA). Cellstripper™ was obtained from Mediatech, Inc., (Manassas, VA) and used as received. For the fluorescence visualization experiments, *E. coli* cells were stained with a fluorescein-based cell membrane stain, PKH67, according to the manufacturer's protocol (Sigma-Aldrich, St. Louis, MO). All bacterial cells used (*Staphylococcus aureus*, *Micrococcus luteus*, *Bacillus subtilis*, *Enterobacter aerogenes*, *Escherichia coli* K12) were purchased from Sigma-Aldrich (Milwaukee, WI), and *Escherichia coli* O157:H7 cells were purchased from Kirkegaard & Perry Laboratories Inc. (Gaithersburg, MD). A stock solution of *E. coli* cells was prepared at a concentration of 3×10^9 cfu mL⁻¹ and cell suspensions required for testing were prepared through serial dilution.

4.2.2 Microfluidic Chip Fabrication and Assembly

The microfluidic fabrication procedure involved the following four major steps: (i) mold fabrication using high precision micromilling (HPMM); (ii) hot embossing of the microfluidic structures in a PMMA substrate; (iii) post-processing of the microfluidic including drilling of sample reservoirs, UV-photoactivation of the immobilization beds, cover plate assembly; and (iv) antibody attachment to the capture channel surfaces. Microstructures were milled onto the surface of a 6.3 mm thick brass plate (alloy 353 engravers brass, McMaster-Carr, Atlanta, GA, USA) using a high-precision micromilling machine (KERN MMP 2522, KERN Micro- und Feinwerktechnik GmbH & Co. KG; Germany) as reported previously.²² PMMA was used as the chip substrate and cover plate (0.5 mm thickness) and were purchased from Good Fellow (Berwyn, PA). The microstructures were hot embossed into PMMA substrates via micro-replication from the brass mold master. Before final assembly (attachment of the cover plate to enclose fluidic channels), chips were washed with ~0.5% Alconox solution, rinsed with DI water,

2-propanol, and ultrasonicated for 10 min in DI water. PMMA devices and cover plates were exposed through a mask to ultraviolet radiation (254 nm, 10 min at 15 mW cm⁻²) resulting in the formation of carboxylate moieties only in the UV exposed areas of the PMMA, which in this case was the cell selection bed. The density of the carboxylic acid groups on the surface after a 10 min exposure to UV light has been determined to be $6.6 \times 10^{-10} \pm 0.8 \times 10^{-10}$ mol cm⁻².¹⁷ UV-modified PMMA parts were clamped together between two borosilicate glass plates and the cover plate was thermally fusion bonded to the substrate using a convective oven set to 101 °C, slightly above the glass transition temperature of the UV-modified material. The temperature was increased from 50 °C to 101 °C at a rate of 20 °C min⁻¹ and held at 101 °C for 15 min. Polyimide-coated fused silica capillaries (100 µm i.d., Polymicro Technologies, Phoenix, AZ) were inserted and glued into the inlet port of the assembled device to provide an interconnect for sample introduction into the device.

Each of the 8 devices contained 9.5 mm long, 16 curvilinear channels that were 15 µm in width and 80 µm in depth with a radius of curvature of 120 µm (see Figure 4.1). The surface area of the 16 channels, which defined the cell selection bed, was 40 mm² with a volume of 250 nL. The chip output following selection and release was directed into a PCR microtube. A precell selection rinse of the chip was performed with 100 µL of 150 mM PBS at 50 mm s⁻¹. A programmable syringe pump (Harvard, Holliston, MA) with a syringe equipped with both a luer lock (Hamilton, Reno, NV) and a luer-to-capillary adapter (Inovaquartz, Phoenix, AZ) were used to infuse the water sample into the chip. Then, a cell suspension or water sample was infused into the chip at 0.5, 1.0, 5, 10, 40, 80, and 100 mm s⁻¹ linear velocities. A postcapture rinse with 100 µL of 150 mM PBS at 50 mm s⁻¹ (55.6 µL min⁻¹) was used to remove any nonspecifically adsorbed material.

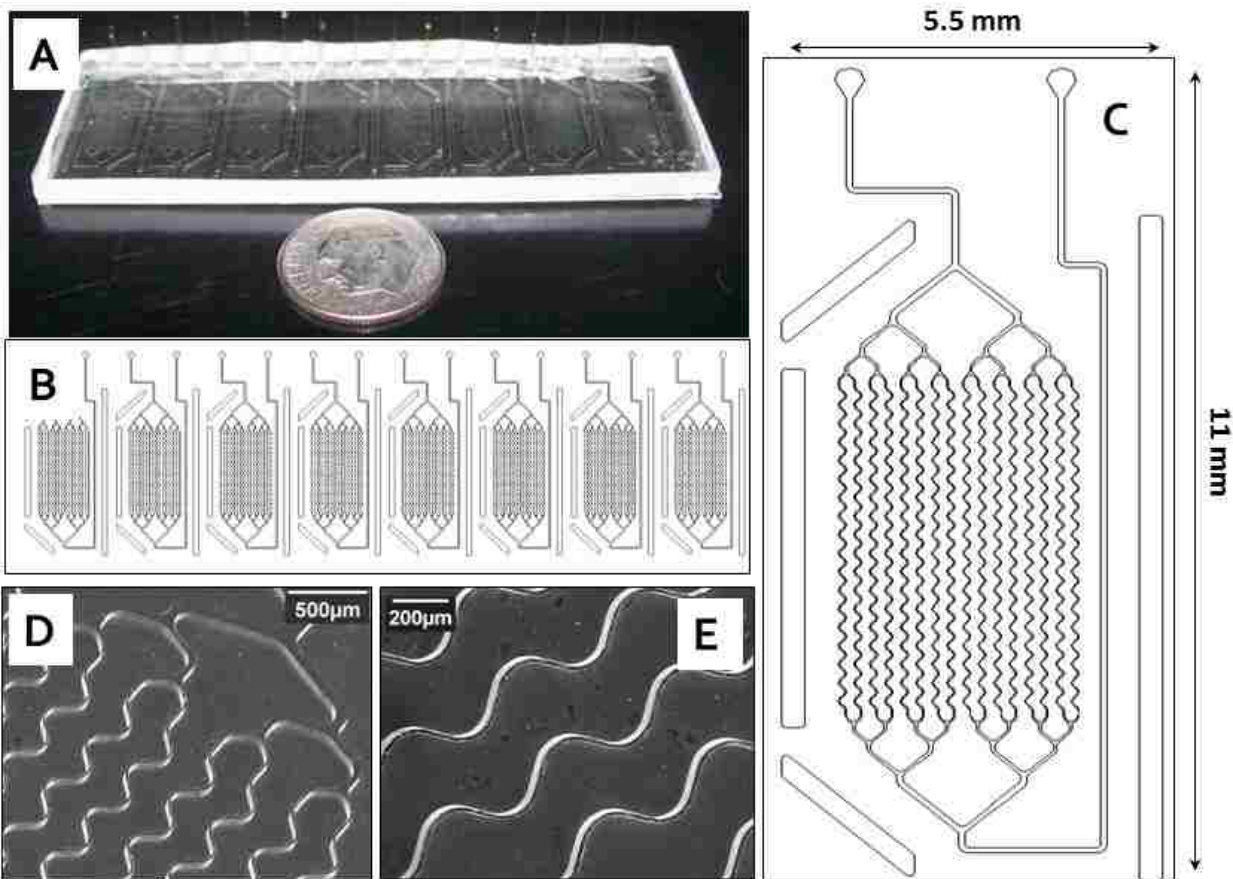


Figure 4.1 (A) A picture of the PMMA fluidic system for the positive selection of rare *E. coli* cells containing 8 different devices with each device comprised of 16 selection channels. (B) Schematic of the entire cell selection chip and (C) an expanded view of an individual cell selection device. Each device contained 9.5 mm long 16 curvilinear channels that were 15 μm in width and 80 μm in depth with a radius of curvature of 120 μm with respect to the channel center. (D-E) SEM of the brass molding tool.

Cells were then stripped from the channel walls using a Cellstripper solution and eluted from the chip in 5 μL of PCR buffer.

4.2.3 Antibody Immobilization

Antibody immobilization onto the photoactivated PMMA chip surface was carried out in a two-step process.⁷ The UV-modified, thermally assembled device was flooded with a solution containing 4 mg mL^{-1} EDC, 40 mg mL^{-1} NHS in a 150 mM MES (pH=6) and kept for 1 h at room temperature to obtain the succinimidyl ester intermediate. After this incubation, the EDC/NHS solution was removed by flushing nuclease-free H_2O

through the device. Then, an aliquot of 10 μL of 1.0 mg mL^{-1} of the polyclonal anti-*E. coli* O157 antibody solution in 150 mM PBS (pH=7.4) was introduced into the channels and allowed to react for 4 h in a high humidity box. The device was then rinsed with a solution of PBS (pH=7.4) to remove any non-specifically bound anti-*E. coli* O157 antibodies. The molecular weight of pAb was provided by the manufacturer and reported as ~ 150 kDa. IgG antibodies possess three discrete domains, two Fab fragments and one Fc, known to be flexible, but difficult to predict the exact conformation when immobilized to a solid surface.⁸ Roberts et al. determined IgG molecular dimensions of passively adsorbed IgG antibodies on a polystyrene surface to be 16-19 nm.²³ Dong et al. determined the diameter of covalently attached IgG to a gold surface to be 52.4 nm and determined that $\sim 22\%$ of the Abs were active after covalent attachment.²⁴ Assuming a 52.4 nm IgG diameter, we calculated the pAb density on the PMMA surface to be 4.6×10^{10} molecules cm^{-2} assuming a full monolayer coverage that was limited by the molecular dimensions of the pAb, which is supported by the higher surface density of carboxylic acid functional groups on the PMMA surface following UV exposure.^{25,26}

4.2.4 Fluorescence Microscopy

Observations of fluorescently-labeled cells in the chip's selection channels were accomplished using a Zeiss Axiovert 200M Inverted Microscope with a 40x fluorescence objective equipped with a 480 nm excitation filter. The microscope was fitted with a JAI CV 252 monochrome video camera. The images were captured directly to the hard drive of a Dell Precision 500M workstation via a Pinnacle Systems DV500 video capture card that was interfaced to a Pinnacle Systems Bluebox (Pinnacle Systems, Inc., Mountain View, CA). Adobe Premiere 6.0 (Adobe Systems, Inc., San Jose, CA) was

used for image acquisition and processing. In order to analyze the cell flow profiles and cell radial distribution in the selection channels, trajectories of fluorescently labeled *E. coli* O157:H7 cells flowing in an unmodified channel were investigated. Cell trajectories were captured via video microscopy and micrographs containing one half of the curved channels were extracted from the video. One hundred cellular events were located in the micrographs and the distance between the center of the cell event and the channel wall was determined using ImageJ 1.38x software (National Institute of Health, USA).

4.2.5 Flow Dynamics

To evaluate the flow dynamics of bacterial cells in the microchannel operated with hydrodynamic pumping, the Reynolds numbers (R_e) were calculated²⁷ using the equation, $R_e = \rho U d_h / \mu$, where, ρ , U , and μ are the density (997.04 kg m^{-3}), velocity (m s^{-1}), and viscosity ($8.9 \times 10^{-4} \text{ Pa s}^{-1}$) of the fluid, respectively, and d_h is the hydraulic diameter, defined as $2wh/(w+h)$, where w and h are the channel width and height, respectively. For a rectangular channel with $15 \text{ }\mu\text{m} \times 80 \text{ }\mu\text{m}$ dimensions, $d_h = 2.53 \times 10^{-5} \text{ m}$. R_e was calculated to be in the range of 0.01 to 2.83, for 0.5, and 100 mm s^{-1} linear velocities, respectively, indicating fully developed laminar flow within the tested flow range.

4.2.6 Water Sample Collection

Lake water samples were secured from two different sites: (i) Baton Rouge University Lake, LA (USA), which is a small man-made lake on the LSU campus created in the early 1920s with the damming of Bayou Duplantier, and (ii) Lake Granbury, TX (USA), which is a reservoir on the Brazos River constructed in 1969. The sampling depth was about 6 in. below the water surface. The University Lake is a part of the Lakes District System, which consists of six man-made lakes located approximately 1.2 miles east of the Mississippi River and 2.5 miles southeast of downtown Baton

Rouge, LA. Creation of the lakes began in the early 1920s with the damming of Bayou Duplantier, which flooded the old cypress swamp. There are approximately 140 outflows entering the lakes from storm drains of the watershed. University Lake is the largest lake of the system at approximately 195 acres in size. The lake has an average depth of 1.5 feet with some areas as low as 0.5 feet and a hydraulic retention time of ~50 days (<http://www.mvn.usace.army.mil/pd/projectsList/ProjectData/108824/reports/University%20Lakes%20PRP.pdf>).

Lake Granbury's surface area and volume are 34 km² and 167×10⁶ m³, with inflows primarily through the Brazos River. Upstream of Lake Granbury, the Brazos River watershed is dominated by rangeland. For extended periods of the year, inflows can be near-zero. When inflow events occur, they last several days and can exceed flushing rates of 20 d⁻¹.²⁸ Much of the shoreline of Lake Granbury is residential, with only a portion of this area serviced by a sewage system. In addition, some areas of Lake Granbury are protected from flushing (*i.e.*, coves with longer hydraulic residence times). *E. coli* concentrations can become problematic in this lake system (Roelke, unpublished data), where the likely source of contamination is aging septic systems that leak into the lake. *E. coli* concentrations are able to accumulate in areas of low flushing. For this study, water samples were collected by hand from multiple coves of Lake Granbury.

4.2.7 Water Sample Filtration

Water samples from recreational lakes (100 mL) and wastewater samples (1 mL) were filtered using hydrophilic (PVP-coated) polycarbonate track etched membranes (PCTE, Sterlitech, Kent, WA) membrane filters. The pore size of the membranes used was 10 µm for the prefiltration to remove large particulates and 0.1 µm for further

filtration and volume reduction prior to input into the microfluidic device. Water samples were filtered through the 10 μm pore size membranes at 10 mL min^{-1} , and the effluent was collected and filtered through the 0.1 μm pore size membranes at 2.5 mL min^{-1} . The membrane was rinsed with ~ 1 mL of pure water to exhaustively remove material from the surface and used as the input to the microfluidic chip. The 10 μm pore size membrane filter did not change the total volume of the sample; however, it did remove solid particulates and debris.

4.2.8 *E. coli* Detection via Culturing

E. coli were in some cases analyzed from membranes using a modified membrane-Thermotolerant *E. coli* agar (Modified mTEC EPA Method 1603), which uses a membrane filter procedure for the detection and enumeration of *E. coli* bacteria in ambient waters and disinfected waste waters. The modified medium contained a chromogen (5-bromo-6-chloro-3-indolyl- β -D-glucuronide), which is catabolized to glucuronic acid producing a red- or magenta-colored compound by *E. coli* that produces the enzyme, β -glucuronidase. A sample was filtered through a 0.1 μm pore diameter membrane, which retained the bacteria. After filtration, the membrane was placed on a selective and differential medium, modified mTEC agar, incubated at 35 ± 0.5 $^{\circ}\text{C}$ for 2 ± 0.5 h to resuscitate injured or stressed bacteria and then incubated at 44.5 ± 0.2 $^{\circ}\text{C}$ for 22 ± 2 h. The target colonies on the modified mTEC agar are red or magenta in color after incubation and can be counted manually via visual inspection.

4.2.9 Polymerase Chain Reaction (PCR) and Real-Time qPCR

The primer sequences used for the PCR were as follows: *slt1*, forward primer (FP) – CAG TTA ATG TGG TGG CGA AGG ($T_m=56.3$ $^{\circ}\text{C}$), reverse primer (RP) – CAC CAG ACA ATG TAA CCG CTG ($T_m=56.2$ $^{\circ}\text{C}$) product size – 348 bp; *uidA*, FP – GCA

AAA CTG TGG AAT TGG G ($T_m=54.8$ °C), RP – TGA TGC TCC ATA ACT TCC TG ($T_m=52.0$ °C), product size – 252 bp. These primers were previously reported by Cebula et al. for recognition of *E. coli* O157:H7 through a mismatch amplification mutation assay.⁶ PCR cocktails consisted of 0.5 μ M primers, 0.2 mM dNTP's, 1x PCR buffer, 5 U of *Taq* DNA polymerase, DNA template and ultrapure water. The PCRs were carried out using a commercial thermal cycling machine (Techne, Burlington, NJ) with cycles consisting of an initial denaturation step at 94 °C for 5 min followed by 30 cycles of the following: 94 °C for 30 s, 58 °C for 40 s, 72 °C for 60 s. A final extension at 72 °C for 7 min was followed by a cooling step at 4°C. Real-time qPCRs were performed on a Stratagene Mx4000 real-time PCR machine with Brilliant® II SYBR® Green QPCR Master Mix (Stratagene, La Jolla, CA). The reactions (50 μ L) were prepared by combining nuclease-free water, master mix, primers (final concentration=40 nM), and reference dye ($e_x/e_m=584/612$ nm) to a final concentration of 30 nM. The volume of the template/unknown sample added to the reaction was 5 μ L and was the total volume of the pre-concentrated cells eluted from the microchip (chip pre-concentration factor = 2×10^2). The PCR protocol used involved a three-step cycling procedure: (1) 10 min at 95 °C; (2) 46 cycles 30 s at 95 °C, 60 s at 58 °C, 60 s at 72 °C; and (3) a dissociation step consisting of 81 cycles of ramping the temperature between 55 and 95 °C (0.2 °C s^{-1}). Standard calibration curves were constructed and PCR amplification efficiencies were determined among different experiments.

4.2.10 Slab Gel Electrophoresis

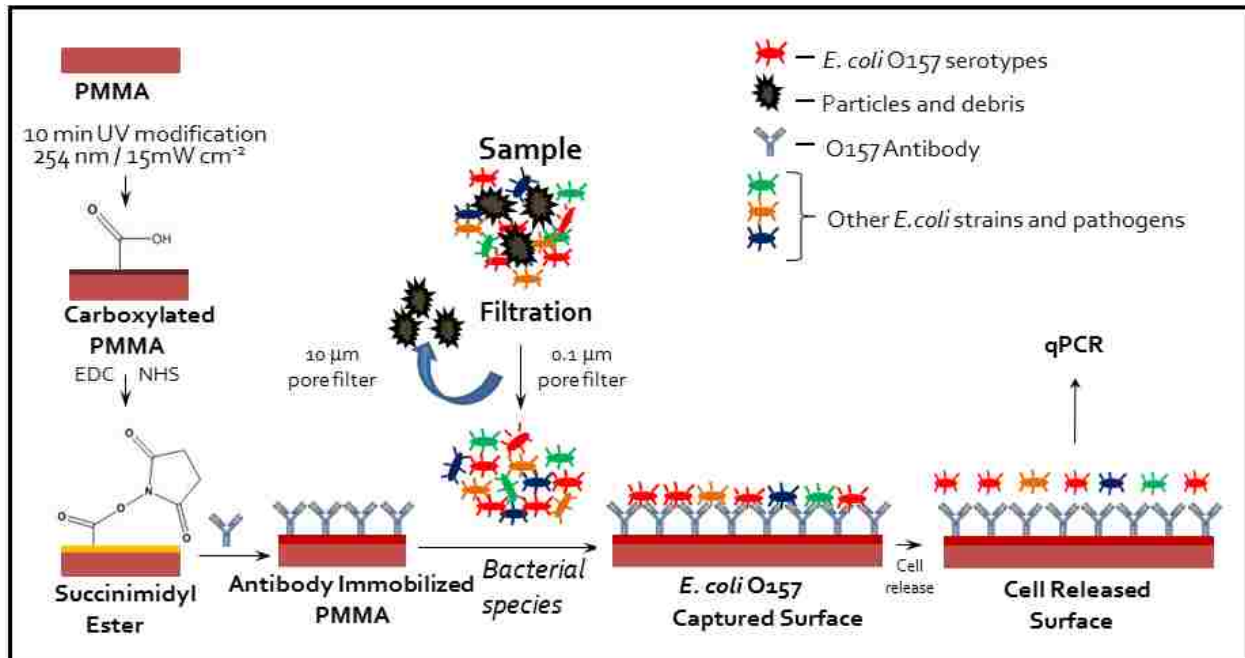
PCR products were electrophoresed using a 2% agarose gel (Bio-Rad Laboratories, Hercules, CA) pre-stained with ethidium bromide. The sample volume loaded onto the gel was 5 μ L with 1 μ L of the loading dye. Amplicons were indexed

against a DNA sizing ladder (50-1,000 bp, Molecular Probes, Eugene, OR). Separation was performed at 4.8 V cm^{-1} in 1x TBE (Tris/Boric Acid/EDTA, Bio-Rad Laboratories). Gels and culturing plates were imaged using a Logic Gel imaging system (Eastman Kodak).

4.3 Results and Discussion

4.3.1 Low-Abundant *E. coli* O157:H7 Cell Processing

Scheme 4.1 presents an overview of the processing strategy used for the selection and identification of *E. coli* O157:H7 cells. The processing steps involved: (i) chip preparation; (ii) sample filtration using PCTE membranes to remove large particulates from the sample and to provide pre-enrichment; (iii) sample processing on the chip and cell release; and (iv) benchtop real-time qPCR quantification of the selected cells. For the recreational water, the time required to filter a 100 mL input using both the 10 and 0.1 μm filters to reduce the total volume to 1 mL was 50 min, producing a volume reduction of 100-fold and, thus, a 10^2 pre-enrichment assuming 100% recovery. Processing a total input volume of 1 mL using the 8 devices poised on the microfluidic chip (Figure 4.1) at a linear flow velocity of 5 mm s^{-1} ($5.3 \mu\text{L min}^{-1}$) required 24 min and produced an enrichment factor of 2×10^2 . Therefore, the 0.1 μm filter and microfluidic chip generated a total enrichment factor of 2×10^4 with a processing time of 74 min. Membranes before and after filtration were inspected under a microscope and showed that the majority if not all of the solid material had been removed from the sample prior to chip processing (see Figure 4.2). To achieve maximum recovery of bacterial cells from the 0.1 μm filter, the filter was washed with 1 mL of water and control experiments with known amounts of cells were performed. Previously, Wang et



Scheme 4.1 Overview for the Processing Strategy Adopted for Analysis of Extremely Low Abundant *E. coli* O157:H7 and Other Serotypes Using Positive Selection and Enrichment via a Microfluidic Chip with Subsequent Quantification through Real-Time qPCR

al. evaluated the performance of these types of membrane filters with pore sizes ranging from 0.1 to 0.45 µm to determine the effect of cell shape and size on bacterial filterability and determined that bacterial shape, rather than their absolute size, was a key factor in determining cell recovery.²⁹ We recovered 92±5% ($n=4$) of *E. coli* O157:H7 microbial material using the 0.1 µm. Bacterial cells were not lysed while on the membrane because this process would not guarantee the high quality quantitative analysis of DNA. A DNA extraction step should be performed to free the sample from any potential inhibitors present on the membrane surface.³⁰ In our approach, the immunocapture of the pathogens of interest using microfluidic channels followed by an extensive wash and subsequent release from the capture surface produced high quality

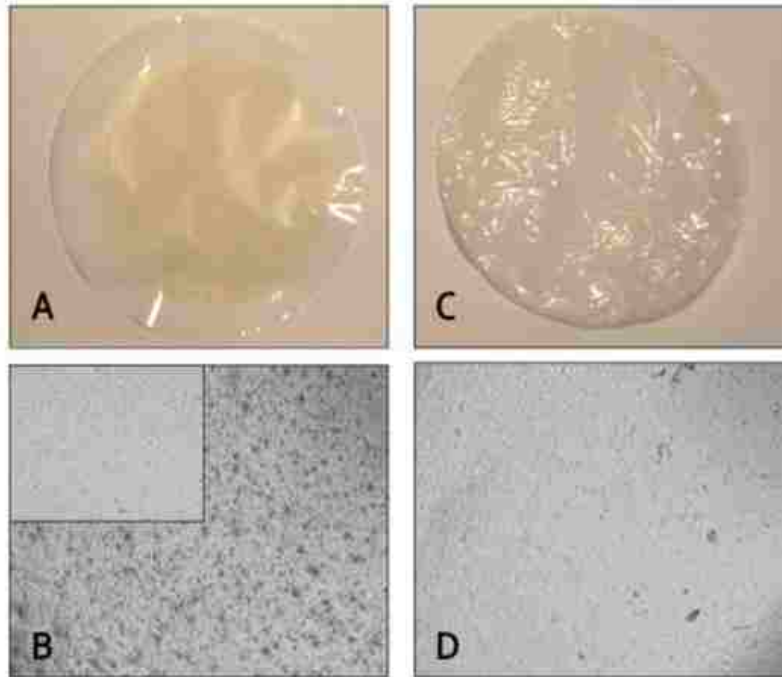


Figure 4.2 **A** and **C** are pictures of 0.1 μm PCTE membranes after filtration and washing, respectively, while **B** and **D** correspond to 40x microscope images of the same membranes after filtration and washing, respectively. The insert in **B** shows a micrograph of the membrane before filtration. The sample processed here was that taken from Lake Granbury in Texas.

qPCR results that were not seen in the case using *E. coli* washed directly from the 0.1 μm filter (data not shown). In addition, the use of the microfluidic device provided high preconcentration factors due to the small selection bed volume, improving the limit-of-detection for the qPCR.

4.3.2 Water Sample Filtration

The water samples (100 mL) were first filtered using a 10 μm pore size Polycarbonate Track Etched membranes (PCTE). Using a vacuum pump with the filter allowed processing water samples at a volume flow rate of 10 mL min^{-1} . This step ensured that large debris was removed from the sample before it entered the microfluidic device. Effluent from that step was subsequently filtered on a 0.1 μm pore size PCTE membrane, on which bacteria and debris larger than 0.1 μm and smaller than 10 μm were retained. Samples were processed at 2.5 mL min^{-1} volume flow rates.

The next step involved washing residual material from the 0.1 μm pore membrane using 1,000 μL of water, which also resuspended the retained bacterial material. This was performed thoroughly making sure none of the retained material was left on the membrane. Membranes before filtration, after filtration and washing were inspected under a microscope. Figure 4.2 presents results from these evaluations.

4.3.3 *E. coli* Flow Dynamics in Microfluidic Channels

As we demonstrated in our previous work discussing the positive-selection of cells via surface-immobilized Abs, hydrodynamic flow through low R_e channels can produce a cell-free layer near the channel wall due to focusing effects, significantly reducing cell:wall interactions and thus, cell recovery.^{17,18} This focusing effect is flow rate dependent, but can be reduced using a channel geometry that is sinusoidally configured, at least for relatively large cells such as tumor cells. Therefore, we investigated cell flow dynamics and possible focusing artifacts for much smaller cells, such as *E. coli*, in curved channels. Radial cell distribution histograms for 1, 5, 40, and 100 mm s^{-1} linear flow velocities are presented in Figures 4.3A-D. Cell distributions indicated that the number of cells at the outer edge of a single curved region increased only slightly with flow velocity compared to the number within the inner edge. For example, the ratio of cells at the outer-to-inner edges of a curve were 1.6, 2.0, 2.5, 3.0, and 11.0 for 1, 10, 40, 80 and 100 mm s^{-1} flow rates, respectively. Similar observations were reported by Mayeed et al.³¹

Previously, we reported that sinusoidal channels were more effective than straight channels for recovering circulating tumor cells at relatively high linear velocities due to the lack of a cell-free marginal zone adjacent to the outer-edge of the wall for a single turn. This resulted from centrifugal forces acting on the cells and increased

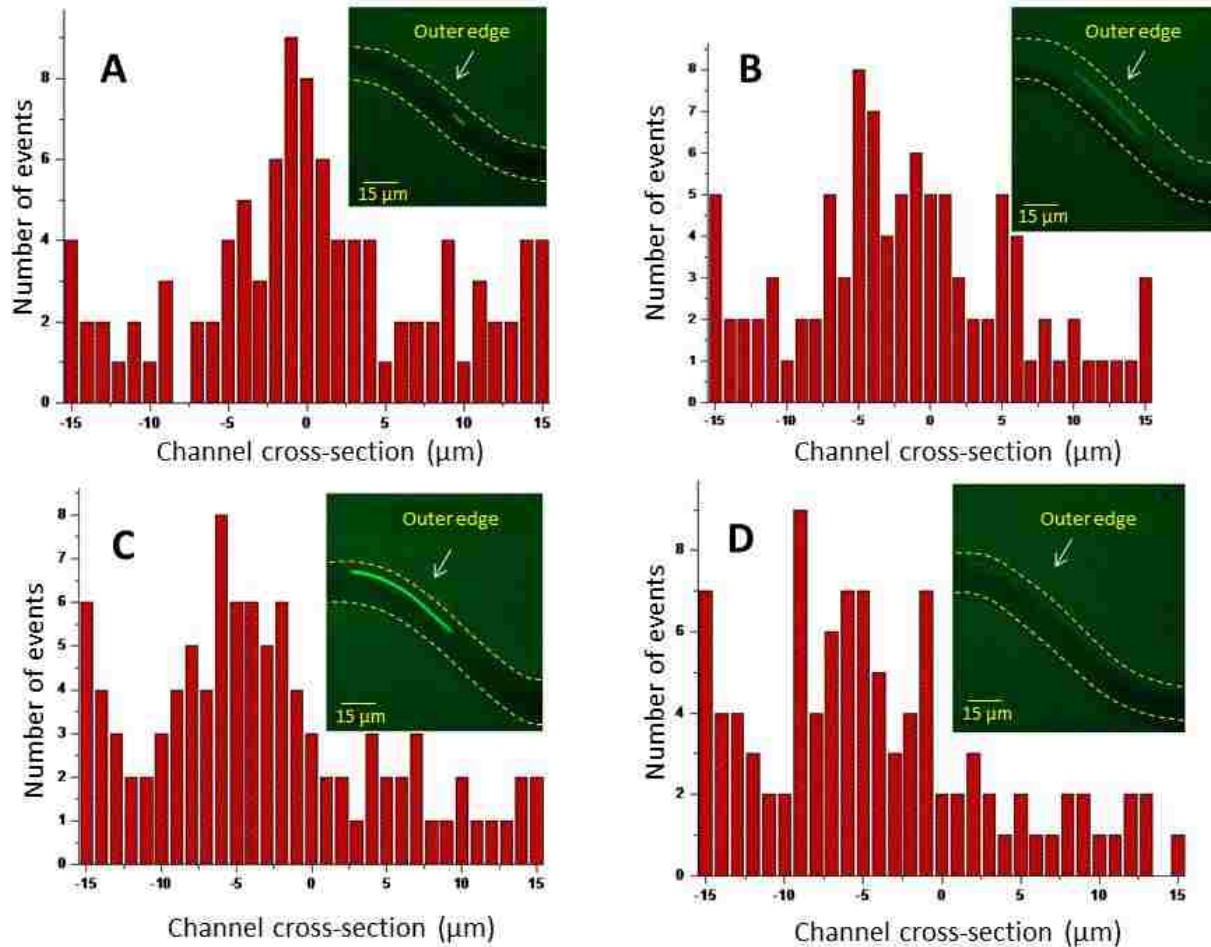


Figure 4.3 Histograms of the radial position of bacterial cells in an unmodified sinusoidally-shaped microchannel at linear velocities of (A) 1, (B) 5, (C) 40, and (D) 100 mm s^{-1} . The dashed lines designate the channel walls. The cells were imaged using fluorescence microscopy with the cells stained using PKH67. The coordinate system adopted used 0 as the channel centroid, (-) values refer to locations with respect to the outer edge of the channel and (+) values represent radial positions in the direction of the inner edge of the channel.

cell:wall interactions generating higher cell recoveries.¹⁷ In the data presented in Figure 4.3, these effects were much less dramatic for the *E. coli* cells most likely due to the smaller size of these cells. In fact, as can be seen from Figure 4.3C, the *E. coli* cells did not cross flow lines through the turns with fully developed laminar flow. Therefore, a much more uniform cellular radial distribution was observed, which indicates that higher flow rates could be used to increase sample processing throughput based solely on the cells' flow dynamics.

4.3.4 Nonspecific Cell Selection

Even though the affinity purified pAb were directed against *E. coli* O157:H7, other types of *E. coli* serotypes such as O157:H12, O157:H42, O157:H29, O157:H19, and O157:H45, could potentially be selected using this reagent as well as other species, such as *S. sonnei* or *C. freundii* (see www.kpl.com). However, even if these bacterial types were selected during microchip enrichment, they would not be transduced during the enumeration process using real-time qPCR because of a lack of the specific marker genes used for reporting specifically on *E. coli* O157:H7.³² We tested the nonspecific selection of *E. coli* K12. Cells were infused into the microfluidic channels at 5 mm s⁻¹, the same conditions used for *E. coli* O157:H7 selection. After a postcapture rinse, fluorescence micrographs indicated that no *E. coli* K12 cells were found in the selection beds when decorated with the *E. coli* O157 pAbs.

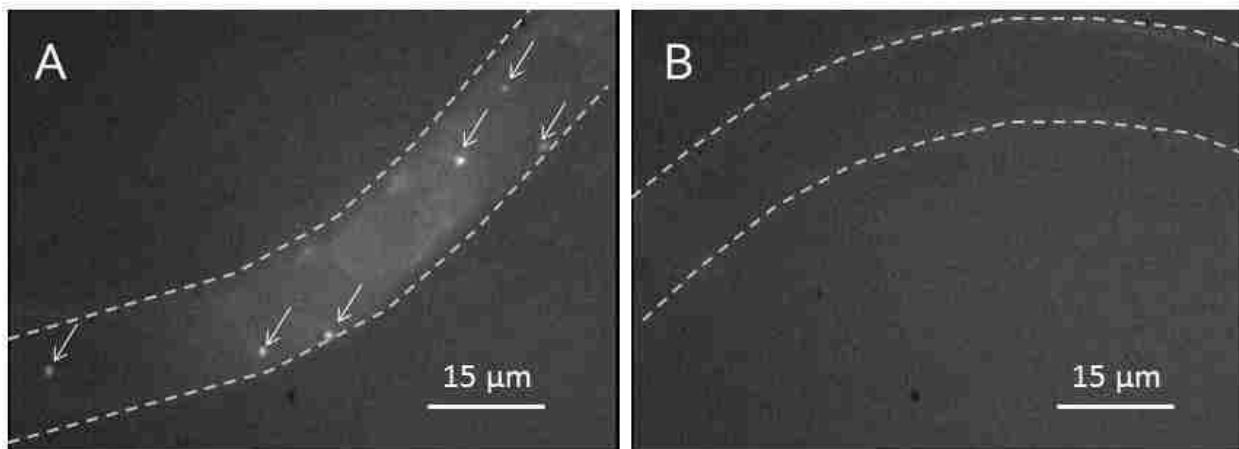


Figure 4.4 Fluorescence images of a microchannel with (A) *E. coli* O157:H7 cells and (B) *E. coli* K12 cells captured on an antibody modified PMMA surface. The dashed lines designate the edges of the channel.

Figure 4.4 shows fluorescence micrographs taken after introducing both types of cells. In Figure 4.4A, one can clearly see multiple events of anchored *E. coli* O157:H7 cells (indicated with arrows), while in Figure 4.4B, there was a lack of any such events

for the K12 serotype. Also, minimal nonspecific cell interactions with the poly(methylmethacrylate), PMMA, channel surface was also found (data not shown) due to the weak adhesion forces and the presence of hydrodynamic shear that could remove any nonspecifically bound cells.¹⁷

4.3.5 *E. coli* O157:H7 Cell Release from the Channel Surface

Due to the strong adhesion between the captured cells and the antibody-modified capture surface, hydrodynamic release from the capture surface to provide intact *E. coli* O157:H7 cells for real-time qPCR interrogation was found to not be feasible (data not shown). Following a postcell capture rinse performed with 150 mM PBS, a Cellstripper solution was infused into the channels to dislodge antibody-induced adhesion of cells to the channel wall. The use of the Cellstripper™ solution, a non-enzymatic cell dissociation solution formulated with a proprietary mixture of chelators, for the release of antibody-captured cells without causing cell disassembly was investigated.

Figure 4.5 shows time-lapse micrographs of a surface-captured cell that was subjected to Cellstripper™ processing. Stoke's forces induced by hydrodynamic shear produced from laminar flow in the presence of the Cellstripper™ solution allowed for efficient release of these cells in less than 4 min. Twenty-five cells were monitored, and the average time required for their release was determined to be 3.4 ± 0.3 min. Following incubation with the stripper solution, the released cells were flushed from the selection amplification. We determined that a concentration of Cellstripper up to 10% in the real-time qPCR cocktail did not affect these results (see Figure 4.6A-D).

4.3.6 Cell Recovery

In order to maximize the recovery of *E. coli* O157:H7 cells from water samples and maintain high sampling throughput, the processing linear flow velocity thru the

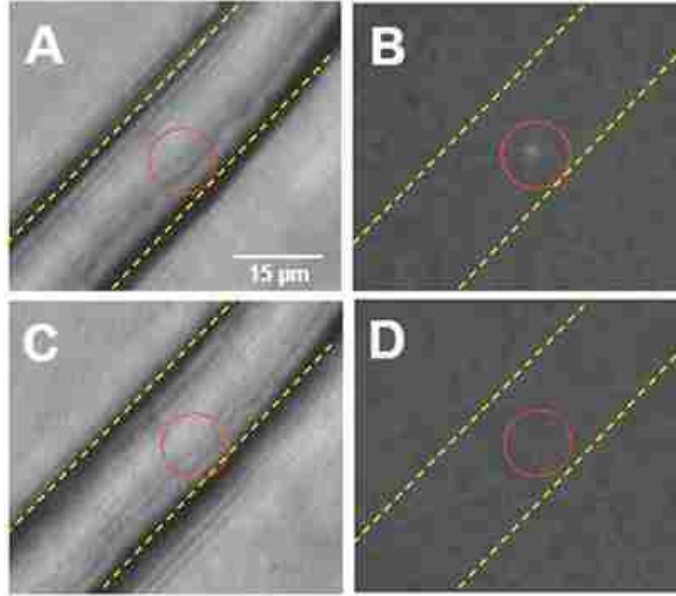


Figure 4.5 Time-lapse micrographs showing Cellstripper™ and hydrodynamic shear-mediated release of a captured fluorescently-labeled *E. coli* O157:H7 cell (circled in red) from the capture surface. (A) A brightfield image prior to exposure of the captured cell to the stripping solution. (B) A fluorescence image of the same spot at $t=0.1$ min following incubation with the Cellstripper™ solution. (C) A bright field image at $t=3.4$ min after introduction of the Cellstripper™ solution was infused into the channel and disruption of the binding complex was evident by the bacterial cell being released from the surface. (D) A fluorescence image at $t=3.5$ min following introduction of the stripping solution – the cell appears to be released from the capture surface. The stripping solution was hydrodynamically pumped through the fluidic chip at a linear velocity of 25 mm s^{-1} .

selection microchannels was optimized. *E. coli* O157:H7 capture efficiency at different flow rates and different cell densities ($3\text{-}30 \times 10^3 \text{ cfu mL}^{-1}$) were determined using real-time qPCR. Linear flow velocities were varied between 0.5 and 100 mm s^{-1} . The results of these experiments are depicted in Figure 4.7A as a plot of *E. coli* O157:H7 capture efficiency (%) vs linear velocity (mm s^{-1}). We observed that a linear flow rate of 5 mm s^{-1} produced the highest recovery; $71.6 \pm 1.4\%$ ($n=5$). The general trends observed in the plot shown in Figure 4.7A can be explained based on the Chang/Hammer model for mobile cell interactions with immobilized association elements.^{17,33} Basically, the two processes that primarily dictate a successful antibody/cell interaction involve: (i) the encounter rate, which describes the rate of delivery of cells to the channel surface and

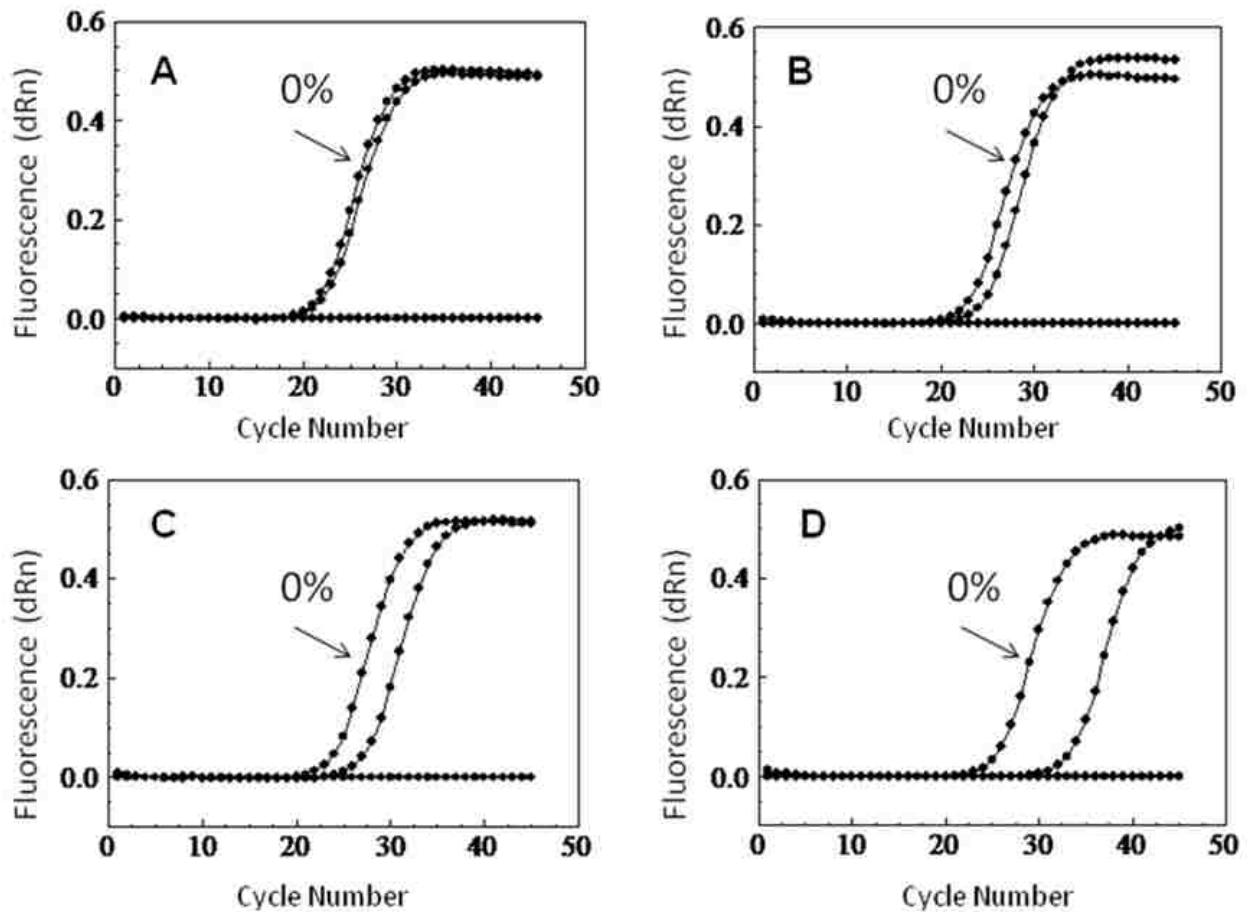


Figure 4.6 Real-time PCR amplification plots for the *stt1* gene using RT qPCR with a master mix containing different concentrations of Cellstripper™ in standard samples (indicated with arrows in the figure). The protocol involved a three-step cycle: (1) 10 min at 95 °C, 46 cycles; (2) 30 s at 95 °C, 60 s at 58 °C; and (3) 60 s at 72 °C. The PCR products were observed in real-time using a SYBR Green dye.

is flow rate dependent with this rate increasing with linear velocity, and (ii) the reaction probability between the surface tethered antibody and the mobile cell antigenic target, which is dependent on the reaction kinetics between the antigen/antibody complex with this probability decreasing at high linear velocities.¹⁷ Therefore, the observed optimal linear velocity ($\sim 5 \text{ mm s}^{-1}$) results from a balance between the reaction kinetics and the encounter rate.

Capture efficiency decreased with increasing channel width as well^{17,18} (see Figure 4.7B). We evaluated the recovery of *E. coli* cells using channels with variable

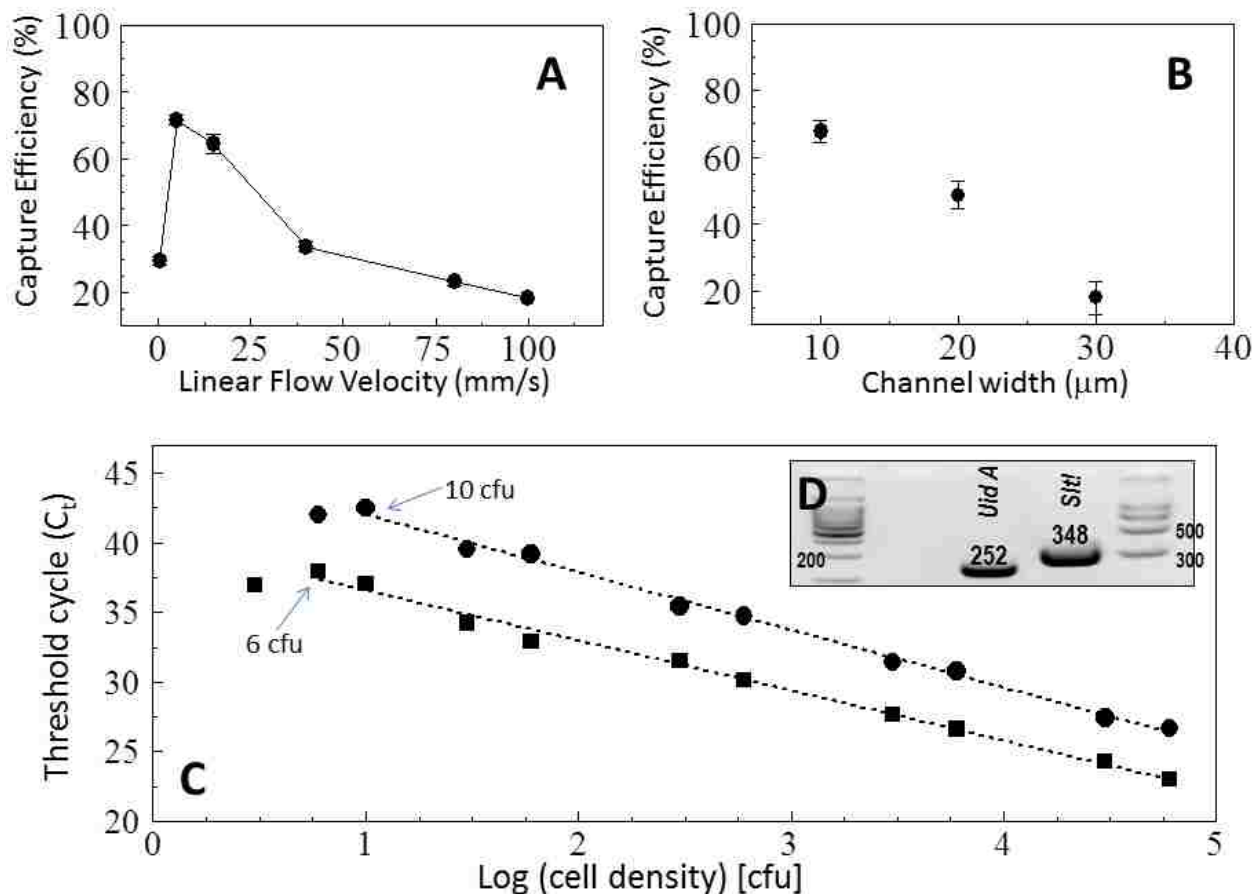


Figure 4.7 (A) Capture efficiency data of *E. coli* O157:H7 as a function of the cells' translational velocity using the microfluidic chip shown in Figure 4.1. The number of captured cells was determined via real-time qPCR. (B) Cell capture efficiency as a function of the channel width using a translational velocity of 5 mm s⁻¹. Channels used contained a variable width (10, 20, and 30 μm) but the same depth (30 μm) and length (3 cm). (C) Standard curves for the real-time, qPCR analysis of *E. coli* O157:H7 using *stt1* (filled squares) and *uidA* (filled circles) genes. C_t values of known samples were plotted against the corresponding cfu of the bacteria. The linear regression analysis for *stt1*: $y = -3.456 \log(x) + 37.12$ ($r^2 = 0.997$) and *uidA*: $y = -3.373 \log(x) + 40.99$ ($r^2 = 0.996$). (D) A fluorescence agarose gel image of the 252 bp and 348 bp PCR products for *uidA* and *stt1* genes, respectively. The amplicons were generated with 10×10^3 cfu/reaction of the *E. coli* O157:H7 serotype.

widths but the same depth (30 μm) and length (3 cm) and cells flowing at 5 mm s⁻¹ linear velocity. We observed much higher recoveries for narrower channels as opposed to wider channels (68%±2%, 49%±2%, and 18%±5% for channel widths of 10, 20, and 30 μm, respectively). We previously demonstrated that cell recoveries are maximized when the channel width approaches the average cell diameter.¹⁷ Unfortunately, we were limited by the micromachining technique employed here to a channel width of 10 μm,

but the use of narrower channels will most likely increase the recovery by increasing the number of cell/wall contacts. Narrower channels can be fabricated using optical lithography to make the molding tool as opposed to high precision micromilling.³⁴

4.3.7 Cell Enumeration in Water Samples

The selective enumeration of *E. coli* O157:H7 used real-time qPCR and two sets of primers targeting the *slt1* and *uidA* genes. Primers for these genes were reported by Cebula et al.³⁴ and were extensively tested for specificity in comparison to other serotypes of *E. coli*. Additionally, we tested these primers with other microbes, some potentially present in the sample. No PCR products were observed for *S. aureus*, *B. subtilis*, *E. aerogenes*, *M. luteus*, or *E. coli* K12 using the *uidA* and *slt1* specific primers. PCR products with the size appropriate for the particular gene being interrogated for *E. coli* O157:H7 were observed (see Figure 4.7D).

Calibration curves for *E. coli* O157:H7 were generated using serial dilutions of standard *E. coli* O157:H7 cell suspensions between 1 cfu and $\sim 3 \times 10^6$ cfu (see Figure 4.7C) in samples containing 100 mL of water. The linearity between the C_t values and the number of target cells was observed over 5 orders of magnitude ($r^2 \geq 0.996$). The slope of the calibration curve, which is directly related to the average amplification efficiency throughout the cycling reaction (efficiency) $10^{(-1/\text{slope})-1}$, was found to be -3.593 ± 0.231 , yielding a $98.5 \pm 1.7\%$ efficiency ($n=5$) for *slt1*, and -3.616 ± 0.372 , for an $89.2 \pm 2.4\%$ efficiency ($n=5$) for the *uidA* gene. The limit-of-detections (expressed as the amount of cells detected in the 100 mL sample at least 95% of the time) were calculated to be 6 cfu for the *slt1* gene and 10 cfu for the *uidA* gene. Similar or higher real-time qPCR limits-of-detections were reported.³⁵

Plots of the real-time normalized fluorescence intensity as a function of cycle number for the *slt1* gene for different cell numbers are presented in Figure 4.8A. The analysis of dissociation curves, plotted as the first derivative of the reference dye-normalized fluorescence intensity reading multiplied by $-1(-Rn'(T))$, as a function of temperature displayed one population with a transition temperature of 80-82 °C, indicating the presence of only a single PCR product of the anticipated sequence content (see Figure 4.8B). Standard curves were generated using serial dilutions of standard *E. coli* O157:H7 cell suspensions ranging from 1 cfu to $\sim 10^6$ cfu per reaction for both *slt1* and *uidA* genes. The linearity between the C_t values and the number of target cells was observed over five orders of magnitude. The C_t values of the known standards were plotted versus logarithm of the cell count for each standard, creating calibration curves from which the unknown concentrations were determined.

Control samples (single blinded studies) were also evaluated in which *E. coli* O157:H7 samples were spiked at levels of 30-800 cfu per 100 mL input. This data was used to construct a calibration plot of C_t versus log (cell density, see Figure 4.7C). For example, the number ($n=3$) of *E. coli* O157:H7 cells determined from the calibration plot was 34 ± 4 (RSD of 12%) at the 30 cfu spike level. At a 400 cfu spike level, the average cell count for the assay was 405 ± 5 with an RSD of 1.2%. A blank sample was also analyzed, and no *E. coli* O157:H7 was detected.

We next evaluated the microchip/real-time qPCR assay to assess the quality of different water samples. These samples consisted of samples from two lakes and sewer water from a purification plant in Baton Rouge. We should also note that *E. coli* obtained directly from the 0.1 μm filter and tested via realtime qPCR without processing in the

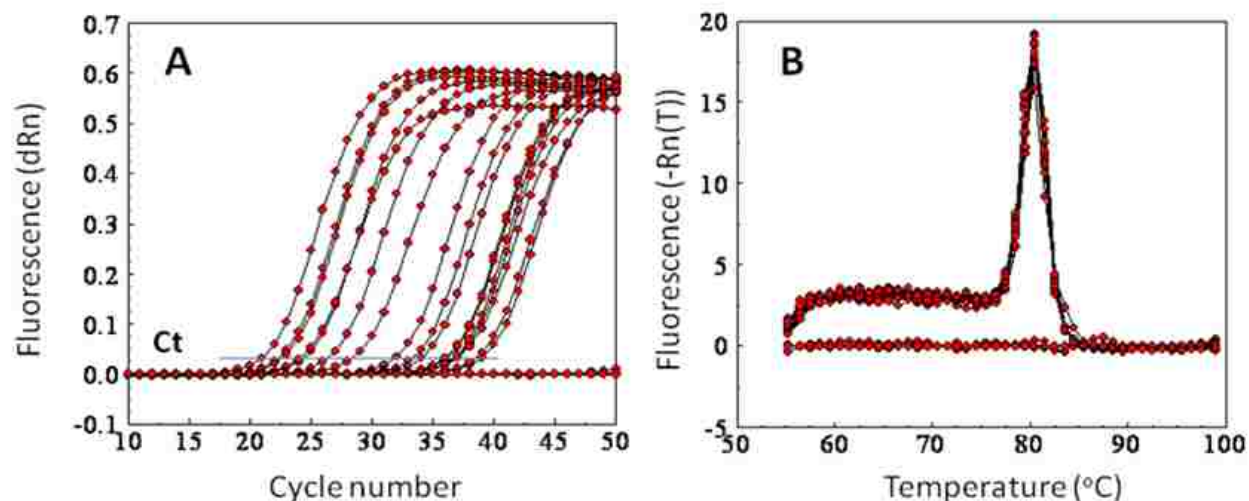


Figure 4.8 (A) Amplification plots for the *slt1* gene using real-time qPCR for serial dilutions of *E. coli* O157:H7 ($6 - 60 \times 10^3$ cfu/reaction). (B) Dissociation curves for amplicons obtain in (A). The PCR protocol used involved a three-step procedure: (1) 10 min at 95 °C; 46 cycles consisting of (2) 30 s at 95 °C, 60 s at 58 °C, 60 s at 72 °C; and (3) 81 cycles of ramping the temperature between 55 and 95 °C ($0.2 \text{ } ^\circ\text{C s}^{-1}$).

microchip produced failed PCR results due most likely to the presence of potential PCR inhibitors that were removed in the fluidic chip following cell selection and rinsing.

In the Lake Granbury sample, the total *E. coli* levels were detected at 5 cfu 100 mL⁻¹ and *E. coli* O157:H7 serotype at 4 cfu 100 mL⁻¹. Water from University Lake in Baton Rouge was evaluated only for the total *E. coli* level using EPA Method 1603 and was determined to be 15 cfu 100 mL⁻¹ (see Figure 4.9A). After performing the assay using the microfluidic chip, we determined that for both of these water samples, the level of *E. coli* O157:H7 was below the limit-of-detection. This is understandable given the fact that the recovery is 72%, and therefore, the approximate numbers of *E. coli* O157:H7 from Lake Granbury would be ~3 cells, which is below the limit-of-detection for both the *slt1* and *uidA* genes.

Next, we evaluated wastewater samples using EPA Method 1603 and found *E. coli* levels of 2.6×10^6 cfu 100 mL⁻¹ (see Figure 4.9B). In wastewater samples, we

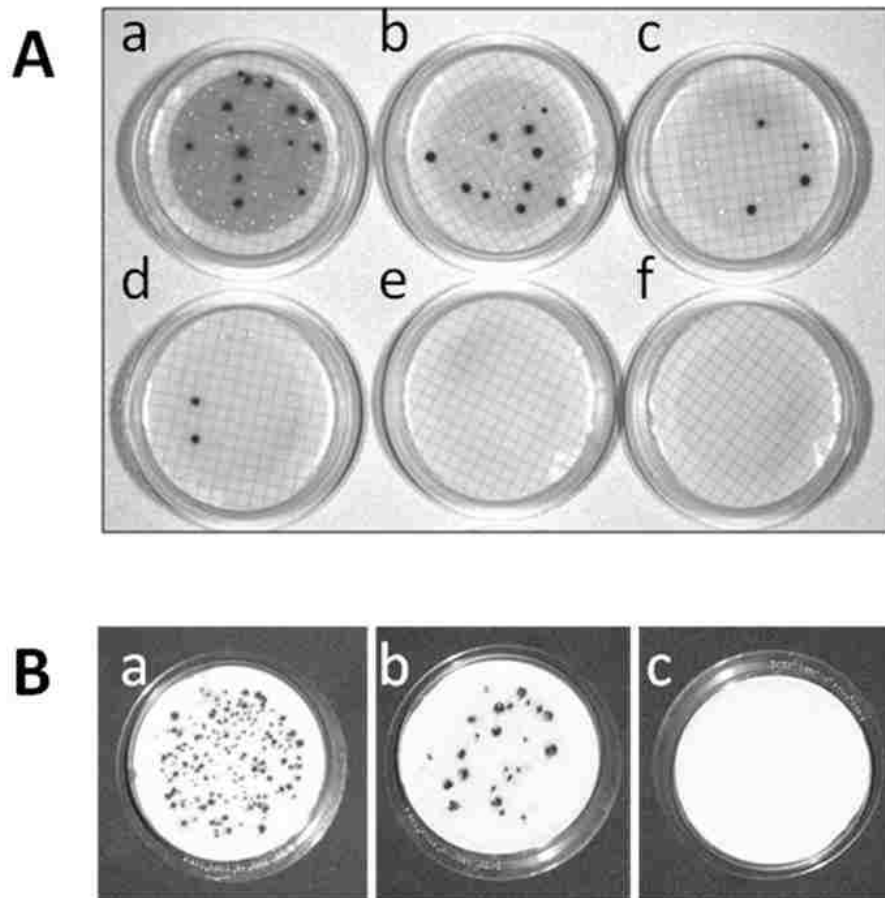


Figure 4.9 *E. coli* colonies formed on the modified mTEC agar surface. The *E. coli* colonies are represented as dark spots. **(A)** Baton Rouge Lake water, filtered volumes: **a** – 100 mL sample, **b** – 25 mL, **c** – 10 mL, **d** – 5 mL, **e** – 0.1 mL, **f** – blank. The membrane filter in sample (a) was used to calculate the number of colonies of *E. coli* per 100 mL of water. The *E. coli* concentration was calculated as (# colonies/volume processed)×100. **(B)** A waste water sample processed using the mTEC agar surface; volumes processed: **a** – 1 mL; **b** – 0.1 mL; **c** – 0 mL (blank). The membrane filter in sample b has the acceptable number of colonies to calculate the number of *E. coli* per 100 mL of waste water.

detected $0.96 \times 10^6 \pm 0.2$ cfu 100 mL^{-1} of *E. coli* with the serotype O157:H7. Also, we calculated the cell capacity of the microchip selection beds possessing a surface area of 40 mm^2 , and this value was determined to be 260×10^6 cells. Thus, the level of cells collected from the wastewater sample is well below the saturation limit.

4.3.8 Cellstripper™ Effects on Real-Time Quantitative PCR (RT qPCR)

The effect of the non-enzymatic cell dissociation solution on the efficiency of RT qPCR was investigated. The amplification plots of baseline-corrected, reference dye-

normalized fluorescence (dRn) as a function of the cycle number for the *slt1* gene for different concentrations of Cellstripper™ with different cell numbers are presented in Figure 4.6A-D. Typically, the reproducibility of qPCR assays determining cell numbers from multiple runs in the absence of the Cellstripper solution was observed to be 2-10%. Based upon these results, variabilities between the Cellstripper and no Cellstripper qPCRs of $\leq 5\%$ for concentrations of Cellstripper™ up to 10% in the RT qPCR cocktail were concluded to not significantly affect these results (see Figure 4.6B).

4.4 Conclusions

I demonstrated the ability to select and quantitatively enumerate the *E. coli* O157:H7 serotype free from other serotype interferences, which is important due to the large number of *E. coli* types and the O157:H7 serotype health-related issues. The strategy developed offered the ability to monitor water quality without the need for a time-consuming cell culture step. I also showed the ability to recover cells with $\sim 72\%$ efficiency from 100 mL input volumes with the real-time qPCR step providing a limit of detection of 6-10 cfu. The entire series of processing steps can be implemented in under 5 h, and this could significantly be reduced by transitioning more of the processing steps to the chip. For example, increasing the throughput of the fluidic chip through the use of more fluidic vials that are deeper can provide the opportunity to process 100 mL of input directly without the need for the intermediate 0.1 μm filtering step. In addition, moving the real-time qPCR step to the chip can also reduce processing time significantly due to the more efficient thermal management properties of microscale PCR.³⁶

The microchip enrichment procedure provided the following advantages: (i) the enrichment step can recognize O157 types in intact and virulent cells and in stressed

and nonculturable cells; (ii) cells enriched on the chip can be isolated from potential contaminants that can interfere with nucleic acid-based analysis; and (iii) the chip can preconcentrate cells to a detectable level with an enrichment of 2×10^2 in its current rendition. I envision the potential to probe for a large number of different strains of enterohemorrhagic *E. coli*, which includes more than 100 different non-O157 strains.³⁷⁻

³⁹ By proper choice of pAbs and specific probes for the real-time qPCR, one could monitor a large panel of suspected *E. coli* strains from a single sample.

4.5 References

1. Ishii, S.; Hansen, DL.; Hicks, RE.; Sadowsky, MJ. *Environ. Sci. Technol.* **2007**, *41*, 2203–2209.
2. Yamahara, KM.; Layton, BA.; Santoro, AE.; Boehm, AB. *Environ. Sci. Technol.* **2007**, *41*, 4515–4521.
3. Frick, WE.; Ge, Z.; Zepp, RG. *Environ. Sci. Technol.* **2008**, *42*, 4818–4824.
4. Whitman, R. L.; Nevers, M. B. *Environ. Sci. Technol.* **2008**, *42*, 9217–9224.
5. Ge, Z.; Frick, WE. *Environ. Sci. Technol.* **2009**, *43*, 1128–1133.
6. Keene, WE.; McAnulty, JM.; Hoesly, FC.; Williams, LP., Jr.; Hedberg, K.; et al., *Engl.J. Med* **1994**, *331*, 579–584.
7. Tracy, BP.; Gaida, SM.; Papoutsakis, ET. *Appl. Environ. Microbiol.* **2008**, *74*, 7497–7506.
8. Brown, DG.; Abramson, A. *Water Res.* **2006**, *40*, 1591–1598.
9. Bessoff, K.; Delorey, M.; Sun, W.; Hunsperger, E. *Clin. Vaccine Immunol.* **2008**, *15*, 1513–1518.
10. Lancioni, CL.; Thomas, JJ.; Rojas, RE. *J. Immunol. Methods* **2009**, *344*, 15–25.
11. Van Poucke, SO.; Nelis, HJ. *J. Appl. Microbiol.* **2000**, *89*, 390–396.
12. Brown, RL.; Cleveland, TE.; Payne, GA.; Woloshuk, CP.; White, DG. *J. Food Prot.* **1997**, *60*, 84–87.

13. Franson, MAM.; Greenberg, AE.; Trussell, RR.; Clesceri, LS.; *Editors Standard Methods for the Examination of Water and Wastewater*, 16th ed.;**1985**.
14. Poitras, C.; Fatisson, J.; Tufenkji, N. *Water Res.* **2009**, *43*, 2631–2638.
15. Juhna, T.; Birzniece, D.; Rubulis, J. *Appl. Environ. Microbiol.* **2007**, *73*, 3755–3758.
16. Muniesa, M.; Jofre, J.; Garcia-Aljaro, C.; Blanch, A. R. *Environ. Sci. Technol.* **2006**, *40*, 7141–7149.
17. Adams, AA.; Okagbare, PI.; Feng, J.; Hupert, ML.; Patterson, D.; et al., *J. Am.Chem. Soc.* **2008**, *130*, 8633–8641.
18. Dharmasiri, U.; Balamurugan, S.; Adams, AA.; Okagbare, PI.; Obubuafo, A.; Soper, SA. *Electrophoresis* **2009**, *30*, 3289–3300.
19. Nagrath, S.; Sequist, LV.; Maheswaran, S.; Bell, DW.; Irimia, D.; et al., *Nature* **2007**, *450*, 1235–1239.
20. Liu, RH.; Yang, J.; Lenigk, R.; Bonanno, J.; Grodzinski, P. *Anal. Chem.* **2004**, *76*, 1824–1831.
21. Beyor, N.; Seo, T. S.; Liu, P.; Mathies, R. A. *Biomed. Microdevices* **2008**, *10*, 909–917.
22. Hupert, ML.; Guy, WJ.; Llopis, SD.; Shadpour, H.; Rani, S.; Nikitopoulos, DE.; et al., *Microfluid. Nanofluid.* **2007**, *3*, 1–11.
23. Roberts, CJ.; Williams, PM.; Davies, J.; Dawkes, AC.; Sefton, J.; et al., *Langmuir* **1995**, *11*, 1822-1826.
24. Dong, Y.; Shannon, C. *Anal. Chem.* **2000**, *72*, 2371-2376.
25. McCarley, RL.; Vaidya, B.; Wei, SY.; Smith, AF.; Patel, AB.; et al., *J. Am. Chem. Soc.* **2005**, *127*, 842-843.
26. Wei, S.; Vaidya, B.; Patel, AB.; Soper, SA.; McCarley, RL. *J. Phys. Chem. B* **2005**, *109*, 16988-16996.
27. Di Carlo, D.; Irimia, D.; Tompkins, RG.; Toner, M. *Proc. Natl. Acad. Sci. U. S. A., Early Ed.* **2007**, 1-6, 6 pp.
28. Roelke, DLG.; G. M.; Valenti.; TW.; Grover, JP.; Brooks, BW.; Pinckney, JL. *Harmful Algae (accepted)* **2009**
29. Wang, Y.; Hammes, F.; Duggelin, M.; Egli, T. *Environ. Sci. Technol.* **2008**, *42*, 6749–6754.

30. Mull, B.; Hill, V. R. *Appl. Environ. Microbiol.* **2009**, *75*, 3593–3597.
31. Mayeed, MS.; Mian, A.; Auner, GW.; Newaz, GM. *J. Biomech. Eng.* **2006**, *128*, 458-461
32. Schmidt, H.; Scheef, J.; Huppertz, Hl.; Frosch, M.; Karch, H. *J. Clin. Microbiol.* **1999**, *37*, 3491–3496.
33. Chang, K-C.; Hammer, DA. *Biophys. J.* **1999**, *76*, 1280–1292.
34. Ford, SM.; Davies, J.; Kar, B.; Qi, SD.; McWhorter, S.; Soper, SA.; Malek, CK. *J. Biomech. Eng.* **1999**, *121*, 13–21.
35. Cebula, TA.; Payne, WL.; Feng, P. *J. Clin. Microbiol.* **1995**, *33*, 248–250.
36. Fitzmaurice, J.; Glennon, M.; Duffy, G.; Sheridan, JJ.; Carroll, C.; Maher, M. *Mol. Cell. Probes* **2004**, *18*, 123–132.
37. Hashimoto, M.; Chen, P-C.; Mitchell, MW.; Nikitopoulos, D. E.; Soper, S. A.; Murphy, M. C. *Lab Chip* **2004**, *4*, 638–645.
38. Bennett, A. R.; MacPhee, S.; Betts, R. P. *Lett. Appl. Microbiol.* **1996**, *22*, 237–243.
39. Martinez-Jehanne, V.; du Merle, L.; Bernier-Febreau, C.; Usein, C.; Gassama-Sow, A.; et al., *Infect. Immun.* **2009**, *77*, 1442–1450.

CHAPTER 5 HIGH-THROUGHPUT SELECTION, ENUMERATION, ELECTROKINETIC MANIPULATION, AND MOLECULAR PROFILING OF LOW-ABUNDANT CIRCULATING TUMOR CELLS USING A MICROFLUIDIC SYSTEM

5.1 Introduction

Colorectal cancer (CRC) accounts for nearly 1,000,000 new cases and 550,000 deaths worldwide each year; it is the fourth most common form of cancer in the United States and the third leading cause of cancer-related deaths in the western world.¹ Diagnostic and/or prognostic tests of CRC consist primarily of looking for bleeding in the stool (fecal occult blood test, FOBT) and/or endoscopic examinations of the colon and/or rectum. While FOBT has reduced mortality rates by 15-33% over the last 30 years, FOBT is more sensitive for the diagnosis of invasive cancer than it is toward advanced adenomas or early-stage lesions.² On the other hand, endoscopic examinations, such as colonoscopy or flexible sigmoidoscopy, can detect early stage lesions but misses proximal lesions when the distal colon is examined. Even in cases where both stool samples and endoscopy are employed, 25% of cases are expected to be missed.³

In cancer patients with either metastatic or localized disease, there is growing evidence that the presence of circulating tumor cells (CTCs) in the blood may be an important indicator of the potential for metastatic disease and thus, poor prognosis.⁴ Various epithelial-based cancers are known to release CTCs into circulation for example breast, bladder, prostate, lung, colorectal, cervical, and pancreatic cancers. The attractive attribute associated with CTCs is their ease of securing the sample; a simple blood draw (~7.5 mL) can be used to allow for the selection and enumeration of these cells.⁵ CTCs can provide valuable clinical information as well, such as early diagnosis of relapse, monitoring the effectiveness of adjuvant therapy and serving as an

independent prognostic factor. For example, while surgical resection of the diseased tissue in conjunction with chemotherapy is seen as an effective mode of treatment for highly localized CRC diseases, 30-50% of these patients ultimately experience recurrence and die.⁶

The high rate of recurrence for CRC could be due to heightened levels of CTCs in peripheral blood following surgery; indeed elevated levels of CTCs were found post-operatively for CRC patients.⁷ Finally, tumors contain genetically heterogeneous cell subpopulations with different propensities to spawn metastatic disease and therefore, if the CTC population responsible for metastasis could be identified through unique genetic profiles, oncologists could match proper therapy to the individual patient.⁸

Early results for CTCs as a biomarker for CRC have been somewhat controversial due to the proximity of the colon to the liver, which can act as a filter to remove malignant cells. In spite of this controversy, promising results have appeared in the literature.⁹ For example, progression free survival and overall survival for metastatic CRC patients with less than 3 CTCs per 7.5 mL of peripheral blood was significantly longer than those with CTC numbers >3 per 7.5 mL of blood. In addition, the diversity of targeted therapies is often times hampered by the acquisition of solid biopsy samples and the use of CTCs has been demonstrated to serve as an important, noninvasive biomarker for pharmacodynamic assessment of new treatment regimens for CRC.⁵

The challenge in any platform directed towards the isolation and pre-concentration of low abundance cells begins with the selection of the target cells from a heterogeneous population in which the target is a minority. However, technological advances have now facilitated the selection, enumeration, and characterization of CTCs using methods such as PCR,¹⁰ flow cytometry,¹¹ image-based immunologic

approaches,¹² immunomagnetic techniques,¹³ and microchip technology.¹⁴ The FDA accepted modality for CTC selection has been the use of the Veridex CellSearch™ system, which uses magnetic beads coated with monoclonal antibodies directed against the epithelial cell adhesion molecule, EpCAM. The processed sample is incubated with ferromagnetic particles coated with anti-EpCAM antibodies and the immunomagnetically-labeled cells are isolated by an external magnetic field. A rigorous evaluation of the performance metrics associated with the CellSearch™ system has indicated that the CTC recovery is ~85%.⁴ Challenges with this technology are the low throughput (8 samples per day) it affords and the high cost per assay.¹⁵ In addition, once selected, the cells must be extracted from the isolation cassette and placed in the imaging station for enumeration. This requires the vessel containing the cells to be opened to the environment, which can run the risk of contamination, especially in a centralized laboratory where many samples are processed.

Microchip technology has the potential to select with high recoveries, enumerate, and characterize rare CTCs in cancer patients, which will provide opportunities for identifying the potential for metastatic disease at very early stages, managing risk stratification in the adjuvant setting, monitoring response to treatment, identifying disease recurrence, and the prospective development of targeted therapies based on molecular characterization of CTCs (*i.e.*, personalized medicine). For example, Nagrath et al. developed a microfluidic device for selecting CTCs directly from peripheral blood.¹⁶ The CTCs originated from a variety of epithelial-based tumors and were selected through the use of anti-EpCAM monoclonal antibodies tethered to a fluidic channel containing 78,000 microposts. Anti-EpCAM monoclonal antibodies provided the specificity for CTC selection from unfractionated blood because EpCAM is

overexpressed only by adenoma carcinomas. The potential utility of this CTC chip in monitoring response to anti-cancer therapy was also investigated.¹⁶ RT-PCR analysis of the selected CTCs indicated the opportunity for CTC-based molecular analyses.

Adams and Dharmasiri et al. generated a polymer-based fluidic device for the high-throughput and high recovery selection and enumeration of CTCs directly from peripheral blood using either anti-EpCAM antibodies or PSMA-specific aptamers as the molecular/cellular recognition elements.^{17,18} The cells were selected directly from whole blood in less than 40 min of processing time with recoveries exceeding 90%. In addition, the selected CTCs could be released from the capture surface and counted quantitatively using a contact conductivity sensor.

Unfortunately, the aforementioned work did not perform any type of molecular analyses on the selected CTCs with the selected CTCs simply dumped to waste following their selection from whole blood. Molecular profiling of CTCs can provide important clinical information that cannot be garnered simply by enumerating the selected cells. As noted, mutations in certain gene fragments carried by CTCs can be used to guide therapy and provide opportunities for personalized treatment of a patient. In the case of colorectal cancer (CRC), patients with mutated *K-ras* oncogenes do not benefit from anti-EGFR mAB therapy, whereas patients with wild-type *K-ras* genotypes do benefit from cetuximab and panitumumab-based treatments.²⁰ Yang and coworkers recently found that 90% of metastatic CRC patients had a *K-ras* mutational status of CTCs similar to the primary tumor as determined by genotyping mRNA surrogates. In addition, it has been noted that non-tumor epithelial cells can also be present in the blood and express antigens that would select these cells. Therefore, to discern differences between CTCs and normal epithelial cells shed into peripheral blood,

molecular profiling is necessary.²¹ The significant challenge with genotyping gDNA from mass-limited samples, such as CTCs isolated from cancer patients, is the small copy number of the assays input material. Indeed, most studies in which molecular profiling has been invoked on CTCs, in particular CRC, has focused on using reverse transcription PCR with mRNA surrogates to record gene activity or the presence/absence of mutations due to the higher copy number of the transcripts compared to the gDNA.²² Therefore pre-concentration of the selected CTCs in a microfluidic for subsequent molecular profiling is crucial for detecting low copy number gDNA mutations.

Many techniques exist to physically manipulate and pre-concentrate cells such as blood, tumor and bacterial cells using microfluidics including optical tweezers,²³ acoustic forces,²⁴ magnetic forces, electromagnetic fields, dielectrophoresis (DEP) and surface modification.²⁵ Magnetoquasistatic fields have been used to manipulate cells either due to their intrinsic magnetizability, such as the iron found in red blood cells,²⁶ or by attaching magnetic materials to the cells for magnetically activated cell sorting.²⁷ The resulting force is due to the interaction of a magnetic dipole with a non-uniform magnetic field and is known as magnetophoresis. Magnetophoresis has the important attribute of being highly specific because the vast majority of material does not respond strongly to magnetic fields. The drawback is that the technique requires a label (except for red blood cells). Electromagnetic fields are the most general case and are commonly used to manipulate particles when used as optical tweezers.²⁸ At low frequencies or in systems that are small compared with the wavelength of the field, the electric and magnetic components of the electromagnetic field decouple and one will dominate.²³ Optical tweezers typically are able to handle only one or a few cells at once. DEP

systems are less suitable due to potentially cytotoxic buffers and/or high temperatures induced by Joule-heating.^{29,30}

Overall, cell manipulation techniques thus far are rather inefficient with the efficiency, defined as the ratio of the number of cells successfully collected to the total number of input cells, is only 10-20%.^{31,32} The low efficiency may not be a problem in many cell assays, but it is a concern when working with cell-limited samples, such as the case with CTCs. To address these limitations, a family of emerging technologies, such as microfluidic, and electrophoresis, can be combined for CTC handling with the potential for high-throughput processing with efficient collection of the target cells for molecular profiling. Electrophoresis has already been demonstrated for the manipulation of biological particles, such as cells, bacteria and viruses.³⁰ Electrophoresis is based on the intrinsic electrical properties of the particles being manipulated and does not require a label, thus it can potentially be more universal and simpler to implement. The small volume liquid handling capability of microfluidic chips should also permit the manipulation of only a few cells within a network of channels with highly efficient recovery.

Detecting mutations in cancer patients can be difficult due to the highly variable nature of the cancer cells in terms of their mutational status with respect to the stage of tumorigenesis and the location and proximity of the sampling site with respect to the primary tumor site.^{32,33} The success and accuracy of genotyping many cancers, such as CRC, depends on the ability to detect low copy numbers of mutated sequences in a vast majority of wild-type DNA. However, through the use of a microfluidic device that can enrich low-abundance CTCs from a mixed-population and recover them with high efficiency and their subsequent release can provide effective molecular profiling results

from low-copy number inputs and alleviate the problem of large wild-type DNA backgrounds.

Ligase detection reaction (LDR) coupled to a primary PCR can be used to identify extremely low abundant mutant DNA due to the double amplification steps the assay employs, even when implemented in a multiplexed fashion.³³ Following PCR amplification of the appropriate genes containing the loci of interest, the amplicon is mixed with two complementary primers (a common primer and a discriminating primer) that flank the mutation locus of interest. The discriminating primer contains a base at its 3' end that coincides with the single-base mutation site being interrogated. Facilitated by a highly specific thermally stable ligase, the allele-specific LDR primers become covalently ligated to adjacent fluorescently labeled primers to form an LDR product if and only if the nucleotide at the potential mutation site is complementary to the 3' end of the discriminating primer. This LDR can then linearly amplify the products during subsequent thermal cycles. The flexible design of the primers used for the LDR assay has allowed for the detection of successful ligation events via a variety of analytical formats,³⁴ such as low-density DNA microarrays,³⁵ high-resolution electrophoresis,³⁶ and spectroscopic techniques employing fluorescence resonance energy transfer.³⁷⁻³⁹

In this report, we describe a microfluidic electrokinetic micromanipulation method for the selection and electrokinetic collection of low-abundance CTCs affinity-selected from whole blood for subsequent molecular profiling of point mutations in the gDNA of the CTCs. The electric field strength and hydrodynamic flow velocity were optimized for the effective collection of CTCs released from the surface containing antibodies specific to the CTCs. The CTCs were directed into a reservoir (2 μ L) for molecular interrogation of potential point mutations within their gDNA. Finally, the optimized system was

integrated to a micro-scale high-throughput microsampling unit (HTMSU) for CTC selection and enumeration directly from whole blood. We recovered SW620 cells, a CRC cell line used as a model, following seeding into peripheral blood. The selected cells were enumerated using an on-chip conductivity sensor and the enumerated cells directed into a reservoir for pre-enrichment. The enriched CTCs were lysed and their DNA was extracted for genotyping gDNA for potential *K-ras* mutations. Because most *K-ras* mutations are localized to codon 12 and to a lesser extent, codons 13 and 61, the PCR/LDR assay was performed on codon 12 of the *K-ras* oncogene to detect the presence/absence of point mutations possessing clinical relevance for the diagnosis/prognosis of colorectal cancers.

5.2 Materials and Methods

5.2.1 Reagents and Cells

PMMA substrates and cover plates (0.5 mm thickness) were purchased from Good Fellow (Berwyn, PA). Platinum wires were purchased from Alfa Aesar (Boston, MA). Polyimide-coated fused silica capillaries were purchased from Polymicro Technologies (Phoenix, AZ). Chemicals used for the PMMA surface cleaning and modification included reagent grade isopropyl alcohol, 1-ethyl-3-[3-dimethylaminopropyl] carbodiimide hydrochloride (EDC), N-hydroxysuccinimide (NHS), fetal bovine serum and 2-(4-morpholino)-ethane sulfonic acid (MES) and these were purchased from Sigma-Aldrich (St. Louis, MO). Monoclonal anti-EpCAM antibody was obtained from R & D Systems (Minneapolis, MN). The SW620 (colorectal cancer cell line), growth media, HEPES buffer, phosphate buffered saline (PBS) and trypsin were purchased from American Type Culture Collection (ATCC, Manassas, VA). Citrated rabbit blood was purchased from Colorado Serum Company (Denver, CO). Tris-Glycine buffer was

obtained from Bio-Rad Laboratories (Hercules, CA). All solutions were prepared in nuclease-free water, Invitrogen (Carlsbad, CA). Nuclease-free microfuge tubes were purchased from Ambion (Foster City, CA) and were used for preparation and storage of all samples and reagents. A fluorescein derivative, PKH67, was purchased from Sigma-Aldrich. Oligonucleotide probes and primers were obtained from two different sources, Integrated DNA technologies (Coralville, IA).

5.2.2 Cell Culturing

SW620 cells were cultured to 80% confluence in Dulbecco's Modified Eagle's Medium supplemented with high glucose containing 1.5 g L^{-1} sodium bicarbonate (NaHCO_3), 15 mM HEPES buffer, and 10% fetal bovine serum. A cell stripper solution was prepared in 150 mM PBS and was used to harvest the SW620 and HT29 cells from the culturing plate. SW620 cells were stained with PKH67 for microscopic visualization experiments using fluorescence microscopy. A modified protocol for cell staining was implemented whereby the dye concentration was increased twofold resulting in more evenly distributed fluorescent labels over the cell's periphery. Cell counts were determined by counting three aliquots of cells in succession using a hemacytometer. The cell count accuracy was within 10%.

5.2.3 Microscopy

In cases where the cells required optical visualization to assist in the operational optimization of the CTC selection, enumeration and manipulation assay, the PMMA devices were fixed onto a programmable motorized stage of an Axiovert 200M (Carl Zeiss, Thornwood, NY) inverted microscope and video images were collected during each experiment at 30 frames s^{-1} using a monochrome CCD (JAI CV252, San Jose,

CA). A Xe arc lamp was used to excite the fluorescent dyes incorporated into the cells' membrane.

5.2.4 Fabrication of HTMSU

The HTMSU and electro-manipulation unit were hot embossed into PMMA substrates via micro-replication from a metal mold master. Fabrication of the HTMSU followed steps previously reported.¹⁷ The HTMSU consisted of a series of 51 high-aspect ratio curvilinear channels that in concert formed the cell selection bed. Each channel was 150 μm (depth) \times 30 μm (width) and shared common inlet/outlet ports (Figure 5.1A). Curvilinear-shaped capture channels were used to improve the cell capture efficiency as described previously.^{17,18} The cell-free marginal zone apparent in straight channels was not observed in curvilinear channels and the cell radial distribution was unaffected by changes in cell translational velocity. Cells migrate to the outside of the curved channels due to centrifugal forces acting on the cells and the cross-stream velocity component due to the reversal of the direction of curvature.¹⁷ The result is an increase in the antibody/antigen encounter rate as the cells moved through the capture beds at the relatively high-linear velocities used here, which resulted in high recoveries of the CTCs. The channel width of the cell selection bed (30 μm) was comparable to the average target cell diameter, which was used to increase the probability of cell–antigen interactions with the solution-borne target cells. The large channel depth (150 μm) was selected to reduce the pressure drop in high-volume flow rate operation and also to increase sample processing throughput.

The electro-manipulation unit possessed one entry, through (a), (see Figure 5.1A) and two exits, via (b) and (c). Entry (a) was connected to a T intersection labeled (e) in Figure 5.1A. All of the channels were rectangular in shape with dimensions of 50 $\mu\text{m}\times$

100 μm , width and depth, respectively. Before final assembly, 1 mm holes were drilled into the electro-manipulation unit for reservoirs, input port and electrodes. Then, the electro-manipulation unit chips were washed with $\sim 0.5\%$ Alconox solution, rinsed and ultrasonicated with DI water followed by rinsing with 2-propanol, and again ultrasonication for 15 min in DI water. The channels were examined under a microscope to ensure they were not filled with debris.

Appropriately cleaned HTMSU substrates and cover plates were exposed through a mask to UV radiation resulting in surface photooxidation only in the exposed areas of the PMMA. The exposed areas were restricted to only the cell selection region of the device. UV irradiation was performed through an aluminum mask for 10 min at 15 mW cm^{-2} to facilitate the formation of the activated surface, which also included a carboxylic acid scaffold.¹⁸

Pt electrodes ($d=76 \mu\text{m}$) served as the contact conductivity sensor in the detection zone of the HTMSU and were placed into guide channels that were positioned orthogonal to the fluidic output channel following thermal assembly. Then, Pt wires positioned in the HTMSU and the cover plate were aligned and clamped together between two borosilicate plates. Insertion of the electrodes was monitored using a microscope to carefully control the inter-electrode gap ($\sim 50 \mu\text{m}$). The cell constant of the Pt conductivity sensor, K , was $\sim 0.01 \mu\text{m}^{-1}$, which allowed for the specific detection of SW620 cells based on their average size (diameter $\approx 23 \mu\text{m}$).¹⁷

The embossed devices were assembled by heat annealing a cover plate made from the same material to the substrate. The cover plate and substrate were clamped together and placed in a convection oven for ~ 20 min at 101 $^{\circ}\text{C}$ for the UV-modified HTMSU and 105 $^{\circ}\text{C}$ for pristine PMMA electro-manipulation unit. After successful heat

annealing, 125 μm diameter Pt wires/electrodes wrapped Cu electrodes were placed into the drilled holes in the electro-manipulation unit.

5.2.5 Antibody Immobilization to the HTMSU

Antibody immobilization was carried out in a two-step process. The UV-modified thermally assembled HTMSU device was loaded with a solution containing 4 mg mL^{-1} EDC, 40 mg mL^{-1} NHS in 150 mM MES (pH = 6) for 1 h at room temperature to obtain the succinimidyl ester intermediate. After this incubation, the EDC/NHS solution was removed by flushing nuclease-free water through the device. Then, an aliquot of 1.0 mg mL^{-1} of the monoclonal anti-EpCAM antibody solution contained in 50 mM PBS (pH=7.4) was introduced into HTMSU and allowed to react for 4 h. The device was then rinsed with a solution of PBS (pH=7.4) to remove any non-specifically bound anti-EpCAM antibodies.¹⁷

5.2.6 SW620 Cell Capture/Release and Enumeration Using the HTMSU

To connect the HTMSU to the pump, a luer lock syringe (Hamilton, Reno, NV) was placed on the pump equipped with a luer-to-capillary adapter (Inovaquartz, Phoenix, AZ). This was then attached to the capillary that was sealed to the input port of the HTMSU. A pre-capture rinse was performed with 0.2 mL of 150 mM PBS at 50 mm s^{-1} linear velocity to maintain isotonic conditions. Then, the appropriate volume of a cell suspension was introduced at the 27.5 $\mu\text{L min}^{-1}$ (2 mm s^{-1}) volumetric flow rate, which was optimized by Adams et al.¹⁷ Next, a post-capture rinse was performed with 0.2 mL of 150 mM PBS at 50 mm s^{-1} to remove any non-specifically adsorbed cells.

Following a post cell capture rinse, a 0.25% trypsin solution in 0.2 mM Tris/19.2 mM Glycine buffer (pH=8.3) was infused into the HTMSU. The captured cells could be

observed using a microscope until they were enzymatically removed with Stoke's forces acting on the cells as well to facilitate release.

5.2.7 Electrokinetic Cell Manipulation

The released cells from the cell selection surface were subjected to electrokinetic cell manipulation after the enumeration. The released cells from the selection surface were traversed into the electro-manipulation unit at $1 \mu\text{L min}^{-1}$ (3.3 mm s^{-1}) transport rate from inlet (a) (see Figure 5.1A). The electric field was applied between (b) and (c) reservoirs in the electro-manipulation unit when the buffer solution containing cells were introduced from the inlet reservoir.

The programmable high voltage power supply was assembled in-house. The unit consisted of 4 individual power supplies (Model UR5PN, Matsusada Precision Inc., Santa Clara, CA) capable of delivering -5 to +5 kV. Each power supply was equipped with an independent Reed relay (Model RR1A07P06, Ross Engineering Corporation, Campbell, CA) that was used to toggle the polarity, ground, and floating states of the power supply. The power supply was computer controlled with a 4 channel 12 bit digital-to-analog board (Model CYDDA 04P, CyberResearch Inc., New Haven, CT) with peripheral component interface (PCI) and software written in Labview (National Instruments, Austin, TX). All experiments were carried out at room temperature. Caution: The electrophoresis uses high voltages and special care should be taken when handling the electrodes.

Cell migration velocities in the present study were calculated by measuring consecutive cell events observed in the video, which had a frame capture rate of 30 frames s^{-1} . The average velocity was based on values obtained from 5 different cell events.

5.2.8 Measurement of the Electroosmotic Flow (EOF)

The EOF in assembled devices was measured using the method described by Zare and co-workers.⁴⁰ EOF values in 0.2 mM Tris/19.2 mM Glycine buffer (pH=8.3) and 0.25% trypsin in 0.2 mM Tris/19.2 mM, Glycine buffer (pH=8.3) were calculated. The procedure involved filling the entire chip with a 0.2 mM Tris and 19.2 mM Glycine buffer. After filling, one reservoir was emptied and filled with the same type of buffer, but of lower ionic strength (0.2 mM Tris/19.2 mM Glycine). An electric field (100 V cm^{-1}) was applied to the reservoirs containing the low and high ionic strength buffers. The current was monitored continuously using a strip-chart recorder (Kipp and Zonen Inc., Bohemia, NY). The time needed for the current to reach a plateau was measured from the plot and the linear velocity calculated. Dividing the linear velocity by the electric field strength produced EOF values ($\text{cm}^2 \text{ V}^{-1} \text{ s}^{-1}$). The electric field was supplied by a Spellman high-voltage power supply (CZ1000R, Plainview, NY). The electroosmotic flow measurements were carried out on pristine PMMA microchips. Electroosmotic mobility data were obtained at room temperature. Each data point was the average of five measurements.

5.2.9 DNA Extraction from SW620 Cells

Genomic DNA (gDNA) was extracted from CTCs using Lyse-and-Go PCR reagent (Pierce Biotechnology, IL, USA). Following manufacturer's recommendations, 5 μL of Lyse-and-Go PCR reagent was added to the selected CTCs and thermocycled using the following temperatures: 65 °C for 30 s; 8 °C for 30 s; 65 °C for 90 s; 97 °C for 180 s; 8 °C for 60 s; 65 °C for 180 s; 97 °C for 60s; 65 °C for 60 s. Prior to the addition of the PCR cocktail, the samples were placed at 80 °C.

5.2.10 PCRs, LDRs, Gel Electrophoresis and Capillary Electrophoresis

PCR amplifications were carried out to generate 300 bp amplicons from SW620 CTCs using the gene-specific primer sequences: exon 1 forward –5' TTA AAA GGT ACT GGT GGA GTA TTT GAT A 3', ($T_m=55.4$ °C) and exon 1 reverse – 5' AAA ATG GTC AGA GAA ACC TTT ATC TGT 3'($T_m=56.3$ °C). Forty-five μL of PCR cocktail consisting of 10 mM Tris–HCl buffer (pH=8.3) containing 50 mM KCl, 1.5 mM MgCl_2 , 200 μM dNTPs, 0.4 μM of each forward and reverse primers was added to the lysate previously held at 800C in the thermocycler. After a 2-min initial denaturation, 1.5 U of AmpliTaq DNA polymerase (Applied Biosystems, Foster City, CA, USA) was added under hot-start conditions and amplification was achieved by thermally cycling for 30 cycles at 95 °C for 30 s, 60 °C for 2 min, and a final extension at 72 °C for 3 min.

To test the fidelity and yield of the PCR, slab gel electrophoresis was run on an aliquot of each reaction. From each aliquot, either 2 μL PCR product for standard cell solutions or 3 μL PCR product from microchip processed solutions was mixed with 1 μL loading dye and 3 μL of 1x TBE buffer for the standard cell solution or 2 μL of 1x TBE buffer for a microchip-processed solution. The mixture was then loaded into an individual well of an ethidium bromide prestained 3% agarose gel (Bio-Rad Laboratories, Hercules, CA). The slab gel electrophoresis was typically run at 5 V cm^{-1} for 30 min. The developed slab gel images were captured using Gel Logic 200 Visualizer (Carestream Molecular imaging, New Haven, CT)

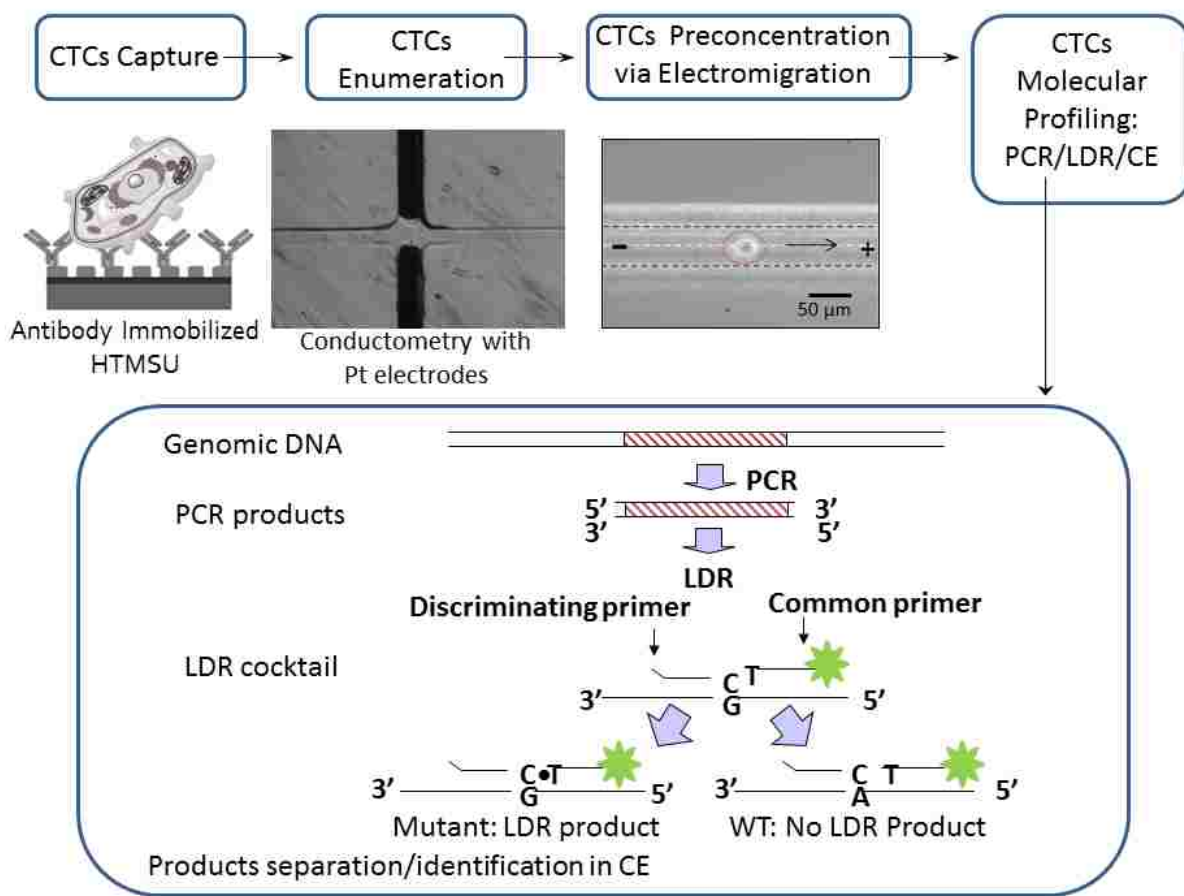
LDRs were executed in a total volume of 20 μL in 0.2 mL polypropylene microtubes using a commercial thermal cycling machine (Eppendorf Thermal Cycler (Brinkmann Instrument, Westbury, NY, USA). The reaction cocktail typically employed in this work consisted of 10 mM Tris–HCl (pH=8.3), 25 mM KCl, 10 mM MgCl_2 , 0.5 mM

NAD⁺ (nicotinic adenine dinucleotide, a cofactor for ligase enzyme), and 0.01% Triton X-100, 2 μ L of 100 nM of the discriminating primer: 5' AAAGTTGTGGTAGTTGGAGCTGT 3' (T_m =71.3 °C) and fluorescently labeled freshly phosphorylated common primer: 5' Phos/TGGCGTAGGCAAGAGTGCCT/Cy5.5Sp 3' (T_m =63.5 °C) and 2 μ L of the PCR product as template. 40 U of Taq DNA ligase (New England Biolabs) was added to the cocktail under hot-start conditions and the reactions were thermally cycled 20 times for 30 s at 94 °C and 2 min at 65 °C. The LDR products were stored at 4 °C until needed for capillary gel electrophoresis (CGE). The LDR products were separated using a CEQ 8000 Genetic Analysis System (Beckman Coulter, Fullerton, CA, USA). Data acquisition was performed using the Beckman P/ACE software.

5.3 Results and Discussion

In the present work, we were interested in the ability to enumerate and enrich CTCs using a microfluidic system with their subsequent molecular characterization by looking for point mutations within certain gene fragments. In these studies, the SW620 cell line was used as a model for CTC selection, enumeration, and enrichment via an integrated HTMSU. SW620 cells over-express the EpCAM membrane antigen and harbor *K-ras* c12.2V oncogene mutations. Circulating colorectal cancer cell line, HT29, which do not harbor *K-ras* c12.2V oncogene mutation, was used as the wild-type for comparison. SW620 and HT29 cells are typically 15-30 μ m in diameter (Avg \approx 23 μ m)⁴¹ and EpCAM occurs at a frequency of 1×10^6 and 2.5×10^5 molecules per cell, respectively.⁴² In the work presented herein, we focused on: (1) The selection and enumeration of low-abundance SW620 cells from peripheral blood; (2) release of the cells from the antibody selection surface; (3) electrokinetic enrichment of the selected

SW620 cells; and (4) molecular profiling of low-abundance cells using a PCR/LDR/electrophoresis assay (see Scheme 5.1). Release of the cells intact is critical because the enumeration process depends on counting via conductivity whole cells and the molecular profiling is performed on rare cells selected from peripheral blood and as such, the genetic material to be analyzed should not be diluted extensively or mixed with potential interfering materials.



Scheme 5.1 Overview for the cell selection, enumeration, electrokinetic enrichment and molecular profiling strategy adopted for analysis of extremely low-abundant SW620 cells resident in peripheral blood.

5.3.1 SW620 Cell Selection

The highly specific selection of SW620 CTCs was based on the recognition capabilities of anti-EpCAM antibodies that were tethered to the HTMSU selection beds. Dynamic interactions between the CTC membrane's receptors and the channel wall containing the recognition elements are important in determining the recovery of these rare CTCs from blood. Curvilinear-shaped channels were employed to provide high recovery.¹⁷ As such, the cell-free marginal zone apparent in straight channels was not observed in these curvilinear channels and the cell radial distribution was unaffected by changes in cell translational velocity.¹⁷ Chang's model of cell adhesion in flowing systems has been applied in previous reports to describe the encounter rate between the solution-borne cells and the surface-tethered cell selection elements.⁴³ Therefore, an optimal linear velocity would be expected to guarantee a high probability of binding between the target molecules and the antigen based upon a balance between the interaction time and the encounter rate. The optimum linear velocity for selection of MCF-7 CTCs, which has the same mean diameter as SW620 CTCs, using EpCAM/anti-EpCAM antibodies ($K_D=3.3\times 10^8 \text{ M}^{-1}$)⁴⁴ was found to be 2.0 mm s^{-1} . Thus, according to the Chang and Hammer model for cell adhesion, efficient CTC/mAb adhesion was determined by two factors; the encounter rate (k_o) and the probability (P) of interaction between the membrane bound antigen and the channel wall's tethered antibody.⁴³ As such, MCF-7 and SW620 CTCs should have a similar optimum linear cell selection velocity of 2 mm s^{-1} , which we employed in these experiments for the selection of SW620 CTCs. The selected cells were observed using fluorescence and brightfield microscopy as shown in Figure 5.1B. As Adams et al. and Dharmasiri et al. reported

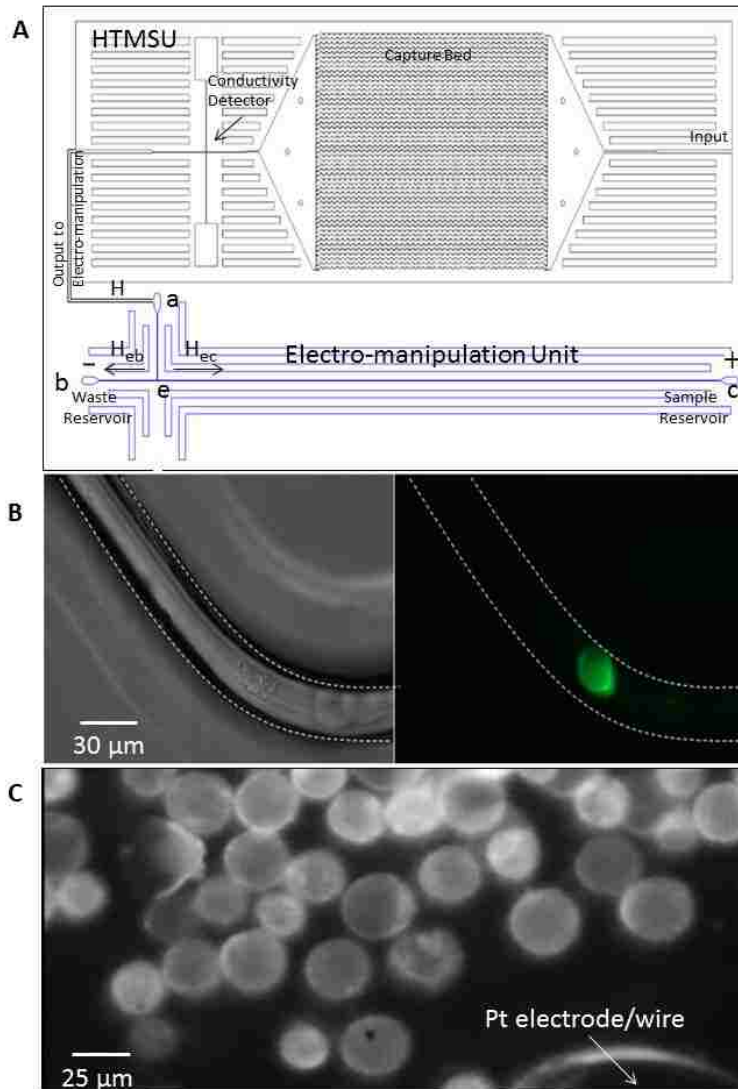


Figure 5.1 Diagrams of the microfluidic system made via micro-replication into PMMA from a metal mold master. **(A)** Cell selection HTMSU. The capture bed consisted of curvilinear 51 channels that were $30\ \mu\text{m}$ wide and $150\ \mu\text{m}$ deep. (Electro-manipulation unit consists of $80\ \mu\text{m}$ wide, $100\ \mu\text{m}$ deep and $5\ \text{cm}$ long linear channels. The solution flow H arriving from HTMSU is divided at the T junction into a major flow (H_{eb}) and a minor flow (H_{ec}). Conductometrically enumerated SW620 cells were introduced to system at 'a' entrance port. The 'a' entrance port connects with b-c channel at the T intersection. 'b' exit is the sample waste reservoir and c exit is cell reservoir. Both 'b' and 'c' reservoirs host Pt external electrodes; cathode and anode embedded in sample reservoir, 'b' and waste reservoir, 'c', respectively. **(B)** Brightfield (left) and fluorescence (right) micrographs (43x) for the positive selection of SW620 cells infused into the HTMSU at a constant linear velocity flow of $2\ \text{mm}\ \text{s}^{-1}$. The cells were suspended in a whole blood ($100\ \text{cells}\ \text{mL}^{-1}$) and following infusion of the cell suspension, the device was washed with PBS buffer prior to imaging. In all cases, the entire capture bed was imaged by scanning the microscope stage. The cells were stained with the fluorescein membrane probe prior to introduction into the HTMSU to allow visualization. **(C)** The selected SW620 cells enriched in the sample reservoir at the end of c channel. Positive Pt electrode is also in the Figure. Total volume of the reservoir is $2\ \mu\text{L}$.

that the CTCs appear to be flattened and elongated upon capture giving better adhesion between the CTC and selection wall. As observed experimentally (see Figure 5.1B), the resulting contact area was determined to be $448 \pm 18 \mu\text{m}^2$. The anti-EpCAM antibody density on the selection bed wall was reported to be 2.3×10^{11} molecules cm^{-2} .¹⁷ Therefore, 2.4×10^5 EpCAM/anti-EpCAM antibody interactions were involved in one cell/antibody binding event. A CTC recovery of $96 \pm 4\%$ was found at a translational velocity of 2.0 mm s^{-1} under the conditions employed in this study.

5.3.2 Cell Detachment from the Capture Surface

Release of intact CTCs from the capture bed is critical for the subsequent conductivity enumeration followed by electrokinetic manipulation and molecular profiling as noted above. Enzymatic digestion of EpCAM and anti-EpCAM was achieved using the proteolytic enzyme, trypsin. Microscopic investigations (data not shown) revealed that the average time for release of the captured SW620 CTCs was ~ 16 min, which was higher than the values recorded for MCF-7 CTC release (~ 7 min).¹⁷ This difference could be accounted for by the EpCAM expression level difference between the two cell lines (MCF-7 = 5×10^5 and SW620 = 1×10^6 EpCAM molecules per cell).¹⁸ Due to the higher expression level of EpCAM present within the SW620 membrane, higher numbers of EpCAM/anti-EpCAM interactions must be degraded.

5.3.3 Conductivity Enumeration of the CTCs

The selected and released CTCs were subsequently enumerated using a conductivity sensor. A typical data streams are shown in Figure 5.2A. The transducer measured changes in the conductivity of the release buffer with respect to the buffer in the presence of a single CTC between the Pt electrode pair. It was found that the peak width for a single CTC was $\sim 150 \text{ ms}$ (see inset to Figure 5.2A). Tris-Glycine buffer was

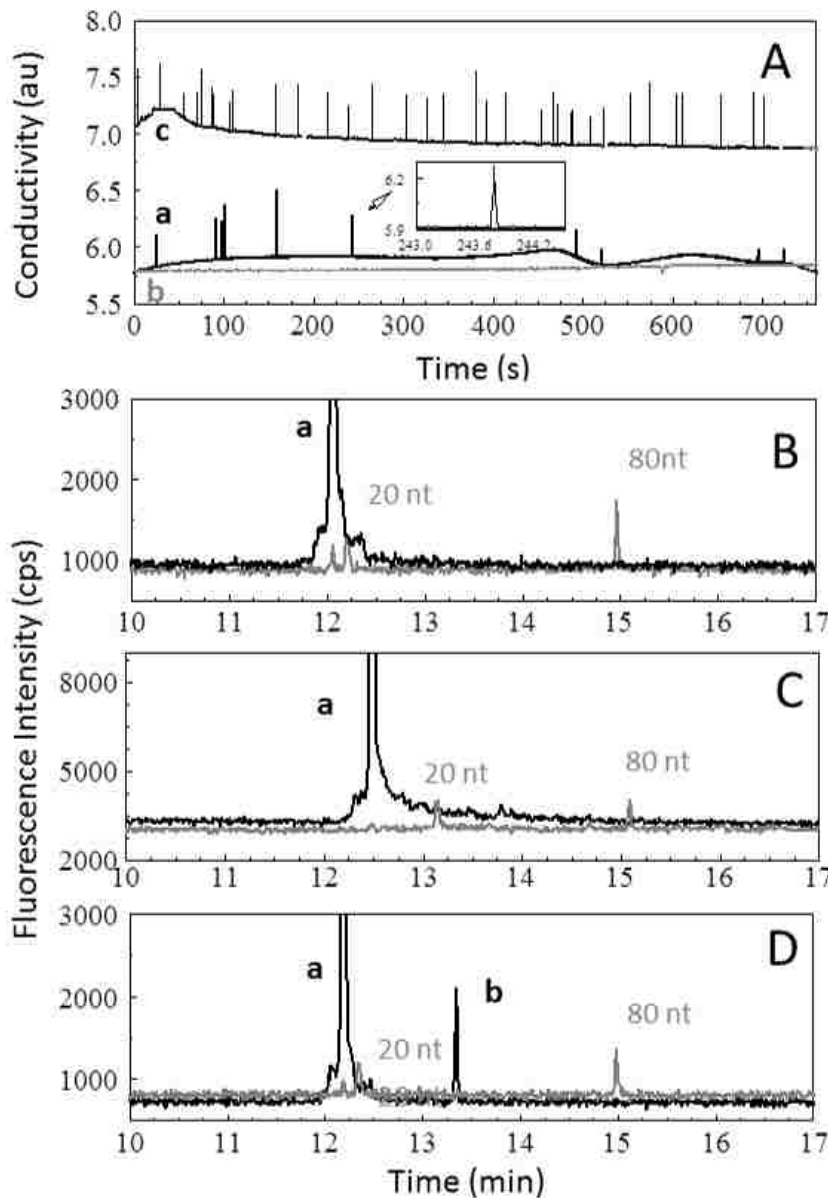


Figure 5.2 (A) Conductometric responses generated for 1.0 mL of whole blood seeded with 10 SW620 cells (a) 0 SW620 cells (ash) (b) and 32 HT29 (c) at a linear flow velocity of 2.0 mm s^{-1} processed using the HTMSU. The captured SW620 cells were released from the capture surface using the release Tris-Glycine buffer comprised of 0.25% w/v trypsin and transported through the conductivity sensor at a volumetric flow rate of $1 \mu\text{L min}^{-1}$. Peaks were identified as SW620/HT29 cells based on a signal-to-noise threshold of 3. The insets shown in the figure represent a magnified view of sections of the data stream. The data presented here was smoothed by the Savitsky-Golay method (25 point smoothing function). The conductometrically enumerated cell samples were subjected to PCR followed LDR analysis. Two μL of amplicons from PCR were used for analyzing point mutation in the *K-ras* gene. The LDR products were analyzed using capillary electrophoresis. The capillary electrophoresis responses for the sample after processing blood with no SW620 (**B**), Sample after processing blood with 50 HT29 cells (**C**) and sample after processing blood with 10 SW620 cells (**D**). Peak 'a' represents the primer and peak 'b' is the LDR product for SW620.

selected as the major component in the release buffer due to its low conductance, which improved the SNR for the conductivity detection of single CTCs. There were 10 peaks observed in the conductance response shown in Figure 5.2A (a) that could be assigned to SW620 cells based on a SNR threshold of 3 (99.7% confidence level) giving a recovery and detection efficiency of ~100% in this case (seed level=10 CTCs mL⁻¹). Enumeration of HT29 cells followed cell capture showed 32 events (seed level=50 CTCs mL⁻¹) in the conductivity response attributed to HT29 cells as shown in Figure 5.2A (b). HT29 recovery was found to be 72% likely due to its lower EpCAM expression. The variations in the peak response for CTC was most likely due to differences in the cells' morphology and chemical composition.

One milliliter of a blank sample, which consisted of whole blood seeded with no SW620 CTCs, was analyzed by the HTMSU and enumeration via conductivity under the same conditions as described for peripheral blood seeded with SW620 CTCs. The resultant trace c is shown in Figure 5.2A. In this case, no single-cell spikes were observed in the conductivity data trace indicating that the signal spikes seen for the SW620 seeded peripheral blood sample was indeed due to CTCs.

The trace for the SW620 spiked blood sample showed a higher background level as well as a slight response drift compared to the blank sample. These artifacts may have been due to non-specific accumulation of dissolved membrane proteins on the Pt electrode surface. Because these deposits are subjected to Joule effects, the electrode surface temperature could change during the readout phases of the measurements, affecting the conductance response.⁴⁵

5.3.4 Electrokinetic Enrichment of SW620 Cells

In the electro-manipulation unit, the total flow (H) arriving from the inlet (a) was divided at the T junction into a major flow (H_{eb}) and a minor flow (H_{ec}) (see Figure 5.1A). The ratio between H_{eb} and H_{ec} was equal to 9:1, which was set by the pressure drop ratio ($\Delta P_{eb}/\Delta P_{ec}=0.1$ at $1 \mu\text{L min}^{-1}$) between the two channels. As such, the device was designed to have only 10% of the hydrodynamic driven input volume from the HTMSU entering the CTC collection reservoir ((c) in Figure 5.1A). Therefore, 90% of the hydrodynamic driven fluid would flow into reservoir (b) as seen in Figure 5.3A-C.

To provide efficient pre-concentration of the selected CTCs, we applied an electric field to specifically select solution-born CTCs from the hydrodynamic flow and divert them into the collection reservoir (c). As shown in Figure 5.1C, cells were electrophoretically diverted from the hydrodynamic flow into (c) due to their intrinsic electrophoretic mobility and the applied electric field, which overcame the force exerted on the cell by the pressure-driven flow. The volume of reservoir (c) was $2 \mu\text{L}$ in this case, providing a 500x enrichment factor for the CTCs (input volume= 1 mL). The electric field applied between (b) and (c) generated an electrokinetic flow. We placed the anode at the exit reservoir of channel (c) and the cathode at reservoir (b).

According to the Smoluchowski equation, the electrophoretic mobility of cells is determined by the surface bound charged groups, such as the sialic and carboxylic acid groups, lysine side chain amino groups, sulfhydryl groups and alkaline phosphatase-susceptible phosphate groups.⁴⁶ Thereby CTCs possess a net negative surface charge (Q) at pH=8.3 of;

$$Q=4\rho \pi r_p^2 \quad (1)$$

whereas ρ is the charge density, $-5.8 \times 10^{-14} \text{ C } \mu\text{m}^{-2}$,⁴⁸ and r_p is the cell radius, $11.5 \mu\text{m}$ for CTCs. Therefore, the average net surface charge (Q) of a typical CTC is approximately $-9.6 \times 10^{-11} \text{ C}$. Because Q is set by protonation/deprotonation of membrane-bound proteins and other groups, the CTCs' charge can be controlled by altering the properties of the buffer solution (i.e., pH, ionic strength, salt composition). This along with the size of the CTC and its zeta potential will determine its electrophoretic mobility.

The electrophoretic force acting on a particle with a net charge Q under an electric field strength of V/d is given by;⁵²

$$F_{EP} = Eq = QV/d \quad (2)$$

where V is the applied voltage and d is the distance between cathode and anode. Therefore, the electrophoretic force acting on the cell was calculated to be $9.6 \times 10^{-9} \text{ N}$. In this study we used PBS (50 mM) and Tris-Glycine buffer in preliminary cell manipulation studies. It was observed that SW620 cells resident in 50 mM PBS were subjected to lysis at the electric field strength of 100 V cm^{-1} . The cell migration velocity calculated to be $100 \pm 16 \mu\text{m s}^{-1}$ at 100 V cm^{-1} electrical field strength. On the other hand, utilization of Tris-Glycine buffer (0.2 mM Tris/19.2 mM Glycine) improved the CTC manipulation conditions dramatically. Tris-Glycine buffer is a lower ionic strength buffer and it has been found to increase the target cells' zeta potentials and mobility.⁴⁹ Buffers of low ionic strength have the additional advantage of minimizing ohmic losses⁵⁰ and consequently, heating effects.

In addition, because electrolysis occurs at the electrodes, the buffer must negate possible changes in pH and maintain a constant charge on the cells being manipulated. Therefore, the SW620 cells were not found to lyse at 100 V cm^{-1} throughout the course

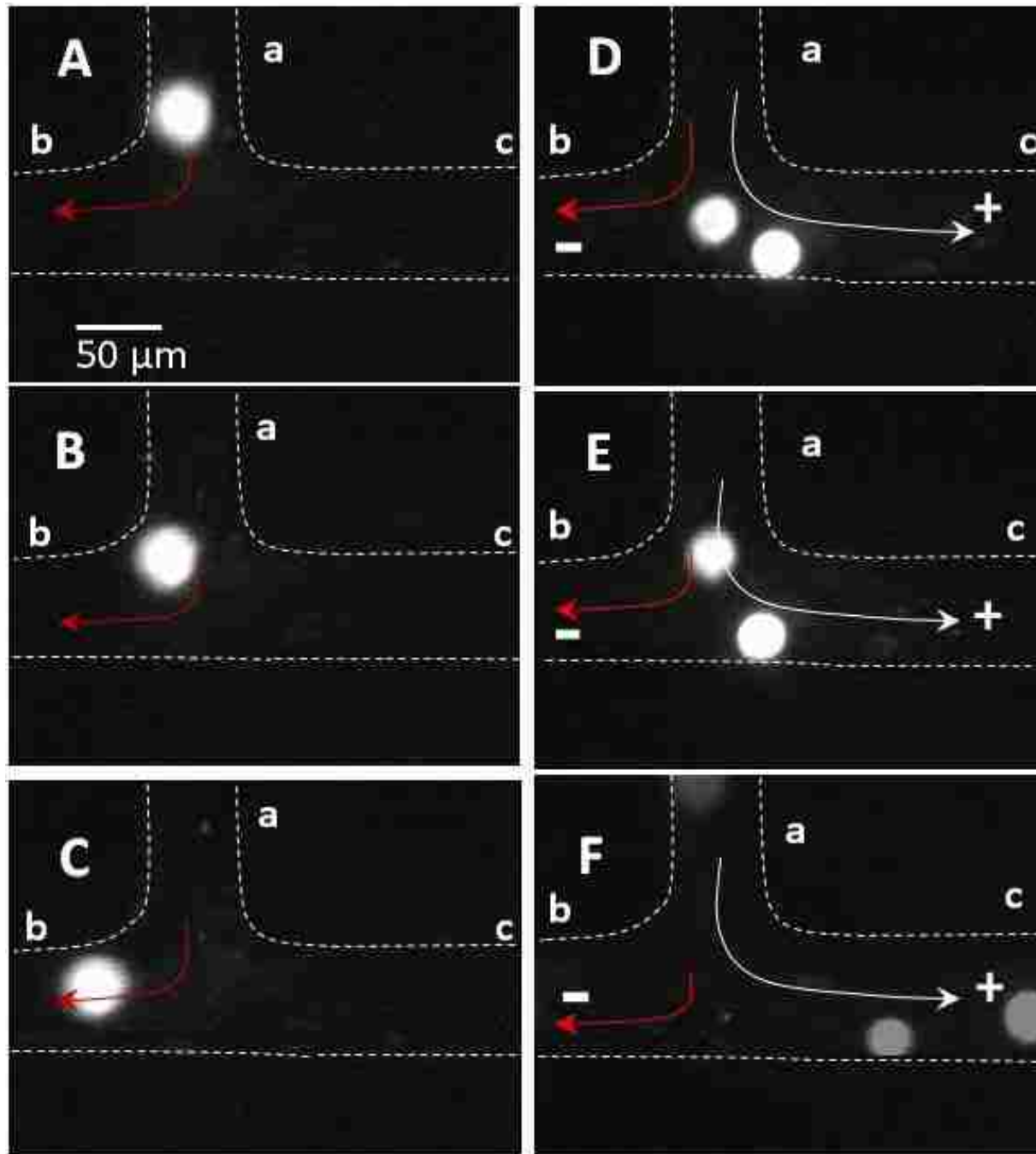


Figure 5.3 Micrographs (43x) showing SW620 cell manipulation in the electro-manipulation unit. The SW620 cells resident in Tris-Glycine buffer were introduced from inlet of channel 'a'. **A, B, C**) The cells are travelling at $1 \mu\text{L min}^{-1}$ flow rate. The hydrodynamic flow direction is given in white arrow. The majority (90%) of the cells are travelling from a-b, which has less pressure drop ($0.7 \text{ psi at } 1 \mu\text{L min}^{-1}$) compared to the pressure drop of a-c ($7 \text{ psi at } 1 \mu\text{L min}^{-1}$). **D, E, F**) The SW620 cells movement in the presence of electric field strength of 100 V cm^{-1} . The electrophoretic movement direction of cells is given in red arrow.

of the cell manipulation and the cell migration velocity was calculated to be $130 \pm 15 \mu\text{m s}^{-1}$. This field may cause membrane permeation but did not result in cell lysis.⁵¹ It took approximately 5 min for the cells to migrate from the T junction to the (c) sample reservoir. We applied higher electric field strengths to speed up the cell migration rate, however, an electric field $\geq 200 \text{ V cm}^{-1}$ resulted in a higher velocity $160 \pm 17 \mu\text{m s}^{-1}$, but also extensive cell lysis. We also found that applying an electric field strength of 100 V cm^{-1} along with a hydrodynamic flow rate of $1 \mu\text{L min}^{-1}$ (linear velocity = 3.3 mm s^{-1}) was sufficient for the CTCs to be effectively collected into (c) reservoir with nearly 100% efficiency. Figure 5.3 D-F illustrates two cells moving in the direction toward the anode. Above $1 \mu\text{L min}^{-1}$ flow rate, cells were not diverted toward the anode and they maintained their traveling direction with the hydrodynamic flow towards the waste reservoir.

For an incompressible Newtonian fluid of low Reynolds number, the fluid motion is governed by the Stoke's equation. In the T junction, The Stoke's frictional force on a charged particle is due to the relative motion of the particle with regard to the EOF and is given by;⁵²

$$F_{Stoke's} = -6\pi\eta r_p(U_h + U_{EOF}) \quad (3)$$

For the present experiments, η the solution viscosity is $7.98 \times 10^{-4} \text{ N s m}^{-2}$,⁵⁴ r_p is the radius of the cell, and U_h is linear velocity of the hydrodynamic flow of H_{eb} ($3.0 \times 10^{-3} \text{ m s}^{-1}$), which is the 90% of optimum linear velocity ($3.3 \times 10^{-3} \text{ m s}^{-1}$) for cell manipulation into reservoir (c). The EOF value for 0.25% w/v trypsin/0.2 mM Tris/19.2 mM Glycine buffer solution has been determined to be $3.1 \times 10^{-4} \pm 0.23 \times 10^{-4} \text{ cm}^2 \text{ V}^{-1} \text{ s}^{-1}$ at pH=8.3. Therefore, the linear velocity (U_{EOF}) for corresponding EOF is $3.1 \times 10^{-4} \text{ m s}^{-1}$. For pristine PMMA,

the apparent surface pK_a value was found to be 4.2, indicative of carboxylic acid functional groups present on the surface. At $pH=8.3$, the PMMA surface consists of negatively charged functional groups producing a cathodic EOF⁵³ in the same direction as the hydrodynamic flow of U_h in the e-b section of the channel. The total Stoke's force on the SW620 cell at the T junction was calculated to be 5.0×10^{-10} N.

At junction T, the electrophoretic force (9.6×10^{-9} N) is larger than the Stoke's force (5.0×10^{-10} N) acting on the cell. Therefore, CTCs are diverted into the collection reservoir (c) (see Figure 5.3D-F). In addition, the linear velocity (U'_h) of the hydrodynamic flow of H_{ec} (3.0×10^{-4} m s⁻¹), which is the 10% of optimum linear velocity (3.3×10^{-3} m s⁻¹) for cell manipulation into reservoir (c) is in opposite direction to the linear velocity (3.1×10^{-4} m s⁻¹) of EOF in the e-c section of the channel. As such, hydrodynamic flow force is cancelled out by the electroosmotic flow in the e-c section of the channel. The apparent electrophoretic mobility of the SW620 cells was calculated to be $1.23 \text{ cm}^2 \text{ V}^{-1} \text{ s}^{-1}$. This value is closely correlated to the experimental value of $1.30 \pm 0.15 \text{ cm}^2 \text{ V}^{-1} \text{ s}^{-1}$.

Chip-to-chip reproducibility of the measured cell flow velocities varied slightly however, the direction of the cell transport was reproducible from chip-to-chip. For example, in 3 different PMMA devices, the RSD for the velocities were 10–15%.

It was found that smaller cells moved slightly faster and thus could climb over the larger cells moving in front, if the centers of the cells were not located on the same line parallel to the applied electric field. The net charge on the cell also depends on its mitosis stage and surface area.⁴⁶ Thus, cells with different negative surface charge densities migrated at different speeds.

In preliminary studies, we used channels of 80 $\mu\text{m}\times 100\ \mu\text{m}$ and 50 $\mu\text{m}\times 100\ \mu\text{m}$ of width and depth, respectively. We observed a near-wall enhancing effect, which was reported by Xuan et al.⁵⁵ As such, the cell velocity observed for the 80 $\mu\text{m}\times 100\ \mu\text{m}$ channel was lower ($110\ \mu\text{m s}^{-1}\pm 10$) at $100\ \text{V cm}^{-1}$ than the velocity observed for 50 $\mu\text{m}\times 100\ \mu\text{m}$ channels ($130\ \mu\text{m s}^{-1}\pm 15$) at $100\ \text{V cm}^{-1}$. When the particle–wall separation distance became smaller, the local electric field in the gap became stronger and hence, the electric force dominated over the viscous friction and the electrophoretic motion increased. In addition to the translational electrokinetic motion, the spherical particle also has a rotational motion due to the asymmetry of the electric field and the flow field. The particle rotational motion was more obvious in the 80 $\mu\text{m}\times 100\ \mu\text{m}$ channels, where the boundary effect was more dominant.⁵⁶

Downstream PCR and LDRs required very sensitive analysis of low-abundant point mutations in the gDNA, and this could be inhibited by the presence of trypsin. However, we were able to perform PCR/LDR reactions effectively; we noted that the trypsin did not inhibit PCR/LDR assays. The cell releasing agent, 0.25% trypsin, possessed a net positive charge at $\text{pH}=8.3$ ($\text{pI}=10.3$).⁵⁷ Therefore, trypsin migrated toward the cathode with the EOF facilitating efficient separation of the CTCs and trypsin. In addition, the surface “softness” (*i.e.*, the rigidity and ion permeability of glycocalices) may be influenced by trypsin treatment of the CTCs.⁵⁸ We did not observe significant variation of the electrophoretic mobility of the CTCs with and without treatment of trypsin for ~ 30 min; it appeared that proteases may remove negative charges from the cell surface but still maintain the electrophoretic mobility.⁵⁹

Because fluorescence microscopy was used for initial cell visualization, the cells were fluorescently labeled using fluorescein derivative, fluorescein isothiocyanate

(FITC), which has a net negative charge at pH=8.3.⁶⁰ In the cell staining process, FITC conjugates with membrane lipids could produce more net negative charges on the cell surface, producing a greater electrophoretic mobility $1.35 \pm 0.11 \text{ cm}^2 \text{ V}^{-1} \text{ s}^{-1}$ than for cells that were stained.

From these experiments, we noticed negligible amounts of cell adhesion of the SW620 cells to the channel walls of the electro-manipulation unit. It was noticed during device operation that some of the immobilized/adsorbed cells could be removed by applying higher electric fields. This was partially caused by an increase in the number of collisions between the flowing and stagnant cells as well as stronger fields that were able to “lift” cells from the polymer surface, suggesting that the adhesion forces of the cell to the polymer surface were not strong enough to withstand the electric force. We have observed less cell adhesion for devices with $50 \text{ }\mu\text{m} \times 100 \text{ }\mu\text{m}$ channel dimensions compared to those of $80 \text{ }\mu\text{m} \times 100 \text{ }\mu\text{m}$ dimensions. This effect may arise from higher frequency of collisions between moving cells and the adhered cells in the smaller channels.

5.3.5 PCR and LDR Mutation Profiling

A method that can detect single point mutations in DNA is the ligase detection reaction (LDR) coupled to a PCR (see Scheme 5.1) and this was used to search for point mutations in the enriched CTCs.^{35,61-68} Following PCR amplification of the appropriate gene fragments, which contain sections of the gene with point mutations, the amplicon is mixed with two LDR primers, a common and discriminating primer that flank the point mutation of interest. The discriminating primer contains a base at its 3'-end that coincides with the single base mutation site. If bases are mismatched, ligation

of the two primers does not occur. A perfect match, however, results in a ligation of the two primers and a product length that is the sum of the two oligonucleotides primers.

In our experiment, enriched CTCs were lysed and the PCR/LDR assay was performed to search for point mutations in codon 12 of the *K-ras* gene (*c12.2V*). Most *K-ras* mutations for colorectal cancer patients are localized within codon 12, but are also

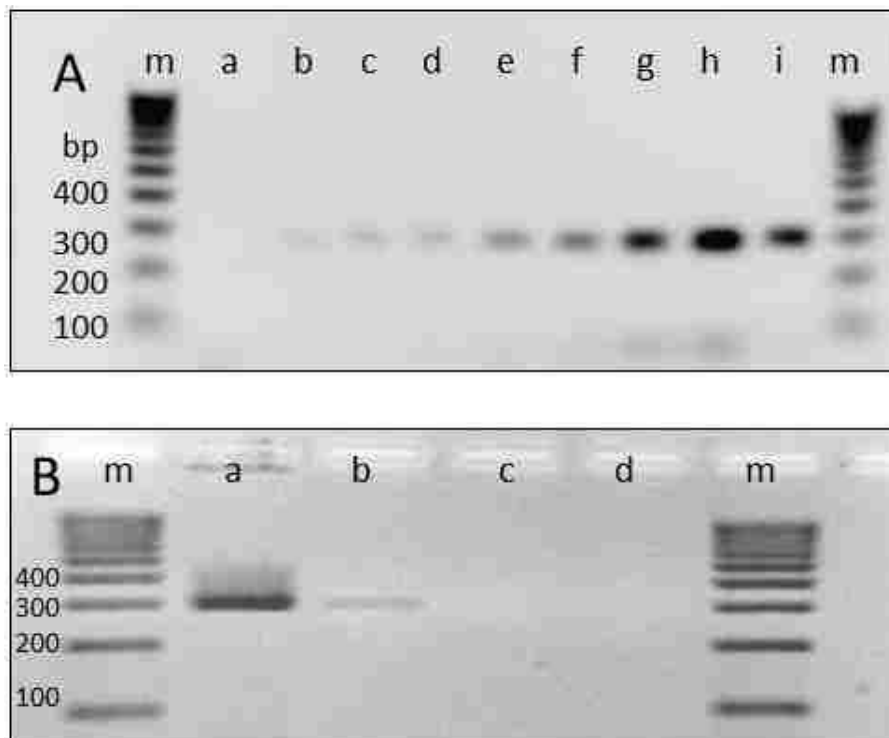


Figure 5.4 Agarose gel electrophoresis of the PCR products. PCR was set for 32 cycles, with initial denaturation of 2 min and final extension of 7 min. Each cycle consisted of: 94 °C (30 s), 60 °C (30 s), 72 °C (40 s). Gel stained with ethidium bromide were run at 4.8 V cm⁻¹. **(A)** Gel electropherogram for PCR performed on standard SW620 samples (**a**) no gDNA template, Negative control; (**b**) DNA from 10 SW620 cells; (**c**) DNA from 20 SW620 cells; (**d**) DNA from 50 SW620 cells; (**e**) DNA from 100 SW620 cells; (**f**) DNA from 500 SW620 cells; (**g**) DNA from 1,000 SW620 cells; (**h**) DNA from 5,000 SW620 cells; (**i**) gDNA template from SW620, Positive control; Lanes a-i contains 3 µL of DNA amplicons. **(B)** Gel Electropherogram for PCR performed on SW620 cells obtained from HTMSU selection followed by electrokinetic enrichment (**a**) gDNA template from SW620, Positive control; (**b**) PCR product from 10 SW620 cells selected from whole blood using HTMSU (**c**) PCR product from whole blood with no SW620 cells (**d**) no gDNA template, negative control. Lanes a-d contains 3 µL of DNA amplicons.

present in codons 13 and 61;⁶⁹⁻⁷⁶ they are found in nearly 35–50% of all patients with colorectal cancer.⁷⁷⁻⁷⁹ Once acquired, *K-ras* mutations are conserved throughout the

course of disease progression. The PCR phase of the assay was first evaluated using different numbers of SW620 cells, ranging from 10-5,000 cells in control experiments. In these experiments, the required number of cells was added to a PCR tube, thermally lysed and the PCR reagents added to the tube. As shown in Figure 5.4A, cells ranging from 5,000 to as low as 10 were successfully amplified to yield 300 bp PCR products based on the primers used for the PCR amplification of codon 12 of the SW620 cells.

To demonstrate the capability of our integrated HTMSU with cell enrichment for subsequent molecular profiling, 1 mL of whole blood containing low-abundance CTCs was processed. Ten SW620 cells were selected and enriched from 1 mL of whole blood and subjected to PCR yielding the results shown in the Figure 5.4B lane (b). The success of the PCR reaction on 10 CTC was confirmed by the positive and negative control experiments as shown in the Figure 5.4B lane (a) and (d) respectively. As expected, no PCR amplicon was generated from the whole blood as shown in Figure 5.4 lane (c). The presence of mutations within the amplicon (~300 bp) was analyzed by LDR. The LDR common primer possessed a Cy5.5 fluorescent label and a 5' phosphorylation modification to facilitate covalent coupling with the discriminating primer for the detection of successful ligation events produced as a result of the LDR and the subsequent analysis using capillary gel electrophoresis with laser-induced fluorescence detection. Point mutations were identified through the observation of a 43 nt product. The capillary gel electrophoresis results of LDR products generated from different numbers of CTCs processed using the HTMSU and electro-manipulation unit are shown in Figures 5.5A-G. Clearly, the results indicated the ability to identify point mutations from as few as 10 CTCs seeded into the whole blood sample and subjected to CTC selection and enrichment. The HT29 (wild-type) lacks *K-ras c12.2V* point mutation in the

K-ras gene, which was confirmed by the absence of 43 nt LDR product, as shown by capillary gel electrophoresis results of the LDR products generated from 50 HT29 cells in Figure 5.5H. Three samples, one containing whole blood without CTCs, a second one

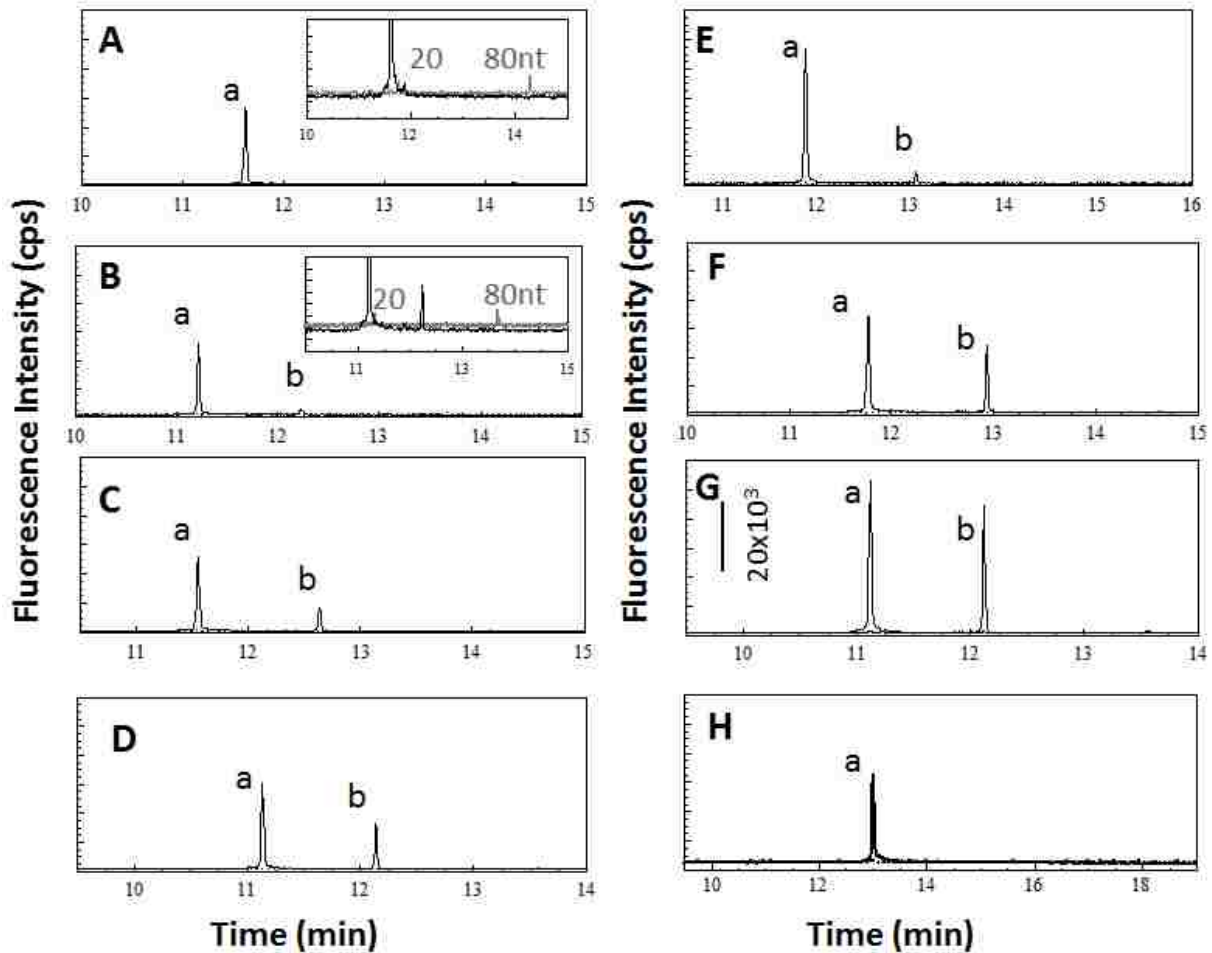


Figure 5.5 The LDR mixtures with a discriminating and common primers for *K-ras c12.2V*, could selectively detect this mutation. Two μL of amplicons from PCR with SW620 (mutant) and HT29 were used for analyzing point mutation in the *K-ras* gene. LDR was set for 20 cycles. Initial denaturation 95 °C for 2 min. Each cycle consisted of: 95 °C (30s), 65 °C (2 min), and 4 °C as final hold. LDR was performed at capillary temperature of 60°C, denaturation temperature of 90 °C (3 min), Injection at 2.0 kV (30 s) and separation at 6.0 kV (20 min). Peak a represent the primer and peak b represents the LDR product. Capillary electrophoresis products for **A**) 0 **B**) 10 **C**) 20 **D**) 50 **E**) 100 **F**) 500 and **G**) 5000 cells of SW620. The insets in **A** and **B** show the magnified scaled plot of products. **H**) LDR product for 50 cells of HT29.

containing 32 cells from HT29 cells, and a third sample containing 10 SW620 cells were processed via the HTMSU and enriched with the electro-manipulation unit. The three

samples were subjected to PCR/LDR/capillary gel electrophoresis and yielded the results shown in Figures 5.2B-D. As expected, our results showed the presence of no mutations in the whole blood that contained no CTCs (Figure 5.2B) which served as a negative control. The sample containing 34 HT29 cells did not show any product (Figure 5.2C) because it does not harbor 12.2V point mutation and served as a wild-type in this assay. Conversely, the results of whole blood that contained 10 SW620 cells produced 43 nt long LDR product indicative of 12.2V point mutation as shown in Figure 5.2D.

5.4 Conclusions

Previously, it has been reported a positive selection of MCF-7 and LNCaP cancer cells from peripheral blood using affinity agents such as antibodies and aptamers immobilized HTMSU. In here, I have integrated HTMSU with electrokinetic enrichment microfluidic unit for performance of single recombinant low-abundance CTC cell-based assay. A series of analytical processes were carried out, including immunoaffinity selection of rare CTCs, quantification of selected cells via conductivity impedance and electrophoretic enrichment of selected cells for PCR/LDR/CE interrogation for detection of low abundant point mutations in genomic DNA. We also showed the ability to recover cells with $\sim 96 \pm 4\%$ efficiency from the whole blood and $\sim 100\%$ efficient electrokinetic enrichment of selected CTCs for molecular profiling. The strategy developed offered the ability to effectively profile low-abundant point mutations harbored in rare CTCs in patients' blood without the interferences of highly abundant leukocytes. The entire series of processing steps can be implemented in under 40 min for 1 mL of blood sample, and the processing volume could significantly be increased by increasing the throughput of the fluidic chip through the use of more fluidic vials that are deeper can provide the opportunity to process 10 mL of input blood directly. In addition, moving the

PCR/LDR step to the chip can also reduce processing time significantly and improve the sensitivity due to the more efficient thermal management properties of microscale molecular profiling.

5.5 References

1. Peek, RM., Jr. *Cancer Chemother. Pharmacol.* **2004**, *54*, S50.
2. Ang, C-S.; Nice, EC. *J. Proteome Res.* ACS ASAP.
3. Takahashi, H.; Hosono, K.; Uchiyama, T.; Sugiyama, M.; Sakai, E.; et al., *PPAR Res.* **2010**, No pp given.
4. Allard, WJ.; Matera, J.; Miller, MC.; Repollet, M.; Connelly MC.; et al., *Clin. Cancer Res.* **2004**, *10*, 6897.
5. Vidaurreta, M.; Sastre, J.; Sanz-Casla MT.; Maestro ML.; Rafael, S.; et al., *Med. Clin.* **2007**, *129*, 333.
6. Midgley, RS.; Kerr, DJ. *Expert Rev. Anticancer Ther.***2003**, *3*, 63.
7. Cristofanilli, M.; Budd, GT.; Ellis, MJ.; Stopeck, A.; Matera, J.; et al., *New England J. Med.* **2004**, *351*, 781.
8. Helo, P.; Cronin, AM.; Danila, DC.; Wenske, S.; Gonzalez-Espinoza, R.; et al., *Clin. Chem.* **2009**, *55*, 765.
9. Han, HJ.; Yanagisawa, A.; Kato, Y.; Park, JG.; Nakamura, Y. *Cancer Res.* **1993**, *53*, 5087.
10. Sieuwerts, AM.; Kraan, J.; Bolt-de VJ.; Spoel, P.; Mostert, B.; et al., *Breast Cancer Res. Treat.* **2009**, *118*, 455.
11. Cohen, SJ.; Alpaugh, RK.; Gross, S.; O'Hara, SM.; Smirnov, DA.; et al., *Clin. Colorectal Cancer* **2006**, *6*, 125.
12. Allan AL.; Keeney, M. *J. Oncol.* **2010**, *2010*, 426218.
13. Campos, M.; Prior, C.; Warleta, F.; Zudaire, I.; Ruiz-Mora, J.; et al., *J. Histochem. Cytochem.* **2008**, *56*, 667.
14. Wlodkowic, D.; Faley, S.; Skommer, J.; McGuinness, D.; Cooper, J. M. *Anal. Chem.* **2009**, *81*, 9828.

15. Hou, J-M.; Greystoke, A.; Lancashire, L.; Cummings, J.; Ward, T.; et al., *American J. Pathol.* **2009**, *175*, 808.
16. Nagrath, S.; Sequist, LV.; Maheswaran, S.; Bell, DW.; Irimia, D.; et al., *Nature* **2007**, *450*, 1235.
17. Adams, AA.; Okagbare, PI.; Feng, J.; Hupert, ML.; Patterson, D.; et al., *J. Am. Chem. Soc.* **2008**, *130*, 8633.
18. Dharmasiri, U.; Balamurugan, S.; Adams, AA.; Okagbare, PI.; Obubuafo, A.; Soper, SA. *Electrophoresis* **2009**, *30*, 3289.
19. Miller, MC.; Doyle Gerald, V.; Terstappen Leon, WMM. *J. Oncol.* **2010**, *2010*, 617421.
20. Bouche, O.; Beretta, GD.; Alfonso, PG.; Geissler, M. *Cancer Treat. Rev.* **2010**, *36*, S1.
21. Yang, M-J.; Chiu, H-H.; Wang, H-M.; Yen, L-C.; Tsao, D-A.; et al., *Ann. Surg. Oncol.* **2010**, *17*, 624.
22. Bilchik, AJ.; Nora, DT.; Saha, S.; Turner, R.; Wiese, D.; et al., *Arch. Surg.* **2002**, *137*, 1377.
23. Svoboda, K.; Block, SM. *Annu. Rev. Biophys. Biomol. Struct.* **1994**, *23*, 247.
24. Wu, JR. *J. Acoust. Soc. Am.* **1991**, *89*, 2140.
25. Jung, DR.; Kapur, R.; Adams, T.; Giuliano, K. A.; Mrksich, M.; et al., *Crit. Rev. Biotechnol.* **2001**, *21*, 111.
26. Melville, D.; Paul, F.; Roath, S. *IEEE Trans. Magn.* **1975**, *MAG11*, 1701.
27. Radbruch, A.; Mechtold, B.; Thiel, A.; Miltenyi, S.; Pfluger, E. *Methods Cell Biol.* **1994**, *42 Pt B*, 387.
28. Grimm, S. *Nat. Rev. Genet.* **2004**, *5*, 179.
29. Andersson, H.; van den BA. *Curr. Opin. Biotechnol.* **2003**, *15*, 44.
30. Voldman, J.; Gray, ML.; Schmidt, MA. *Annu. Rev. Biomed. Eng.* **1999**, *1*, 401.
31. Faley, S.; Seale, K.; Hughey, J.; Schaffer, DK.; VanCompernelle, S.; et al., *Lab Chip* **2008**, *8*, 1700.
32. Wlodkowic, D.; Faley, S.; Zagnoni, M.; Wikswa JP.; Cooper JM. *Anal. Chem.* **2009**, *81*, 5517.

33. Hashimoto, M.; Barany, F.; Soper, SA. *Biosensors & Bioelectronics* **2006**, 21, 1915.
34. Sinville, R.; Coyne, J.; Meayher, RJ.; Cheng, YW.; Barany, F.; et al., *Electrophoresis* **2008**, 29, 4751.
35. Gerry, NP.; Witowski, NE.; Day, J.; Hammer, RP.; Barany, G.; et al., *Mol. Biol.* **1999**, 292, 251.
36. Khanna, M.; Cao, WG.; Zirvi, M.; Paty, P.; Barany, F. *Clin. Biochem.* **1999**, 32, 287.
37. Hashimoto, M.; Barany, F.; Soper, SA. *Biosensors & Bioelectronics* **2006**, 21, 1915.
38. Thomas, G.; Sinville, R.; Sutton, S.; Farquar, H.; Hammer, RP.; et al., *Electrophoresis* **2004**, 25, 1668.
39. Wabuyele, MB.; Farquar, H.; Stryjewski, W.; Hammer, RP.; Soper, SA.; et al., *J. Am. Chem. Soc.* **2003**, 125, 6937.
40. Huang, X.; Gordon, MJ.; Zare, RN. *Anal. Chem.* **1988**, 60, 1837.
41. Hosokawa, M.; Hayata, T.; Fukuda, Y.; Arakaki, A.; Yoshino, T.; et al., *Anal. Chem.* **2010**, 82, 6629.
42. Stephan JP.; Schanz, S.; Wong, A.; Schow, P.; Wong WLT. *Am. J. Pathol.* **2002**, 161, 787.
43. Chang, K-C.; Hammer, DA. *Biophys. J.* **1999**, 76, 1280.
44. Willuda, J.; Honegger, A.; Waibel, R.; Schubiger, PA.; Stahel, R.; et al., *Cancer Res.* **1999**, 59, 5758.
45. Ayadi, MA.; Leuliet, JC.; Chopard, F.; Berthou, M.; Lebouche, M. *Innovative Food Science Emerging Tech.* **2004**, 5, 465.
46. Mehrishi, JN.; Bauer, J. *Electrophoresis* **2002**, 23, 1984.
47. Weiss, L. *Exp. Cell Res.* **1974**, 86, 223.
48. Lipman, KM.; Dodelson, R.; Hays, RM. *J.Gen. Physiol.* **1966**, 49, 501.
49. Righetti, PG. *Electrokinet. Sep. Methods* **1979**, 389.
50. Kuhr, WG. *Anal. Chem.* **1990**, 62, 403R.
51. Li, PCH.; Harrison, DJ. *Anal. Chem.* **1997**, 69, 1564.

52. Kang, Y.; Li, D. *Microfluid. Nanofluid.* **2009**, *6*, 431.
53. Witek, MA.; Wei, S.; Vaidya, B.; Adams, AA.; Zhu, L.; et al., *Lab Chip* **2004**, *4*, 464.
54. Korson, L.; Drost-Hansen, W.; Millero, FJ. *J. Phys. Chem.* **1969**, *73*, 34.
55. Xuan, X.; Raghbizadeh, S.; Li, D. *J. Colloid Interface Science* **2006**, *296*, 743.
56. Keh, HJ.; Chiou, JY. *AIChE J.* **1996**, *42*, 1397.
57. Novillo, C.; Castanera, P.; Ortego, F. *Insect Biochem. Mol. Biol.* **1999**, *29*, 177.
58. Mazda, T.; Makino, K.; Ohshima, H. *Colloids Surfaces, B: Biointerfaces* **1995**, *5*, 75.
59. Uhlenbruck, G.; Rothe, A.; Pardoe, GI. *Immunol.* **1968**, *136*, 79.
60. The, TH.; Feltkamp, TEW. *Immunol.* **1970**, *18*, 865.
61. Hashimoto, M.; Hupert, ML.; Murphy, MC.; Soper, SA.; Cheng, Y-W.; et al., *Anal. Chem.* **2005**, *77*, 3243.
62. Barany, F. *Proc. Natl. Acad. Sci. USA.* **1991**, *88*, 189.
63. Favis, R.; Day, JP.; Gerry, NP.; Phelan, C.; Narod, S.; et al., *Nature Biotech.* **2000**, *18*, 561.
64. Khanna, M.; Park, P.; Zirvi, M.; Cao, W.; Picon, A.; et al., *Oncogene* **1999**, *18*, 27.
65. Wang, Y.; Vaidya, B.; Farquar, H. D.; Stryjewski, W.; Hammer, R. P.; et al., *Anal. Chem.* **2003**, *75*, 1130.
66. Situma, C.; Wang, Y.; Hupert, M.; Barany, F.; McCarley, et al., *Anal. Biochem.* **2005**, *340*, 123.
67. Khanna, M.; Cao, W.; Zirvi, M.; Paty, P.; Barany, F. *Clin. Biochem.* **1999**, *32*, 287.
68. Cheng, YW.; Shawber, C.; Notterman, D.; Paty, P.; Barany, F. *Genome Res.* **2006**, *16*, 282.
69. Bos, JL. *Mutat. Res.* **1988**, *195*, 255.
70. Breivik, J.; Meling, GI.; Spurkland, A.; Rognum, TO.; Gaudernack, G. *Br. J. Cancer* **1994**, *69*, 367.
71. Capella, G.; Cronauer-Mitra, S.; Pienado, MA.; Perucho, M. *Environ. Health Perspect.* **1991**, *93*, 125.

72. Finkelstein, SD.; Sayegh, R.; Bakker, A.; Swalsky, P. *Arch. Surg.* **1993**, 128, 526.
73. Forrester, K.; Almoguera, C.; Han, K.; Grizzle, WE.; Perucho, M. *Nature* **1987**, 327, 298.
74. Losi, L.; Benhattar, J.; Costa, J. *Eur. J. Cancer* **1992**, 28A, 1115.
75. Smith, AJ.; Stern, HS.; Penner, M.; Hay, K.; Mitri, A.; et al., *Cancer Res.* **1994**, 54, 5527.
76. Vogelstein, B.; Fearon, ER.; Hamilton, SR.; Kern, SE.; Preisinger, AC.; et al., *N. Engl. J. Med.* **1988**, 319, 525.
77. Andersen, SN.; Lovig, T.; Breivik, J.; Lund, E.; Gaudernack, G.; et al., *Scand J Gastroenterol.* **1997**, 32, 62.
78. Chiang, JM. *Cancer Lett.* **1998**, 126, 179.
79. Rothschild, CB.; Brewer, CS.; Loggie, B.; Beard, GA.; Triscott, MX. *J. Immunol. Methods* **1997**, 206, 11.

CHAPTER 6 FUTURE WORK: HIGHLY EFFICIENT SEPARATION OF PURE HEMATOPOIETIC STEM CELLS FROM WHOLE BLOOD

6.1 Introduction

The stem cells that generate blood and immune cells are termed as hematopoietic stem cells (HSCs). Recently, it has been found that HSCs are able to form epithelial cells, such as muscle, blood vessels, and bone.¹ Lagasse et al. demonstrated that the liver can be repaired by purified HSCs; therefore, HSCs have the potential to integrate into and grow in some epithelial tissues. This may eventually make it possible to use HSCs to replace a wider array of cells and tissues.² In addition, there have been suggestions that umbilical cord blood contains stem cells having the capability of developing cells of multiple germ layers (multipotent) or even all germ layers, e.g., endoderm, ectoderm, and mesoderm (pluripotent).³ Another potential use of HSCs is in the treatment of hereditary blood disorders such as aplastic anemia, beta-thalassemia, Blackfan-Diamond syndrome, globoid cell leukodystrophy, sickle-cell anemia, severe combined immunodeficiency, X-linked lymphoproliferative syndrome, and Wiskott-Aldrich syndrome.⁴ Also, HSCs can be utilized for the replacement of blood cells that are destroyed by chemotherapy. Thus, these cells can be stored while the patient undergoes intensive chemotherapy or radiotherapy that is used to destroy the cancer cells. Once the drugs are washed out of the patient's body, the patient receives a transfusion using the stored HSCs.⁵ One problem with the use of autologous HSCs transplants in cancer therapy is that circulating tumor cells (CTCs) are sometimes inadvertently collected and reinfused into the patient along with the HSCs. Reintroduction of CTCs can be eliminated by specific selection and separation of HSCs from whole blood.⁶

To harvest HSCs, an intravenous tube is inserted into the donor's vein and the blood is passed through a filtering system that pulls out CD34 white blood cells (WBCs) and returns the red blood cells (RBCs) to the donor. The most common approach to identify HSCs is to utilize membrane markers such as CD34, CD59, CD38, Thy1 and/or SCA-1.⁹ Unfortunately, these markers are non-specific for HSCs and they have been occasionally expressed in WBCs and RBCs when in an activated state.¹⁰ Therefore, of the cells collected, only 5-20% are genuine HSCs and the remainder are a mixture of WBCs of various degrees of maturity.⁷

In addition, another major issue with selection of HSC levels is the low-abundance or rare-event nature of these cells among a higher number of spectator cells in peripheral blood. For example, ~1,000 HSCs are in whole blood, which is composed of $>10^9$ erythrocytes and $>10^6$ leukocytes per mL. In addition, there are multiple types of stem cells with rare, long-term replicating ability, which are morphologically similar to WBCs or bone marrow cells.⁸

SELEX (systematic evolution of ligands by exponential enrichment) is a method used to generate DNA or RNA aptamers from a combinatorial library. Aptamers with high affinity and specificity for cells have already been produced successfully, demonstrating that complex targets, including tumor cells and tissues, are compatible with the SELEX process.¹² Guo et al. generated aptamers for the isolation of HSCs from whole bone marrow. When bound to a surface, the aptamers could be used for HSCs tracking. Furthermore, they found that after immobilizing the aptamers targeted against osteoblasts on titanium, the aptamer-coated titanium surface could enrich osteoblasts quickly and efficiently.¹¹

Aptamer technology has been used for protein-protein interaction research and for molecular recognition. It is a robust technology to identify specific targets. The cell-SELEX process allows the selection of highly specific aptamers with high binding affinities without prior knowledge of any biomarkers or proteins on the cell membrane.¹³ It has been reported that cell-SELEX can be used to identify minor molecular-level differences among similar categories of cells.¹⁴ In addition, The cell-SELEX process allows for aptamers to be selected from cells in their native state. In fact, through biomarker discovery, the molecular nature of the membrane can then be explored to derive even more information by the selected aptamers for an understanding of the molecular foundation of the cell membrane, which has been preliminarily demonstrated by Blank and co-workers.¹⁸

On the other hand, improved performance of microsystem technologies is emerging as fundamental to high-sensitivity cellular analysis technologies. In particular, microsystem platforms enable one to handle small numbers of cells without loss.¹⁵ Already, aptamers and antibodies have been incorporated into microsystems to effectively isolate low-abundance CTCs.^{13,16,17} The challenge for imposing low-abundance cell-selection assays to microsystems is sampling; to generate a high statistical probability of selecting the low-abundance cells, large input volumes must be processed and most microsystems cannot handle large-volume inputs in reasonable times. Adams et al. recently reported a microsystem having high-throughput capabilities.^{16,17} In this system, 1 mL of blood could be processed in ~30 min.

Therefore, proposed herein is a novel approach to selectively isolate HSCs from peripheral blood using an ultra-high-throughput microsystem. The cell-SELEX procedure will be implemented to generate HSCs specific aptamers. The developed

HSCs specific aptamers will be immobilized onto ultra-high aspect ratio microstructures for high-throughput selection of HSCs from whole blood. The isolated HSCs will be released into solution using complementary oligonucleotide, pH or ionic strength changes in the medium. As such, viability and physiological integrity of the selected HSCs will be conserved for downstream clinical applications.

6.2 Materials and Methods

6.2.1 Cell Suspensions

HSCs (ATCC) will be cultured to 80% confluence in Dulbecco's Modified Eagle's Medium supplemented with high glucose containing 1.5 g L⁻¹ sodium bicarbonate (NaHCO₃), 15 mM HEPES buffer, and 10% fetal bovine serum. A cell stripper (Mediatech, Inc.) solution will be used to harvest the HSCs from the culturing plate. HSCs will be stained with PKH67 for microscopic visualization experiments using fluorescence. Cell counts for seeding experiments into whole blood will be determined by counting three aliquots of cells in succession using a hemacytometer.

6.2.2 Cell-SELEX Library and Primers

The HPLC-purified library will contain a central randomized sequence of 45 nucleotides (nt) flanked by 20-nt primer hybridization sites (ACGCTCGGATGCCACTACAG-45nt-CTCATGGACGTGCTGGTGAC) (Applied Biosystems). 5'-primer (5'-FITC- ACGCTCGGATGCCACTACAG-3') and a biotinylated (Bio) 3'-primer (5'-Bio- GTCACCAGCACGTCCATGAG-3') (Applied Biosystems) will be used in the PCR reactions for the synthesis of DNA molecules. After denaturing in 0.2 M NaOH, the ssDNA aptamer will be separated from the biotinylated antisense ssDNA strand by streptavidin-coated sepharose beads (Amersham Bioscience) and used for next round selection.¹⁴

6.2.3 Cell-SELEX Procedures for Generation of Panel of Aptamers for HSCs

The ssDNA pool will be dissolved in a binding buffer. The binding buffer will be prepared by adding yeast tRNA (0.1 mg mL⁻¹; Sigma) and BSA (1 mg mL⁻¹) (Fisher) into wash buffer. Then, the ssDNA pool will be incubated with a target HSCs (ATCC) monolayer in a T25 flask on ice for 30 min. The adherent cells will be scraped from the culturing medium and washed. The bound DNAs on the cells' membrane will be eluted by heating at 95 °C for 5 min in a binding buffer. The eluted DNAs will then be incubated with a WBC and RBC monolayer in a dish (control cells) for counter selection on ice for 1 h. The supernatant will be desalted with a NAP 5 column (GE Healthcare) and then amplified by PCR with biotin-labeled primers (10-20 cycles of 0.5 min at 94 °C, 0.5 min at 58 °C, and 0.5 min at 72 °C, followed by 5 min at 72 °C; Taq-polymerase and dNTP's). The selected sense ssDNA will be separated from the biotinylated antisense ssDNA strand by streptavidin-coated sepharose beads. In the first round, the amount of initial ssDNA pool will be dissolved in 1 mL of binding buffer and the counter selection step will be eliminated. In order to acquire aptamers with high affinity and specificity, the wash strength will be enhanced gradually by extending wash time (e.g. from 1 to 10 min), increasing the volume of the wash buffer (e.g. from 1 to 5 mL) and the number of washes (e.g. from 3 to 5). Additionally, 20% FBS and 50-300-fold molar excess of an 88-mer random DNA library will be added to the incubation solution to reduce the nonspecific binding of the selected pool. After 16 rounds of selection, the selected ssDNA pool will be PCR-amplified using unmodified primers and cloned into *Escherichia coli* using the TA cloning kit (Invitrogen). Cloned sequences will be determined by genome sequencing.¹⁴

6.2.4 ultra-High-Throughput Microsampling Unit (uHTMSU) Fabrication

The proposed microfluidic will consist of multiple fluidic conduits (460) to reduce the pressure drop across the device while allowing for high volume throughput. (e.g. 10 mL of blood in 20 mins at 2 mm s^{-1} linear velocity flow). The device will consist of a series parallel high-aspect ratio channels sharing common input/output ports. Initially, microstructures will be milled onto the surface of a brass plate with a high-precision micromilling machine (KERN MMP 2522, KERN Micro-und Feinwerktechnik GmbH & Co.KG; Germany). The devices will be replicated from a mold masters using hot embossing. The substrate selected for the HTMSU will be PMMA due to its high fidelity of forming structures with high-aspect ratios via micro-replication, minimal non-specific adsorption of biological components to its surface and its ability to generate functional surface-scaffolds through UV irradiation for the attachment of a variety of biological moieties.

6.2.5 Aptamer Immobilization

The uHTMSU devices will be loaded with a 10 mM aptamer solution also containing 4 mg mL^{-1} EDC and 40 mg mL^{-1} NHS in 150 mM MES (pH=6). The solution will be allowed to incubate in the device for 2 h at room temperature. The device will then be rinsed with a solution of PBS (pH=7.4) to remove any non-specifically bound constituents.

6.2.6 HSCs Selection Using the uHTMSU

The blood/reagent container will be made up in 50 mL thin wall plastic tubes. Helium gas will be used to pressurize the system for infusing the solution into the uHTMSU. The reagent/blood container will be connected to a helium gas regulator and to the input port of the HTMSU via a plastic tube with $250 \text{ }\mu\text{m}$ internal diameter. The

flow rate of the system will be proportional to the helium gas pressure applied. Therefore, the flow rate of the input blood/solution can be controlled by regulating the helium gas pressure.

The aptamer immobilized uHTMSU will be subjected to a pre-cell capture rinse with 0.2 mL of 150 mM PBS at 50 mm s⁻¹ linear velocity. Then, the appropriate volume of cell (~10 mL) suspension will be introduced into the uHTMSU at the appropriate linear velocity to isolate the HSCs. Next, a post-capture rinse will be performed with 0.2 mL of 150 mM PBS at 50 mm s⁻¹ to remove any non-specifically adsorbed cells. In cases where the cells require optical visualization to assist in the operational optimization of the uHTMSU, the PMMA devices will be fixed to a programmable motorized stage of an Axiovert 200M (Carl Zeiss, Thornwood, NY) microscope and video images were collected during each experiment at 30 frames per second using a monochrome CCD (JAI CV252, San Jose, CA).

6.2.7 HSCs Release from the uHTMSU

Following a post cell capture rinse performed with 0.2 mL of 150 mM PBS, the cell releasing step can be implemented. The released cells should be viable and have conserved physiological integrity for downstream clinical applications. It has been reported that aptamer-target complexes can be disrupted by changing medium pH, ionic strength or introducing the complementary oligonucleotide. Each method will be implemented to find the ideal conditions for releasing viable HSCs into solution. The cell releasing process will be observed via microscopy.

6.3 Expected Results and Significance

The HSCs specific aptamers will be tethered to the channel walls, dynamic interactions between aptamer specific cell membrane's receptors and the channel wall

is important for the recovery of HSCs. An optimal linear velocity would be expected to guarantee the highest frequency of interaction between surface bound aptamers and HSCs. The optimum linear velocity depends upon the association constant between cell membrane antigen and the aptamer. Here, panel of aptamers will be utilized and multiple cell surface biomarkers will be targeted. Therefore, determination of optimum linear velocity for maximum cell recovery in the presence of multiple interactions will be an interesting factor to investigate.

The panel of aptamers will selectively and specifically immobilize HSCs without prior knowledge of any cell membrane biomarkers. Isolated cells will be released using the complementary aptamers,¹³ changing pH or changing ionic strength of the medium.¹⁴ These cell releasing methods will have minimal impact on the integrity and viability of the cell. Therefore, the cells harvested will be suitable for downstream applications such as clinical cell implantations.

6.4 Dissertation Summary

After brief overview of low-abundance cell selection techniques in chapter 1 and circulating tumor cells in chapter 2, this dissertation initially focuses on the development of aptamer incorporated high-throughput microfluidic techniques to select rare circulation prostate cancer cells (LNCaP) directly from whole blood. The compelling advantage of this methodology was that no sample pre-treatment was necessary and the throughput, recovery, and purity were extremely high, contrary to what has been seen in other low-abundance cell selection formats utilizing size or affinity capture. The ability to quantify the selected cells with near 100% detection efficiency using a conductivity readout format allows for the use of this simple system at the point-of-care for the management of cancer-related diseases from a simple blood test.

Then, we extended the technology to environmental samples to improve sensitivity and portability of traditional groundwater assessment. As a model bio-pathogen, *E. coli* O157:H7 was chosen due to its toxicity and adverse impact on recreational waters. Low-abundance (<100 cells mL⁻¹) *E. coli* O157:H7 cells were isolated and enriched from environmental water samples using a microfluidic chip that its capture beds were covalently decorated with *E.coli* O157:H7 specific polyclonal antibodies. After cell selection, the cells were released and enumerated using bench-top real-time quantitative polymerase chain reaction (PCR), targeting genes which effectively discriminated the O157:H7 serotype from other nonpathogenic bacteria. The strategy developed offered the ability to monitor water quality without the need for a time-consuming cell culture step. We subsequently performed analysis of lake and wastewater samples. The simplicity in manufacturing and ease of operation makes this device attractive for the selection of pathogenic species from a variety of water supplies suspected of containing bacterial pathogens at extremely low frequencies. We envision the potential to probe for a large number of different strains of enterohemorrhagic *E. coli*, which includes more than 100 different non-O157 strains. By proper choice of pAbs and specific probes for the real-time qPCR, one could monitor a large panel of suspected *E. coli* strains from a single sample.

Finally, we have integrated HTMSU with electrokinetic enrichment microfluidic unit for performance of single recombinant low-abundance CTC cell-based assay. A series of analytical processes were carried out, including immunoaffinity selection of rare CTCs, quantification of selected cells via conductivity impedance and electrophoretic enrichment of selected cells for PCR/LDR/CE interrogation for detection of low-abundance point mutations in genomic DNA. The HTMSU was equipped with a

conductivity sensor utilized for CTC selection and automatic quantitation. Following enumeration of the CTCs, they were hydrodynamically transported to an on-chip electro-manipulation unit for pre-concentration of the CTCs into a receiving reservoir in a controlled manner. The pre-concentrated CTCs could then be genetically profiled to search for point mutations using a PCR/LDR/CE assay. The DNA was extracted from the CTCs and subjected to a primary polymerase chain reaction (PCR) with the amplicons used for a ligase detection reaction (LDR) to probe for *K-ras G12.2V* oncogene mutations. This system directs towards a self-contained and fully integrated fluidic system for the molecular profiling of low-abundance CTCs (~ 10 cell mL⁻¹ of whole blood) scattered among peripheral-blood nucleated cells ($\sim 10^6$ cells mL⁻¹ of whole blood).

6.5 Immediate Projections

With minor modifications to the techniques, such as increasing the number of capture channels, changing the channels dimensions, changing the immobilized affinity agents, changing the releasing agent and changing the electric field strength of the cell manipulation section, this technology will be widely applicable for different cell selection, and enrichment assays. In addition, moving the PCR/LDR step to the chip can also reduce processing time significantly and improve the sensitivity greatly due to the more efficient thermal management properties of microscale molecular profiling. In addition, the cells can be subjected to further investigations such as viability and culturing for development of new array of personalized cell lines. Experimental optimization of the parameters will have significant impact on extending the applicability in disease diagnostics and prognostics. Further, in the environmental regime, investigation with

these devices will yield assessment of environmental samples for low-abundance bio-pathogens.

6.6 References

1. Alison, MR.; Poulosom, R.; Jeffery, R.; Dhillon, AP.; Quaglia, A.; et al., *Nature* **2000**, *406*, 257.
2. Lagasse, E.; Connors, H.; Al-Dhalimy, M.; Reitsma, M.; Dohse, M.; et al., *Nature* **2000**, *6*, 1229.
3. Dzierzak, E.; Medvinsky, A.; de Bruijn, M. *Immun.* **1998**, *19*, 228.
4. Dzierzak, E. *Ann. N.Y. Acad. Sci.* **1999**, *872*, 256.
5. Cutler, C.; Li, S.; Kim, HT.; Laglenne, P.; Szeto, KC.; Hoffmeister, L.; et al., *Bio. Blood and Marrow Trans.* **2005**, *11*, 383.
6. Bittner, R. E.; Schofer, C.; Weipoltshammer, K.; Ivanova, S.; Streubel, B.; et al., *Anat. Embry.* **1999**, *199*, 391.
7. Baum, C. M.; Weissman, IL.; Tsukamoto, AS.; Buckle, AM.; Peault, B. *Proc. Natl. Acad. Sci. U.S.A.* **1992**, *89*, 2804.
8. Chen, J.; Astle, CM.; Harrison, DE. *Exp. Hematol.* **1999**, *27*, 928.
9. Weissman, IL.; Anderson, DJ.; Gage, F. *Ann. Rev. Cell Dev. Biol.* **2001**, *17*, 387.
10. Audet, J.; Miller, CL.; Rose-John, S.; Piret, JM.; Eaves, CJ. *Proc. Natl. Aca. Sci. U.S.A.* **2001**, *98*, 1757.
11. Guo, K-T.; Paul, A.; Schichor, C.; Ziemer, G.; Wendel, HP. *Intl. J. Mol. Sci.* **2008**, *9*, 668.
12. Jayasena, SD. *Clin. Chem.* **1999**, *45*, 1628.
13. Shangguan, D.; Meng, L.; Cao, Z. C.; Xiao, Z.; Fang, X.; et al., *Anal. Chem.* **2008**, *80*, 721.
14. Shangguan, D.; Li, Y.; Tang, Z.; Cao, Z. C.; Chen, H. W.; Mallikaratchy, P.; et al., *Proc. Natl. Aca. Sci. U.S.A.* **2006**, *103*, 11838.
15. Dharmasiri, U.; Witek MA.; Adams AA.; Soper SA. *Ann. Rev. Anal. Chem.* **2010**, *3*, 409.

16. Dharmasiri, U.; Balamurugan, S.; Adams, AA.; Okagbare, PI.; Obubuafo, A.; Soper, SA. *Electrophoresis* **2009**, *30*, 3289.

17. Adams, AA.; Okagbare, PI.; Feng, J.; Hupert, ML.; Patterson, D.; et al., *JACS* **2008**, *130*, 8633.

APPENDIX : PERMISSIONS

Dear Dr. Dharmasiri:

It is the policy of Annual Reviews to obtain a written transfer of copyright ownership from our authors and then **to grant back to authors a broad array of parallel rights**. The transfer of copyright allows Annual Reviews (a nonprofit organization) to publish your article, to recover the costs of publication without immediate commercial competition, and potentially to make arrangements for abstracting, indexing, translating, reprinting, and other distribution services. Further, copyright transfer codifies Annual Reviews' flexibility to produce and disseminate your work as broadly as possible via whatever media and delivery mechanisms are appropriate today and in the future. For a complete explanation of our policy and its underpinnings, please see the Copyright FAQ on our Web site at http://www.annualreviews.org/authors/copyright_mandate-FAQ.aspx.

We ask you, as the author or coauthor of an article now in production, to complete the statement below and sign either (a) or (b). Please return this form to us with your revised manuscript. Note that, in the event of a jointly-authored work, all co-authors will be asked to complete this form.

Copyright Transfer and Authors' Rights Agreement

I, Udara Dharmasiri, am an author or coauthor of the manuscript submitted to Annual Reviews and entitled: Microsystems for the Capture of Low-Abundance Cells, scheduled to appear in Volume 3 of the Annual Review of Analytical Chemistry.

AUTHOR: SIGN ONLY (a) OR (b)


(a) For good and valuable consideration, the receipt and sufficiency of which is hereby acknowledged, the undersigned warrants that the above manuscript is the author's original work and has not been published before, that the work contains no libelous or other unlawful statements, and that the work does not infringe on the rights of others. The work is deemed to include all material submitted for publication and includes the text, figures, tables, and any supplementary material accompanying the work. Effective upon completion of this Transfer Agreement, the author hereby assigns to Annual Reviews all right, title, and interest in and to the work in print and all electronic formats. This includes, but is not limited to, the rights to migrate the work to future formats, translate it, and include it in collections. Again notwithstanding any other rights, Annual Reviews may create adaptations, summaries, extracts, and derivative works and shall retain all rights over such adaptations, summaries, extracts, and derivative works.

Authors' Rights After manuscript acceptance and copyright transfer, substantial rights are granted to the author(s) by Annual Reviews:

- 1.T he retention of **patent and trademark rights** to processes or procedures described within the work.
- 2.T he nonexclusive right to use, reproduce, distribute, perform, update, create derivatives, and make copies of the work (electronically or in print) in **connection with the author's teaching, conference presentations, and lectures**, provided the copies are not offered for sale and proper attribution is given. Note that **self-archiving rights** are treated in items #5 and #6 below.
- 3.T he nonexclusive right to store the publisher-supplied PDF file of the work ("the published version") in **electronic reserve rooms** for access by students at the author's institution as part of the author's teaching activities, so long as these files are made available free of charge and are removed when no longer connected to the author's own teaching.
- 4.T he nonexclusive right to use, reproduce, and distribute the publisher-supplied PDF of the work ("the published version") in **coursepacks**, within the author's own institution, so long as these copies are distributed to students free of charge.
- 5.T he right to **self-archive a "preprint"** version of the work, defined as a manuscript that has not yet been reviewed, edited, or prepared for publication by Annual Reviews, provided (a) any preprint posted to the Web after the completion of this Transfer Agreement states explicitly by which Annual Reviews series the manuscript has been accepted, and (b) after the published version of the work appears on the Annual Reviews Web site, the preprint version is amended to include the following acknowledgment and link: "Posted with permission from the Annual Review of Analytical Chemistry, Volume 3 © 2010 by Annual Reviews, <http://www.annualreviews.org>."
- 6.T he right to **self-archive, after the work's publication, an Annual Reviews-supplied ePrint URL** (a specially-keyed URL that allows nonsubscribers to access an Annual Review article freely via the Annual Reviews Web site) on **one personal Web site and/or one institutional repository**. The ePrint URL provides free access to your article; Annual Reviews does not grant permission to directly self-archive a postprint file or the PDF of the article's published version.
- 7.T he right to distribute an Annual Reviews-supplied **ePrint URL to colleagues** who request reprints.
- 8.T he right to include the work, in whole or in part, in a **dissertation or thesis**.

9. The right to use the work, in whole or in part, with attribution and without revision or modification, **in print compilations or other print publications.**

The author must consistently state that s/he executes any of these rights "with permission from the Annual Review of Analytical Chemistry, Volume 3 © 2010 by Annual Reviews, <http://www.annualreviews.org>."



Signature

2009/Dec/04

Date

OR

(b) I **and all my co-authors** (if applicable) are **United States federal employees** who have created the work within the scope of our official duties.¹ Copyright protection is not available for any work of the United States Government. Therefore, this article should appear with the following footnote to the chapter title: "This paper was authored by employees of the United States Government as part of their official duties and is therefore not subject to copyright." If the work is determined to be copyrightable at a later date, then copyright and all rights included in this will be transferred to Annual Reviews. In that event, all the rights granted to the author(s) by Annual Reviews enumerated in Section (a) above will be granted here as well.

The undersigned warrants that the above article is the author's original work, and has not been published before. The author also warrants that the article contains no libelous or unlawful statements and does not infringe on the rights of others. The work is deemed to include all material submitted for publication and includes the text, figures, tables, and all supplementary material accompanying the work.

Signature

Date

¹ A U.S. federal employee **who created the work outside the scope of his or her employment** owns the copyright in the work despite his/her federal employee status. In this event, the author should complete Section (a) of this Copyright Transfer Agreement. **If any of the work's co-authors is not a U.S. federal employee, all authors should complete Section (a) of this Copyright Transfer Agreement.**

**ELSEVIER LICENSE
TERMS AND CONDITIONS**

Sep 10, 2010

This is a License Agreement between Udara R Dharmasiri ("You") and Elsevier ("Elsevier") provided by Copyright Clearance Center ("CCC"). The license consists of your order details, the terms and conditions provided by Elsevier, and the payment terms and conditions.

All payments must be made in full to CCC. For payment instructions, please see information listed at the bottom of this form.

Supplier	Elsevier Limited The Boulevard, Langford Lane Kidlington, Oxford, OX5 1GB, UK
Registered Company Number	1982084
Customer name	Udara R Dharmasiri
Customer address	LSU, Chemistry Baton Rouge, LA 70802
License number	2505440991260
License date	Sep 10, 2010
Licensed content publisher	Elsevier
Licensed content publication	Trends in Molecular Medicine
Licensed content title	Circulating tumor cells: the 'leukemic phase' of solid cancers
Licensed content author	Simone Mocellin, Ulrich Keilholz, Carlo Riccardo Rossi, Donato Nitti
Licensed content date	March 2006
Licensed content volume number	12
Licensed content issue number	3
Number of pages	10
Type of Use	reuse in a thesis/dissertation
Intended publisher of new work	other
Portion	figures/tables/illustrations
Number of figures/tables /illustrations	1
Format	print
Are you the author of this Elsevier article?	No
Will you be translating?	No
Order reference number	

Title of your thesis/dissertation	HIGHLY EFFICIENT SELECTION, ENUMERATION, ENRICHMENT AND MOLECULAR PROFILING OF LOW-ABUNDANCE BIOLOGICAL CELLS
Expected completion date	Sep 2010
Estimated size (number of pages)	200
Elsevier VAT number	GB 494 6272 12
Terms and Conditions	

INTRODUCTION

1. The publisher for this copyrighted material is Elsevier. By clicking "accept" in connection with completing this licensing transaction, you agree that the following terms and conditions apply to this transaction (along with the Billing and Payment terms and conditions established by Copyright Clearance Center, Inc. ("CCC"), at the time that you opened your Rightslink account and that are available at any time at <http://myaccount.copyright.com>).

GENERAL TERMS

2. Elsevier hereby grants you permission to reproduce the aforementioned material subject to the terms and conditions indicated.

3. Acknowledgement: If any part of the material to be used (for example, figures) has appeared in our publication with credit or acknowledgement to another source, permission must also be sought from that source. If such permission is not obtained then that material may not be included in your publication/copies. Suitable acknowledgement to the source must be made, either as a footnote or in a reference list at the end of your publication, as follows:

"Reprinted from Publication title, Vol /edition number, Author(s), Title of article / title of chapter, Pages No., Copyright (Year), with permission from Elsevier [OR APPLICABLE SOCIETY COPYRIGHT OWNER]." Also Lancet special credit - "Reprinted from The Lancet, Vol. number, Author(s), Title of article, Pages No., Copyright (Year), with permission from Elsevier."

4. Reproduction of this material is confined to the purpose and/or media for which permission is hereby given.

5. Altering/Modifying Material: Not Permitted. However figures and illustrations may be altered/adapted minimally to serve your work. Any other abbreviations, additions, deletions and/or any other alterations shall be made only with prior written authorization of Elsevier Ltd. (Please contact Elsevier at permissions@elsevier.com)

6. If the permission fee for the requested use of our material is waived in this instance, please be advised that your future requests for Elsevier materials may attract a fee.

7. Reservation of Rights: Publisher reserves all rights not specifically granted in the combination of (i) the license details provided by you and accepted in the course of this licensing transaction, (ii) these terms and conditions and (iii) CCC's Billing and Payment terms and conditions.

terms and conditions.

8. License Contingent Upon Payment: While you may exercise the rights licensed immediately upon issuance of the license at the end of the licensing process for the transaction, provided that you have disclosed complete and accurate details of your proposed use, no license is finally effective unless and until full payment is received from you (either by publisher or by CCC) as provided in CCC's Billing and Payment terms and conditions. If full payment is not received on a timely basis, then any license preliminarily granted shall be deemed automatically revoked and shall be void as if never granted. Further, in the event that you breach any of these terms and conditions or any of CCC's Billing and Payment terms and conditions, the license is automatically revoked and shall be void as if never granted. Use of materials as described in a revoked license, as well as any use of the materials beyond the scope of an unrevoked license, may constitute copyright infringement and publisher reserves the right to take any and all action to protect its copyright in the materials.

9. Warranties: Publisher makes no representations or warranties with respect to the licensed material.

10. Indemnity: You hereby indemnify and agree to hold harmless publisher and CCC, and their respective officers, directors, employees and agents, from and against any and all claims arising out of your use of the licensed material other than as specifically authorized pursuant to this license.

11. No Transfer of License: This license is personal to you and may not be sublicensed, assigned, or transferred by you to any other person without publisher's written permission.

12. No Amendment Except in Writing: This license may not be amended except in a writing signed by both parties (or, in the case of publisher, by CCC on publisher's behalf).

13. Objection to Contrary Terms: Publisher hereby objects to any terms contained in any purchase order, acknowledgment, check endorsement or other writing prepared by you, which terms are inconsistent with these terms and conditions or CCC's Billing and Payment terms and conditions. These terms and conditions, together with CCC's Billing and Payment terms and conditions (which are incorporated herein), comprise the entire agreement between you and publisher (and CCC) concerning this licensing transaction. In the event of any conflict between your obligations established by these terms and conditions and those established by CCC's Billing and Payment terms and conditions, these terms and conditions shall control.

14. Revocation: Elsevier or Copyright Clearance Center may deny the permissions described in this License at their sole discretion, for any reason or no reason, with a full refund payable to you. Notice of such denial will be made using the contact information provided by you. Failure to receive such notice will not alter or invalidate the denial. In no event will Elsevier or Copyright Clearance Center be responsible or liable for any costs, expenses or damage incurred by you as a result of a denial of your permission request, other than a refund of the amount(s) paid by you to Elsevier and/or Copyright Clearance Center for denied permissions.

LIMITED LICENSE

The following terms and conditions apply only to specific license types:

15. **Translation:** This permission is granted for non-exclusive world **English** rights only unless your license was granted for translation rights. If you licensed translation rights you may only translate this content into the languages you requested. A professional translator must perform all translations and reproduce the content word for word preserving the integrity of the article. If this license is to re-use 1 or 2 figures then permission is granted for non-exclusive world rights in all languages.

16. **Website:** The following terms and conditions apply to electronic reserve and author websites:

Electronic reserve: If licensed material is to be posted to website, the web site is to be password-protected and made available only to bona fide students registered on a relevant course if:

This license was made in connection with a course,

This permission is granted for 1 year only. You may obtain a license for future website posting,

All content posted to the web site must maintain the copyright information line on the bottom of each image,

A hyper-text must be included to the Homepage of the journal from which you are licensing at <http://www.sciencedirect.com/science/journal/xxxxx> or the Elsevier homepage for books at <http://www.elsevier.com> , and

Central Storage: This license does not include permission for a scanned version of the material to be stored in a central repository such as that provided by Heron/XanEdu.

17. **Author website** for journals with the following additional clauses:

All content posted to the web site must maintain the copyright information line on the bottom of each image, and

the permission granted is limited to the personal version of your paper. You are not allowed to download and post the published electronic version of your article (whether PDF or HTML, proof or final version), nor may you scan the printed edition to create an electronic version,

A hyper-text must be included to the Homepage of the journal from which you are licensing at <http://www.sciencedirect.com/science/journal/xxxxx> , As part of our normal production process, you will receive an e-mail notice when your article appears on Elsevier's online service ScienceDirect (www.sciencedirect.com). That e-mail will include the article's Digital Object Identifier (DOI). This number provides the electronic link to the published article and should be included in the posting of your personal version. We ask that you wait until you receive this e-mail and have the DOI to do any posting.

Central Storage: This license does not include permission for a scanned version of the material to be stored in a central repository such as that provided by Heron/XanEdu.

18. **Author website** for books with the following additional clauses:

Authors are permitted to place a brief summary of their work online only.

A hyper-text must be included to the Elsevier homepage at <http://www.elsevier.com>

All content posted to the web site must maintain the copyright information line on the bottom of each image

**ELSEVIER LICENSE
TERMS AND CONDITIONS**

Sep 09, 2010

This is a License Agreement between Udara R Dharmasiri ("You") and Elsevier ("Elsevier") provided by Copyright Clearance Center ("CCC"). The license consists of your order details, the terms and conditions provided by Elsevier, and the payment terms and conditions.

All payments must be made in full to CCC. For payment instructions, please see information listed at the bottom of this form.

Supplier	Elsevier Limited The Boulevard, Langford Lane Kidlington, Oxford, OX5 1GB, UK
Registered Company Number	1982084
Customer name	Udara R Dharmasiri
Customer address	LSU, Chemistry Baton Rouge, LA 70802
License number	2504960087212
License date	Sep 09, 2010
Licensed content publisher	Elsevier
Licensed content publication	Human Pathology
Licensed content title	Case study of the morphologic variation of circulating tumor cells
Licensed content author	Dena Marrinucci, Kelly Bethel, Richard H. Bruce, Douglas N. Curry, Ben Hsieh, Mark Humphrey, Robert T. Krivacic, Joan Kroener, Lindsay Kroener, Andras Ladanyi, Nicole H. Lazarus, Jorge Nieva, Peter Kuhn
Licensed content date	March 2007
Licensed content volume number	38
Licensed content issue number	3
Number of pages	6
Type of Use	reuse in a thesis/dissertation
Intended publisher of new work	other
Portion	figures/tables/illustrations
Number of figures/tables /illustrations	2
Format	print
Are you the author of this Elsevier article?	No
Will you be translating?	No

Order reference number	
Title of your thesis/dissertation	HIGHLY EFFICIENT SELECTION, ENUMERATION, ENRICHMENT AND MOLECULAR PROFILING OF LOW-ABUNDANCE BIOLOGICAL CELLS
Expected completion date	Sep 2010
Estimated size (number of pages)	200
Elsevier VAT number	GB 494 6272 12
Terms and Conditions	

INTRODUCTION

1. The publisher for this copyrighted material is Elsevier. By clicking "accept" in connection with completing this licensing transaction, you agree that the following terms and conditions apply to this transaction (along with the Billing and Payment terms and conditions established by Copyright Clearance Center, Inc. ("CCC"), at the time that you opened your Rightslink account and that are available at any time at <http://myaccount.copyright.com>).

GENERAL TERMS

2. Elsevier hereby grants you permission to reproduce the aforementioned material subject to the terms and conditions indicated.

3. Acknowledgement: If any part of the material to be used (for example, figures) has appeared in our publication with credit or acknowledgement to another source, permission must also be sought from that source. If such permission is not obtained then that material may not be included in your publication/copies. Suitable acknowledgement to the source must be made, either as a footnote or in a reference list at the end of your publication, as follows:

"Reprinted from Publication title, Vol /edition number, Author(s), Title of article / title of chapter, Pages No., Copyright (Year), with permission from Elsevier [OR APPLICABLE SOCIETY COPYRIGHT OWNER]." Also Lancet special credit - "Reprinted from The Lancet, Vol. number, Author(s), Title of article, Pages No., Copyright (Year), with permission from Elsevier."

4. Reproduction of this material is confined to the purpose and/or media for which permission is hereby given.

5. Altering/Modifying Material: Not Permitted. However figures and illustrations may be altered/adapted minimally to serve your work. Any other abbreviations, additions, deletions and/or any other alterations shall be made only with prior written authorization of Elsevier Ltd. (Please contact Elsevier at permissions@elsevier.com)

6. If the permission fee for the requested use of our material is waived in this instance, please be advised that your future requests for Elsevier materials may attract a fee.

7. Reservation of Rights: Publisher reserves all rights not specifically granted in the combination of (i) the license details provided by you and accepted in the course of this licensing transaction, (ii) these terms and conditions and (iii) CCC's Billing and Payment

terms and conditions.

8. License Contingent Upon Payment: While you may exercise the rights licensed immediately upon issuance of the license at the end of the licensing process for the transaction, provided that you have disclosed complete and accurate details of your proposed use, no license is finally effective unless and until full payment is received from you (either by publisher or by CCC) as provided in CCC's Billing and Payment terms and conditions. If full payment is not received on a timely basis, then any license preliminarily granted shall be deemed automatically revoked and shall be void as if never granted. Further, in the event that you breach any of these terms and conditions or any of CCC's Billing and Payment terms and conditions, the license is automatically revoked and shall be void as if never granted. Use of materials as described in a revoked license, as well as any use of the materials beyond the scope of an unrevoked license, may constitute copyright infringement and publisher reserves the right to take any and all action to protect its copyright in the materials.

9. Warranties: Publisher makes no representations or warranties with respect to the licensed material.

10. Indemnity: You hereby indemnify and agree to hold harmless publisher and CCC, and their respective officers, directors, employees and agents, from and against any and all claims arising out of your use of the licensed material other than as specifically authorized pursuant to this license.

11. No Transfer of License: This license is personal to you and may not be sublicensed, assigned, or transferred by you to any other person without publisher's written permission.

12. No Amendment Except in Writing: This license may not be amended except in a writing signed by both parties (or, in the case of publisher, by CCC on publisher's behalf).

13. Objection to Contrary Terms: Publisher hereby objects to any terms contained in any purchase order, acknowledgment, check endorsement or other writing prepared by you, which terms are inconsistent with these terms and conditions or CCC's Billing and Payment terms and conditions. These terms and conditions, together with CCC's Billing and Payment terms and conditions (which are incorporated herein), comprise the entire agreement between you and publisher (and CCC) concerning this licensing transaction. In the event of any conflict between your obligations established by these terms and conditions and those established by CCC's Billing and Payment terms and conditions, these terms and conditions shall control.

14. Revocation: Elsevier or Copyright Clearance Center may deny the permissions described in this License at their sole discretion, for any reason or no reason, with a full refund payable to you. Notice of such denial will be made using the contact information provided by you. Failure to receive such notice will not alter or invalidate the denial. In no event will Elsevier or Copyright Clearance Center be responsible or liable for any costs, expenses or damage incurred by you as a result of a denial of your permission request, other than a refund of the amount(s) paid by you to Elsevier and/or Copyright Clearance Center for denied permissions.

LIMITED LICENSE



The Publishing Division
of the Massachusetts Medical Society

MMS Reference Number: PS - 2011 - 1187
MMS Invoice Number: RY - 2011 - 1187

Publishers of
*The New England Journal of Medicine, Journal Watch Newsletters,
& AIDS Clinical Care*

Grant of Permission

September 10, 2010

LSU
Dr. Udara Dharmasiri
LSU Chemistry

Baton Rouge, LA 70802

Dear Dr. Dharmasiri,

Thank you for your interest in our copyrighted material, and for requesting permission for its use.

Permission is granted for limited, non-exclusive educational use of the material requested, subject to all the terms and conditions outlined throughout this document. Please review all of the following pages, including the "Basic Provisions of Grant of Permission" as well as "Items Covered by Grant of Permission." A Permissions Invoice is included as the last page, if applicable.

Thank you for your patience while your request was being processed. If you wish to contact us further, please use the address below, and cite our reference numbers on any correspondence.

Sincerely,

Jennifer Moran

A handwritten signature in cursive script that reads "Jennifer A. Moran".

Sr. Rights & Permissions Representative

Page 1

Publishing Division of the Massachusetts Medical Society
Department of Permissions & Licensing
860 Winter Street, Waltham, Massachusetts 02451-1413 USA
Tel: (781) 434 7382 · Fax: (781) 434 7633 · permissions@nejm.org

September 10, 2010

BASIC PROVISIONS of GRANT OF PERMISSION

- This permission applies only to copyrighted material that the Massachusetts Medical Society ("MMS") owns, and not to copyrighted text or illustrations from other sources. If material appears in our work with credit to another source, you must also obtain permission from the original source cited in our work.
- All content reproduced from copyrighted material owned by the MMS remains the sole and exclusive property of the MMS. The right to grant permission to a third party is reserved solely by the MMS.
- MMS' copyrighted content may not be used in any manner that implies endorsement, sponsorship, or promotion of any entity, product or service by the MMS or its publications. MMS cannot and does not authorize the use of any author's name on promotional materials; such approval must be obtained directly from the author.
- **CREDIT LINE:** This permission requires a full credit line either in close proximity to where MMS text or illustration appears, or on the copyright page of any publication that incorporates the MMS' content. This credit line must include reference to the original article in standard citation format, together with a notice of copyright ownership, as follows: Copyright © [year of publication] Massachusetts Medical Society. All rights reserved.
- This permission is a one-time, non-exclusive grant limited only to the specific use, format(s), language(s) and edition(s) specified on the "Items Covered by Grant of Permission" page. It is not a "blanket" permission allowing unrestricted use of this material in future reproductions, editions, revisions, ancillary products, or other derivative works.
- This permission gives distribution rights throughout the world.
- This grant of permission is issued for the material to be used as originally published by MMS. MMS does not approve adaptations or modifications.
- Formatting and stylistic changes and any explanatory material or figure legends used by the requester must accurately reflect the material as originally published by MMS.
- Unless fees have been waived, this permission is contingent on payment in a timely manner of any fees associated with this use. **IMPORTANT:** Please reference MMS' original invoice number to ensure proper credit.

Items Covered by Grant of Permission



The Publishing Division
of the Massachusetts Medical Society
Department of Permissions & Licensing
 860 Winter Street, Waltham, Massachusetts 02451-1413 USA
 Telephone: (781) 434-7382 fax: (781) 893-8103

MMS Reference Number: PS - 2011 - 1187
 MMS Invoice Number: RY - 2011 - 1187

Source Information						
Volume	Pages	Pub. Date	Author(s)	Article Title	Type	Format
351	781- 791	8/19/2004	Cristofanilli, Budd, Ellis, Slopeck, Maitra, Miller, Reuben, Doyle, Allard	Circulating Tumor Cells, Disease Progression, and Survival in Metastatic Breast	F/T	Print & Electronic
						Translations Rights English
						Number of Figures / Tables 1

The following information has been provided for us in your letter of request.

End Use: Dissertation
User: students
Sponsor: Louisiana State University
Date of Use: 5 years
Number of Copies:



Udara Dharmasiri <udharm1@tigers.lsu.edu>

AW: Form: Permission request

3 messages

Rights DE <RIGHTS-and-LICENCES@wiley-vch.de>
To: "udharm1@lsu.edu" <udharm1@lsu.edu>

Mon, Aug 23, 2010 at 1:47 AM

Dear Customer,

Thank you for your email.

Are you the author of the requested material? If yes - will the dissertation be published electronically?

With kind regards

Bettina Loycke

Bettina Loycke
Senior Rights Manager
Wiley-VCH Verlag GmbH & Co. KGaA
Boschstr. 12
69469 Weinheim
Germany

Phone: +49 (0) 62 01- 606 - 280
Fax: +49 (0) 62 01 - 606 - 332
Email: rights@wiley-vch.de

Wiley-VCH Verlag GmbH & Co. KGaA
Location of the Company: Weinheim
Chairman of the Supervisory Board: Stephen Michael Smith
Trade Register: Mannheim, HRB 432833
General Partner: John Wiley & Sons GmbH, Location: Weinheim
Trade Register Mannheim, HRB 432296
Managing Directors : Christopher J. Dicks, Bijan Ghawami, William Pesce

-----Ursprüngliche Nachricht-----
Von: udharm1@lsu.edu [mailto:udharm1@lsu.edu]
Gesendet: Freitag, 20. August 2010 19:15
An: Rights DE
Betreff: Form: Permission request

Form: Permission request
Path: Service Permission Request
Language: en

Adress
First Name: Udara
Surname: Dharmasiri
Street: LSU, Departmeny of Chemistry
Zip code: 70803
City: Baton Rouge
Country: USA
Fax: 225529427
E-mail: udharm1@lsu.edu
Media Type: book
Author or Editor: Udara Dharmasiri
ISBN: Dissertation
Journal Title: Electrophoresis
Journal Month: April 28
Journal Year: 2009
Journal Volume: 30
Media Type: book
Page No: 1-12
Website or Intranet: yes
University/Institute: Louisiana State University
Instructor: Prof. Steven A. Soper
Course: Dissertation
Wiley Author: yes

Udara Dharmasiri <udharm1@tigers.lsu.edu>

Mon, Aug 23, 2010 at 11:21 AM

To: Rights DE <RIGHTS-and-LICENCES@wiley-vch.de>

Hello,

Thank you for the reply. Yes, I am the author. It will be in LSU library system and LSU library will publish it electronically.

Thank you

Udara

[Quoted text hidden]

--

Udara Dharmasiri
PhD Candidate
204, Choppin Hall
Department of Chemistry
Louisiana State University
Baton Rouge, LA, 70803

Office Phone # 225-578-7709

Cell Phone # 225-588-9678

Rights DE <RIGHTS-and-LICENCES@wiley-vch.de>

Tue, Aug 24, 2010 at 3:18 AM

To: Udara Dharmasiri <udharm1@tigers.lsu.edu>

Dear Udara Dharmasiri,

Thank you for your email.

We hereby grant permission for the requested use expected that due credit is given to the original source.

Please note that the author's permission is also required.

Please note that we only grant rights for a printed version, but not the rights for an electronic/ online/ web/ microfiche publication, but you are free to create a link to the article in question which is posted on our website (<http://www3.interscience.wiley.com>)

δ You may use the version of the contribution as originally submitted for publication for an electronic presentation of the thesis. The contribution may not be updated or replaced with the published version. The version posted must contain a legend as follows: This is the pre-peer reviewed version of the following article: FULL CITE.

With kind regards

Bettina Loycke

Bettina Loycke

Senior Rights Manager

Wiley-VCH Verlag GmbH & Co. KGaA

Boschstr. 12

69469 Weinheim

Germany

Phone: +49 (0) 62 01- 606 - 280

Fax: +49 (0) 62 01 - 606 - 332

Email: rights@wiley-vch.de

Wiley-VCH Verlag GmbH & Co. KGaA

**AMERICAN CHEMICAL SOCIETY LICENSE
TERMS AND CONDITIONS**

Sep 09, 2010

This is a License Agreement between Udara R Dharmasiri ("You") and American Chemical Society ("American Chemical Society") provided by Copyright Clearance Center ("CCC"). The license consists of your order details, the terms and conditions provided by American Chemical Society, and the payment terms and conditions.

All payments must be made in full to CCC. For payment instructions, please see information listed at the bottom of this form.

License Number	2504951288701
License Date	Sep 09, 2010
Licensed content publisher	American Chemical Society
Licensed content publication	Analytical Chemistry
Licensed content title	Enrichment and Detection of Escherichia coli O157:H7 from Water Samples Using an Antibody Modified Microfluidic Chip
Licensed content author	Udara Dharmasiri et al.
Licensed content date	Apr 1, 2010
Volume number	82
Issue number	7
Type of Use	Thesis/Dissertation
Requestor type ¹¹	Not specified
Format	Print
Portion	Full article
Author of this ACS article	Yes
Order reference number	
Title of the thesis / dissertation	HIGHLY EFFICIENT SELECTION, ENUMERATION, ENRICHMENT AND MOLECULAR PROFILING OF LOW-ABUNDANCE BIOLOGICAL CELLS
Expected completion date	Sep 2010
Estimated size(pages)	200
Billing Type	Invoice
Billing Address	LSU, Chemistry
	Baton Rouge, LA 70802
	United States
Customer reference info	
Total	0.00 USD
Terms and Conditions	

Thesis/Dissertation

ACS / RIGHTS LINK TERMS & CONDITIONS THESIS/DISSERTATION

INTRODUCTION

The publisher for this copyrighted material is the American Chemical Society. By clicking "accept" in connection with completing this licensing transaction, you agree that the following terms and conditions apply to this transaction (along with the Billing and Payment terms and conditions established by Copyright Clearance Center, Inc. ("CCC"), at the time that you opened your Rightslink account and that are available at any time at <<http://myaccount.copyright.com>>).

LIMITED LICENSE

Publisher hereby grants to you a non-exclusive license to use this material. Licenses are for one-time use only with a maximum distribution equal to the number that you identified in the licensing process; any form of republication must be completed within 60 days from the date hereof (although copies prepared before then may be distributed thereafter).

GEOGRAPHIC RIGHTS: SCOPE

Licenses may be exercised anywhere in the world.

RESERVATION OF RIGHTS

Publisher reserves all rights not specifically granted in the combination of (i) the license details provided by you and accepted in the course of this licensing transaction, (ii) these terms and conditions and (iii) CCC's Billing and Payment terms and conditions.

PORTION RIGHTS STATEMENT: DISCLAIMER

If you seek to reuse a portion from an ACS publication, it is your responsibility to examine each portion as published to determine whether a credit to, or copyright notice of, a third party owner was published adjacent to the item. You may only obtain permission via Rightslink to use material owned by ACS. Permission to use any material published in an ACS publication, journal, or article which is reprinted with permission of a third party must be obtained from the third party owner. ACS disclaims any responsibility for any use you make of items owned by third parties without their permission.

REVOCAATION

The American Chemical Society reserves the right to revoke a license for any reason, including but not limited to advertising and promotional uses of ACS content, third party usage, and incorrect figure source attribution.

LICENSE CONTINGENT ON PAYMENT

While you may exercise the rights licensed immediately upon issuance of the license at the end of the licensing process for the transaction, provided that you have disclosed complete and accurate details of your proposed use, no license is finally effective unless and until full payment is received from you (by CCC) as provided in CCC's Billing and Payment terms and conditions. If full payment is not received on a timely basis, then any license preliminarily granted shall be deemed automatically revoked and shall be void as if never

may be evaluated on a case-by-case basis by the journal's editor. If an ACS journal editor considers Web posting to be "prior publication", the paper will not be accepted for publication in that journal. If you intend to submit your unpublished paper to ACS for publication, check with the appropriate editor prior to posting your manuscript electronically.

If your paper has already been published by ACS and you want to include the text or portions of the text in your thesis/dissertation in **print or microfilm formats**, please print the ACS copyright credit line on the first page of your article: "Reproduced (or 'Reproduced in part') with permission from [FULL REFERENCE CITATION.] Copyright [YEAR] American Chemical Society." Include appropriate information.

Submission to a Dissertation Distributor: If you plan to submit your thesis to UMI or to another dissertation distributor, you should not include the unpublished ACS paper in your thesis if the thesis will be disseminated electronically, until ACS has published your paper. After publication of the paper by ACS, you may release the entire thesis (not the individual ACS article by itself) for electronic dissemination through the distributor; ACS's copyright credit line should be printed on the first page of the ACS paper.

Use on an Intranet: The inclusion of your ACS unpublished or published manuscript is permitted in your thesis in print and microfilm formats. If ACS has published your paper you may include the manuscript in your thesis on an intranet that is not publicly available. Your ACS article cannot be posted electronically on a publicly available medium (i.e. one that is not password protected), such as but not limited to, electronic archives, Internet, library server, etc. The only material from your paper that can be posted on a public electronic medium is the article abstract, figures, and tables, and you may link to the article's DOI or post the article's author-directed URL link provided by ACS. This paragraph does not pertain to the dissertation distributor paragraph above.

Other conditions:

v1.1

Gratis licenses (referencing \$0 in the Total field) are free. Please retain this printable license for your reference. No payment is required.

If you would like to pay for this license now, please remit this license along with your payment made payable to "COPYRIGHT CLEARANCE CENTER" otherwise you will be invoiced within 48 hours of the license date. Payment should be in the form of a check or money order referencing your account number and this invoice number RLNK10846319.

Once you receive your invoice for this order, you may pay your invoice by credit card. Please follow instructions provided at that time.

**Make Payment To:
Copyright Clearance Center
Dept 001
P.O. Box 843006
Boston, MA 02284-3006**

If you find copyrighted material related to this license will not be used and wish to cancel, please contact us referencing this license number 2504951288701 and noting the reason for cancellation.

Vita

Udara Rasika Dharmasiri was born to Mr. A.W. Dharmasiri and Mrs. S.C. Kaldera in Kandy, Sri Lanka. He attended Ananda College, Colombo, Sri Lanka, from 1991–2000. Shortly after the schooling, Udara enrolled at University of Peradeniya, Sri Lanka. He obtained Bachelor of Science in Chemistry in April, 2004. Upon receiving the degree he was recruited as a Teaching Assistant in the Department of Chemistry, University of Peradeniya. In April 2005, Udara entered the postgraduate Institute of Science, University of Peradeniya, where he obtained Master of Science in analytical chemistry in August 2006. While still at the University of Peradeniya, he followed Chartered Institute of Management Accountants (CIMA) (UK) exams and completed CIMA degree up to Intermediate level. In the Fall of 2006, he was accepted to Graduate School doctoral program at Louisiana State University (LSU) in the Department of Chemistry. In the graduate school, he received the James W. Robinson Award for Outstanding Research in Analytical Sciences. He has been a member the American Chemical Society (ACS), Louisiana Volunteers in Action (LAVA) and Chartered Institute of Management Accountants (CIMA). He is also a member of two national honor societies: Phi Kappa Phi and Gamma Beta Phi. Udara Rasika Dharmasiri is currently a candidate for the Doctor of Philosophy in bioanalytical chemistry, which will be awarded to him at the December 2010 Commencement at LSU, Baton Rouge.